

RESEARCH MEMORANDUM

JUN 26 1947

AN INVESTIGATION OF THE LATERAL-CONTROL CHARACTERISTICS
OF SPOILERS ON A HIGH-ASPECT-RATIO WING OF NACA 65-210
SECTION IN THE LANGLEY 8-FOOT HIGH-SPEED TUNNEL

By

Arvo A. Luoma

Langley Memorial Aeronautical Laboratory
Langley Field, Va.

CLASSIFIED DOCUMENT

This document contains classified information affecting the National Defense of the United States within the meaning of the Espionage Act, USC 50131 and 32. Its transmission or the revelation of its contents in any manner to an unauthorized person is prohibited by law. Information so classified may be imparted only to persons in the military and naval services of the United States, appropriate civilian officers and employees of the Federal Government who have a legitimate interest therein, and to United States citizens of known loyalty and discretion who of necessity must be informed thereof.

CLASSIFICATION CANCELLED

Authority: J. W. Crowley Date: 10/21/53
By: J. W. Crowley 12/11/53 See NACA
Del. for #1571

NATIONAL ADVISORY COMMITTEE FOR AERONAUTICS

WASHINGTON
June 24, 1947

UNCLASSIFIED



10-15-58

NATIONAL ADVISORY COMMITTEE FOR AERONAUTICS

RESEARCH MEMORANDUM

AN INVESTIGATION OF THE LATERAL-CONTROL CHARACTERISTICS
OF SPOILERS ON A HIGH-ASPECT-RATIO WING OF NACA 65-210
SECTION IN THE LANGLEY 8-FOOT HIGH-SPEED TUNNEL

By Arvo A. Luoma

SUMMARY

A three-dimensional lateral-control investigation was made of 3- and 6-percent-chord spoilers projecting on the upper surface of a wing of high-aspect ratio. The spoilers were located ahead of conventional 0.20-chord straight-sided-profile plain ailerons and tests were made with the spoilers at the 60- and 70-percent-chord locations. Ailerons and spoilers had the same span of 37.5-percent wing semispan. Spanwise loadings and moments and rolling-moment coefficients were determined from pressure-distribution measurements. Hinge-moment data for the conventional aileron were obtained by an electrical strain gage. Data were obtained for Mach numbers up to 0.925.

The spoilers gave large rolling moments at Mach numbers below the Mach number corresponding to the break in the rolling-moment-coefficient curves. There was an appreciable increase in spoiler control with increase in Mach number at speeds below the rolling-moment-break Mach number; at speeds above the rolling-moment-break Mach number there was an abrupt decrease in rolling-moment coefficient. At high supercritical speeds the 6-percent-chord spoilers still developed notable rolling-moment coefficients. The effectiveness of the 3-percent-chord spoilers at high supercritical speeds varied from completely ineffective to relatively effective (compared to the effectiveness of the 6-percent-chord spoilers), depending on Mach number and angle of attack. The spoilers at the 60-percent-chord location were found to be superior to the spoilers at the 70-percent-chord location for developing rolling moment. Calculations at a Mach number of 0.88 indicated that for the same rolling effectiveness spoilers at the 60-percent-chord location gave smaller wing-twisting moments than at the 70-percent-chord location and that spoilers at either location gave appreciably smaller wing-twisting moments than did the plain ailerons. Spoilers reduced aileron hinge moments for

UNCLASSIFIED

Mach numbers to approximately 0.83. At higher speeds the effect of the spoilers on aileron hinge moments was irregular.

INTRODUCTION

A comprehensive wind-tunnel research program has been undertaken by the National Advisory Committee for Aeronautics to provide aerodynamic data for use in the design of a military airplane to operate at level flight speeds of 80 percent of the speed of sound. The various phases of this program are reported in references 1 to 7.

Tests to determine the aerodynamic characteristics of 0.20-chord plain ailerons on a high-aspect-ratio wing (reference 1) showed that the conventional ailerons experienced appreciable losses in effectiveness at high supercritical speeds as a result of adverse compressibility effects. Additional losses in rolling due to wing twist become serious at these speeds, especially when thin wings of large span are used. Wind-tunnel investigations have indicated that spoilers show promise of use as a lateral-control device at high speeds, either alone or in combination with conventional ailerons, because spoilers retain a large degree of control at high speeds (references 8 and 9) and produce less wing twist than conventional ailerons of equal effectiveness (reference 10).

The present tests were made to determine the suitability of spoilers as a means of improving the rolling-moment and wing-twist characteristics at high supercritical speeds of the wing-aileron combination reported in reference 1. Two spoiler projections and two chordwise locations on the upper surface of the wing were tested. Spanwise loadings and rolling and pitching characteristics were obtained from pressure-distribution measurements. The effect of the spoiler on the hinge-moment coefficient of the conventional aileron was also determined. Test data were obtained for Mach numbers from 0.40 to 0.925.

SYMBOLS

The symbols used herein are defined as follows:

- α angle of attack of finite-span wing
- V velocity in undisturbed stream

- p static pressure in undisturbed stream
- p_l local static pressure at a point on airfoil section
- ρ mass density in undisturbed stream
- a speed of sound in undisturbed stream
- q dynamic pressure in undisturbed stream $\left(\frac{1}{2}\rho v^2\right)$
- P pressure coefficient $\left(\frac{p_l - p}{q}\right)$
- P_{cr} critical pressure coefficient; that is, the pressure coefficient at any point on airfoil surface where the local velocity is equal to the local velocity of sound
- M Mach number (V/a)
- δ_a aileron deflection; positive for downward deflection
- $\Delta\delta_a$ absolute value of total aileron deflection with ailerons at equal positive and negative deflections
- b span of wing; model value, 3.15 feet
- y distance along semispan from reflection plane
- y_1 distance along semispan from reflection plane to inboard end of aileron
- y_0 distance along semispan from reflection plane to outboard end of aileron
- b_a span of aileron and spoiler; model value, 0.590 ft ($b_a = y_0 - y_1$)
- c section chord of wing
- x distance along chord from leading edge of airfoil section
- x_s distance along chord from leading edge of airfoil section to location of spoiler on surface of wing (fig. 3)
- h_s spoiler projection normal to wing surface (fig. 3)
- x_s/c spoiler location at a section in terms of the local section chord of wing

h_s/c spoiler projection at a section in terms of the local section chord of wing

S area of complete wing; model value, 1.10 square feet

c' mean aerodynamic chord of wing; model value, 0.37 foot

$$\left(c' = \frac{2}{S} \int_0^{b/2} c^2 dy \right)$$

c_a section aileron chord measured along airfoil chord line from hinge axis of aileron to trailing edge of airfoil

\bar{c}_a root-mean-square chord of aileron; model value, 0.0534 foot

$$\left(\bar{c}_a = \sqrt{\frac{1}{b_a} \int_{y_i}^{y_o} c_a^2 dy} \right)$$

H_a aileron hinge moment

C_{h_a} aileron hinge-moment coefficient $\left(\frac{H_a}{q b_a \bar{c}_a^2} \right)$

ΔP resultant pressure coefficient across aileron seal
($\Delta P = (\text{value of } P \text{ below seal}) - (\text{value of } P \text{ above seal})$)

c_n section normal-force coefficient of wing from pressure-

distribution data $c_n = \frac{1}{c} \int_0^c (P_L - P_U) dx$

Δc_n change in section normal-force coefficient of airfoil due to spoiler projection and/or aileron deflection

$$\Delta c_n = \frac{1}{c} \int_0^c \left[(P_L - P_U) - (P_L - P_U)_{\substack{\delta_a=0^\circ \\ h_s/c=0}} \right] dx$$

c_m section pitching-moment coefficient of airfoil about quarter-chord point from pressure-distribution data; pitching moment due to chord forces not included

$$c_m = \frac{1}{c^2} \int_0^c (P_U - P_L) \left(x - \frac{c}{4} \right) dx$$

Δc_m change in section pitching-moment coefficient of airfoil about quarter-chord point due to spoiler projection and/or aileron deflection

$$\Delta c_m = \frac{1}{c^2} \int_0^c \left[(P_U - P_L) - (P_U - P_L)_{\substack{\delta_s=0 \\ h_s/c=0}} \right] \left(x - \frac{c}{4} \right) dx$$

C_N normal-force coefficient of semispan wing

$$C_N = \frac{2}{S} \int_0^{b/2} c_n c dy$$

C_m pitching-moment coefficient of semispan wing about quarter-chord line of wing

$$C_m = \frac{2}{Sc^3} \int_0^{b/2} c_m c^2 dy$$

ΔC_m change in pitching-moment coefficient of semispan wing about quarter-chord line of wing due to spoiler projection and/or aileron deflection

$$\Delta C_m = \frac{2}{Sc^3} \int_0^{b/2} \Delta c_m c^2 dy$$

C_z rolling-moment coefficient, due to spoiler projection and/or aileron deflection, about axis collinear with chord line in reflection plane

$$C_z = - \frac{1}{Sb} \int_0^{b/2} \Delta c_n c y dy$$

Subscripts:

U upper surface

L lower surface

APPARATUS AND METHODS

Apparatus.- The tests were made in the Langley 8-foot high-speed tunnel, which is a single-return closed-throat tunnel with an air-stream turbulence that is small but slightly higher than free air.

The wing used for the lateral-control investigation of the spoilers was the same wing used in the aileron tests of reference 1. The wing was supported in the wind tunnel on a vertical steel plate as shown in figure 1(a). This plate has a modified-ellipse section of 50-inch chord and a maximum thickness of 1.5-percent plate chord. A spoiler mounted on the upper surface of the wing is shown in figures 1(b) and 1(c). The wing had an NACA 65-210 airfoil section, an aspect ratio of 9.0, a taper ratio of 2.5:1.0, no sweepback of the quarter-chord line, no twist, or dihedral, and a tip which had the dimensions given in table I. (See also fig. 2.) The effective span of the model wing was 37.8 inches, the root chord was 6 inches, and the tip chord was 2.4 inches. Ordinates of the NACA 65-210 airfoil section are given in table II. A more complete description of the model and additional information concerning the test setup are to be found in reference 3.

Steel spoilers having a cross section approximately triangular were mounted on the upper surface of the wing directly in front of the conventional ailerons. The spoilers had a smooth, solid, plane surface normal to the wing surface and facing the air flow (fig. 3). The span of the spoiler was the same as that of the aileron, 37.5 percent of the wing semispan, with the inboard end of the spoiler and aileron at the 60-percent-semispan station (fig. 2). Tests were made with the spoilers located at the 0.70-chord line of the wing surface and also at the 0.60-chord line of the wing surface. Two spoiler projections of 3 and 6 percent of the local wing chord were included in the tests.

The aileron was of the plain type with no aerodynamic nose balance. The profile of the aileron was straight sided, defined by straight lines tangent to the aileron nose radius and passing to the trailing edge, resulting in a trailing-edge angle of 11.1° (fig. 3). The aileron had a chord 20 percent of the local wing chord and was supported on two hinges located approximately 25 percent of the aileron span from either end of the aileron.

Twenty static-pressure orifices were placed at each of eight stations along the wing span (fig. 4). The spanwise locations of these stations in percent of the semispan were 11, 20, 30, 43, 56, 64, 80, and 95. The four inboard stations were placed on the left half of the wing, and the four outboard stations on the right half. Pressure data at stations within the aileron span were obtained at stations 64, 80, and 95 percent of the semispan.

Test procedure.- Normal-force, pitching-moment, and rolling-moment data were obtained from static pressure-distribution measurements and are for aileron sealed-gap conditions. Hinge-moment data for the aileron were obtained by electrical strain-gage measurements and are for an unsealed aileron with a gap approximately 0.003 of the wing chord. Aerodynamic data were obtained for angles of attack of -2° , 0° , 2° , 4° , 7° , and 10° at Mach numbers of 0.40 and 0.60 and for angles of attack of -2° , 0° , 2° , 4° , and 7° at Mach numbers of 0.76, 0.80, 0.83, 0.88, 0.91, and 0.925. The Reynolds number based on the mean aerodynamic chord of the model wing (0.37 ft) varied from 900,000 at a Mach number of 0.40 to 1,400,000 at a Mach number of 0.91.

Static pressure-distribution and aileron hinge-moment measurements were made for the spoiler configurations at the 70-percent-chord location at aileron deflections of approximately 0° , -3° , and -6° . Pressure measurements for the spoiler configurations at the 60-percent-chord location were made at aileron deflections of approximately 0° and -3° . Aileron hinge-moment data were obtained for the configuration with the 6-percent-chord spoiler at the 60-percent-chord location at aileron deflections of approximately 0° and -3° and for the configuration with the 3-percent-chord spoiler at the 60-percent-chord location at an aileron deflection of approximately 0° .

Corrections.- Tunnel-wall interference corrections based on model, or solid, constriction and wake constriction have been applied to the Mach number and the dynamic pressure except at the highest Mach number. The corrections were very small and amounted to a maximum of about 1 percent at a Mach number of 0.91 as determined from calculations using the methods of references 11, 12, 13, 14 and the drag data of references 3 and 5. The tunnel choked in the present tests at an uncorrected Mach number of 0.95. Some tendency toward choking could be expected at an uncorrected Mach number of 0.925 as indicated by measurements made in the tests of reference 3. Since the methods used in estimating tunnel-wall interference corrections become unreliable at Mach numbers in the vicinity of choke, no corrections have been made at an uncorrected Mach number of 0.925. There is also question about the reliability of wind-tunnel data at speeds in the vicinity of choke. The general trends shown by the data at an uncorrected Mach number of 0.925, however, are believed to be correct. No corrections have been applied to the rolling-moment or hinge-moment coefficients. A discussion of corrections to lateral-control coefficients is given in references 15 and 16.

RESULTS

In the reduction of the data, plots were made of the section pressure distributions and these plots were then mechanically integrated

to give section normal-force and pitching-moment coefficients. These section coefficients were used in determining spanwise force- and moment-loading diagrams. Wing normal-force and rolling-moment coefficients were determined from mechanical integration of the spanwise force-loading plots, and wing pitching-moment coefficients were obtained from mechanical integration of the spanwise moment-loading plots. Previous tests (reference 1) had shown that the spanwise-loading curves could be satisfactorily faired without test points at the 20- and 43-percent-semispan stations, and in order to reduce the large amount of computing required, the pressure data for these two stations were not worked up.

Chordwise pressure distributions at the 80-percent-semispan station (approx. midspan of aileron and spoiler) for the wing with and without spoilers are shown in figures 5 to 8. Data for angles of attack of 0° , 2° , 4° , and 7° and for Mach numbers to 0.925 have been included. The aileron deflection for the various configurations was approximately 0° . Difficulty was experienced in accurately setting the aileron deflection at any particular value, but the effects of the variation in deflection are small and have been neglected in the discussion of these figures.

The rolling-moment coefficient for the spoiler and the sealed aileron are plotted against Mach number in figure 9 and against aileron deflection in figure 10. Also included in figure 10 for comparative purposes are rolling-moment data for the wing with no spoiler from the tests of reference 1. Figure 11 is a comparison of the compressibility effects on the rolling-moment coefficient of the spoilers and the total rolling-moment coefficient of the wing with no spoiler at equal positive and negative aileron deflections. The total aileron deflection is designated $\Delta\delta_a$.

Plots of wing normal-force coefficient against Mach number are given in figure 12. In figure 13 are shown average values of normal-force-curve slope $\Delta C_N / \Delta\alpha$ obtained between angles of attack of 0° and 4° as a function of Mach number for an aileron deflection of 0° . Spanwise section loadings $c_n cb/S$ are shown in figures 14 to 23 for two spoiler projections and two chordwise locations on the upper surface of the wing with the aileron approximately neutral and at small negative deflections. For purposes of comparison, spanwise section loading data from reference 1 for the "no-spoiler" configuration at an aileron deflection of 0.5° have been included in figure 14. Spanwise distributions of section moment factor $c_m c^2 b^2 / S^2$ are given in figures 24 to 33. Experimental data of the nature shown in figures 14 to 33 at the speeds covered in the present tests are meager and not readily available for reference. It is believed that these plots will be found to be of general interest in bringing out the effects of compressibility on spanwise loadings and of specific

usefulness for design purposes. Wing pitching-moment coefficients based on the wing mean aerodynamic chord are plotted against Mach number in figure 34, and incremental wing pitching-moment coefficients ΔC_m due to spoiler projection are plotted against Mach number in figure 35.

Figure 36 shows aileron hinge-moment coefficient plotted against aileron deflection for the several spoiler configurations. Hinge-moment data for the unsealed aileron with no spoiler from the tests of reference 1 are also included in figure 36. The variation of the hinge-moment coefficient of the aileron with Mach number and angle of attack are shown in figures 37 and 38, respectively. A comparison of the effects of compressibility on the aileron hinge-moment coefficient at equal positive and negative aileron deflections with and without a spoiler ahead of the upgoing aileron is shown in figure 39. The total aileron deflection is designated $\Delta\delta_a$. The hinge-moment data are for an unsealed aileron with a gap approximately 0.003 of the local wing chord. The smallness of the electrical strain gage which had to be used with the model wing coupled with severe operating conditions of high speeds, temperatures, and aileron loads impaired the accuracy of the hinge-moment measurements. An idea of the precision of the data can be obtained from the scatter of test points of figure 36. The general compressibility effects on hinge-moment characteristics, however, are well brought out by the data.

Data of average resultant-pressure coefficient across the aileron seal are given in figure 40. The data of figure 40 are for totally sealed conditions and are not directly applicable to the hinge-moment data of these tests which are for an unsealed aileron. The seal pressures are presented to show the compressibility trends and for use in estimating the amount of aerodynamic balance of an internally balanced sealed aileron system.

DISCUSSION

Section Pressure Distributions

The general nature of the action of a spoiler on the air flow about a wing for Mach numbers to 0.925 is illustrated by the chordwise pressure distributions shown in figures 5 to 8 for the wing with and without spoilers. These pressure data are for the 80-percent-semispan station, which is approximately the midspan of the spoiler and aileron.

A spoiler mounted on the upper surface of a wing generally modifies the flow of air about the wing by slowing up the air on the upper surface ahead of the spoiler and by speeding up the air along the lower surface. The speeding up of the flow probably can be explained by the more negative pressures (due to the separated flow aft of the spoiler) existing at the trailing edge of the wing which would tend to accelerate the lower-surface flow, and by the change in flow about the airfoil nose due to the more positive pressures ahead of the spoiler. The control produced by the spoiler at low speeds as indicated by the pressure data of these tests is due from one-half to two-thirds to retarding the flow on the upper surface. At high supercritical Mach numbers the effect of the spoiler is almost wholly due to retarding the flow on the upper surface, the velocities along the lower surface being only slightly affected for the most part. If the flow is already supersonic at the trailing edge, then the separated flow from a spoiler would not be expected to affect the lower-surface flow to any appreciable extent. Under such conditions, however, if the action of the spoiler is great enough to give subsonic velocities ahead of it on the upper surface extending to the leading edge of the airfoil then the lower-surface flow may still be affected to some extent as indicated by figures 6(a) and 8(a).

Since the performance of a spoiler is a function of the boundary-layer thickness at the spoiler location, an increase in boundary-layer thickness in terms of the spoiler projection can be expected to result in a decrease in spoiler effectiveness. Aggravating the adverse pressure gradients on an airfoil results in a thickening of the boundary layer, and if the pressure gradients are severe and associated with compression shock, as is generally true at supercritical speeds, then a separation of the flow may result. An increase in angle of attack usually aggravates the adverse pressure gradients on the upper surface of an airfoil and a loss in spoiler effectiveness generally results with increase in angle of attack as shown in figures 5 to 8. This loss is indicated in the pressure plots by the smaller extent of the more positive pressures ahead of the spoiler. At high supercritical speeds a loss in spoiler effectiveness occurs, particularly for the 3-percent-chord spoilers (figs. 5 and 7). Apparently, a thick boundary layer or separation of the flow has resulted. The Mach number at which this loss in effectiveness occurs decreases, as would be expected, with an increase in angle of attack. At very high supercritical speeds where the flow over the upper surface is completely supersonic, except in the vicinity of the leading edge, the pressure gradients tend to become favorable and there probably is improvement in the boundary-layer conditions with the separation point moving toward the spoiler. This is the probable explanation for the gain in effectiveness as shown by figure 5(d), for example, at the highest speeds.

Rolling-Moment Characteristics

General compressibility effects.- The general effects of compressibility on rolling-moment coefficient are similar for all spoiler configurations (fig. 9). There is first an appreciable improvement in rolling-moment coefficient with Mach number and then at speeds above the Mach number corresponding to the break in the rolling-moment-coefficient curves there is an abrupt decrease in rolling-moment coefficient. Both the increase and decrease in rolling-moment coefficient with Mach number become more gradual at an angle of attack of 7° . At any given angle of attack the rolling-moment-break Mach number is approximately the same for all the spoiler configurations tested, and varies from 0.83 at an angle of attack of -2° to about 0.57 at an angle of attack of 7° (fig. 9).

At very high supercritical speeds all the spoiler configurations show a notable increase in rolling-moment coefficient at an angle of attack of 7° . The same improvement in effectiveness at very high supercritical speeds is also shown to a lesser extent by the data at an angle of attack of 4° . This gain in effectiveness probably is associated with the improvement of the pressure gradients on the upper surface of the airfoil at these speeds and the consequent improvement in boundary-layer conditions and separation tendencies.

Figure 11 is a comparison of the compressibility effects on the rolling-moment coefficient of the spoiler configurations and the wing with no spoiler at equal positive and negative aileron deflections. It should be noted that the total span of the two ailerons for which data are presented in figure 11 was twice that of the spoiler. Spoiler span is not limited by trailing-edge flaps as ailerons would be, so that insufficiency of spoiler control at low speeds could be remedied by increasing the spoiler span. The improvement in rolling-moment coefficient with Mach number is seen to be greater for the spoiler configurations. At low angles of attack the rolling-moment-break Mach number is higher for the spoiler configurations and the decrease in coefficient at supercritical Mach numbers is less for the spoiler configurations. At low angles of attack and high supercritical speeds the 6-percent-chord spoiler produces more rolling moment than the plain ailerons deflected $\pm 10^\circ$. At large angles of attack and high supercritical speeds the plain ailerons are relatively more effective than the spoilers and do not show the large decrease in rolling-moment coefficient at supercritical speeds characteristic of the spoilers.

Spoiler projection.- The increase in rolling-moment coefficient with Mach number and the sharpness of the decrease of rolling-moment coefficient at supercritical speeds are essentially the same for the 3- and 6-percent-chord spoilers at a given spoiler location (figs. 9(a), 9(b), 9(c), and 9(d)). In spite of the large decrease in rolling-moment coefficient at supercritical speeds the 6-percent-chord

spoilers still develop a rolling-moment coefficient at a Mach number of 0.90 from 50 to 100 percent of the values developed at a Mach number of 0.40. The effectiveness of the 3-percent-chord spoilers at high supercritical speeds varies from completely ineffective to relatively effective (compared to the effectiveness of the 6-percent-chord spoilers), depending on Mach number and angle of attack (fig. 10).

Spoiler location.- At the lowest angle of attack at low speeds a change in spoiler location from the 70- to the 60-percent-chord location had little effect on the rolling-moment coefficient of either the 3- or 6-percent-chord spoilers (fig. 10). With increase in angle of attack, however, the effectiveness of the spoilers at the 60-percent-chord location over that at the 70-percent-chord location generally becomes increasingly greater. This difference in effectiveness with angle of attack probably can be attributed to the smaller growth in boundary layer with increase in angle of attack at the more forward spoiler location.

The rise in rolling-moment coefficient with Mach number is generally greater for the spoilers at the 60-percent-chord location and the sharpness of the decrease in rolling-moment coefficient at supercritical speeds is approximately the same for both locations.

The 60-percent-chord spoiler location is seen to be superior to the 70-percent-chord location for developing rolling moment. Two-dimensional wind-tunnel tests made at the Ames Laboratory conclude that when spoilers are used on an NACA 65-210 airfoil section for lateral-control purposes the 50-percent-chord location is better than the 30- and 70-percent-chord locations on the basis of more satisfactory rolling and yawing characteristics.

Aileron effectiveness.- The variation of rolling-moment coefficient with aileron deflection is generally less for the spoiler configurations than for the no-spoiler configuration at speeds below the rolling-moment-break Mach number and approximately the same at speeds above the rolling-moment-break Mach number (fig. 10). In other words, the spoilers generally effect the slope $dC_l/d\delta_a$ adversely at low speeds and have small effect at high supercritical speeds. At an angle of attack of 7° , however, the slope $dC_l/d\delta_a$ is generally affected adversely throughout the speed range and the data show that for certain ranges of aileron deflection at high supercritical speeds the combined effectiveness of the 3-percent-chord spoilers and the aileron is less than that of the aileron alone (fig. 10(e)).

Normal-Force Characteristics

Wing normal-force coefficient.- Compressibility effects on wing normal-force coefficient are very similar for all spoiler configurations (fig. 12). The magnitude of the compressibility effects is not as great as that shown by the wing with undeflected aileron and no spoiler (fig. 12(a)) but is quite like that of the plain aileron at large negative deflections (reference 1). The Mach number corresponding to the break in the wing normal-force-coefficient curves is approximately the same as the Mach number corresponding to the break in the rolling-moment-coefficient curves at moderate angles of attack and is somewhat greater at the largest angles of attack (figs. 12 and 9). The variation of wing normal-force coefficient with aileron deflection is quite similar for the various spoiler configurations (fig. 12). The spoilers at the 60-percent-chord location have a greater effect, for the most part, in reducing the wing normal-force coefficient than the spoilers at the 70-percent-chord location (fig. 12). The effect of the spoilers at supercritical Mach numbers is to increase the normal-force-curve slope $\Delta C_N/\Delta\alpha$ over that of the plain wing (fig. 13). An increase in normal-force-curve slope means a greater damping-moment coefficient in roll at these high speeds for the wing with spoilers. A similar increase in lift-curve slope at supercritical speeds is shown by the two-dimensional wind-tunnel tests made at the Ames Laboratory of spoilers on the NACA 65-210 airfoil section for the 50- and 70-percent-chord locations.

Spanwise loading.- The curves of spanwise loading c_{ncb}/S for the spoiler configurations (figs. 14 to 23) are similar to those for the conventional plain aileron at negative deflections (reference 1). The irregular load distributions and large changes in angle of zero normal force at Mach numbers above 0.83, characteristic of this particular wing and observed in previous tests (references 1 and 3), are also evident in the results of the present investigation.

At Mach numbers where the 3-percent-chord spoiler shows a high degree of effectiveness the influence of the spoiler extends to the wing root (fig. 14). At high supercritical speeds where the effect of the 3-percent-chord spoiler has appreciably diminished, the 3-percent-chord spoiler generally modifies the span loading only over the outboard half of the semispan, the inboard stations being essentially unaffected. On comparing the spanwise plots for the 6-percent-chord spoiler with the no-spoiler data shown in figure 14, it can be seen that the 6-percent-chord spoiler modifies the loading over the entire span at those Mach numbers where the spoiler is most effective, as was true of the 3-percent-chord spoiler. At high supercritical speeds, however, where the effectiveness of

the spoiler decreases, the influence of the 6-percent-chord spoiler is seen to still extend to the wing root for several of the angle-of-attack and Mach number combinations.

Pitching-Moment Characteristics

Large and somewhat irregular variations in the spanwise section moment factor $c_{m\alpha} c^2 b^2 / S^2$ at high supercritical speeds noted in reference 1 for the wing with the plain aileron are also characteristic of the wing with spoilers (figs. 24 to 33). These changes are fundamentally associated with the unsymmetrical effects of shock and shock movement on the upper and lower surfaces of the airfoil and are indicated by the pressure plots of figures 5 to 8. At Mach numbers in the approximate range from 0.82 to 0.90 the rearward movement of shock with the change in the negative direction of the pressures on the lower surface of the airfoil predominated in affecting the aerodynamic characteristics. At Mach numbers above approximately 0.90 the pressures on the aft half of the upper surface are reduced more than the pressures on the corresponding portion of the lower surface and the direction of the changes in aerodynamic coefficients just noted below a Mach number of 0.90 are therefore reversed.

The general effects of compressibility on wing pitching-moment coefficient are very similar for all spoiler configurations (fig. 34) and the trends are the same as for the plain wing. The variation of wing pitching-moment coefficient with angle of attack and small negative aileron deflections is quite similar for all spoiler configurations. The general variation of the incremental wing pitching-moment coefficient ΔC_m with Mach number (fig. 35) is essentially the same for all spoiler configurations, the magnitude of the variation due to compressibility being somewhat greater for the larger spoiler. The magnitude of the incremental pitching-moment coefficient is approximately the same at both spoiler locations for the 3-percent-chord spoiler and generally has smaller positive values at the 60-percent-chord location for the 6-percent-chord spoiler.

At speeds where the problem of wing twist in roll becomes serious, consideration must be given to the pitching moment, caused by a control, in relation to the rolling moment developed by the control and the damping characteristics of the wing (reference 10).

Wing-Torsional Considerations

Torsional-stiffness calculations were made in the analysis of reference 1 for an airplane of 104.5-foot span with plain ailerons

for lateral control. It was determined that in order for this airplane to retain at least 25 percent of the rigid-wing-rolling effectiveness at a Mach number of 0.88 and sea-level conditions, a wing with a minimum torsional stiffness at the midspan of the ailerons of 6,400,000 foot-pounds per radian was necessary. Similar calculations have been made for this airplane at a Mach number of 0.88 and sea-level conditions with spoilers used for lateral control. For the same rolling effectiveness, it was found that if spoilers are used for lateral control the 60-percent-chord-spoiler location gave smaller wing-twisting moments than the 70-percent-chord location, and that spoilers at either location gave appreciably smaller wing-twisting moments than did the plain ailerons. As a consequence, a wing about one-half as rigid torsionally as the wing with plain ailerons would be satisfactory when the spoilers are used for lateral control. These results are in line with the conclusions of reference 10.

Hinge-Moment Characteristics

For Mach numbers up to approximately 0.83 for most of the angle-of-attack range, the spoilers change the hinge-moment coefficient of the aileron in a negative direction and compressibility has small effect on the coefficient up to this Mach number (figs. 36 and 37). As mentioned previously, the hinge-moment data of these tests are for an unsealed aileron. At high supercritical speeds, where marked changes occur in airfoil characteristics as a result of critical shock conditions, large variations in aileron hinge-moment coefficient quite similar to those noted for the no-spoiler configuration occur (fig. 37). At these high supercritical speeds the effect of the spoilers on the aileron hinge-moment coefficient varies. For some conditions of angle of attack, aileron deflection, and Mach number the spoilers change the aileron hinge-moment coefficient in a positive direction. At the highest speeds, for the most part, the change appears to be negative as at lower speeds. The variation of aileron hinge-moment coefficient against angle of attack (fig. 38) is quite regular for speeds to a Mach number of approximately 0.83. At higher speeds, large irregularities similar to those previously noted occur.

The present tests indicate that a spoiler used in conjunction with ailerons for lateral control on the wing investigated could be expected to reduce stick forces for speeds up to a Mach number of approximately 0.83. At speeds above this Mach number, however, where the large changes in aerodynamic characteristics occur the data indicate that the spoilers could be expected to increase stick forces for some of the speed conditions and generally would be unsatisfactory in improving hinge-moment characteristics (fig. 39).

CONCLUDING REMARKS

A three-dimensional investigation of spoilers for lateral control at high speeds was made in the Langley 8-foot high-speed tunnel. Three- and 6-percent-chord spoilers were tested on the upper surface of a high-aspect-ratio wing at 60- and 70-percent wing chord. The spoilers were mounted ahead of conventional, 20-percent-chord, straight-sided-profile ailerons. Both the spoilers and ailerons had the same span of 37.5 percent of the wing semispan. The following statements specifically applying to the wing investigated can be made from the results of these wind-tunnel tests:

1. At Mach numbers below the Mach number corresponding to the break in the rolling-moment-coefficient curves the spoiler configurations investigated gave large rolling moments. There was appreciable improvement in rolling-moment coefficient with rise in Mach number at speeds below the rolling-moment-break Mach number. At Mach numbers above the rolling-moment-break Mach number there was an abrupt decrease in spoiler rolling-moment coefficient. The 6-percent-chord spoilers, however, still retained a notable amount of their effectiveness at high supercritical speeds. The effectiveness of the 3-percent-chord spoilers at high supercritical speeds varied from ineffective to moderately effective (compared to the effectiveness of the 6-percent-chord spoilers), depending on Mach number and angle of attack.

2. The 60-percent-chord-spoiler location was found to be superior to the 70-percent-chord location as regards developing greater rolling moment.

3. Calculations at a Mach number of 0.88 indicated that for the same rolling effectiveness the spoilers at the 60-percent-chord location produced less twisting of the wing than at the 70-percent-chord location, and that spoilers at either location produced appreciably smaller wing-twisting moments than 20-percent-chord plain ailerons. As a consequence, if spoilers are used for lateral control a wing having about one-half the torsional stiffness of the wing with plain ailerons would be satisfactory.

4. Spoilers used in conjunction with ailerons could be expected to reduce aileron stick forces for Mach numbers to approximately 0.83. At higher speeds the effect of the spoilers on aileron hinge moments was found to be irregular.

Langley Memorial Aeronautical Laboratory
National Advisory Committee for Aeronautics
Langley Field, Va.

REFERENCES

1. Luoma, Arvo A.: An Investigation of a High-Aspect-Ratio Wing Having 0.20-Chord Plain Ailerons in the Langley 8-Foot High-Speed Tunnel. NACA RM No. L6H28d, 1946.
2. Luoma, Arvo A., and Liccini, Luke L.: An Investigation of the Hinge-Moment Fluctuations of 0.20-Chord Plain Ailerons on a High-Aspect-Ratio Wing in the Langley 8-Foot High-Speed Tunnel. NACA RM No. L6L10a, 1947.
3. Whitcomb, Richard T.: Investigation of the Characteristics of a High-Aspect-Ratio Wing in the Langley 8-Foot High-Speed Tunnel. NACA RM No. L6H28a, 1946.
4. Ferri, Antonio: Preliminary Investigation of Downwash Fluctuations of a High-Aspect-Ratio Wing in the Langley 8-Foot High-Speed Tunnel. NACA RM No. L6H28b, 1946.
5. Mattson, Axel T.: Investigation of Dive Brakes and a Dive-Recovery Flap on a High-Aspect-Ratio Wing in the Langley 8-Foot High-Speed Tunnel. NACA RM No. L6H28c, 1946.
6. Whitcomb, Richard T.: An Investigation of the Downwash at the Probable Tail Location behind a High-Aspect-Ratio Wing in the Langley 8-Foot High-Speed Tunnel. NACA RM No. L7B12, 1947.
7. Bielat, Ralph P.: Investigation at High Speeds of a Horizontal-Tail Model in the Langley 8-Foot High-Speed Tunnel. NACA RM No. L6L10b, 1947.
8. Laitone, Edmund V.: An Investigation of the High-Speed Lateral-Control Characteristics of a Spoiler. NACA ACR No. 4C23, 1944.
9. Laitone, Edmund V., and Summers, James L.: An Additional Investigation of the High-Speed Lateral-Control Characteristics of Spoilers. NACA ACR No. 5D28, 1945.
10. Purser, Paul E., and McKinney, Elizabeth G.: Comparison of Pitching Moments Produced by Plain Flaps and by Spoilers and Some Aerodynamic Characteristics of an NACA 23012 Airfoil with Various Types of Aileron. NACA ACR No. L5C24a, 1945.
11. Glauert, H.: Wind Tunnel Interference on Wings, Bodies and Airscrews. R. & M. No. 1566, British A.R.C., 1933.

12. Thom, A.: Blockage Corrections in a Closed High-Speed Tunnel. R. & M. No. 2033, British A.R.C., 1943.
13. Goldstein, S., and Young, A. D.: The Linear Perturbation Theory of Compressible Flow, with Applications to Wind-Tunnel Interference. R. & M. No. 1909, British A.R.C., 1943.
14. Allen, H. Julian, and Vincenti, Walter G.: The Wall Interference in a Two-Dimensional-Flow Wind Tunnel with Consideration of the Effect of Compressibility. NACA Rep. No. 782, 1944.
15. Swanson, Robert S., and Toll, Thomas A.: Jet-Boundary Corrections for Reflection-Plane Models in Rectangular Wind Tunnels. NACA ARR No. 3E22, 1943.
16. Sivells, James C., and Deters, Owen J.: Jet-Boundary and Plan-Form Corrections for Partial-Span Models with Reflection Plane, End Plate, or No End Plate in a Closed Circular Wind Tunnel. NACA TN No. 1077, 1946.

TABLE I
DIMENSIONS OF WING-TIP SHAPE

(See fig. 2.)

Plan-forma contour		
Distance from tip, y_t (in.)	Distance forward of 25-percent-chord line, x_f (in.)	Distance rearward of 25-percent-chord line, x_r (in.)
0	-0.360	0.360
.026	.041	.963
.053	.176	1.168
.079	.268	1.307
.105	.337	1.413
.158	.436	1.565
.236	.529	1.710
.341	.595	1.817
.473	.623	1.868
Section contour at B-B, fig. 2		
Distance from tip, y_t (in.)	Upper-surface ordinate, z_U (in.)	Lower-surface ordinate, z_L (in.)
0.026	0.076	0.024
.053	.093	.041
.079	.103	.052
.105	.113	.061
.158	.126	.074
.236	.138	.086
.341	.147	.094
.473	.151	.098

TABLE II

ORDINATES FOR NACA 65-210 AIRFOIL

[Stations and ordinates in percent wing chord]

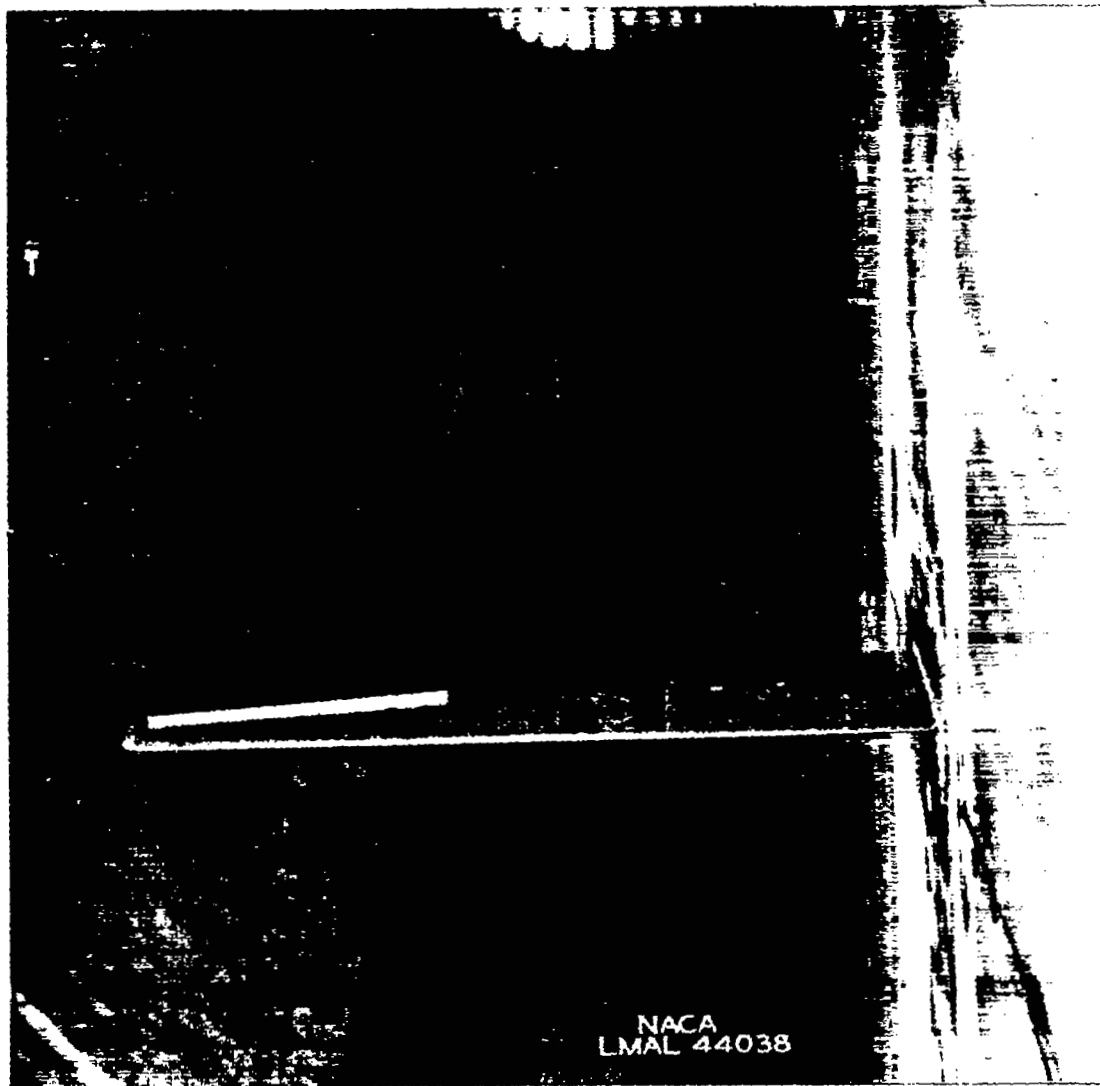
Upper surface		Lower surface	
Station	Ordinate	Station	Ordinate
0	0	0	0
.435	.819	.565	-.719
.678	.999	.822	-.859
1.169	1.273	1.331	-1.059
2.408	1.757	2.592	-1.385
4.898	2.491	5.102	-1.859
7.394	3.069	7.606	-2.221
9.894	3.555	10.106	-2.521
14.899	4.338	15.101	-2.992
19.909	4.938	20.091	-3.346
24.921	5.397	25.079	-3.607
29.936	5.732	30.064	-3.788
34.951	5.954	35.049	-3.894
39.968	6.067	40.032	-3.925
44.984	6.058	45.016	-3.868
50.000	5.915	50.000	-3.709
55.014	5.625	54.986	-3.435
60.027	5.217	59.973	-3.075
65.036	4.712	64.964	-2.652
70.043	4.128	69.957	-2.184
75.045	3.479	74.955	-1.689
80.044	2.783	79.956	-1.191
85.038	2.057	84.962	-.711
90.028	1.327	89.972	-.293
95.014	.622	94.986	.010
100.000	0	100.000	0

L. E. radius: 0.687. Slope of radius through end of chord: 0.084

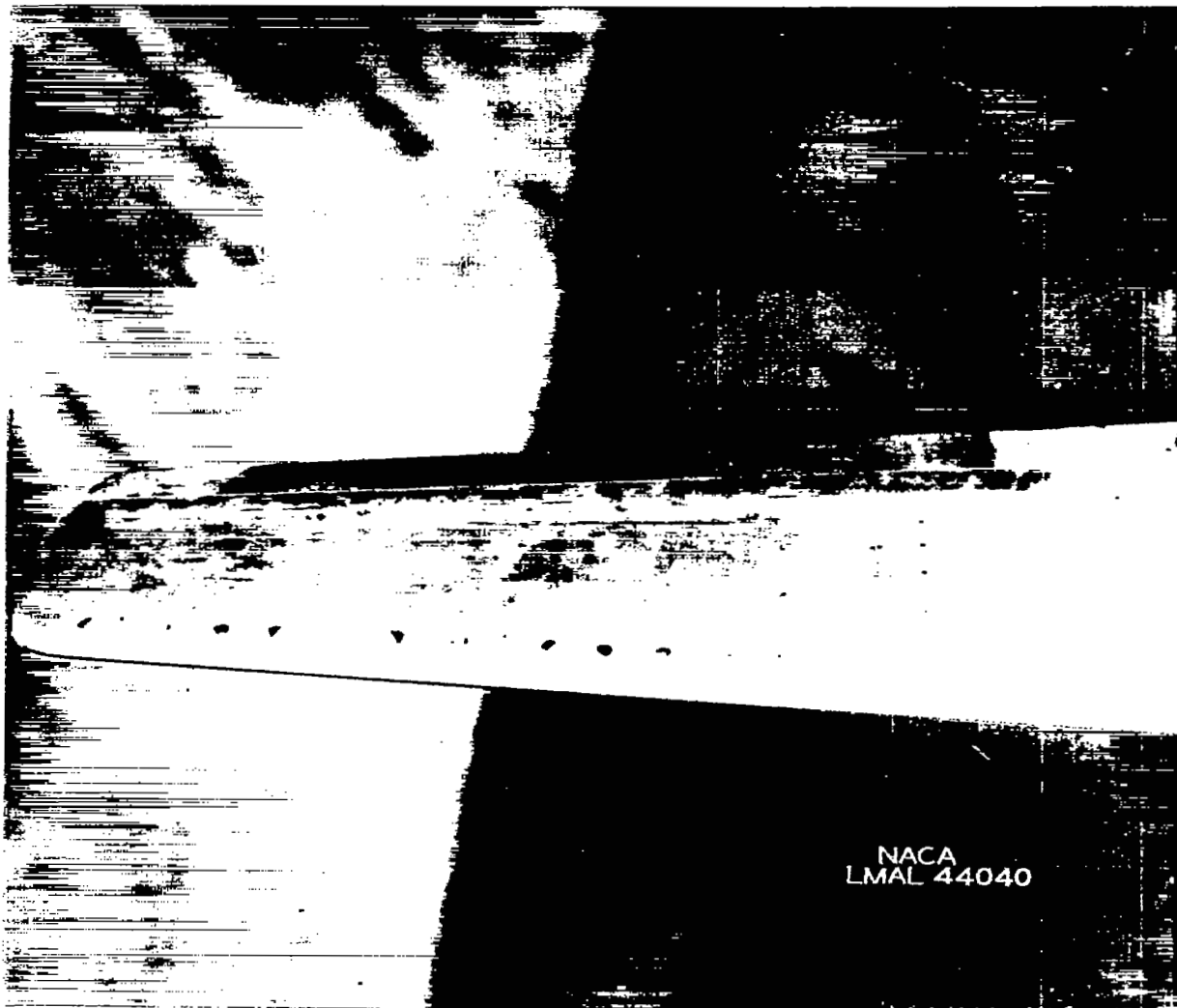


(a) Front view.

Figure 1.- Wing of high-aspect ratio mounted on vertical support plate in Langley 8-foot high-speed tunnel.



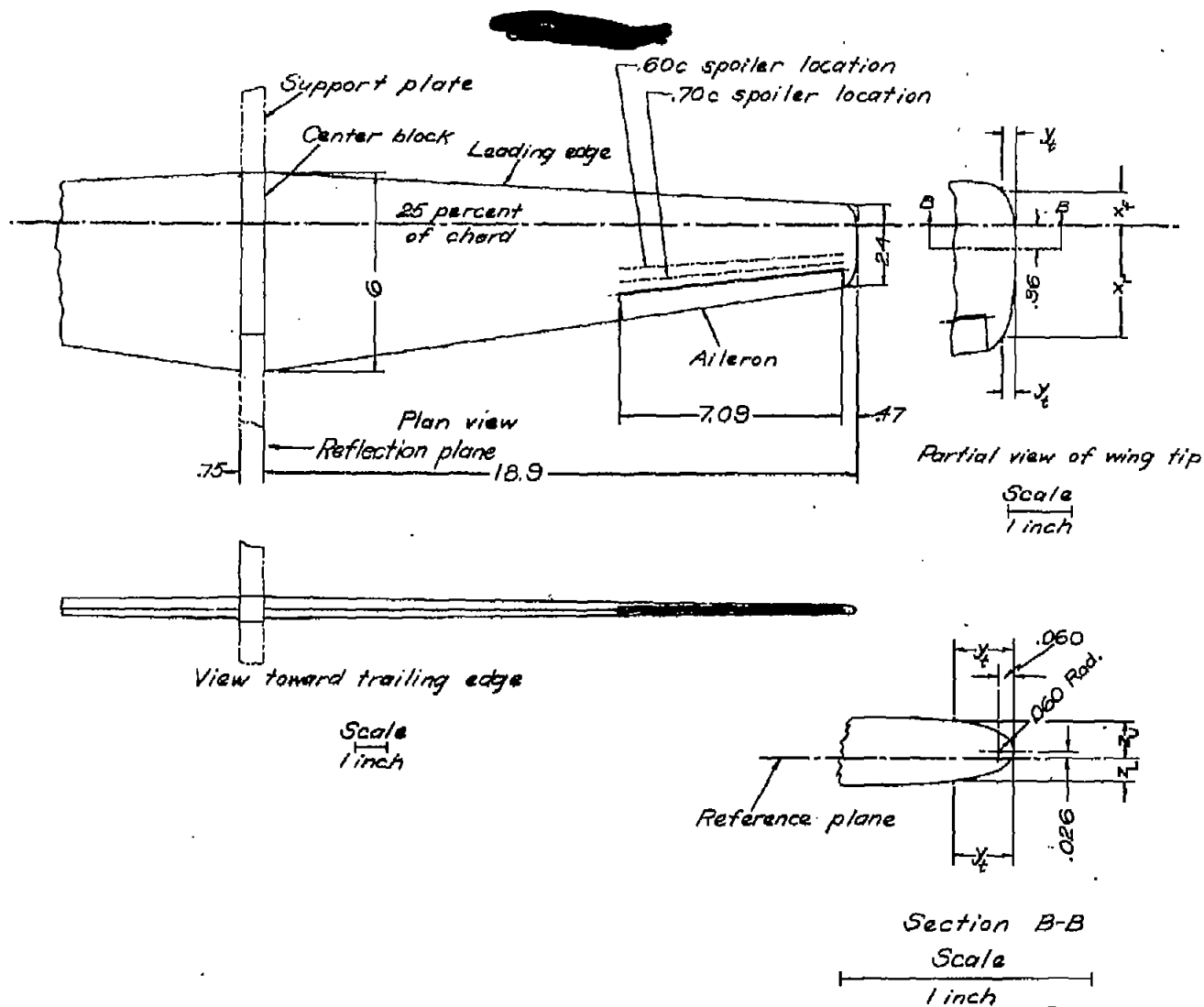
(b) View of right wing showing 6-percent-chord spoiler mounted on upper surface of wing at 70-percent-chord location.



(c) Close-up of right wing tip showing 6-percent-chord spoiler mounted on upper surface of wing at 70-percent-chord location.

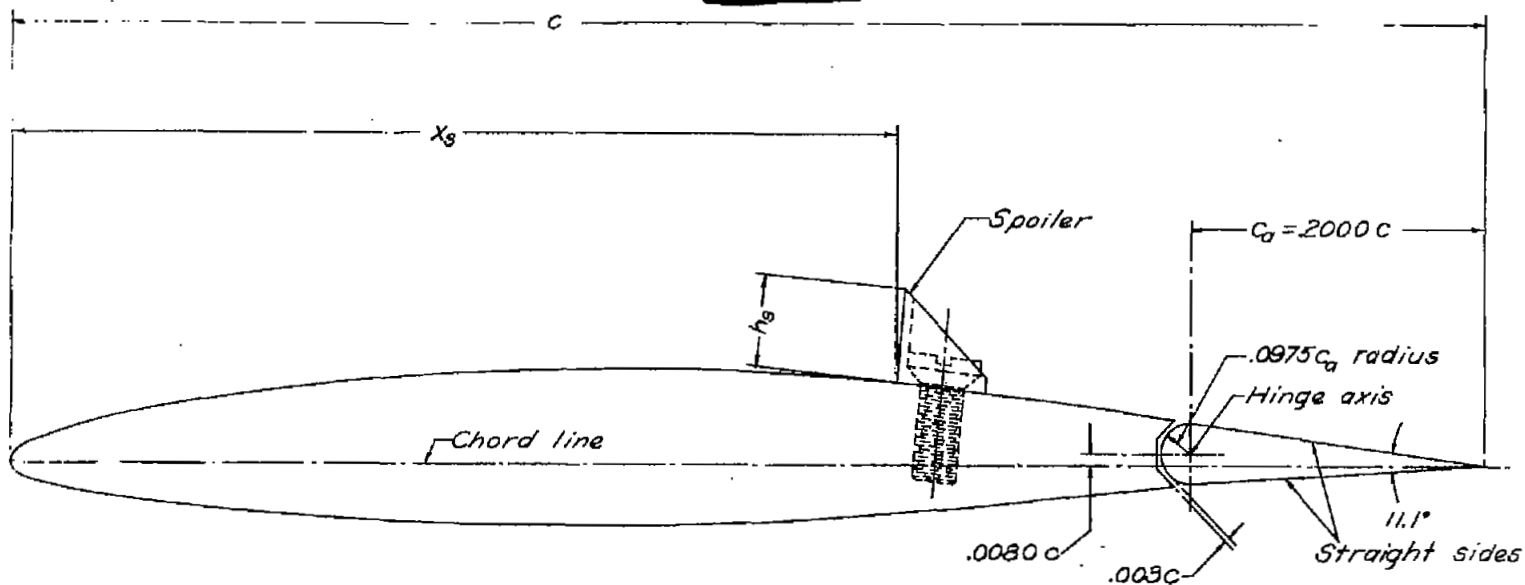
Figure 1.- Concluded.

CONFIDENTIAL



NATIONAL ADVISORY
COMMITTEE FOR AERONAUTICS

Figure 2- Dimensions of model wing. (All dimensions in inches).



NATIONAL ADVISORY
COMMITTEE FOR AERONAUTICS

Figure 3.- Cross-section of the wing within the aileron span showing the dimensions of the 0.20-chord plain ailerons and the mounting of the solid spoilers on the upper surface of the wing.

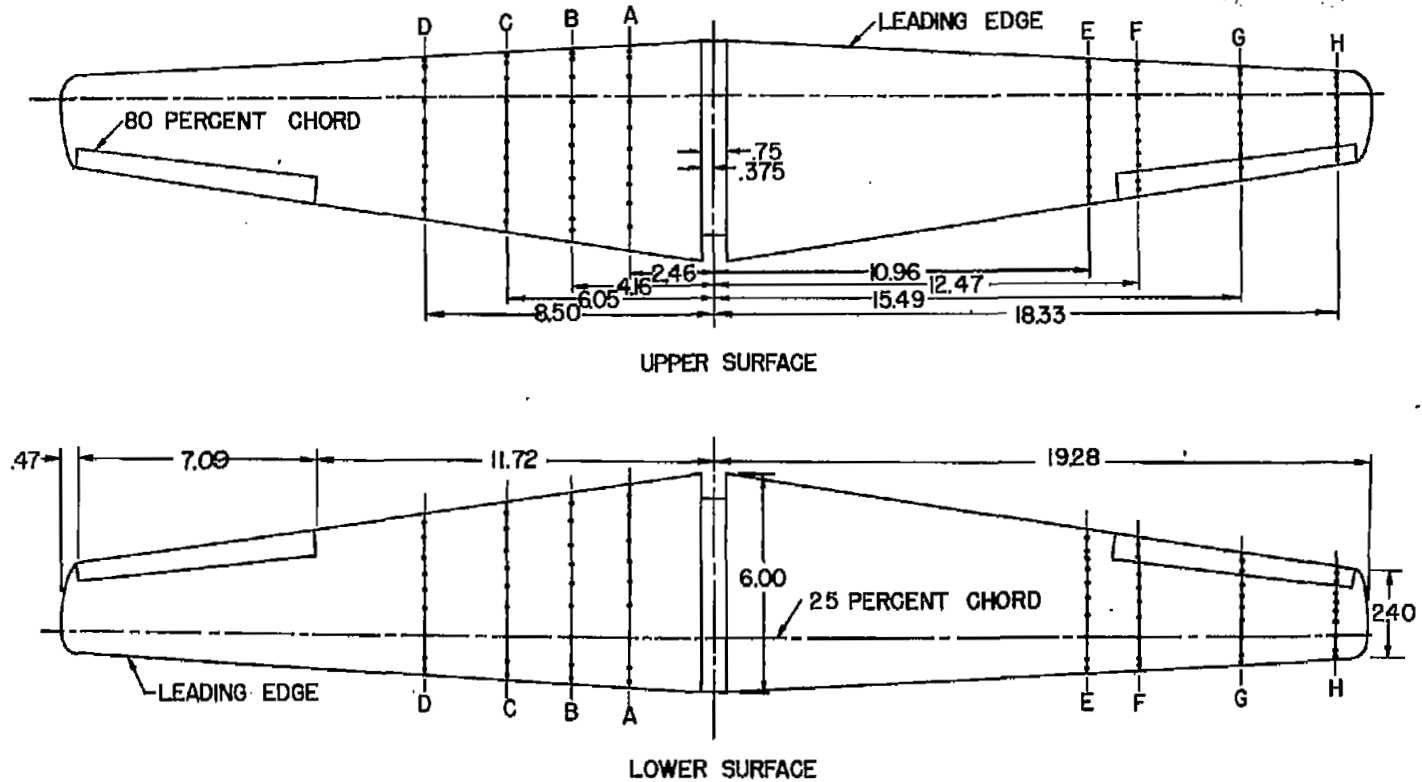


FIGURE 4.- SPAN LOCATIONS OF PRESSURE ORIFICES.
(ALL DIMENSIONS ARE IN INCHES.)

NATIONAL ADVISORY
COMMITTEE FOR AERONAUTICS

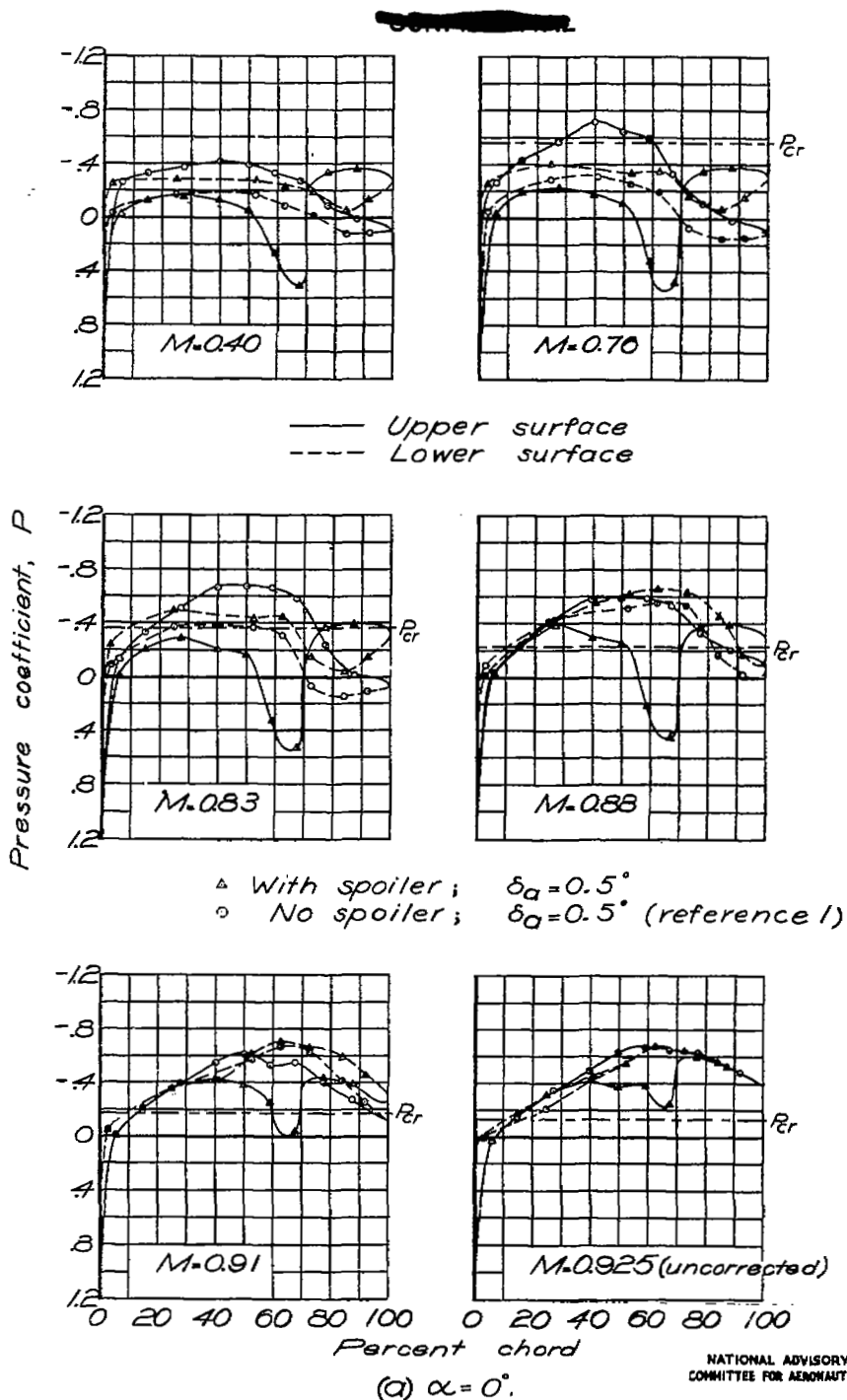


Figure 5 — Pressure distribution about the wing and aileron, at the 80-percent-semispan station. $\frac{h_s}{c} = 0.03$; $\frac{x_s}{c} = 0.70$.

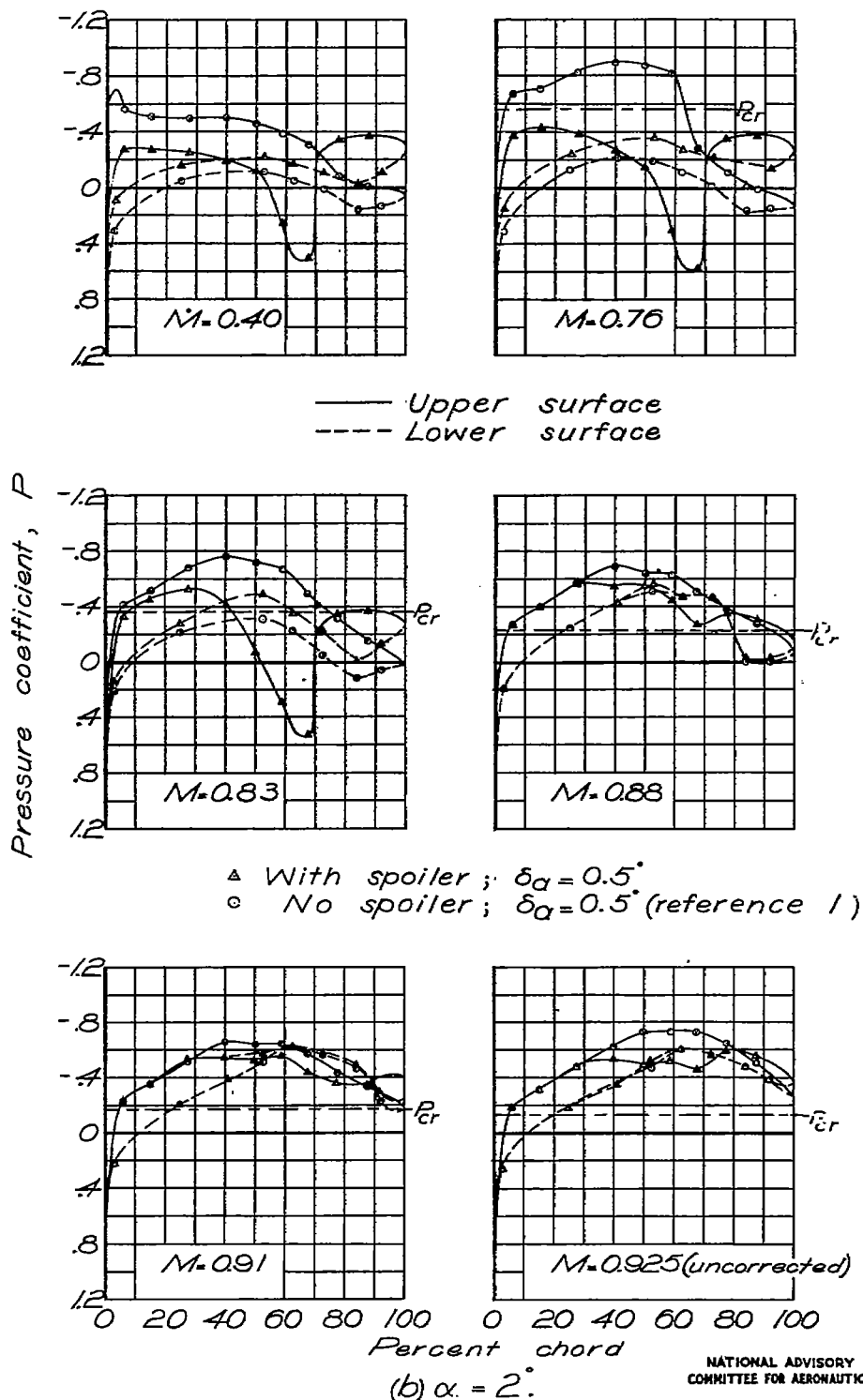
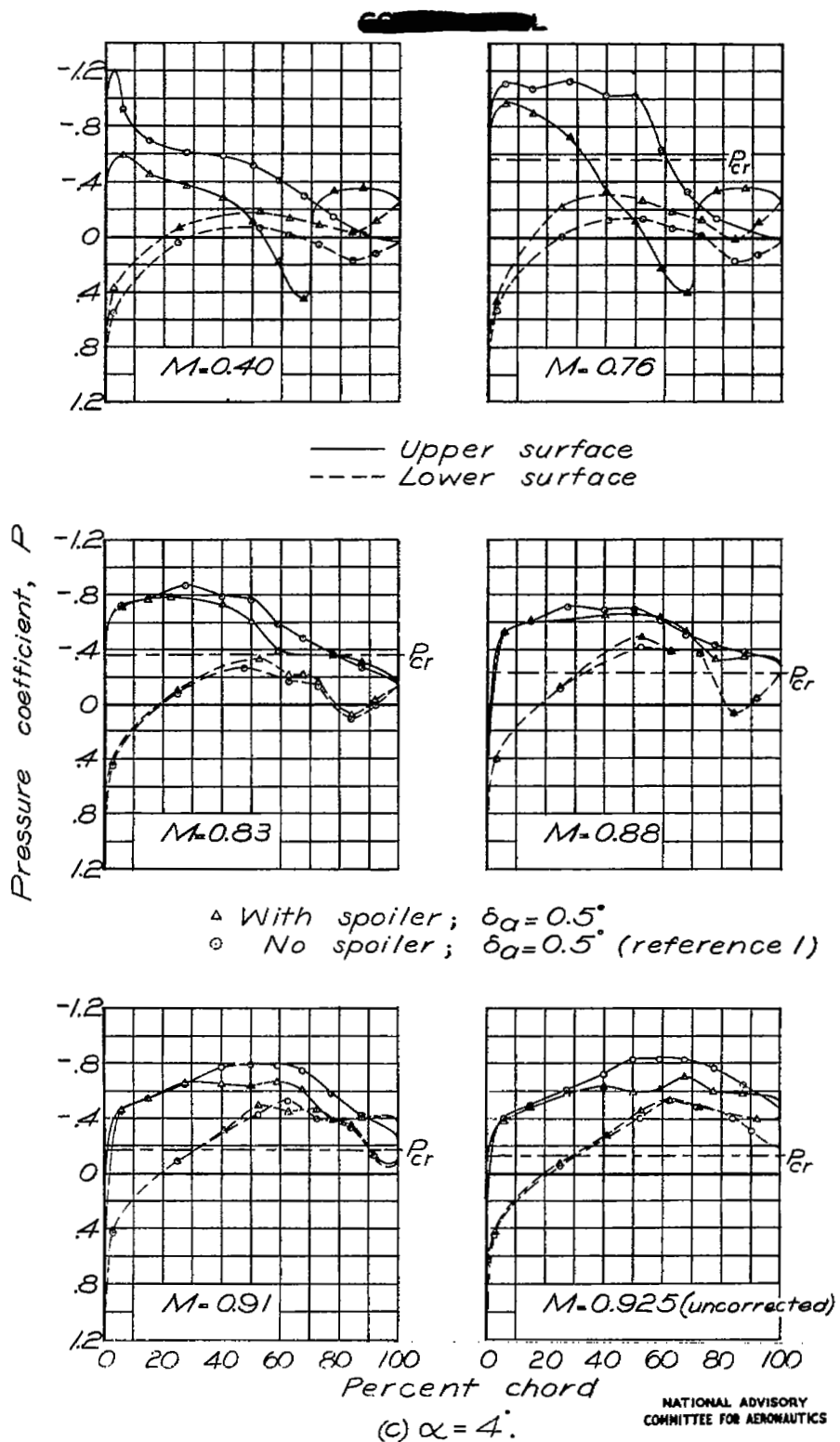
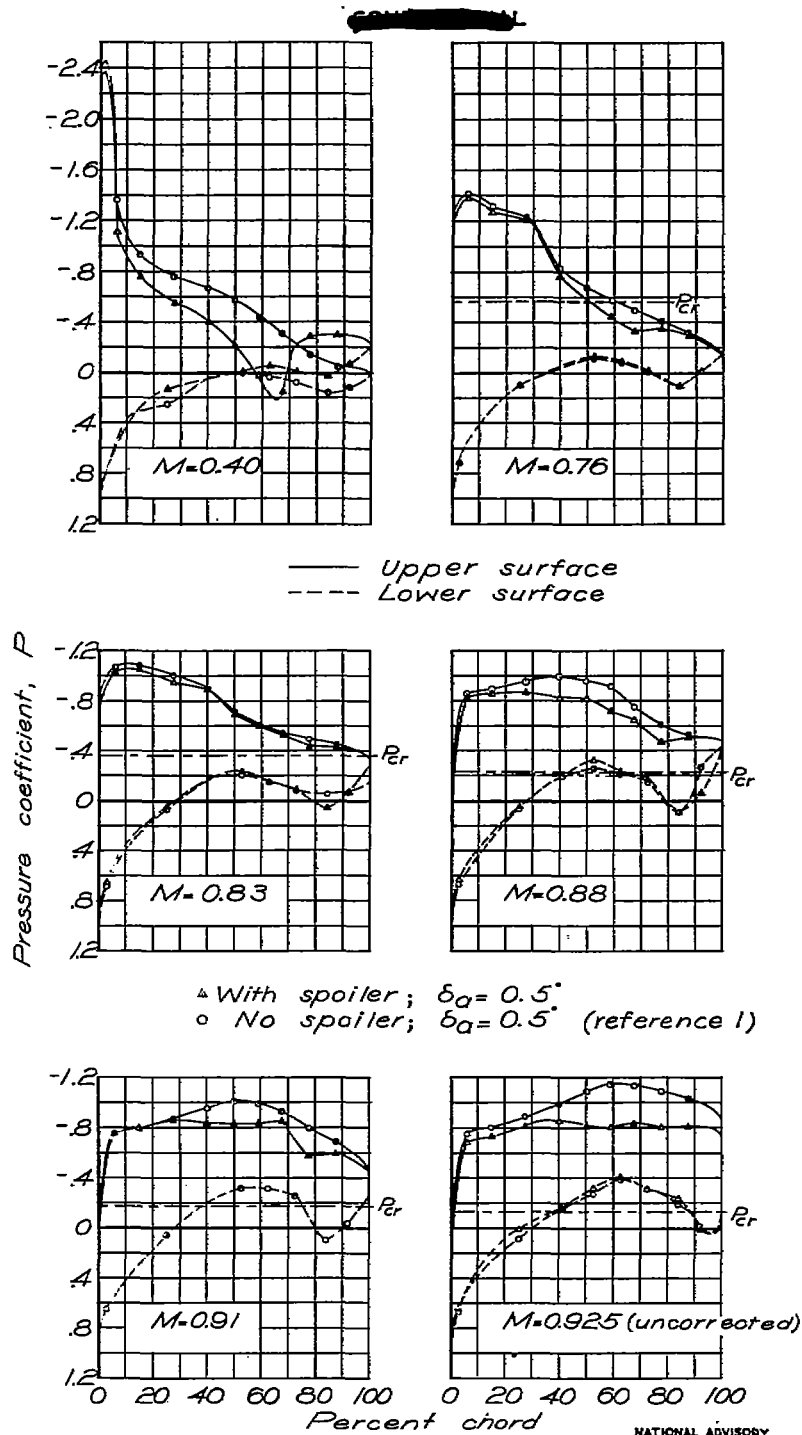


Figure 5.—Continued. $h_s/c = 0.03$; $x_s/c = 0.70$.



NATIONAL ADVISORY COMMITTEE FOR AERONAUTICS

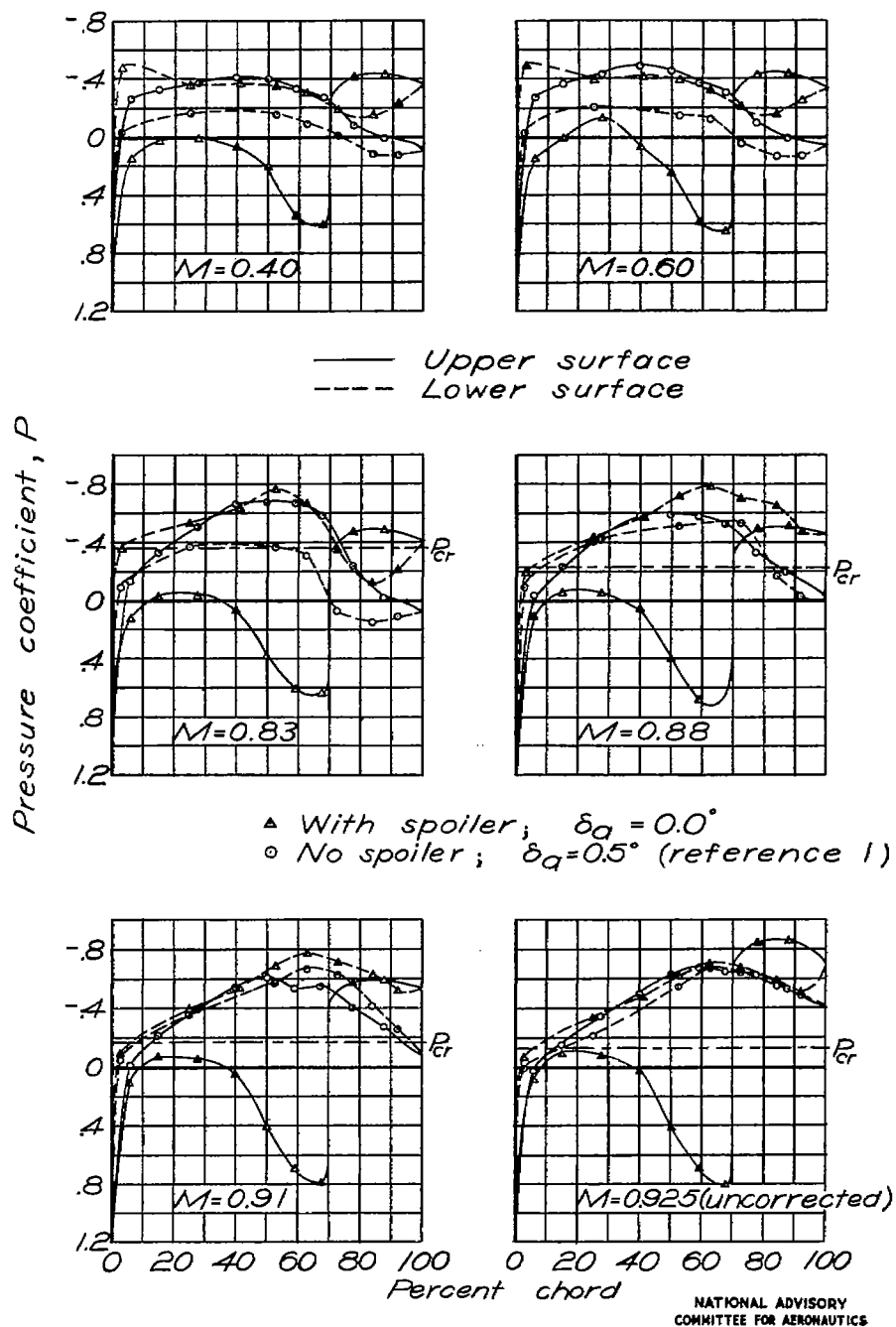
Figure 5 — Continued. $\frac{h_s}{c} = 0.03$; $\frac{x_s}{c} = 0.70$.



\triangle With spoiler; $\delta\alpha = 0.5^\circ$
 \circ No spoiler; $\delta\alpha = 0.5^\circ$ (reference 1)

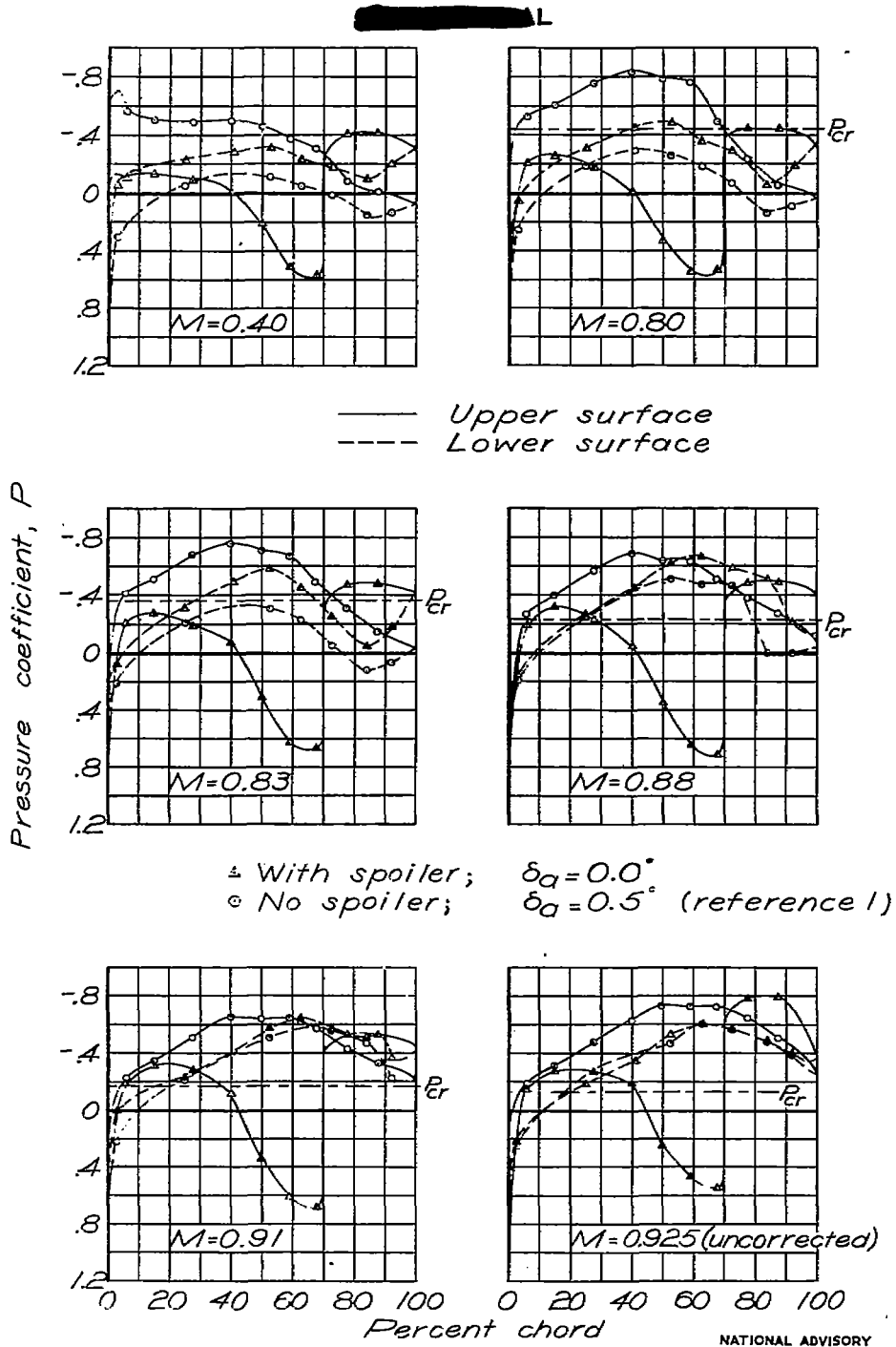
(d) $\alpha = 7^\circ$

Figure 5 — Concluded. $\frac{h_s}{c} = 0.03$; $\frac{x_s}{c} = 0.70$.



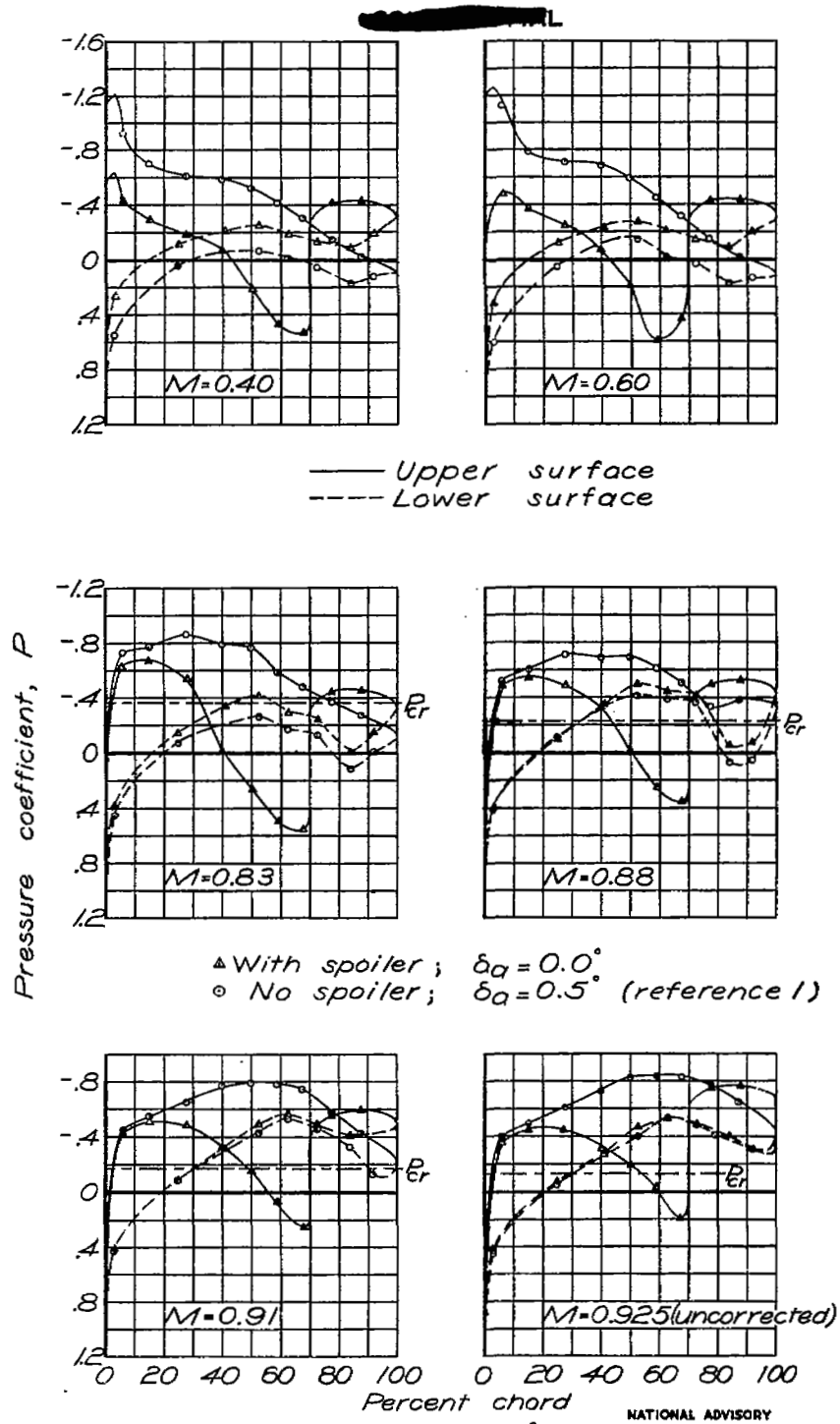
(a) $\alpha = 0^\circ$.
 Figure 6 — Pressure distribution about the wing and aileron at the 80-percent-semispan station. $\frac{h_s}{c} = 0.06$; $\frac{x_s}{c} = 0.70$.

NATIONAL ADVISORY
 COMMITTEE FOR AERONAUTICS



(b) $\alpha = 2^\circ$.

Figure 6.—Continued. $\frac{h_s}{c} = 0.06$; $\frac{x_s}{c} = 0.70$.



(c) $\alpha = 4^\circ$.
 Figure 6.- Continued. $\frac{h_s}{c} = 0.06$; $\frac{x_s}{c} = 0.70$.

NATIONAL ADVISORY
 COMMITTEE FOR AERONAUTICS

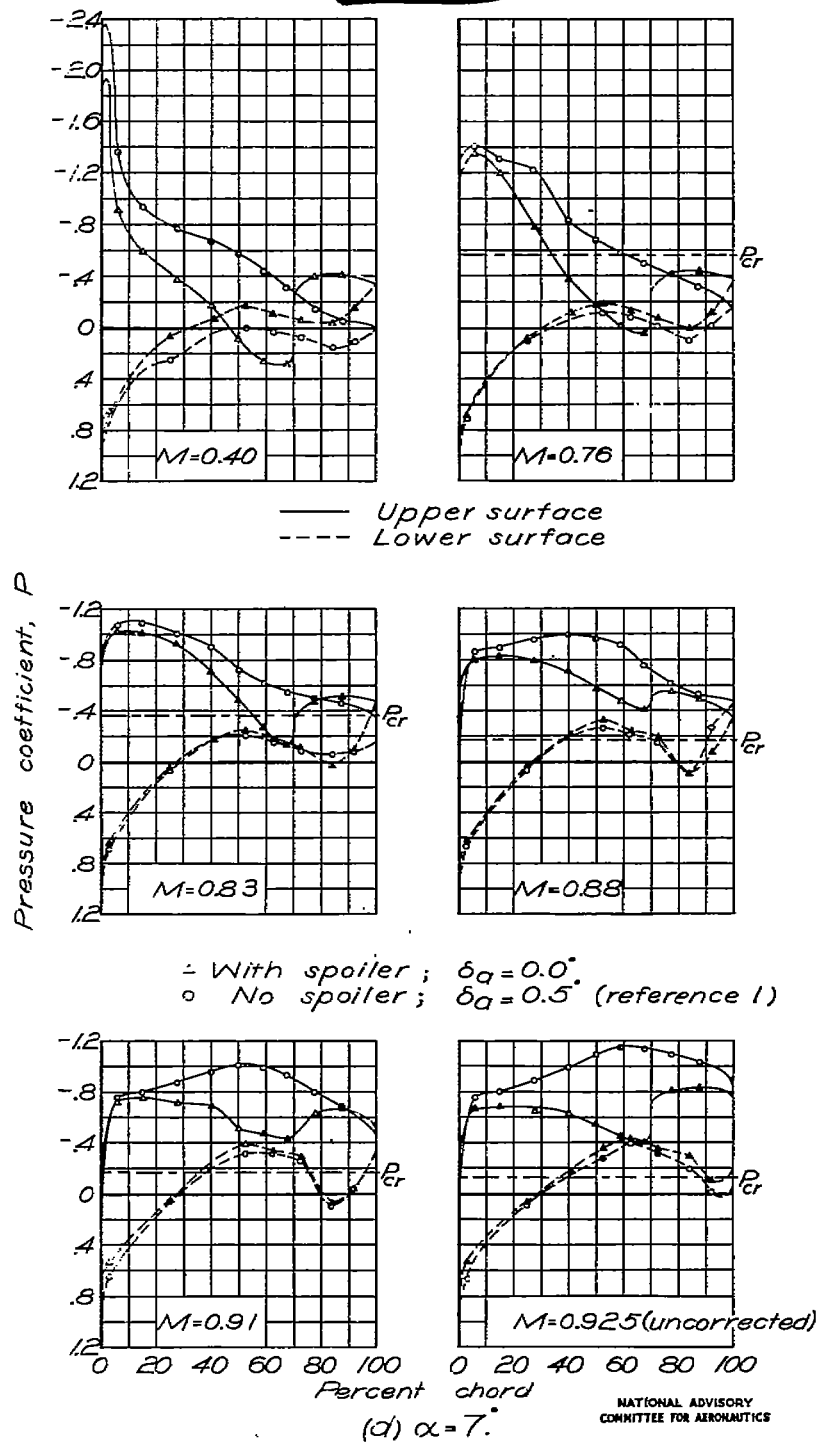


Figure 6 .— Concluded. $\frac{h_s}{c} = 0.06$; $\frac{x_s}{c} = 0.70$.

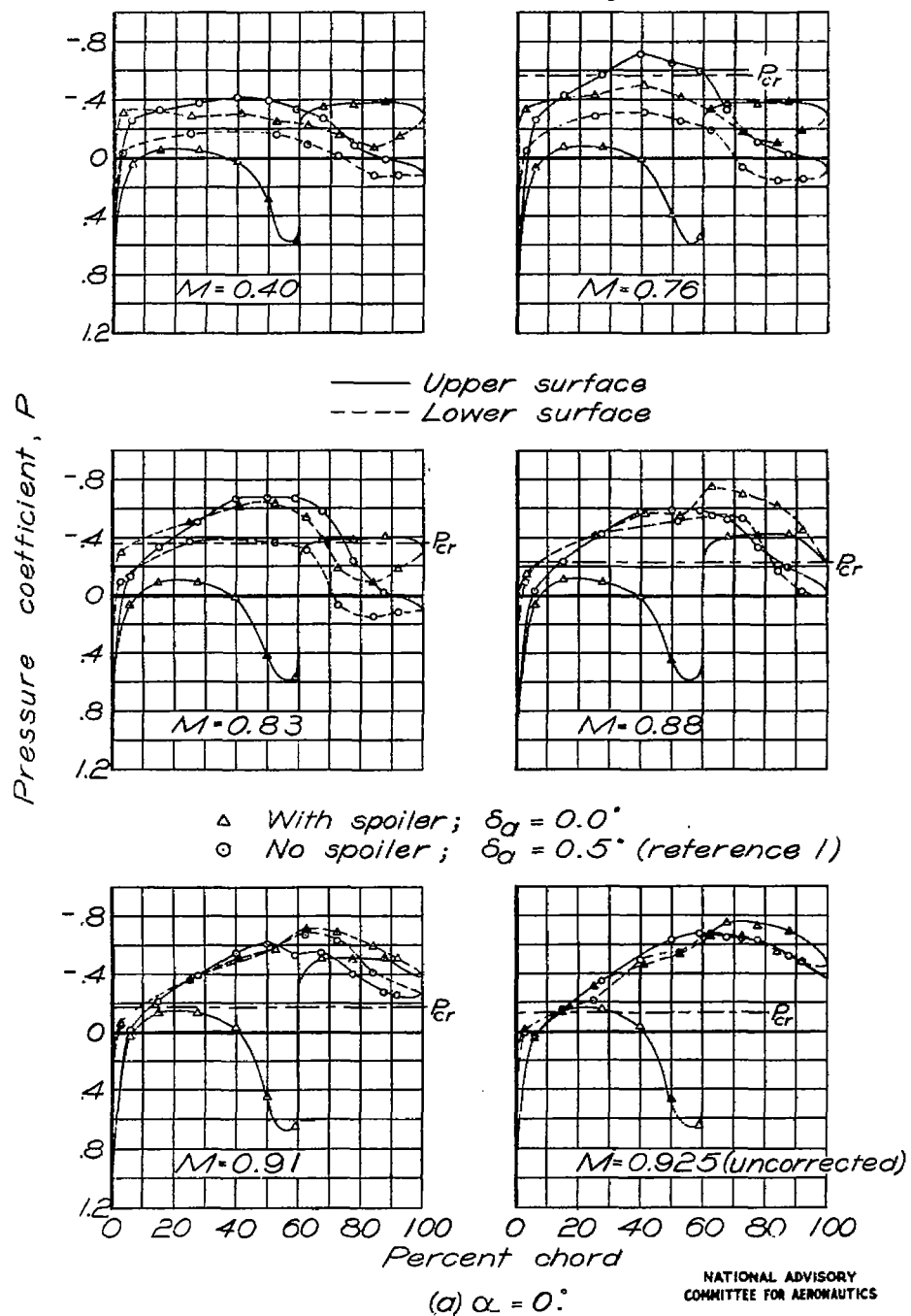
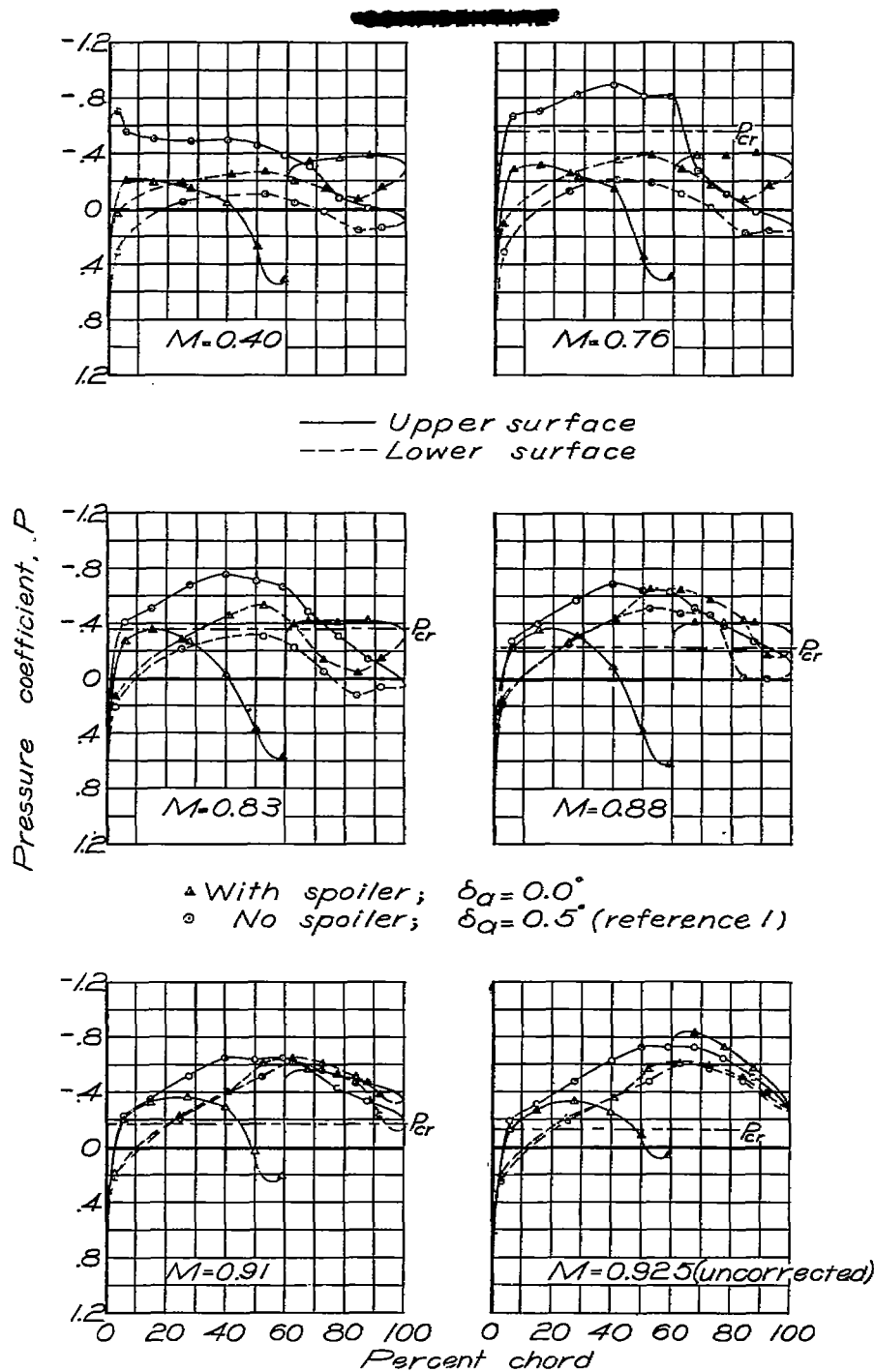


Figure 7.- Pressure distribution about the wing and aileron at the 80-percent-semispan station.

$$\frac{h_s}{c} = 0.03; \frac{x_s}{c} = 0.60.$$



(b) $\alpha = 2^\circ$.
 Figure 7 .— Continued. $\frac{h_s}{c} = 0.03$; $\frac{x_s}{c} = 0.60$.

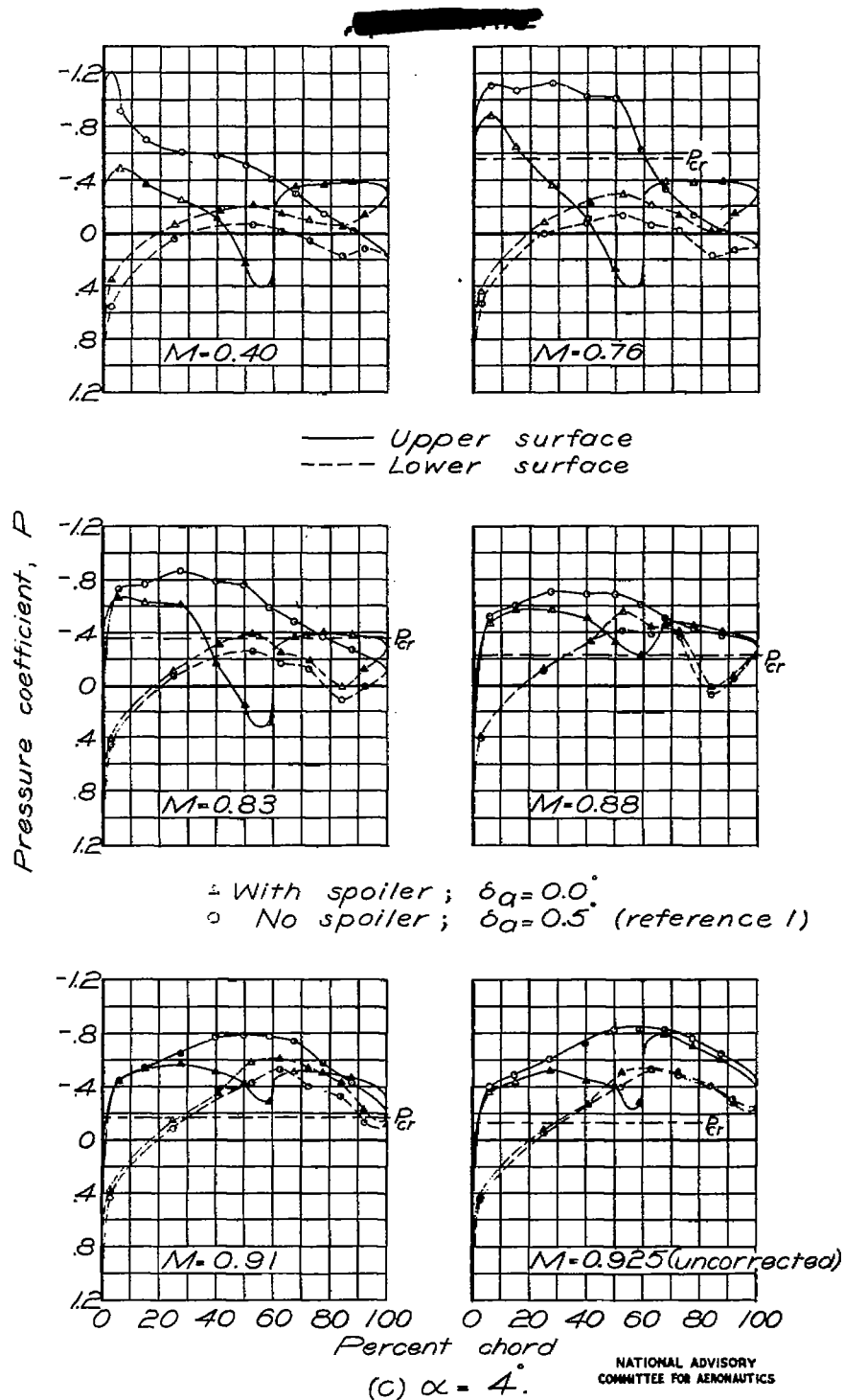


Figure 7 — Continued. $\frac{h_s}{c} = 0.03$; $\frac{x_s}{c} = 0.60$.

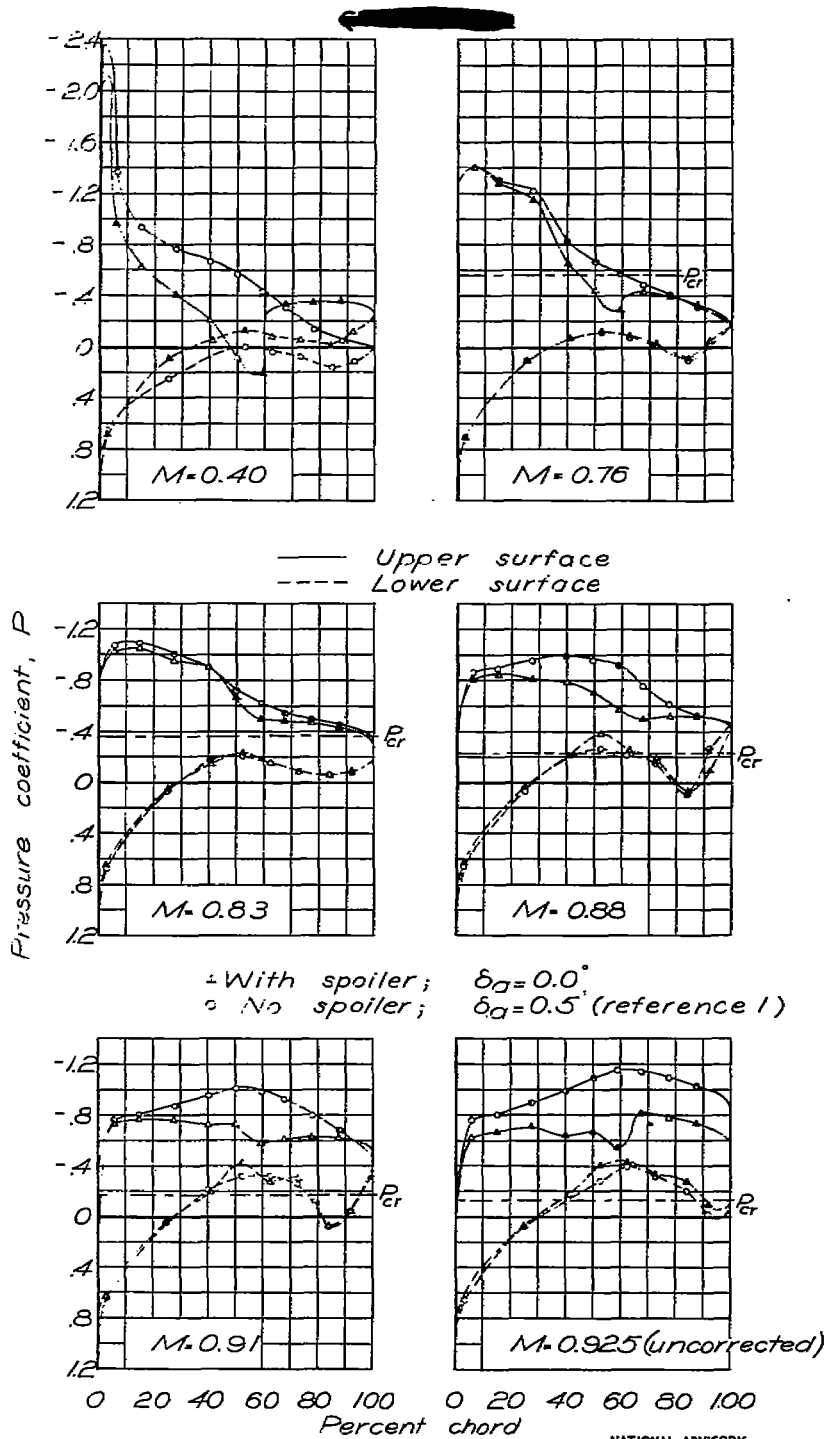
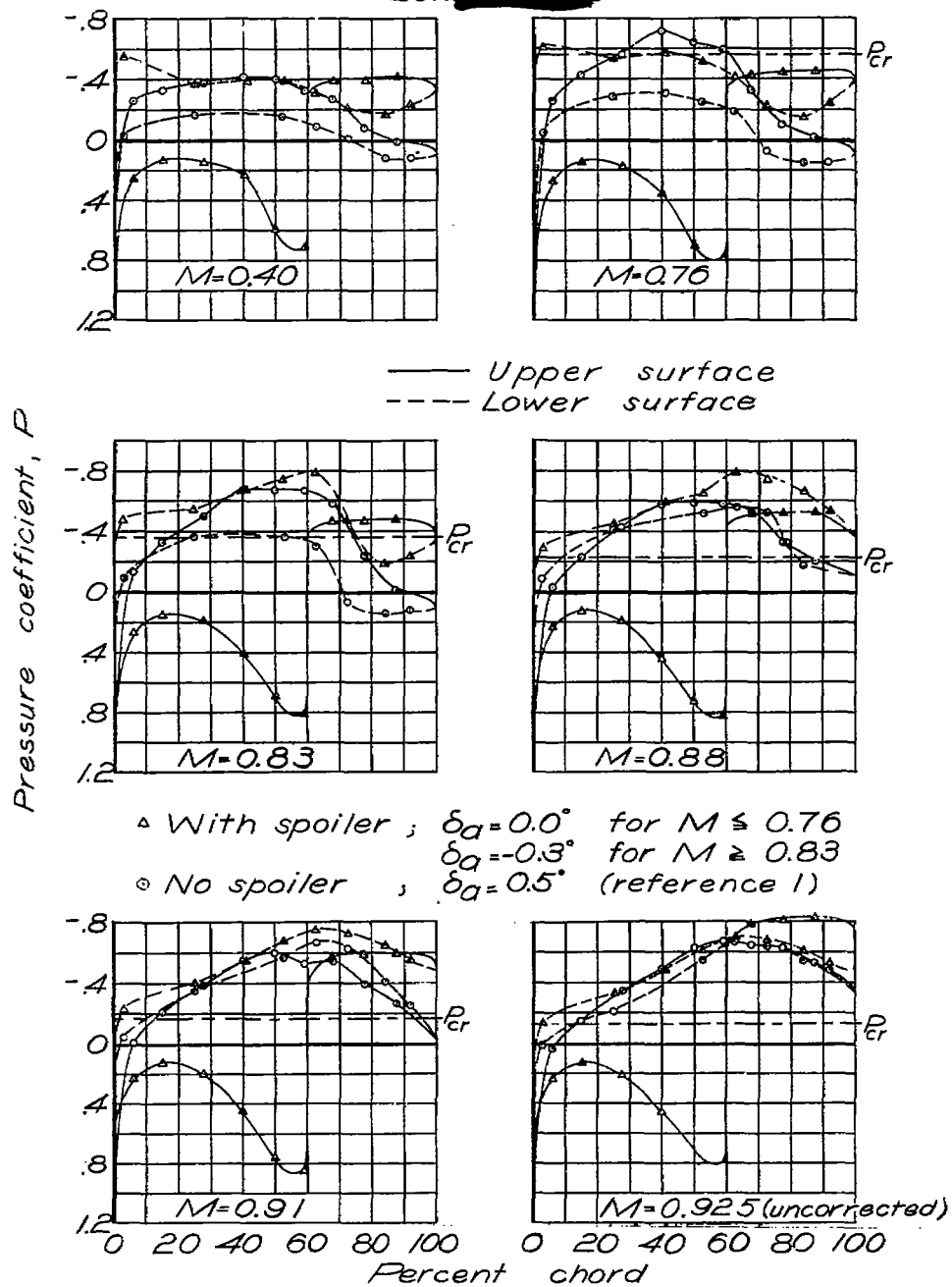


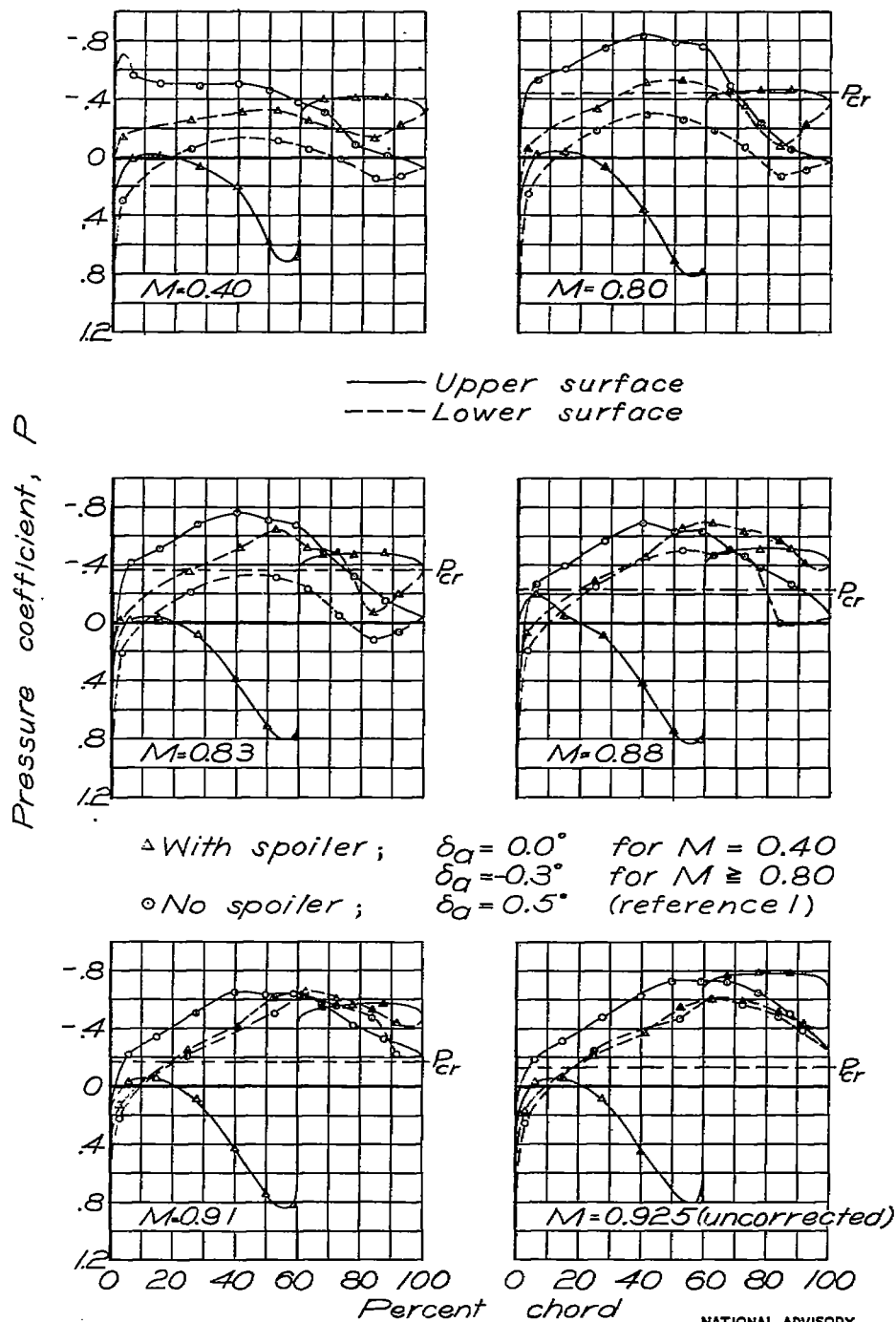
Figure 7. — Concluded. $\frac{h_s}{c} = 0.03$; $\frac{x_s}{c} = 0.60$.



NATIONAL ADVISORY
COMMITTEE FOR AERONAUTICS

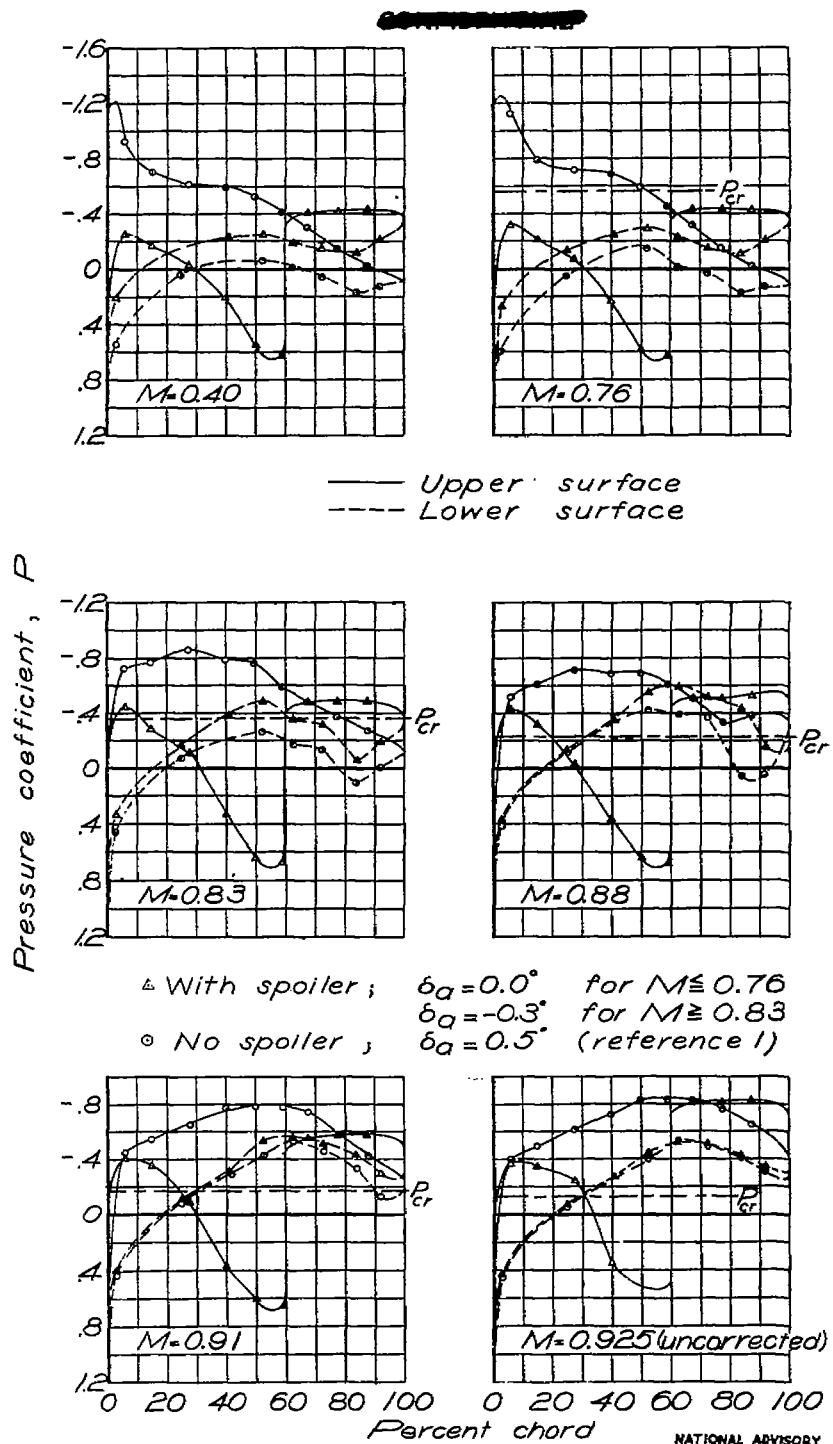
(a) $\alpha = 0^\circ$

Figure 8. — Pressure distribution about the wing and aileron at the 80-percent-semispan station. $\frac{h_s}{c} = 0.06$; $\frac{x_s}{c} = 0.60$.

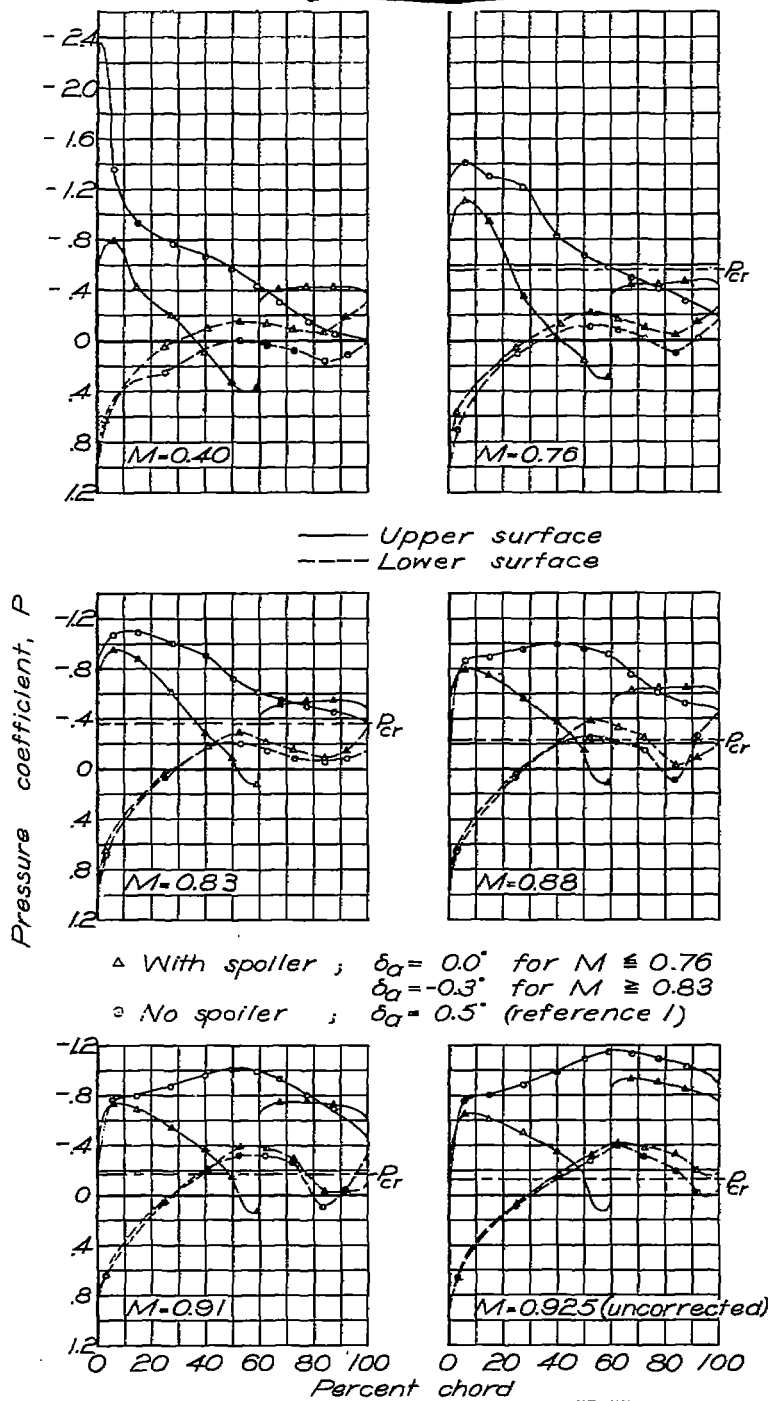


(b) $\alpha = 2^\circ$.

Figure 8 .— Continued. $\frac{h_s}{c} = 0.06$; $\frac{x_s}{c} = 0.60$.



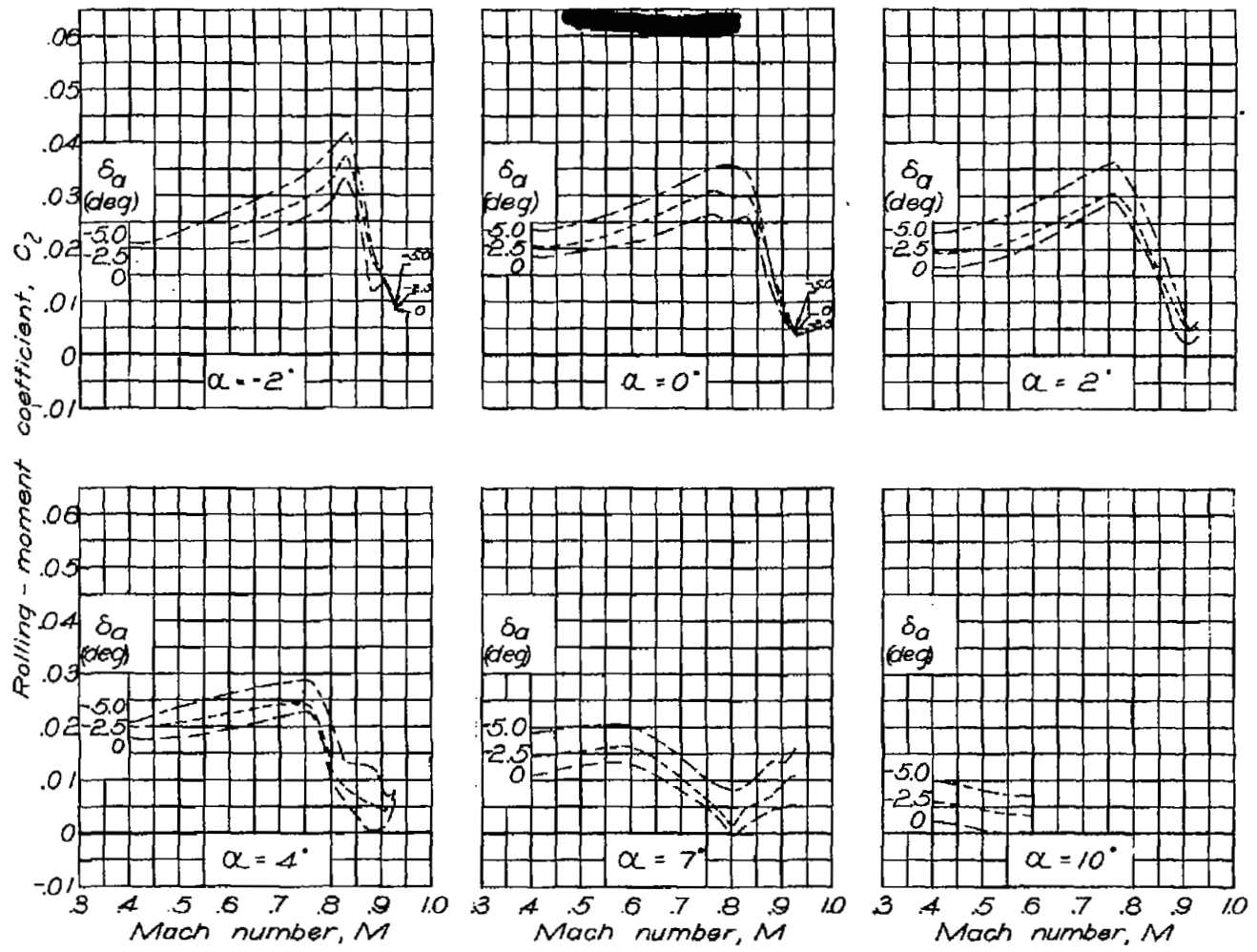
(c) $\alpha = 4^\circ$.
 Figure 8.—Continued. $\frac{h_s}{c} = 0.06$; $\frac{x_s}{c} = 0.60$.



NATIONAL ADVISORY
COMMITTEE FOR AERONAUTICS

(d) $\alpha = 7^\circ$

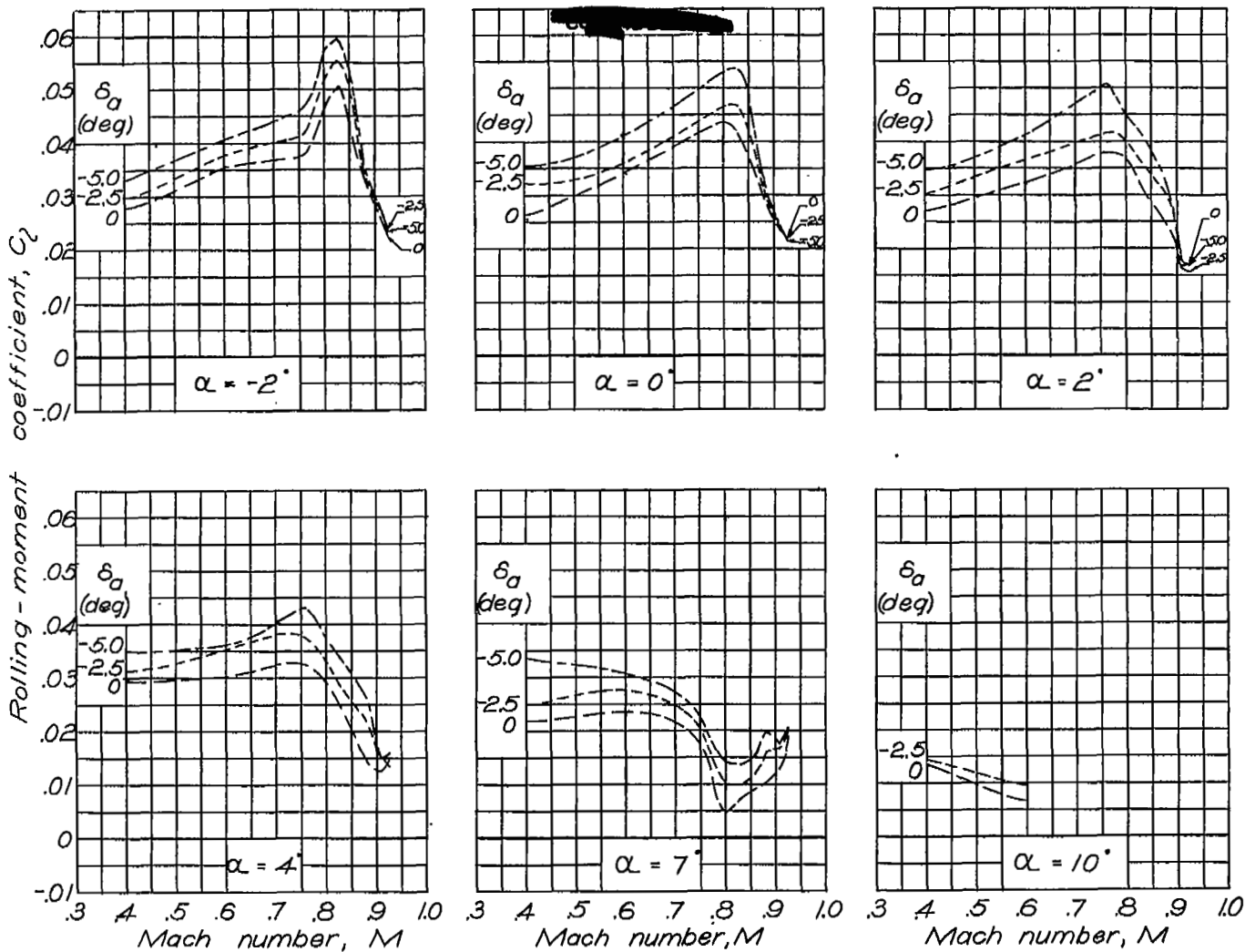
Figure 8 .- Concluded. $\frac{h_s}{c} = 0.06$; $\frac{x_s}{c} = 0.60$.



(a) $\frac{h_s}{c} = 0.03$; $\frac{x_s}{c} = 0.70$.

NATIONAL ADVISORY
COMMITTEE FOR AERONAUTICS

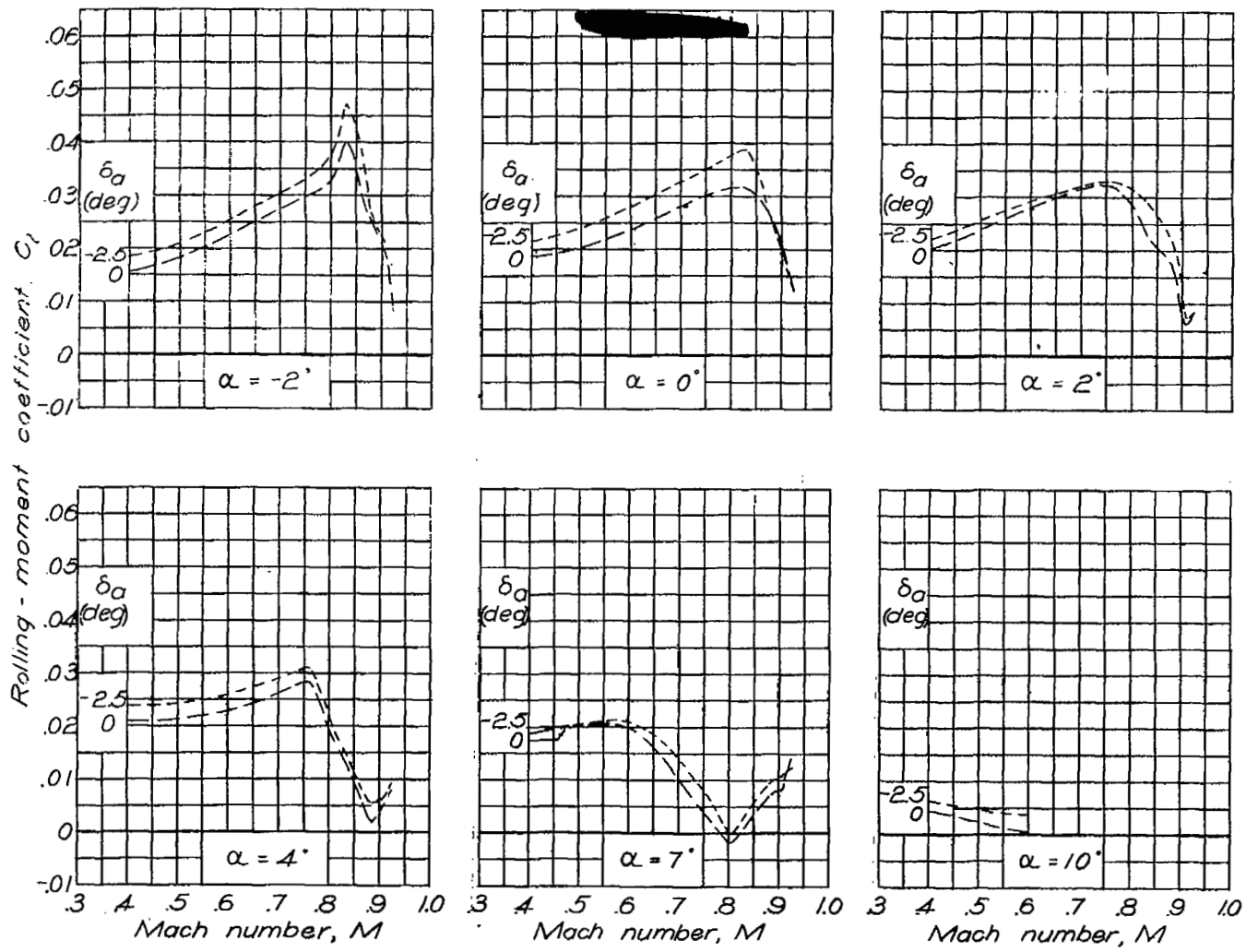
Figure 9.—Variation of rolling-moment coefficient with Mach number.



(b) $\frac{h_s}{c} = 0.06$; $\frac{x_s}{c} = 0.70$.

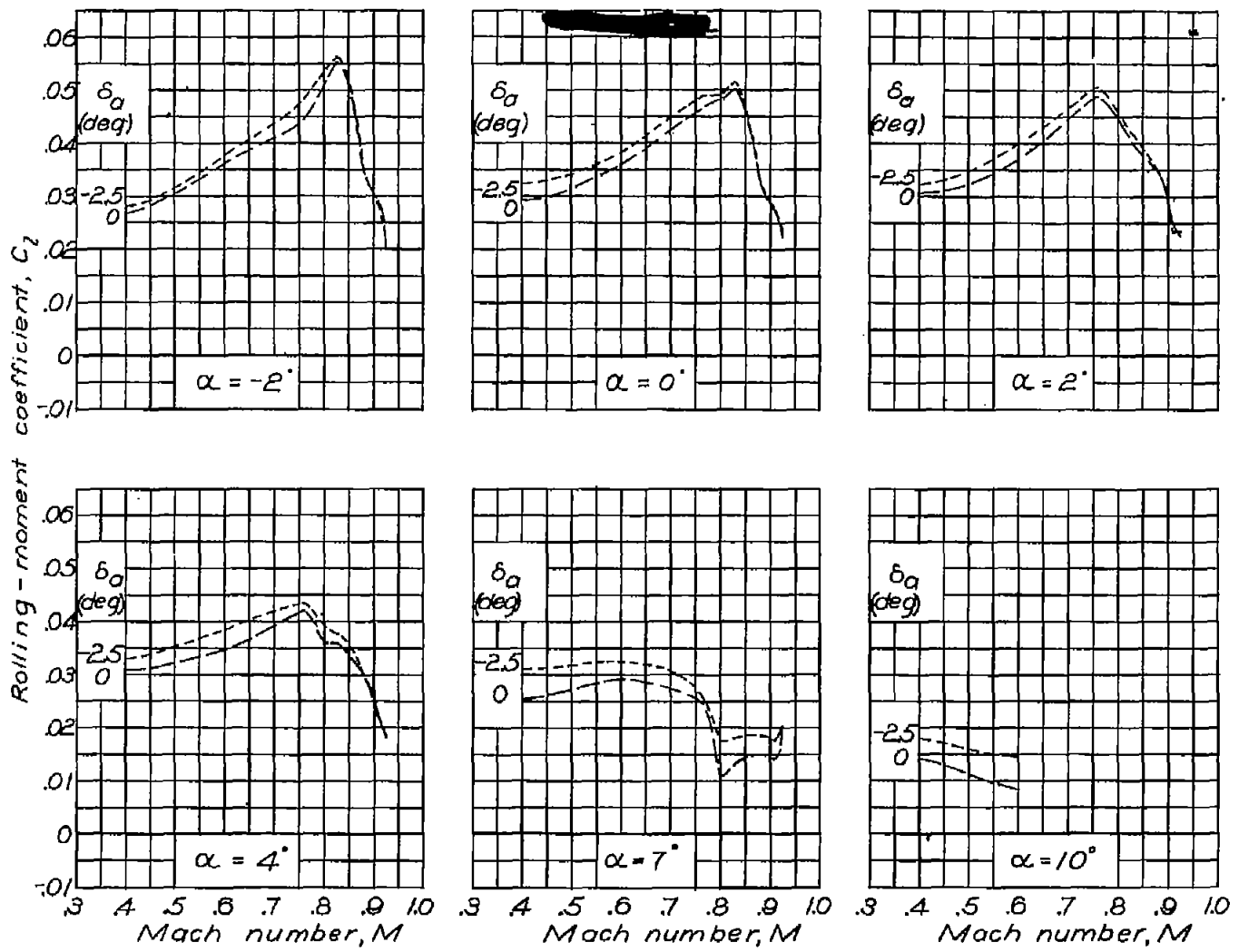
Figure 9 .- Continued.

NATIONAL ADVISORY
COMMITTEE FOR AERONAUTICS



(c) $\frac{h_s}{c} = 0.03$; $\frac{x_s}{c} = 0.60$.

Figure 9 .— Continued.



(d) $\frac{h_s}{c} = 0.06$; $\frac{x_s}{c} = 0.60$.

Figure 9 .- Concluded.

NATIONAL ADVISORY
COMMITTEE FOR AERONAUTICS

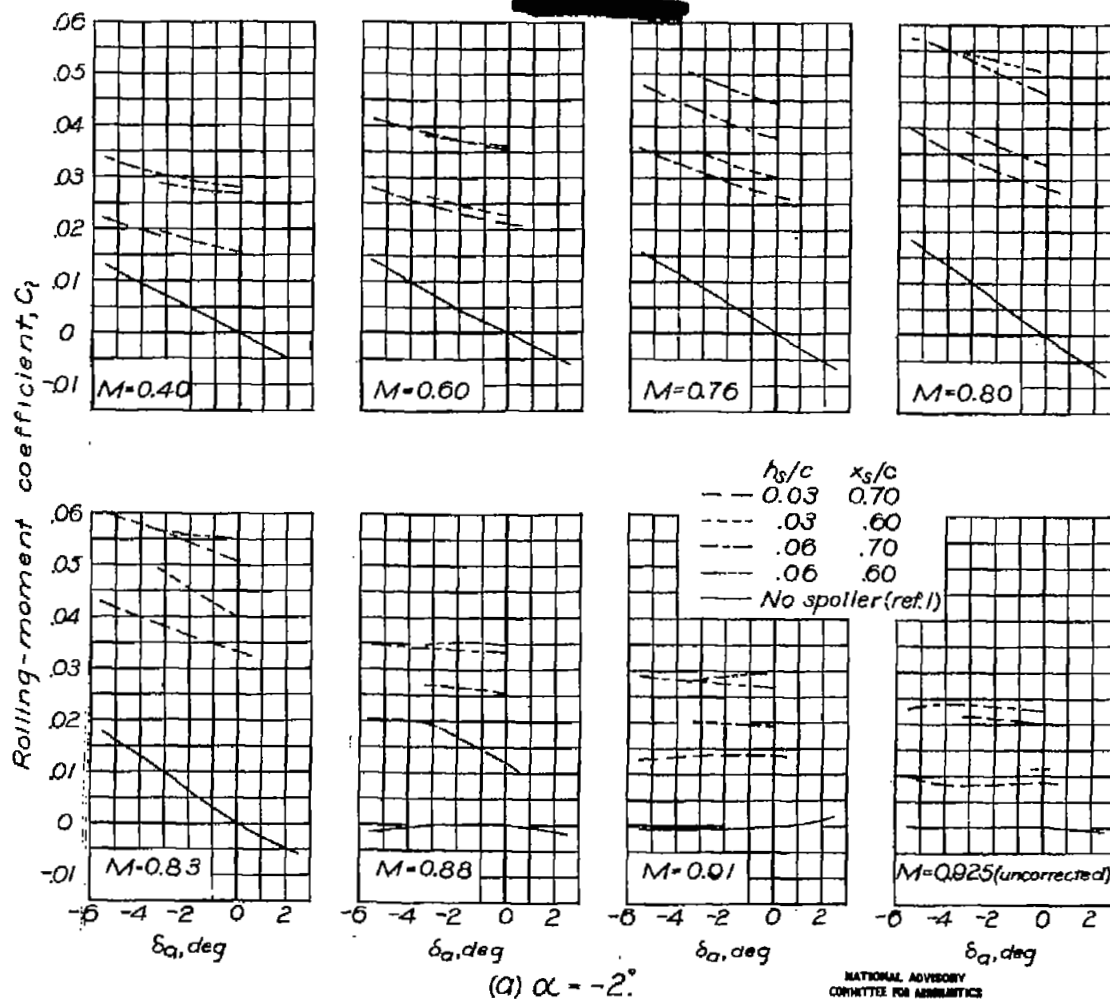


Figure 10 . — Variation of aileron-spoiler rolling-moment coefficient with aileron deflection for two spoiler projections and two chordwise locations on upper surface of wing.

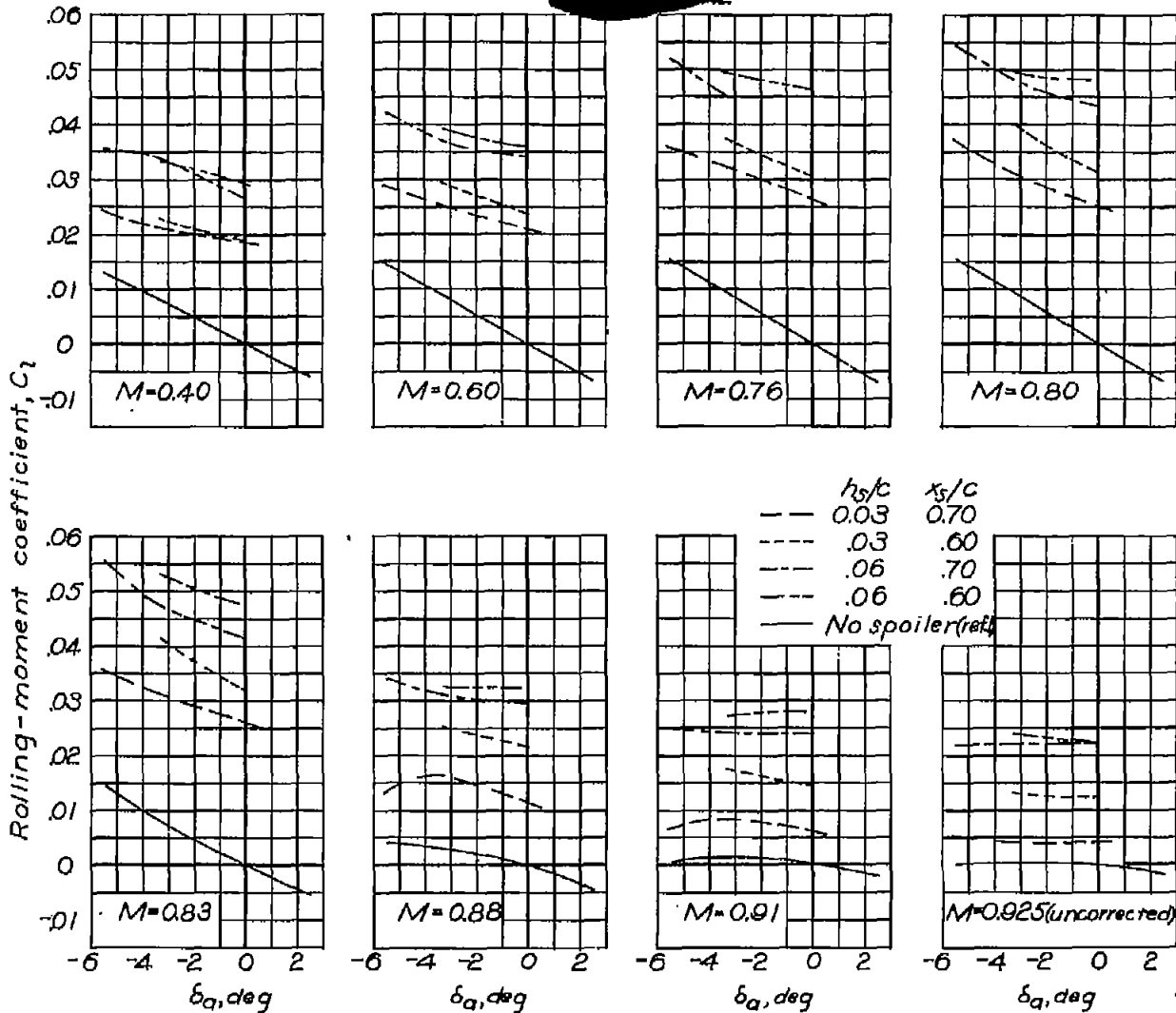
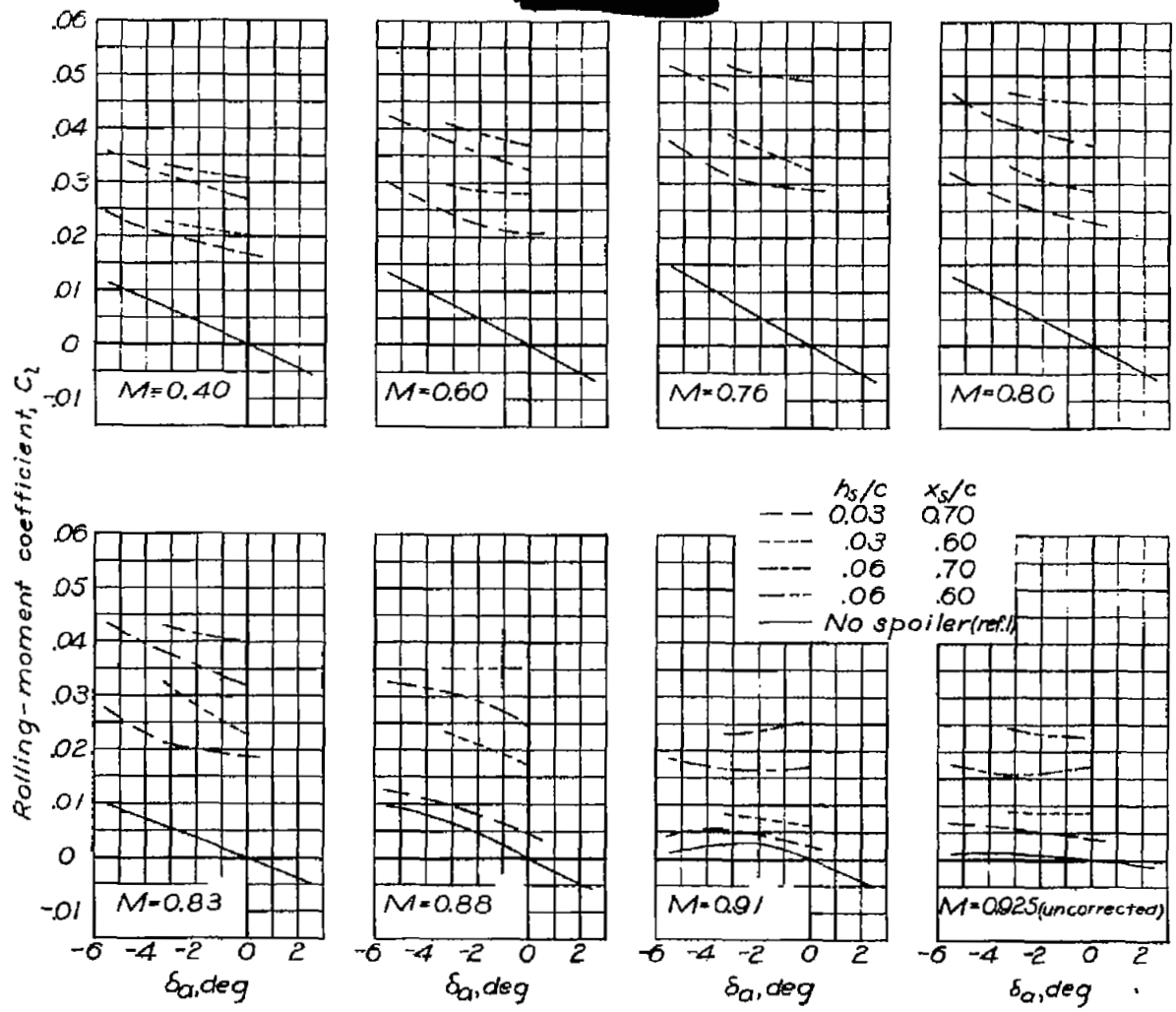


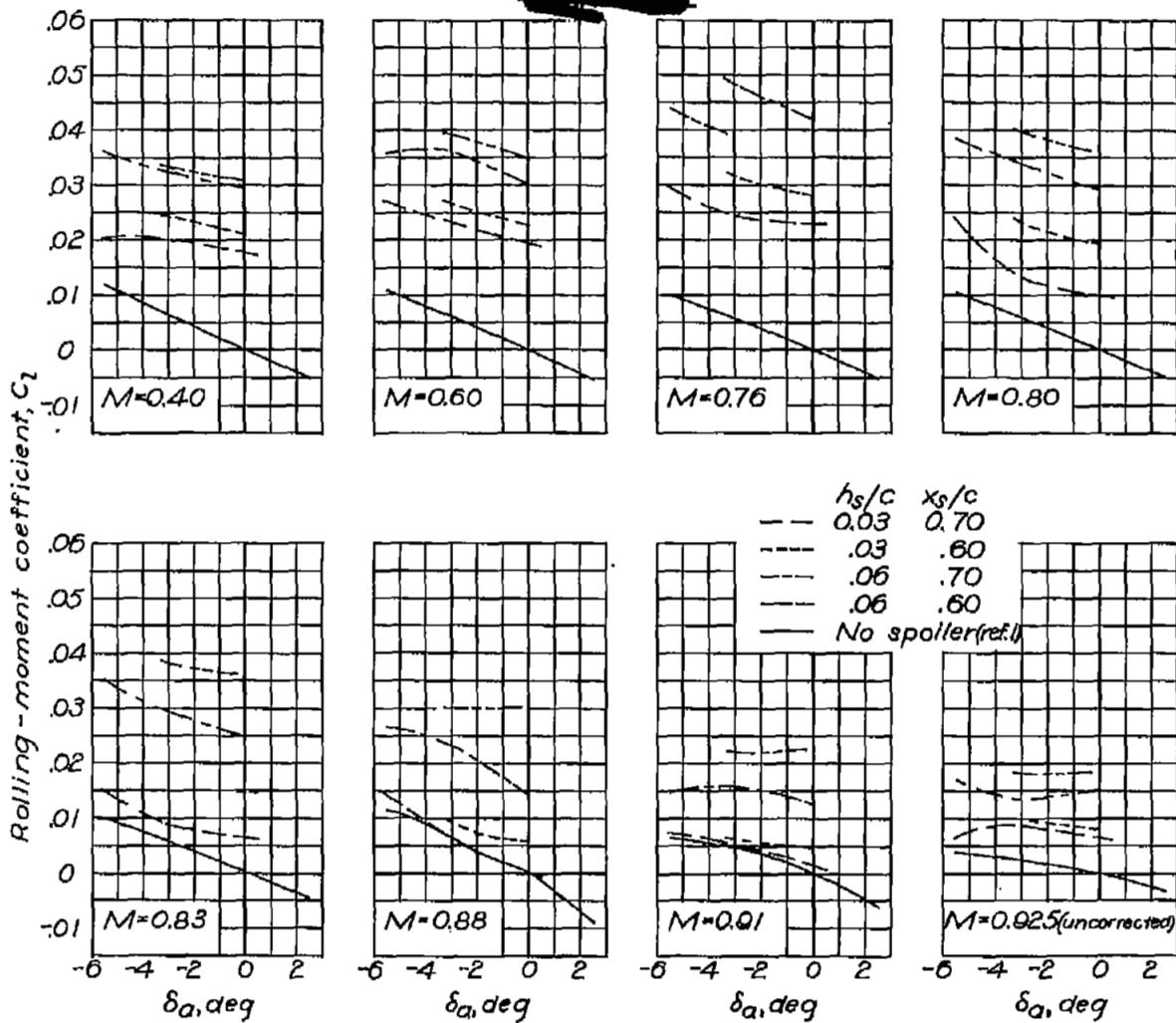
Figure 10 .- Continued. $(b) \alpha = 0^\circ$

NATIONAL ADVISORY
COMMITTEE FOR AERONAUTICS



(c) $\alpha = 2^\circ$

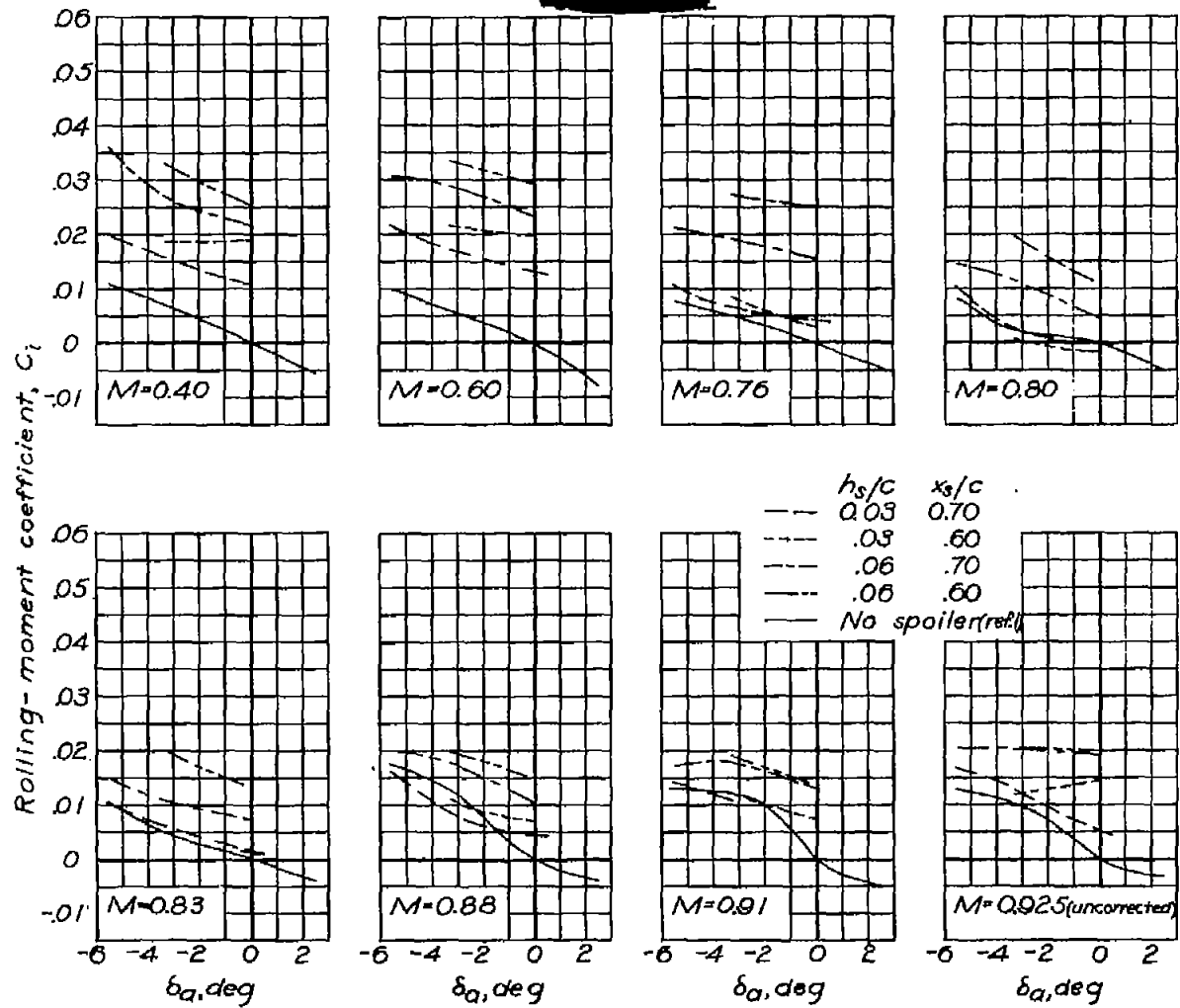
Figure 10.-Continued.



(d) $\alpha = 4^\circ$

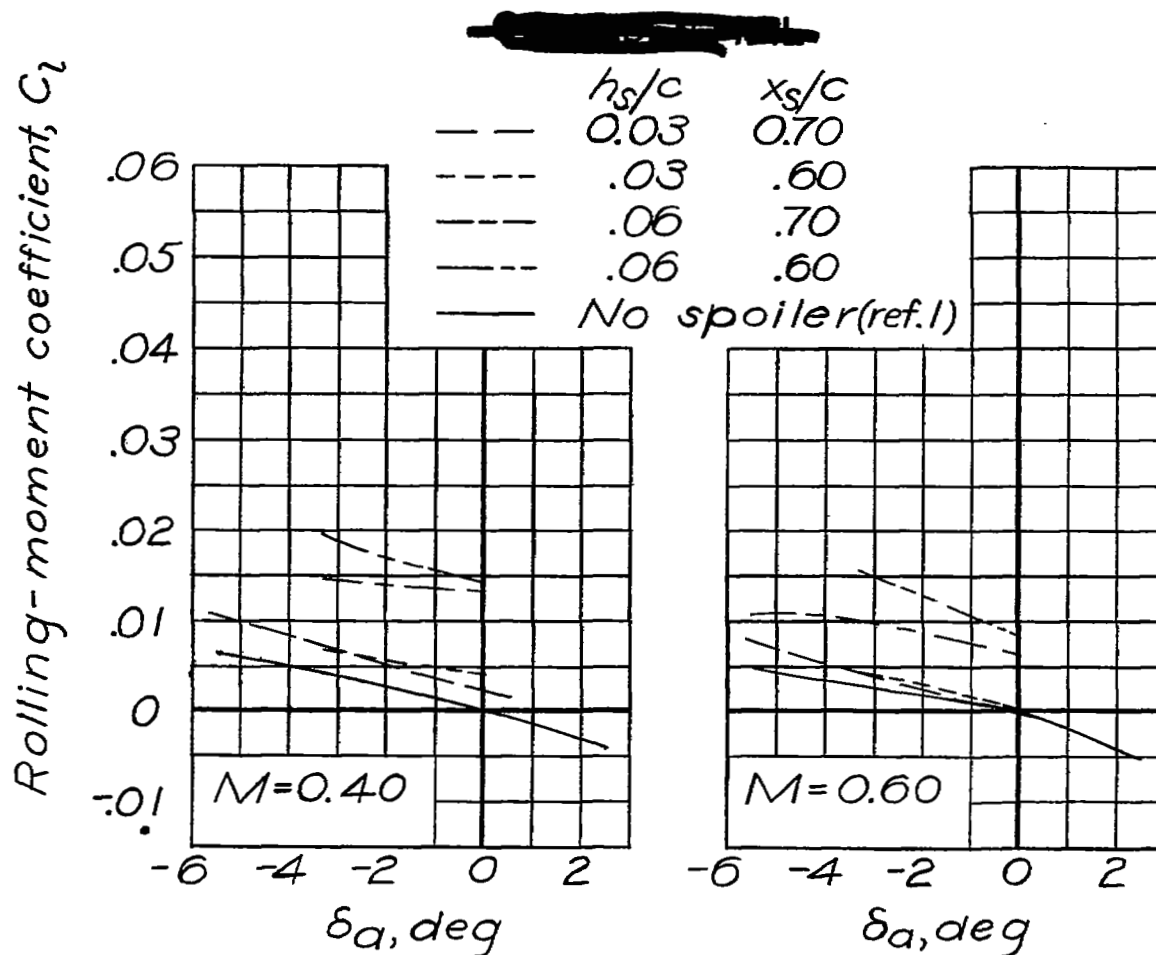
Figure 10.—Continued.

NATIONAL ADVISORY
COMMITTEE FOR AERONAUTICS



(e) $\alpha = 7^\circ$

Figure 10.— Continued.



NATIONAL ADVISORY
COMMITTEE FOR AERONAUTICS

~~CONFIDENTIAL~~

(f) $\alpha = 10^\circ$

Figure 10.— Concluded.

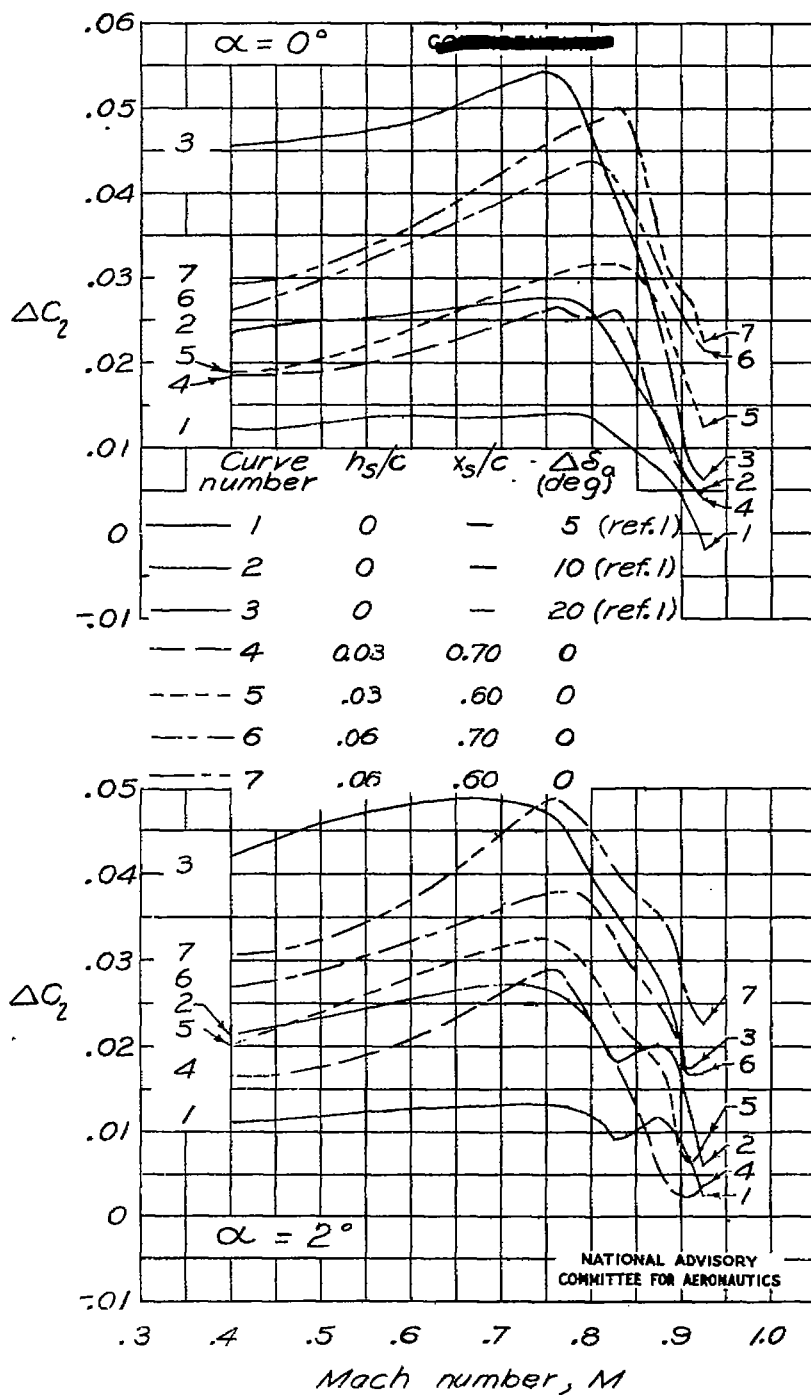


Figure 11.— Comparison of effect of compressibility on rolling-moment coefficient of spoilers and plain ailerons at nondifferential deflections.

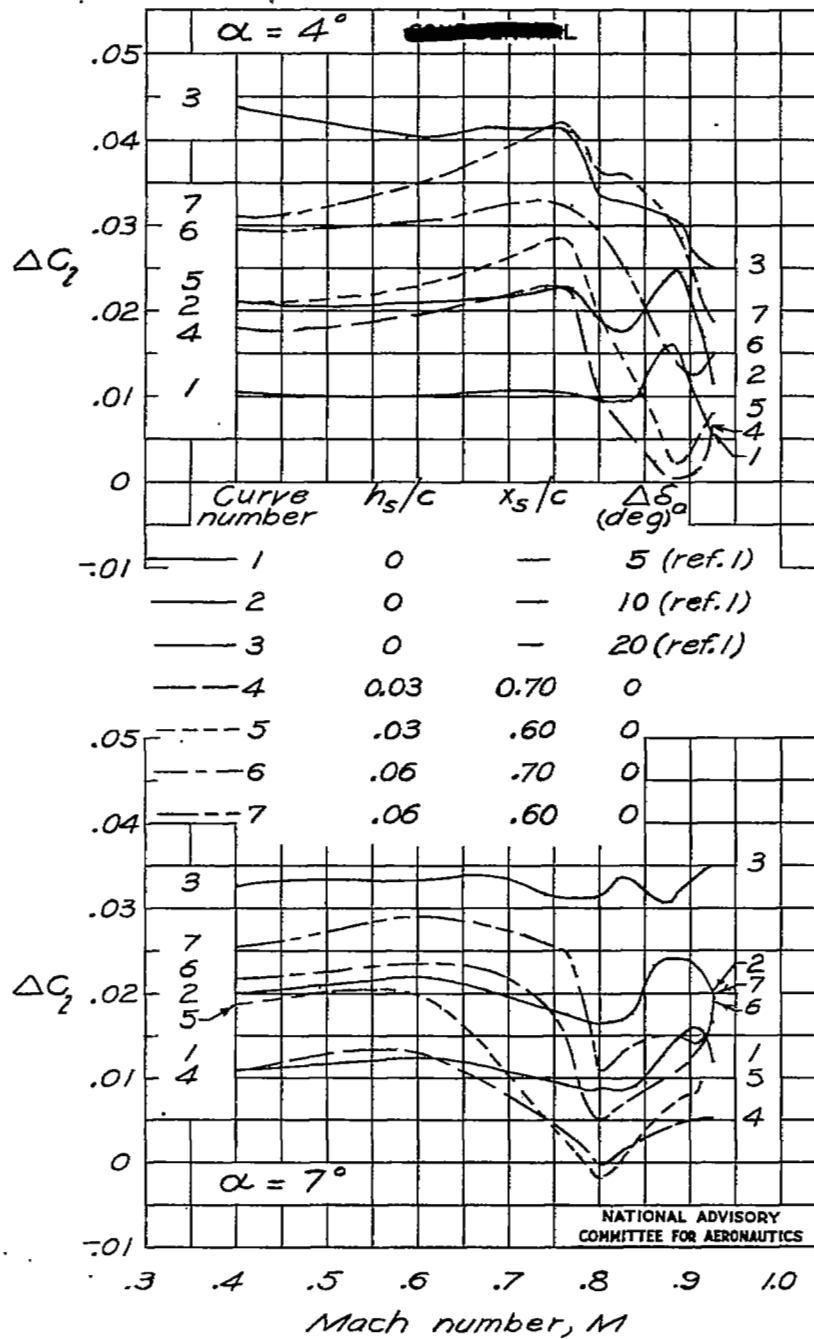
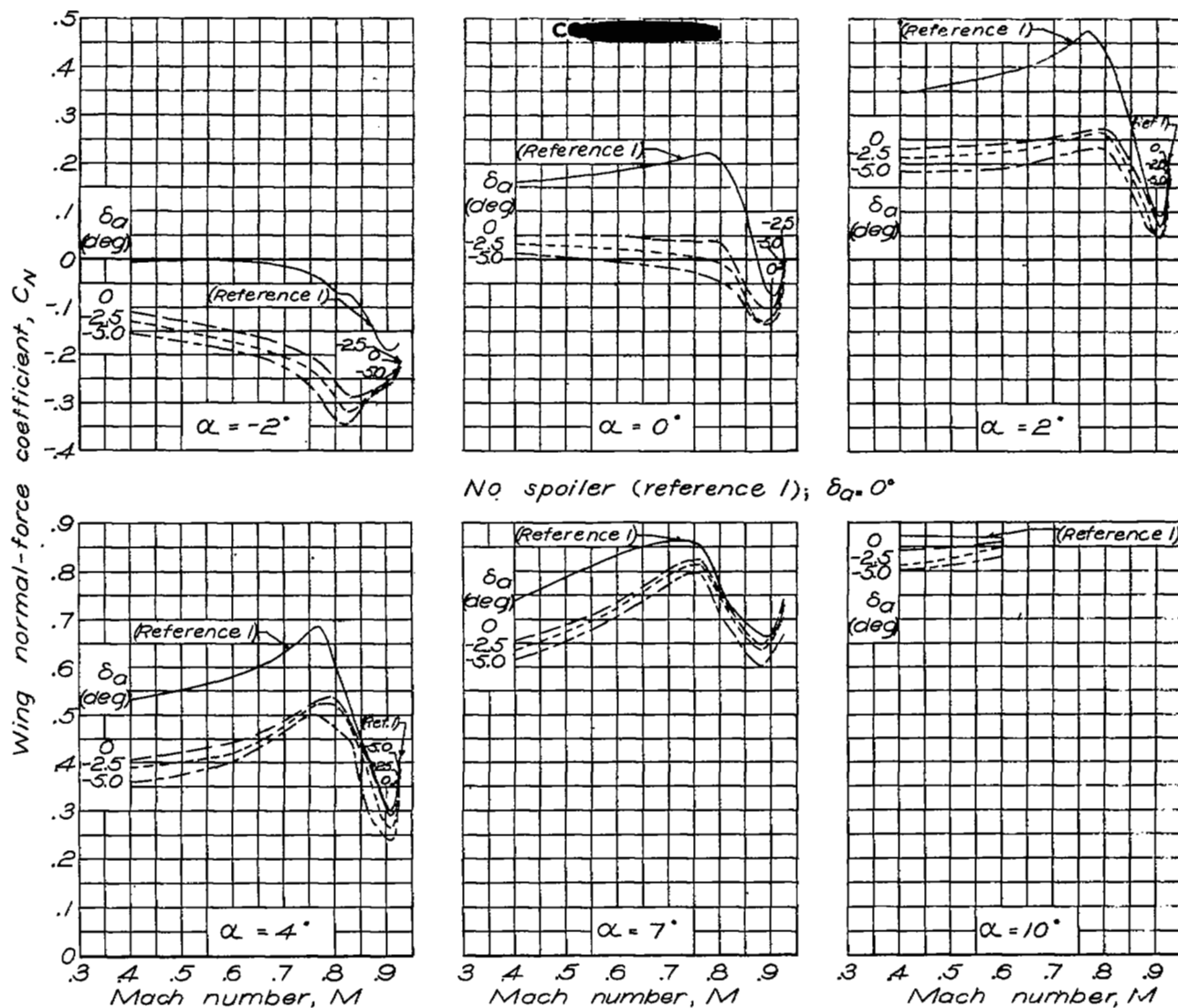
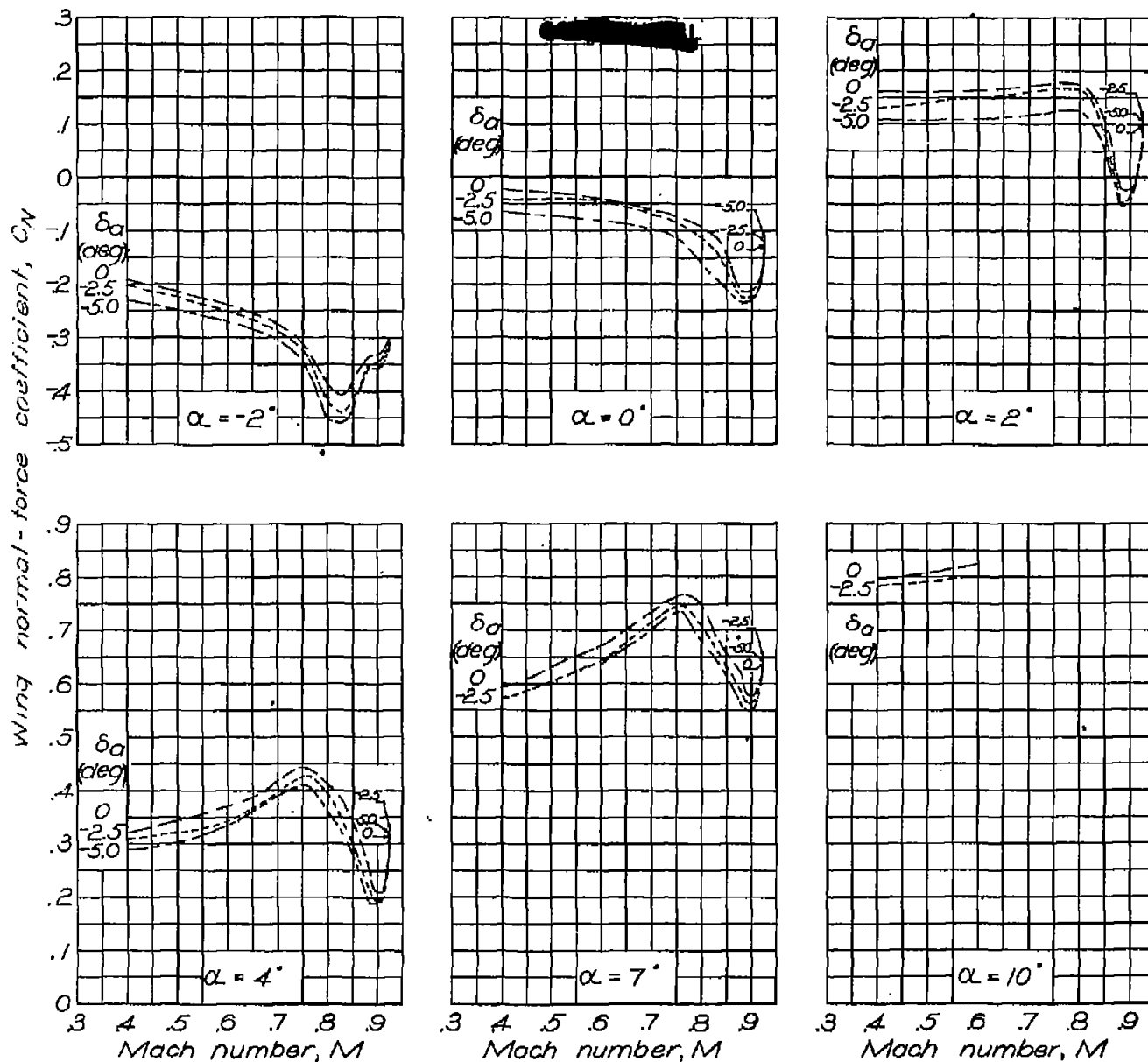


Figure 11.- Concluded.



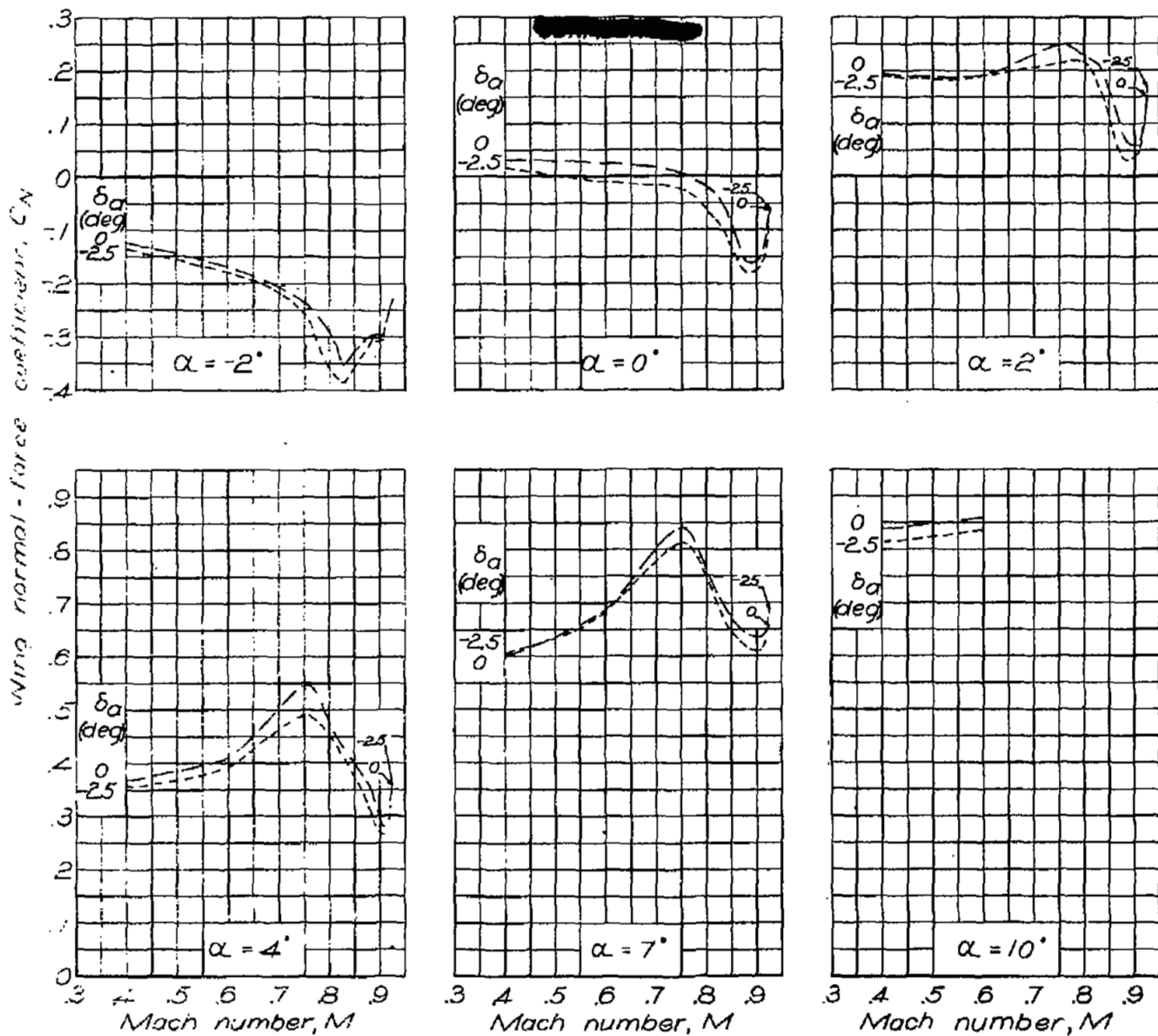
(a) $\frac{h_s}{c} = 0.03$; $\frac{x_s}{c} = 0.70$.

Figure 12. - Variation of wing normal-force coefficient with Mach number.



(b) $\frac{h_s}{c} = 0.06$; $\frac{x_s}{c} = 0.70$.

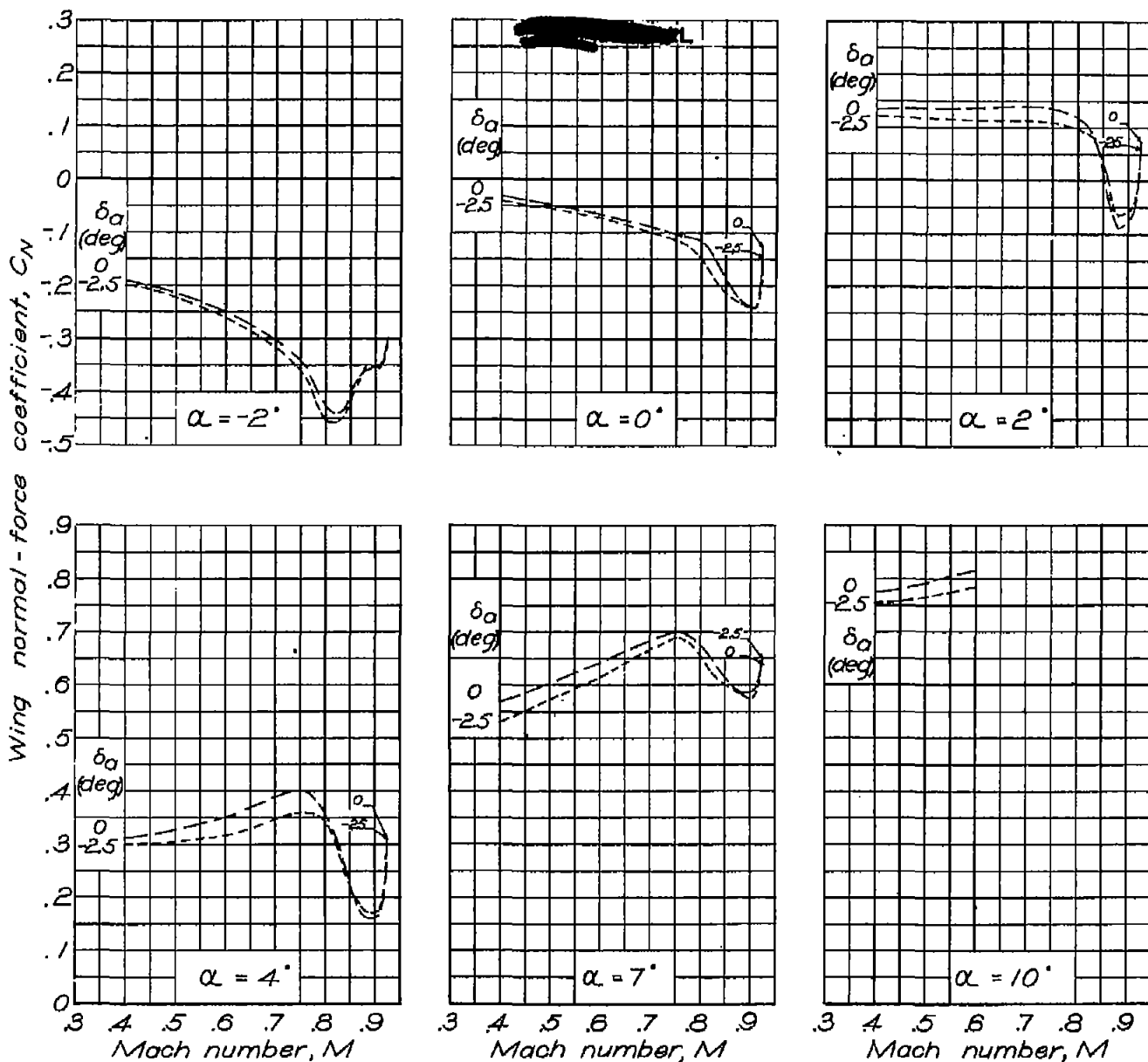
Figure 12.—Continued.



(c) $\frac{\eta_s}{c} = 0.03$; $\frac{\chi_s}{c} = 0.60$.

Figure 12 .- Continued.

NATIONAL ADVISORY
COMMITTEE FOR AERONAUTICS



(d) $\frac{h_s}{c} = 0.06$; $\frac{x_s}{c} = 0.60$.

Figure 12 - Concluded.

NATIONAL ADVISORY
COMMITTEE FOR AERONAUTICS

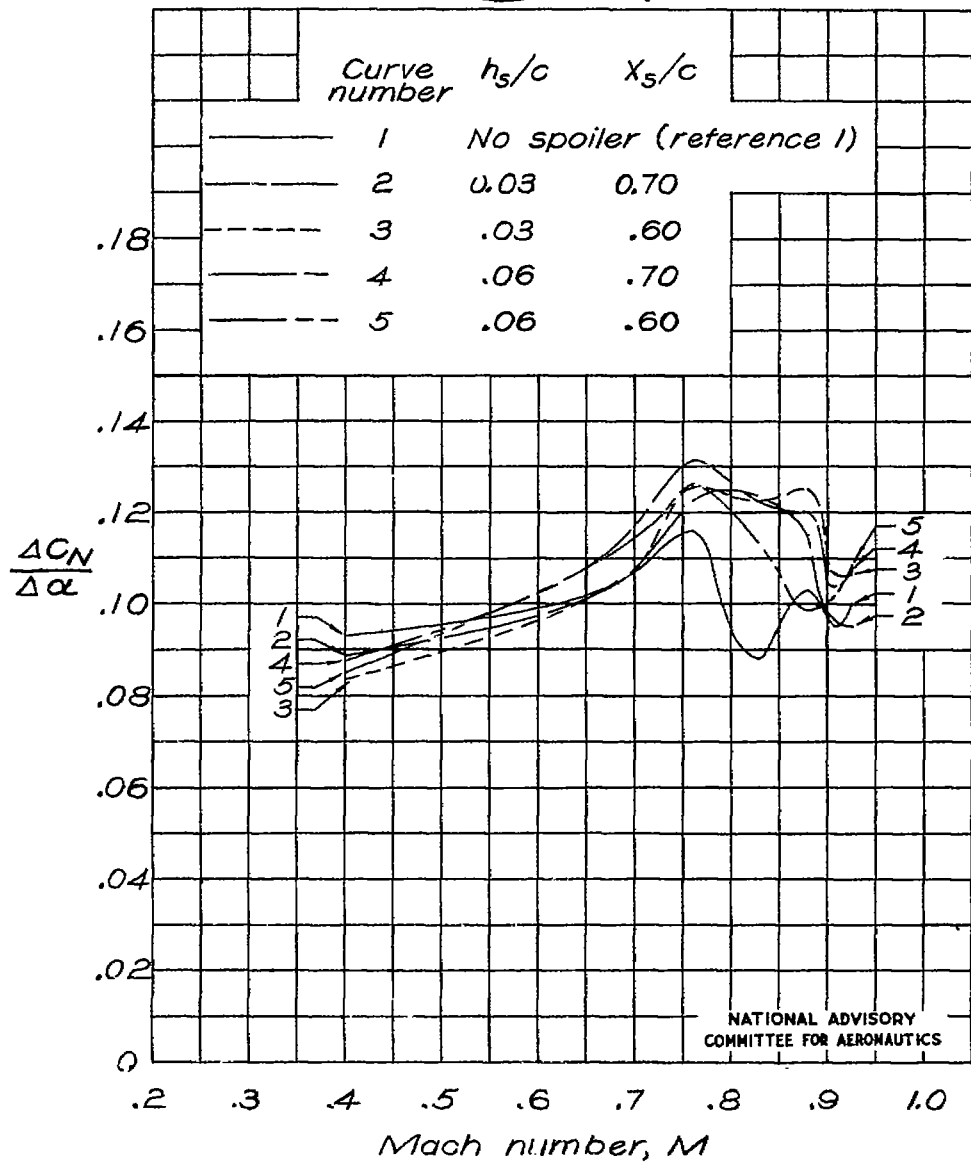


Figure 13.- Effect of compressibility on average normal-force curve slope between angles of attack of 0° and 4°. $\delta_a = 0^\circ$

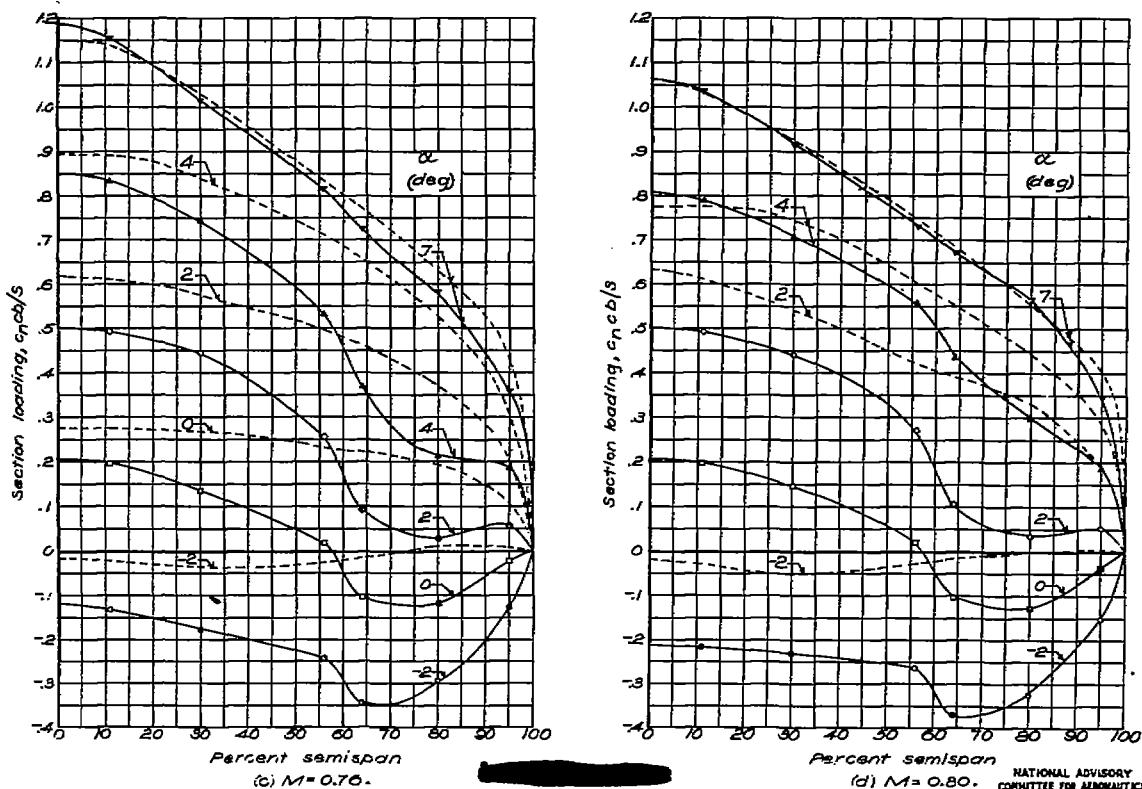
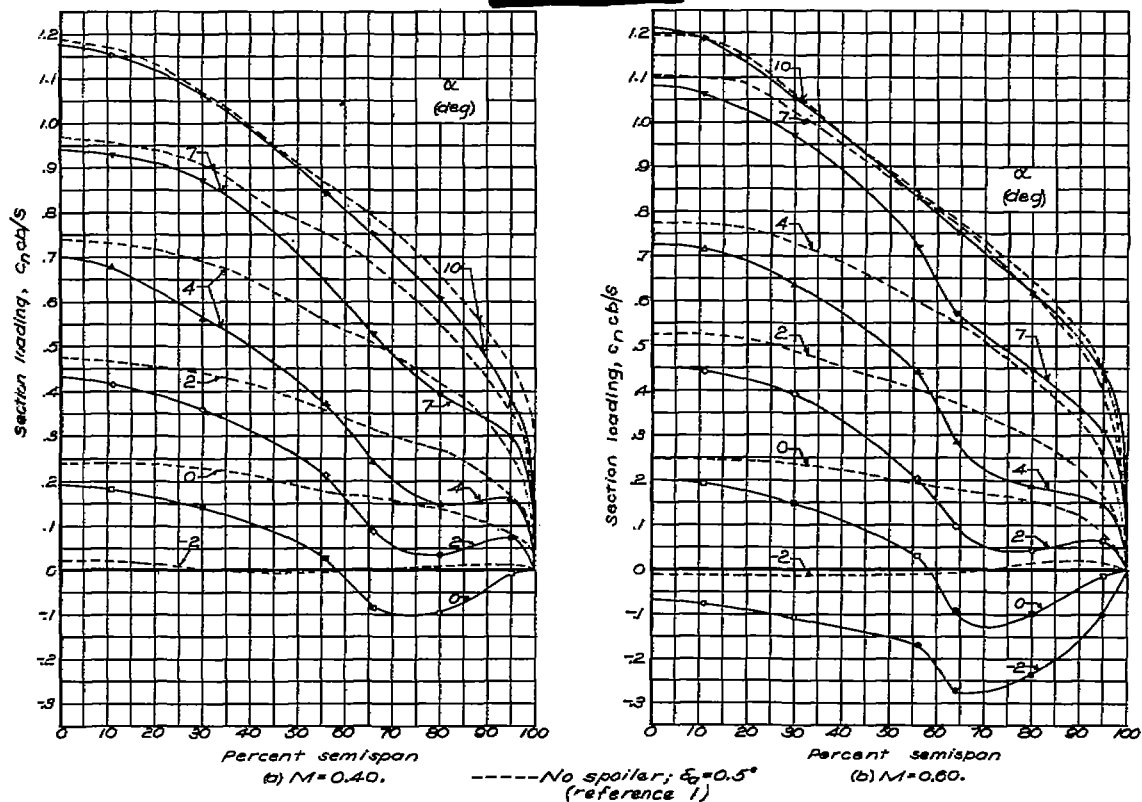


Figure 14.— Spanwise variation in section loading. $\delta_a=0.5^\circ$; $\frac{h}{c}=0.03$; $\frac{x}{c}=0.70$.

NATIONAL ADVISORY
COMMITTEE FOR AERONAUTICS

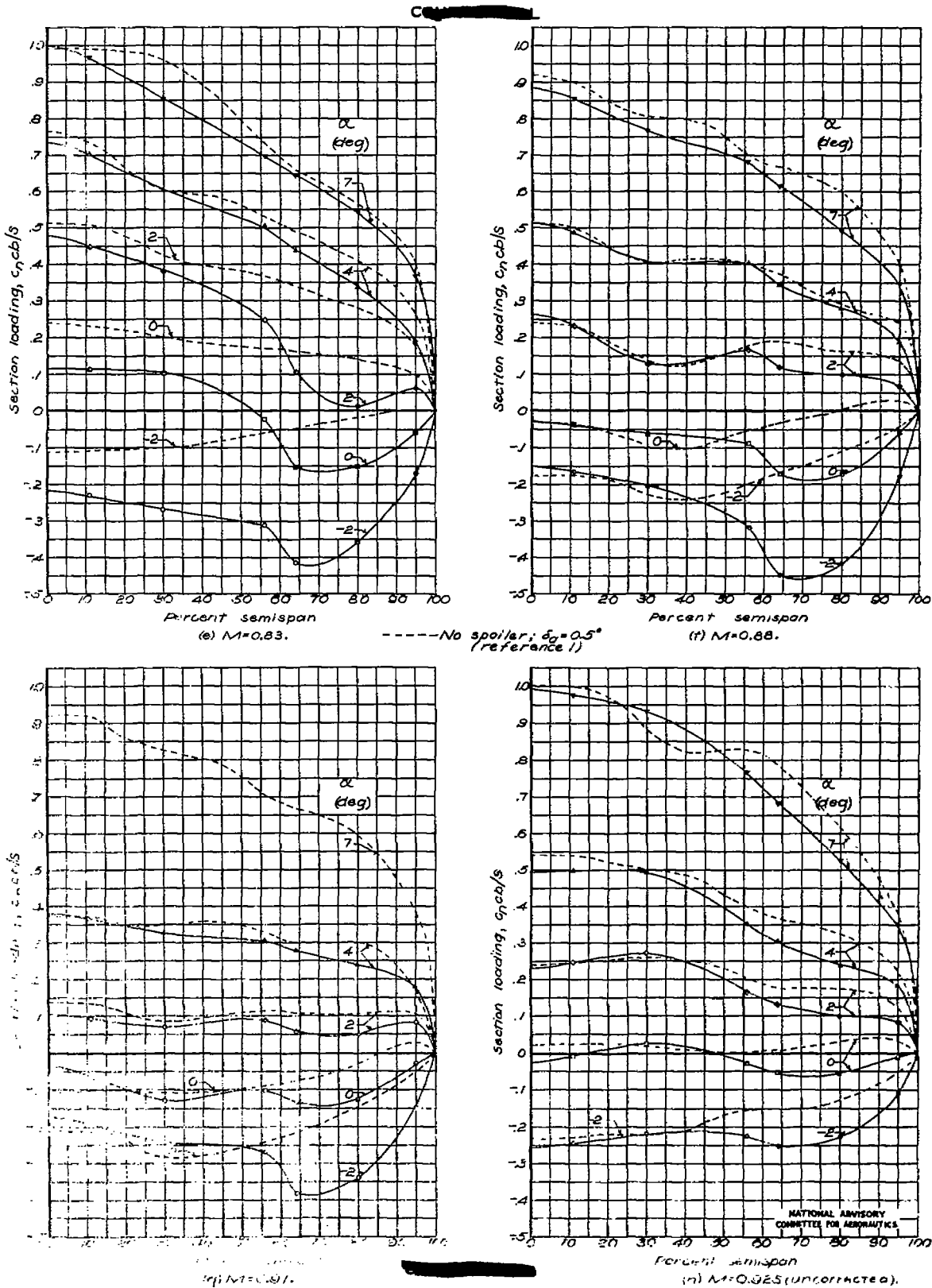


Figure 14 - Continued.

NATIONAL ADVISORY COMMITTEE FOR AERONAUTICS

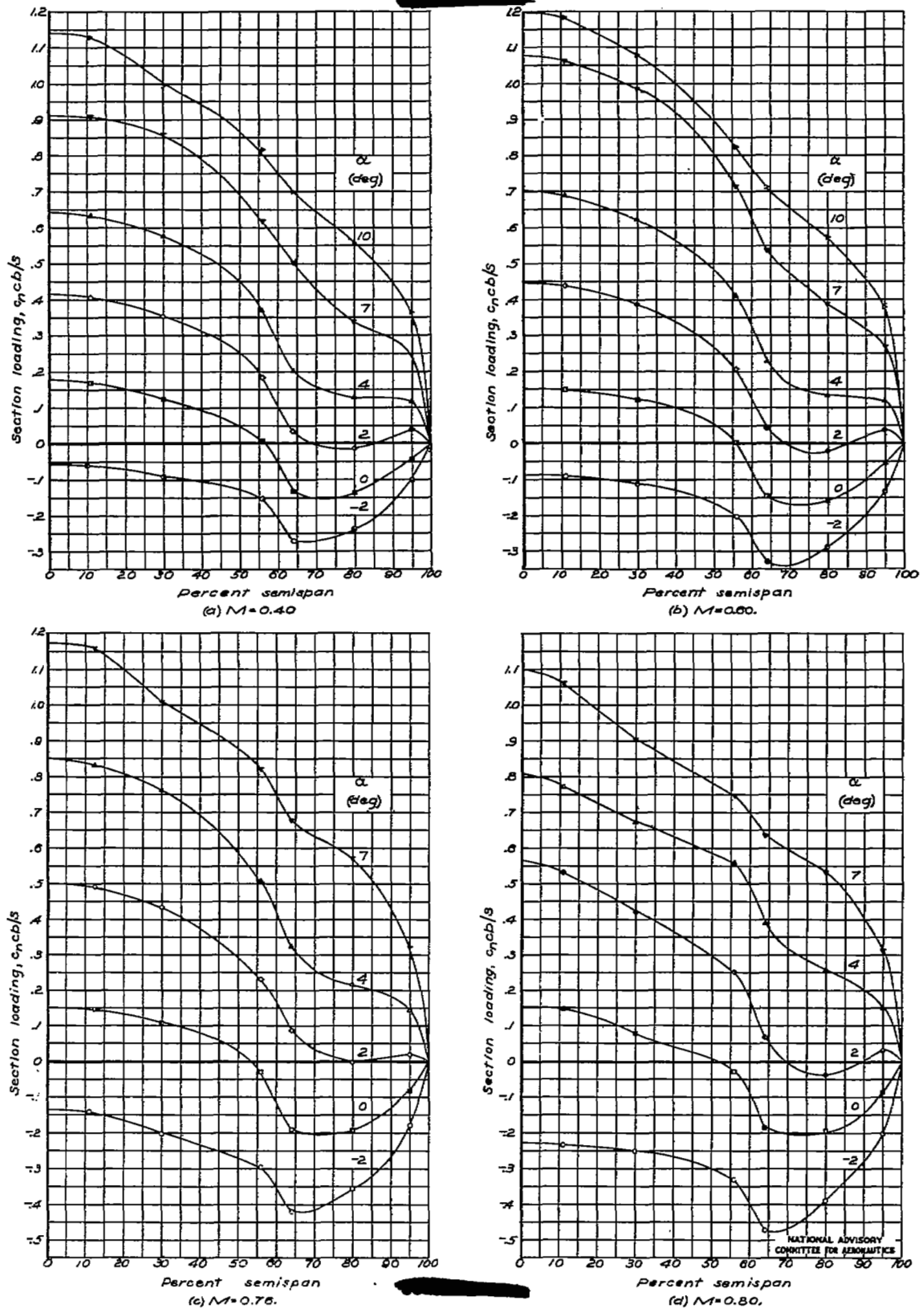


Figure 15. — Spanwise variation in section loading. $\delta_a = 3.3^\circ$; $h/c = 0.03$; $x/c = 0.70$.

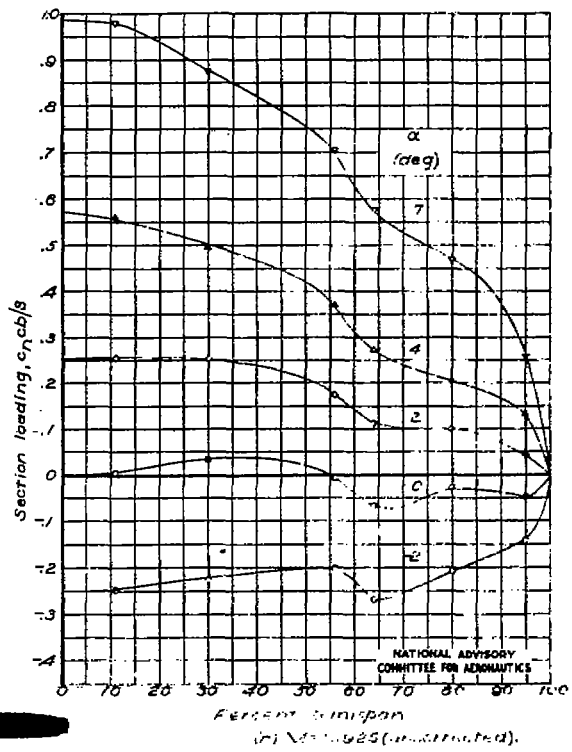
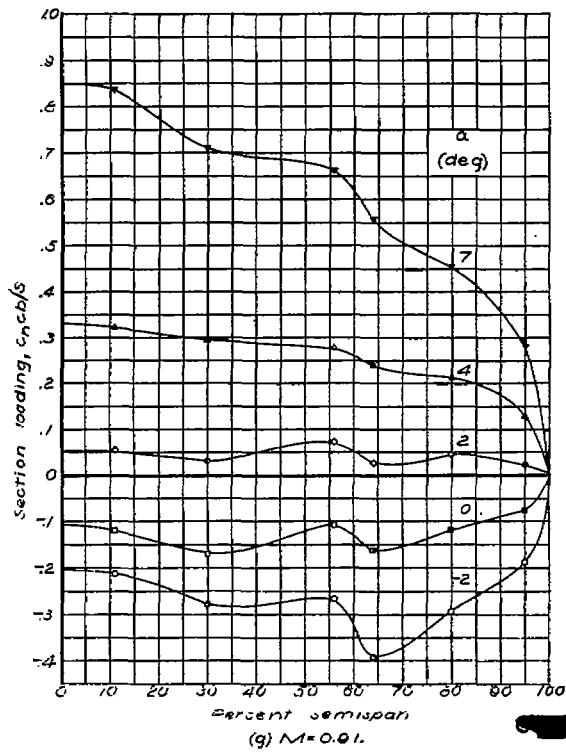
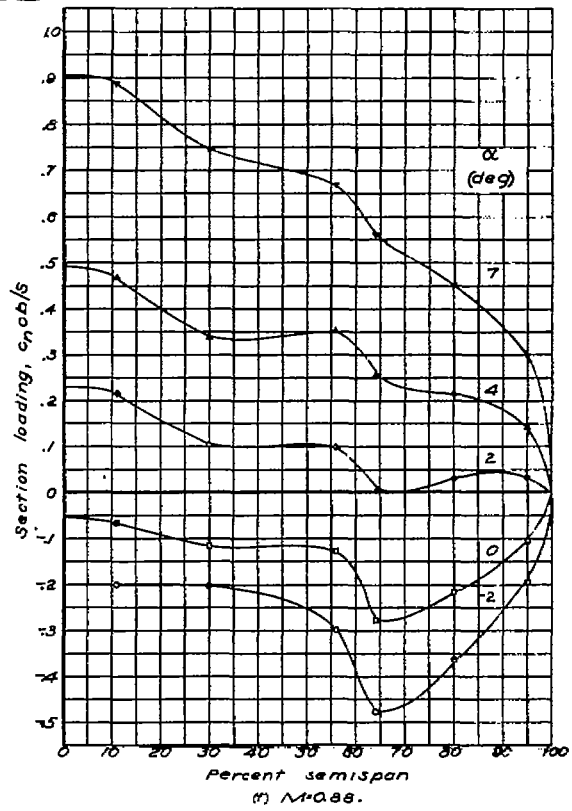
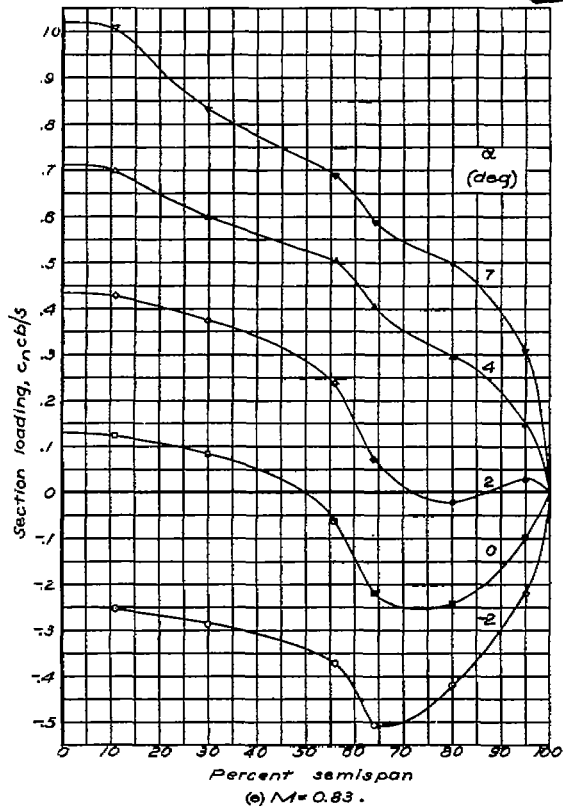


Figure 15 — Concluded.

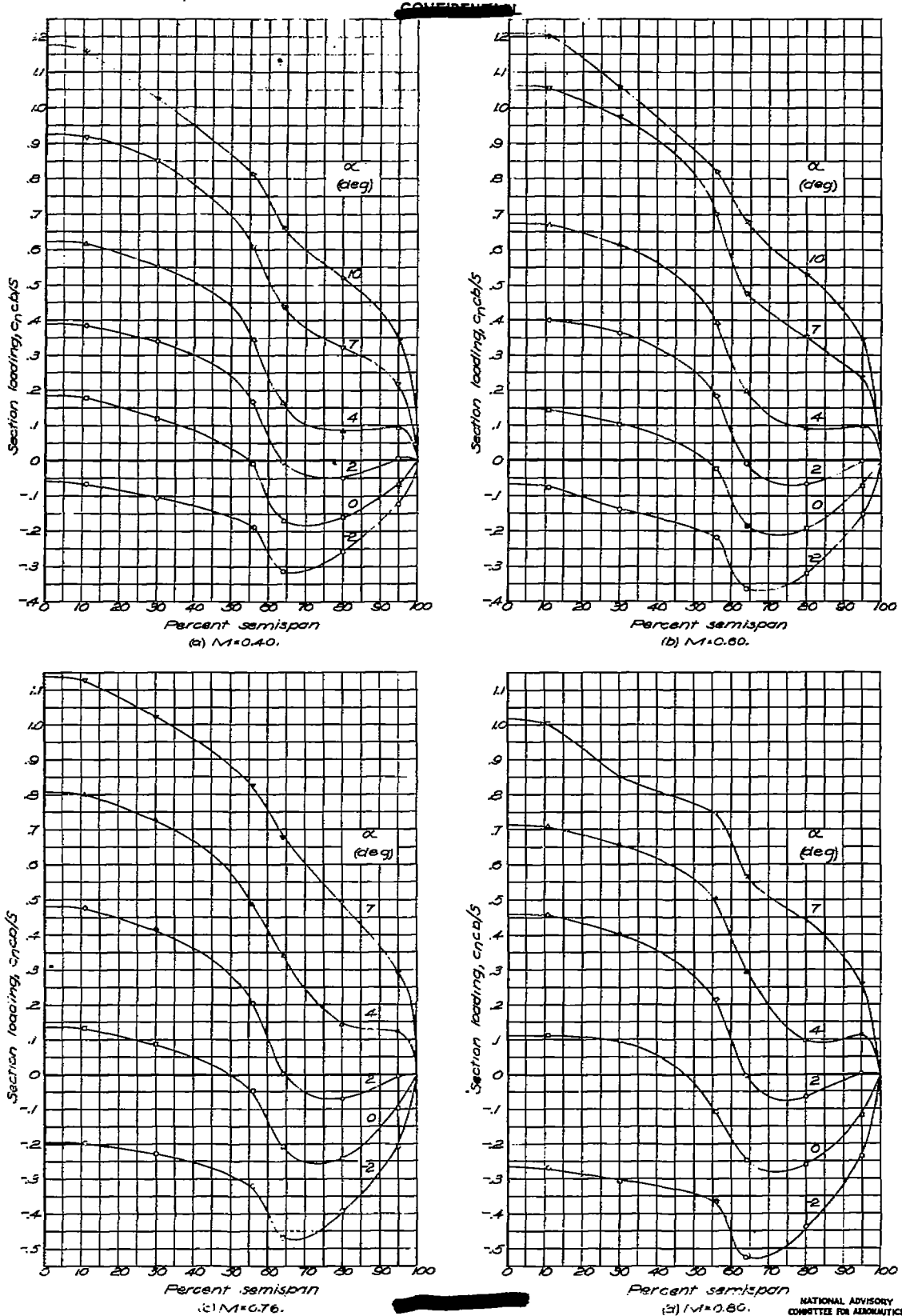


Figure 16.—Spanwise variation in section loading. $\delta\alpha = -5.6^\circ$; $\frac{h_s}{c} = 0.03$; $\frac{x_s}{c} = 0.70$.

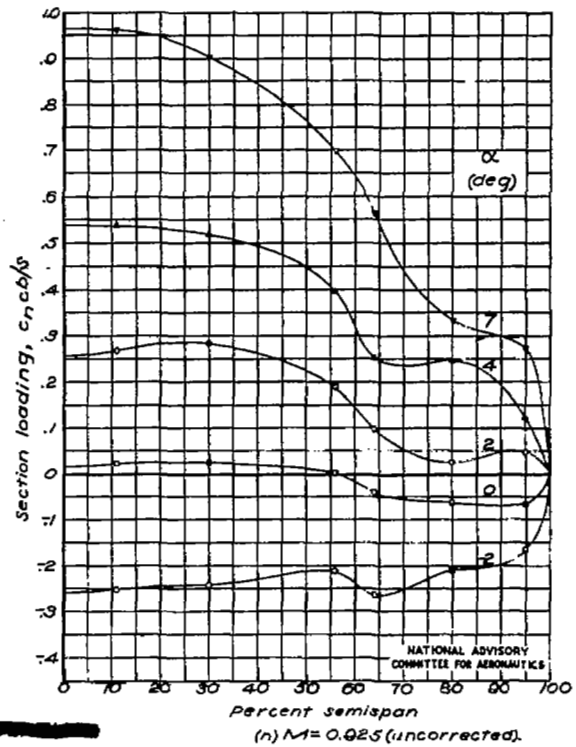
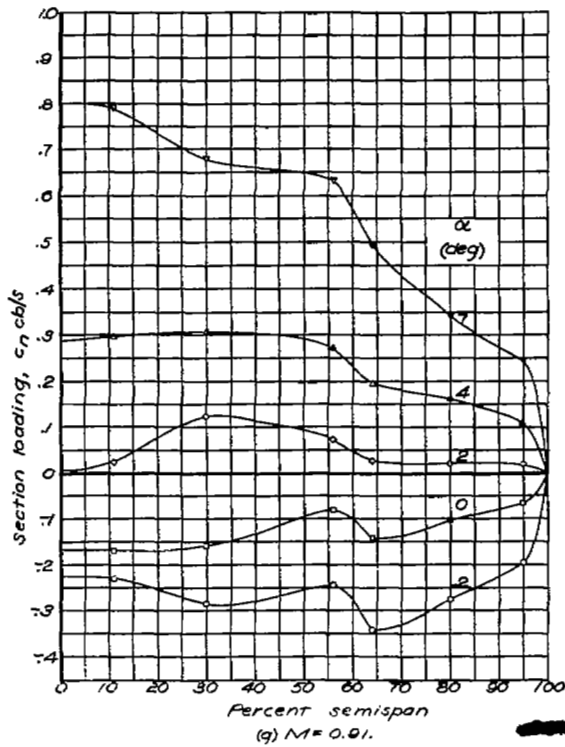
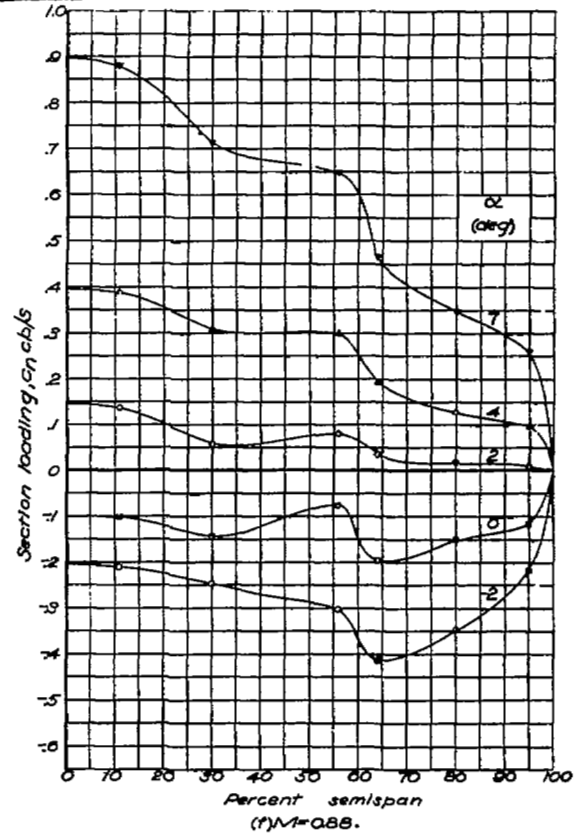
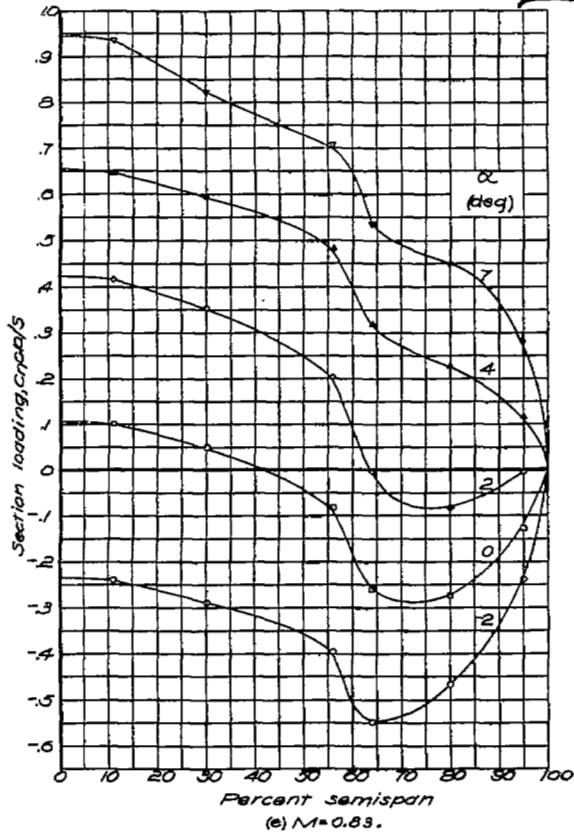


Figure 16. — Concluded.

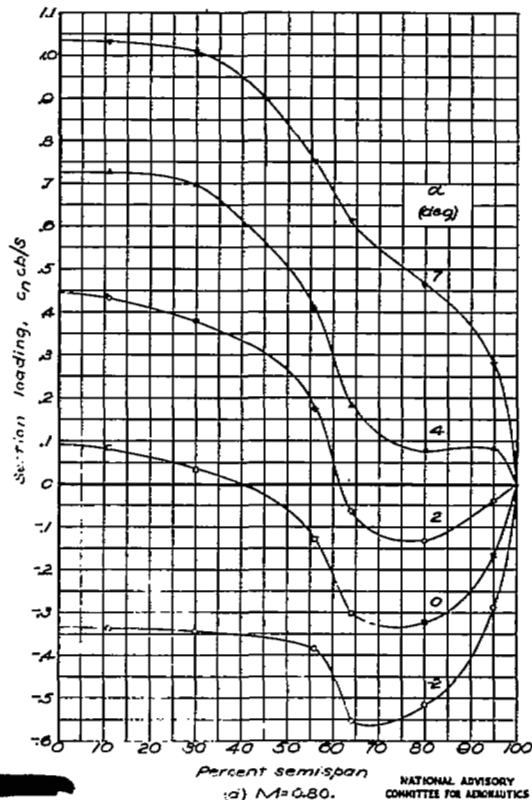
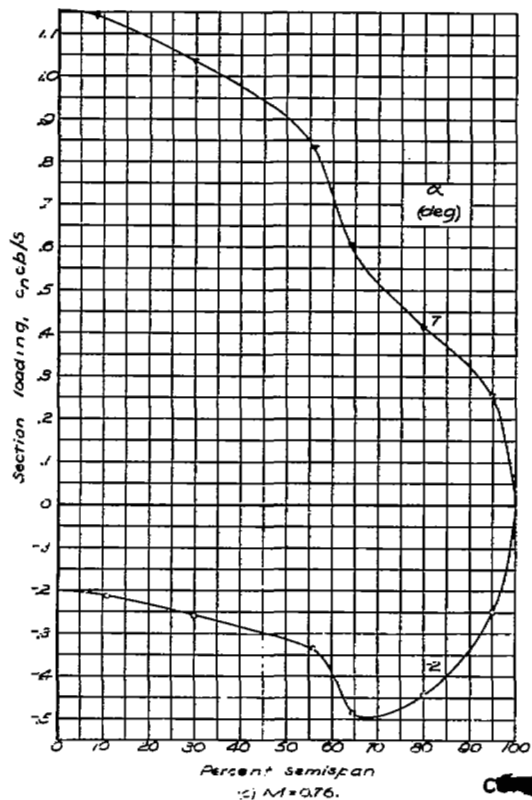
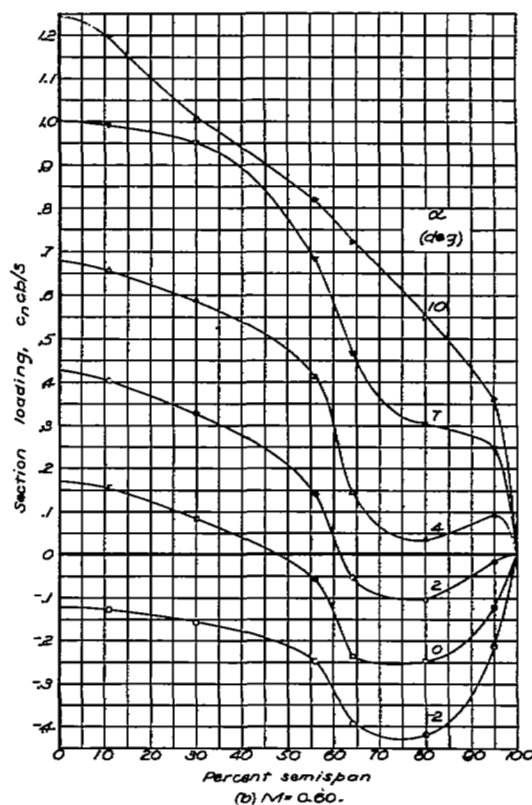
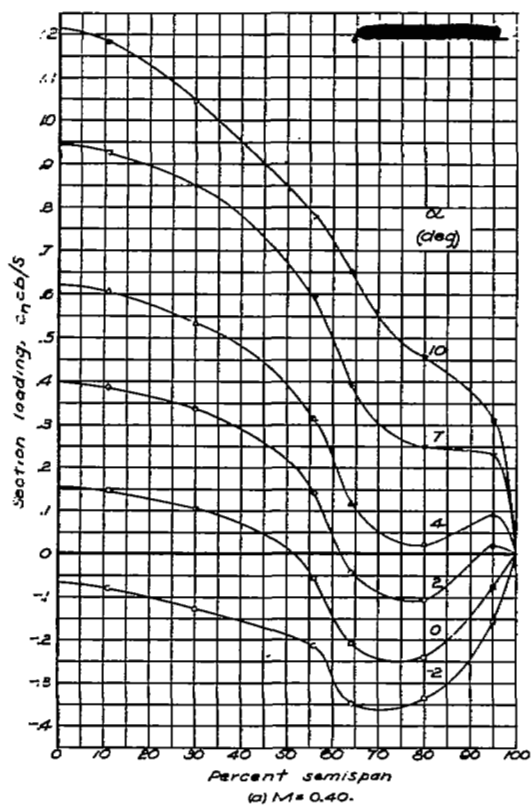


Figure 17. — Spanwise variation in section loading. $\delta_a = 0.0$, $h_s = 0.06$, $x_s = 0.70$.

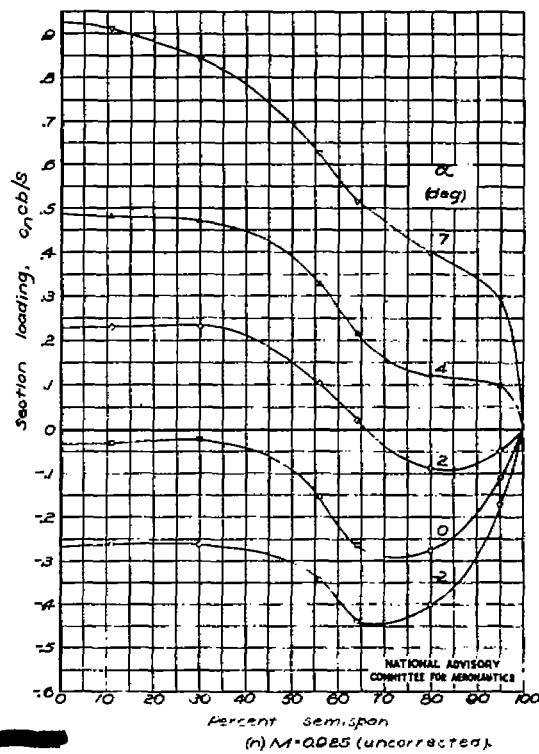
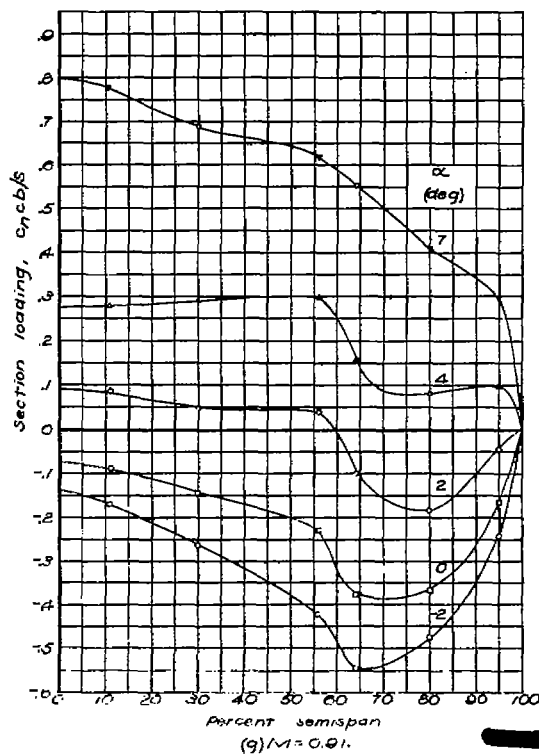
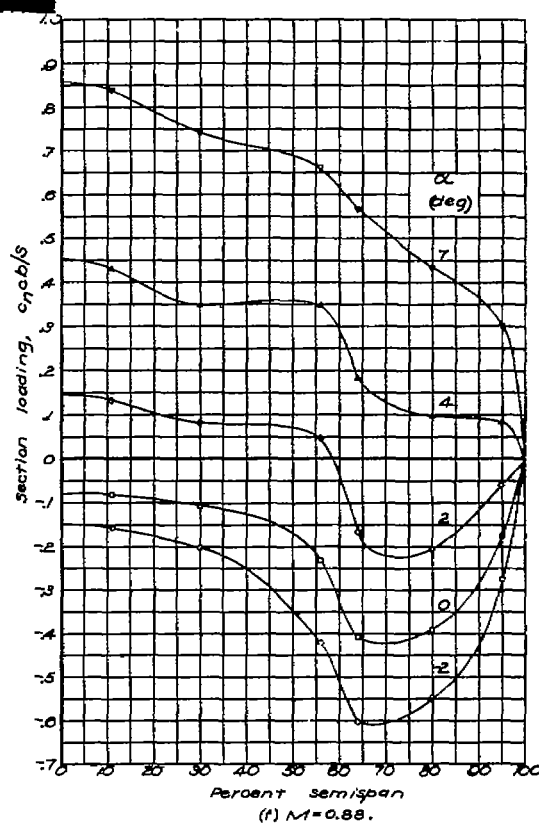
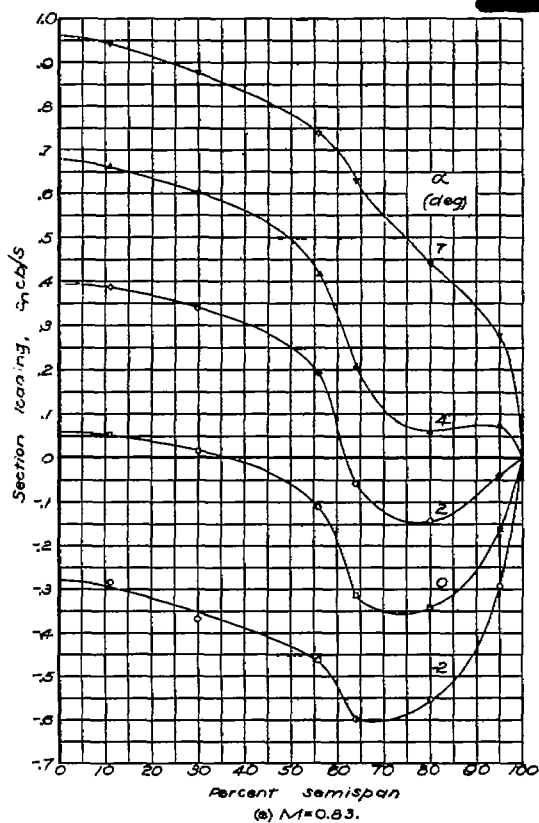


Figure 17. — Concluded.

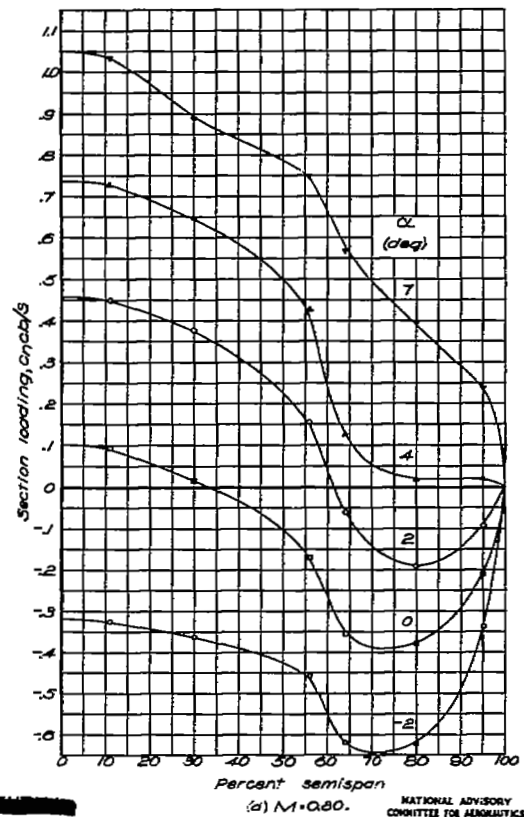
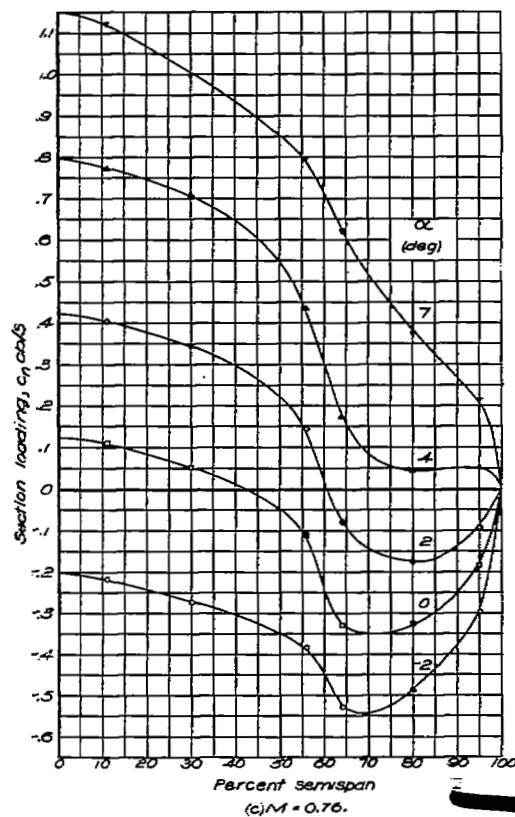
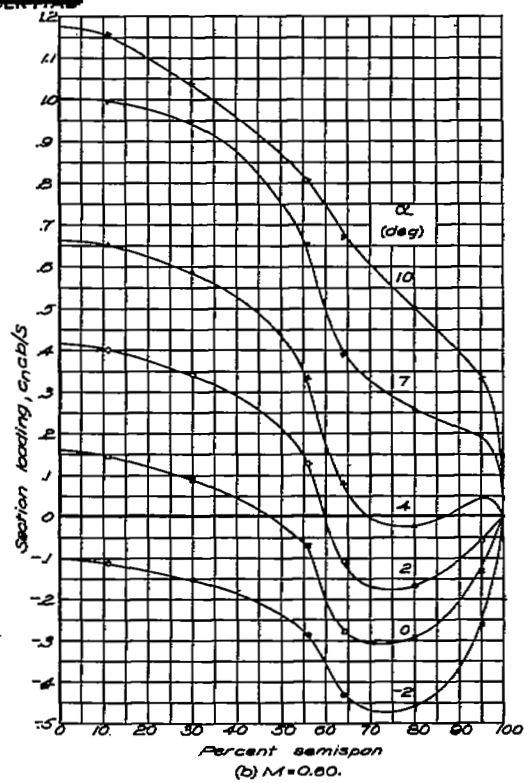
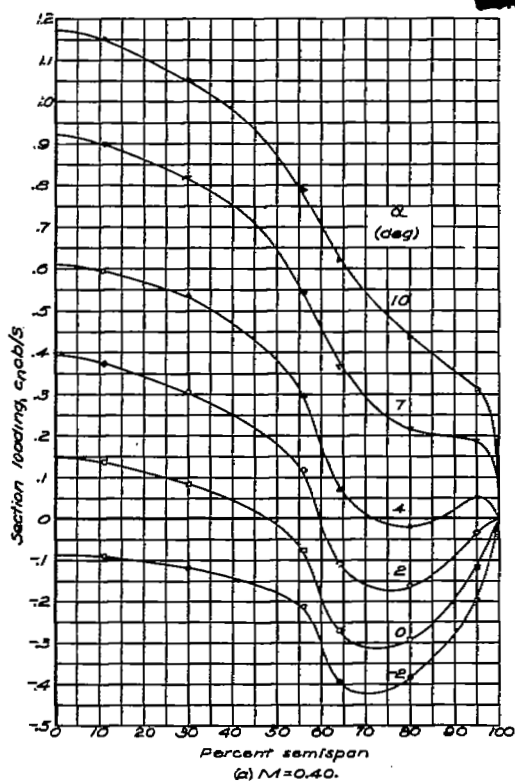


Figure 18. — Spanwise variation in section loading. $\delta_a = -3.3^\circ$; $h_s = 0.06$; $x_s = 0.70$.

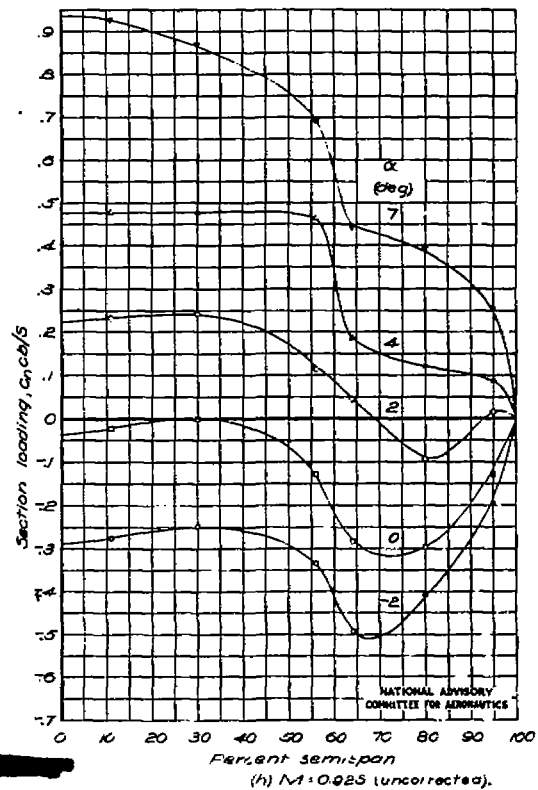
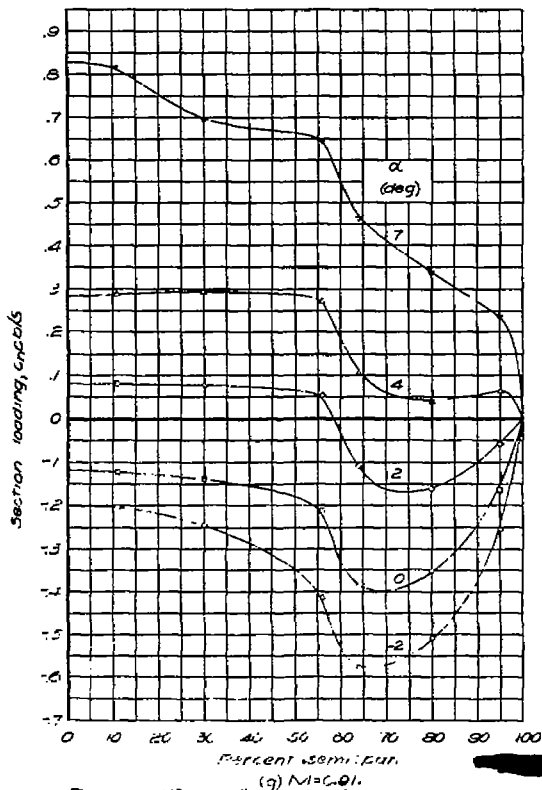
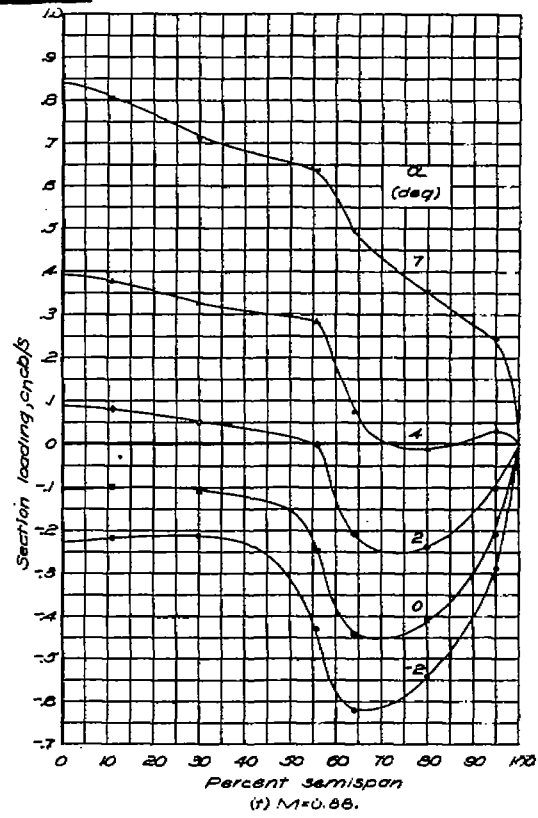
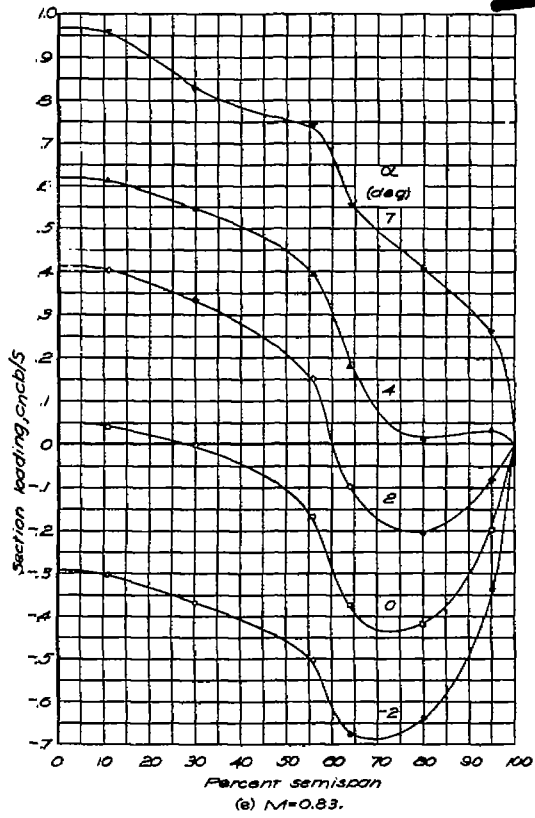


Figure 18 - Concluded.

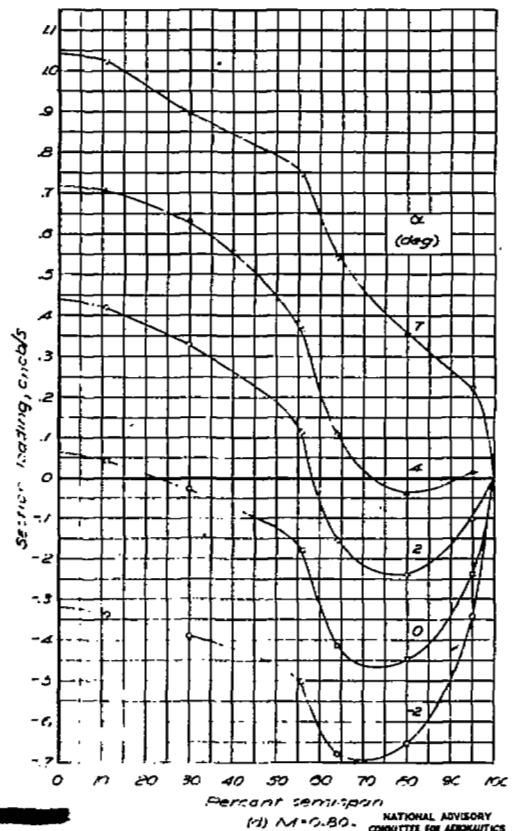
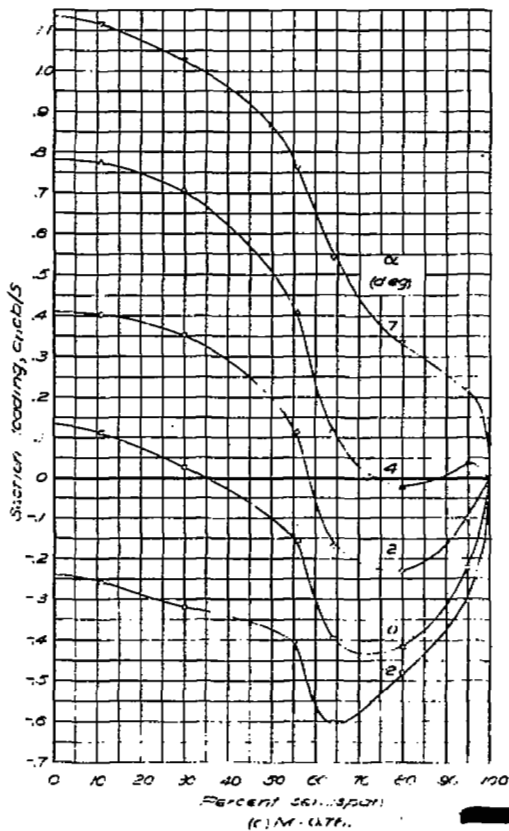
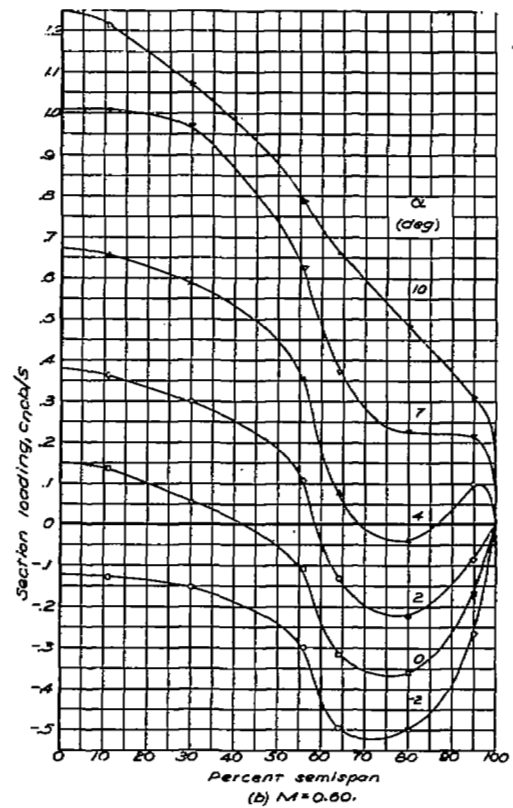
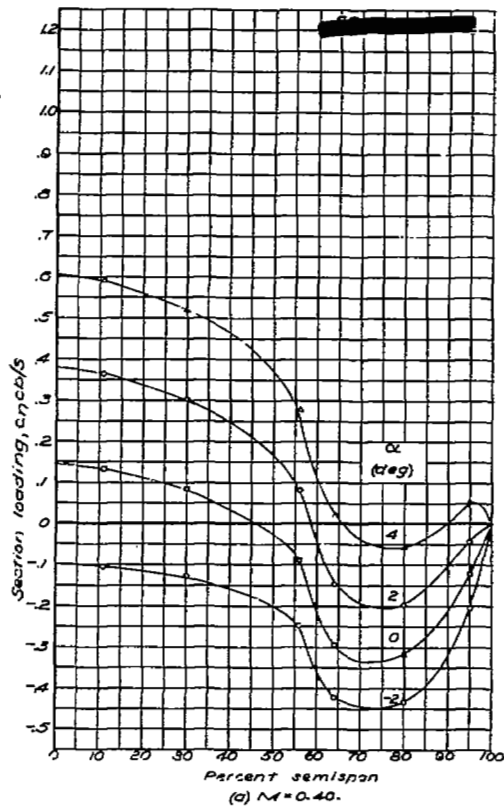


Figure 19. — Spanwise variation in section loading. $\delta_1 = -5.5^\circ$; $\delta_2 = 0.06^\circ$; $\delta_3 = 0.70^\circ$.

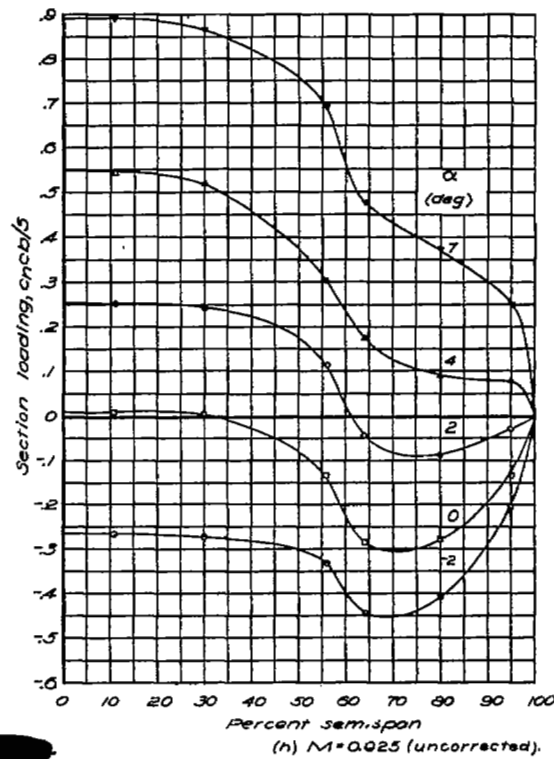
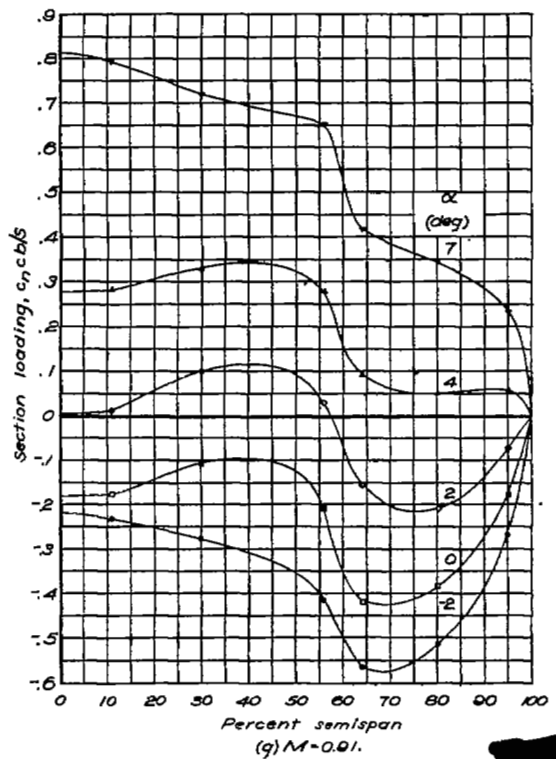
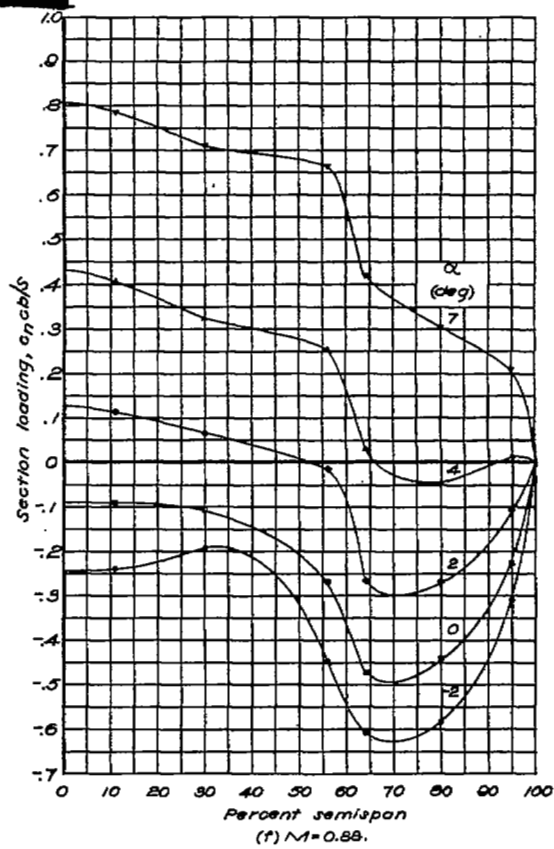
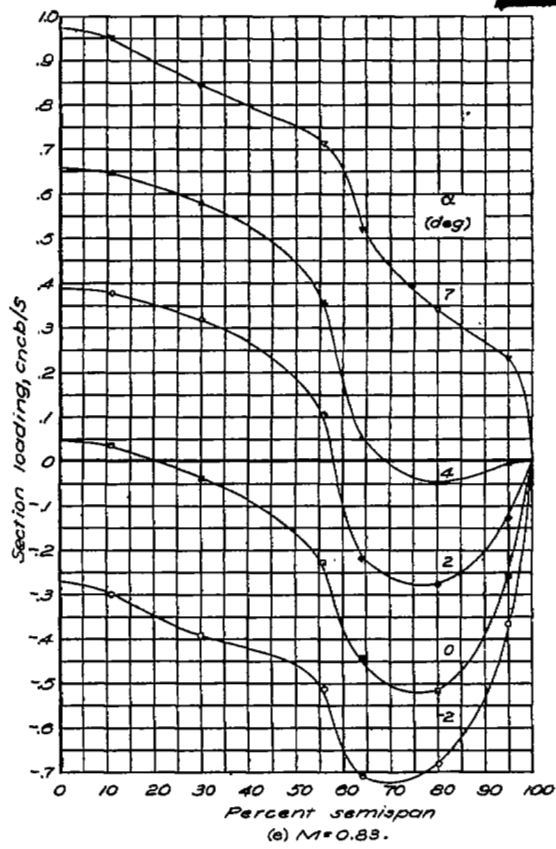


Figure 19 — Concluded.

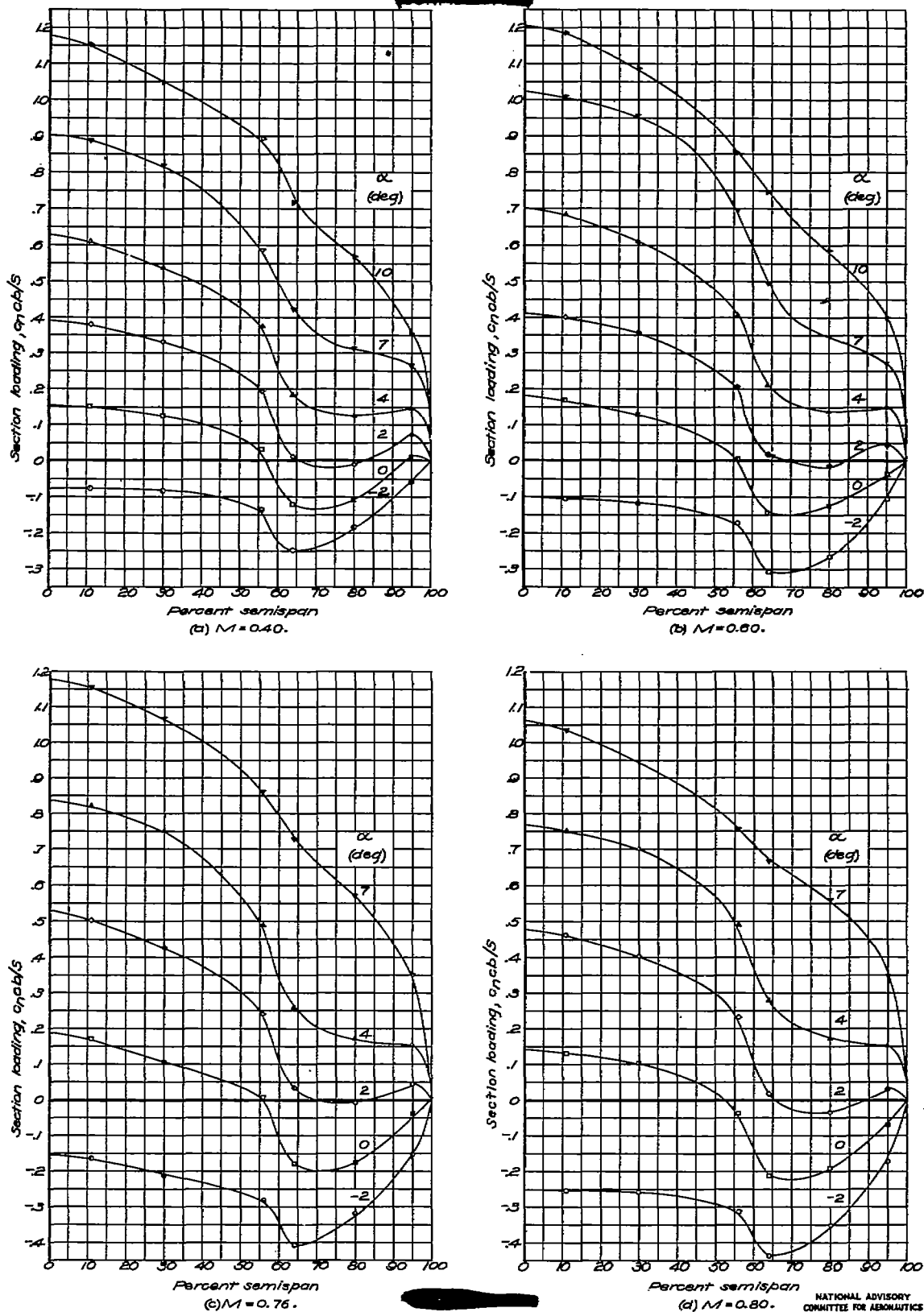


Figure 20. — Spanwise variation in section loading. $\delta_a = 0.0^\circ$; $h_s = 0.03$; $x_s = 0.60$.

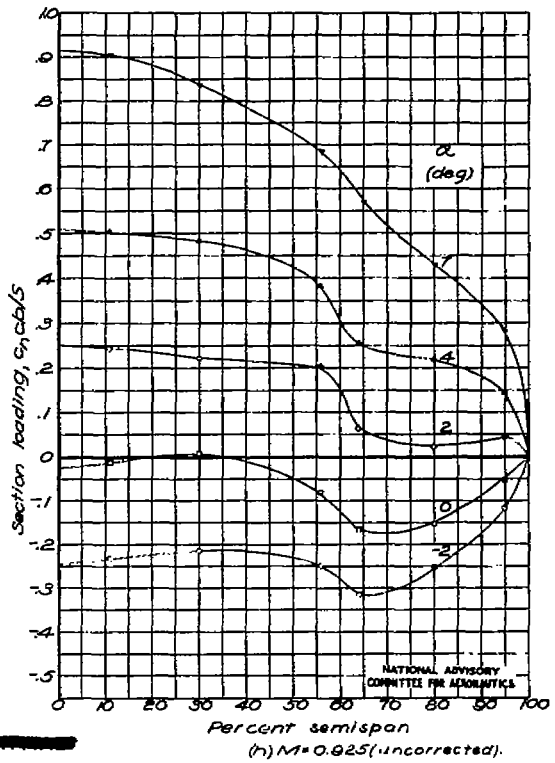
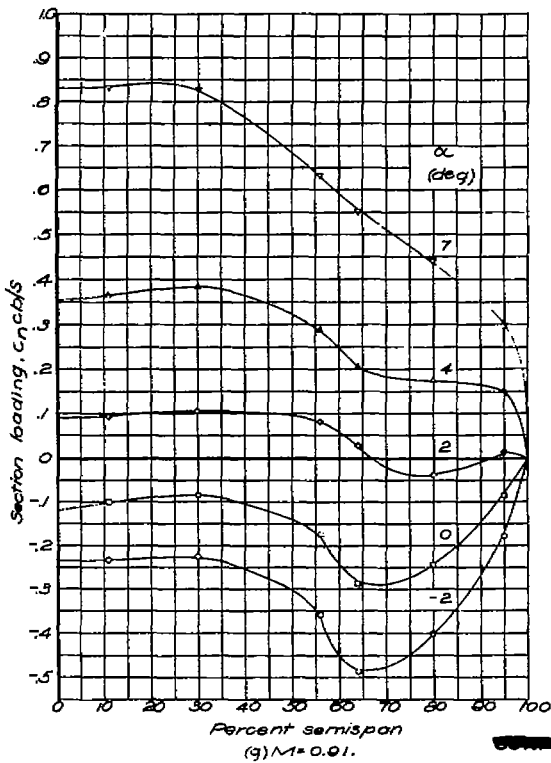
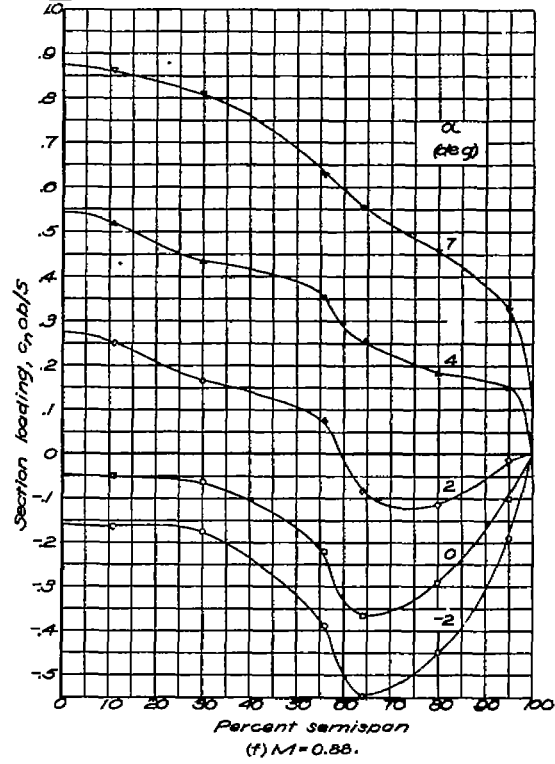
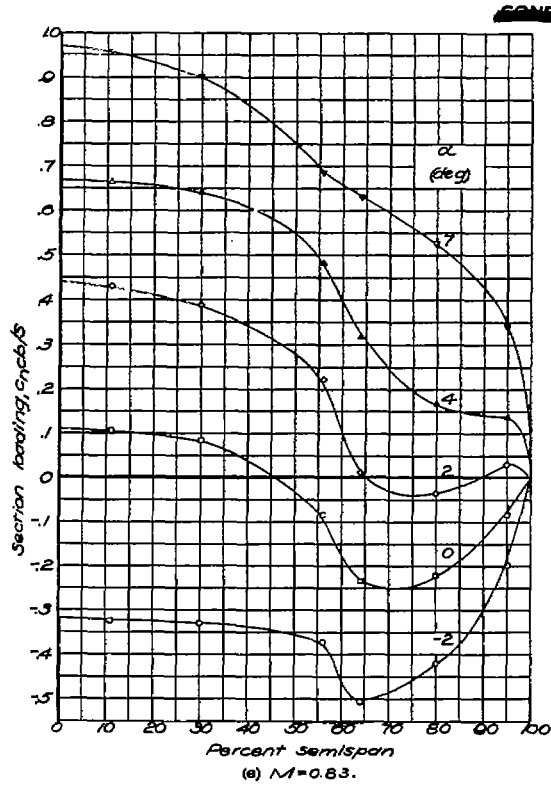


Figure 20. — Concluded.

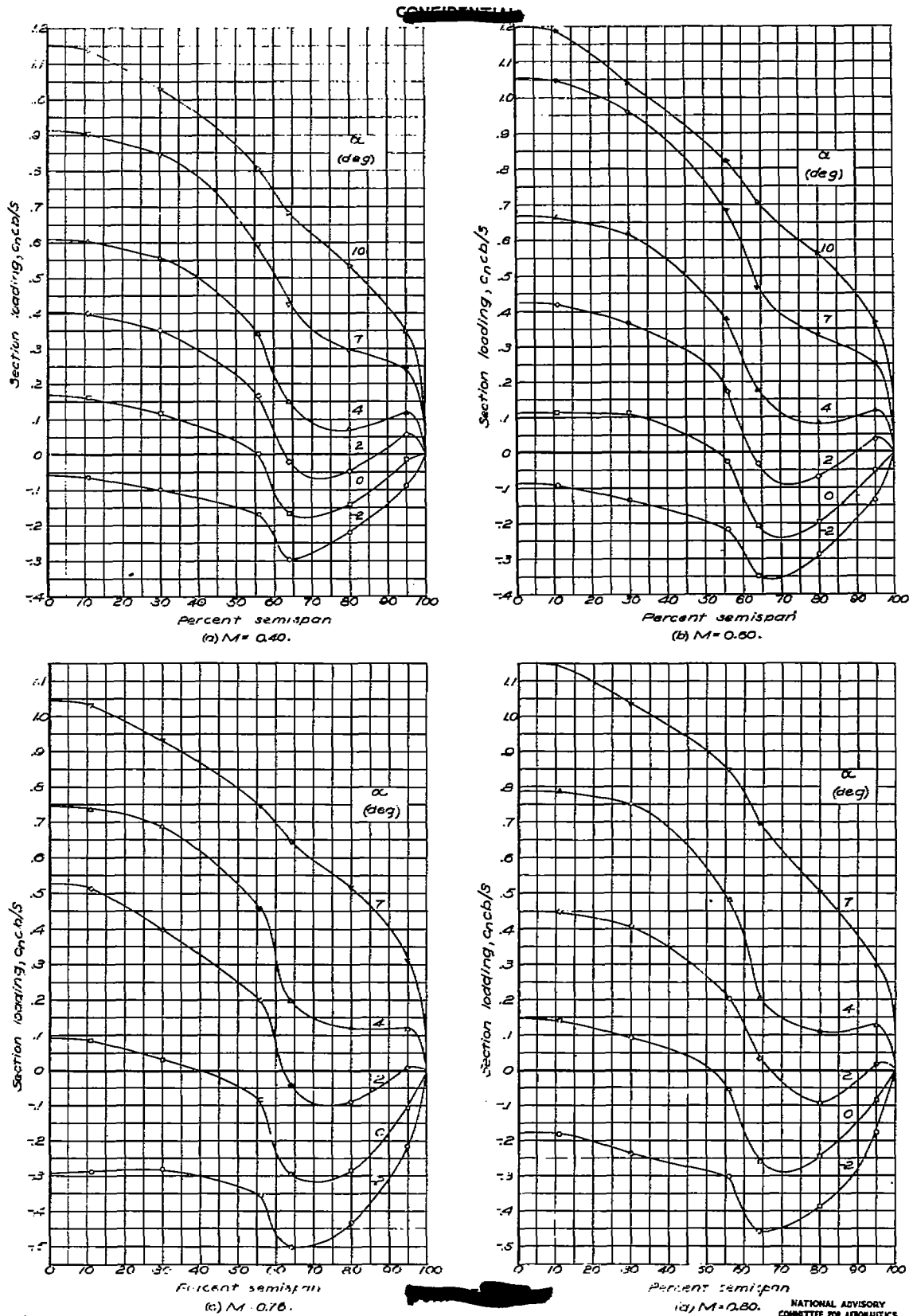


Figure 21. — Spanwise variation in section loading. $\delta_{CP} = 3.3^\circ$; $\frac{h_s}{c} = 0.03$; $\frac{x_s}{c} = 0.60$.

NATIONAL ADVISORY
COMMITTEE FOR AERONAUTICS

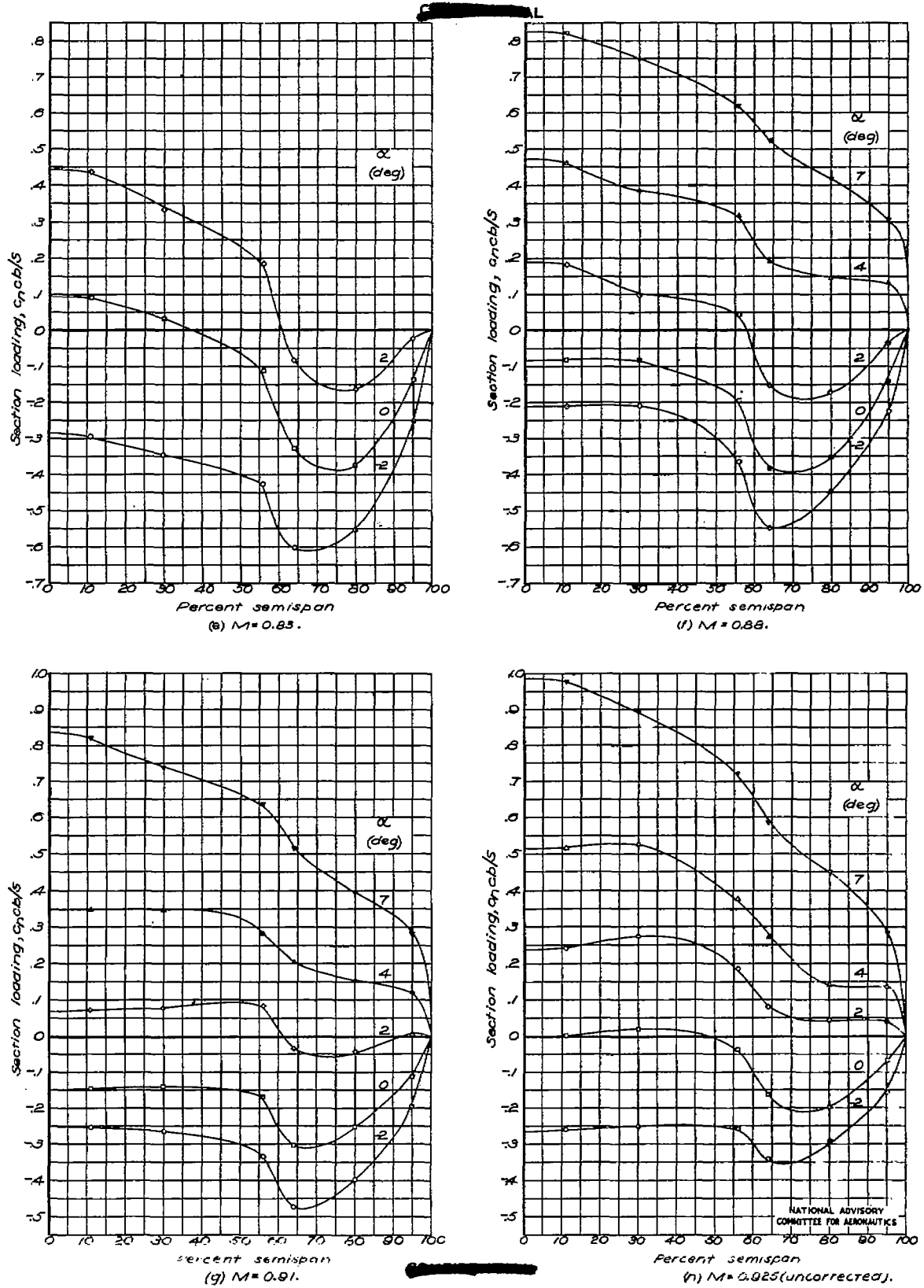


Figure 21 .— Concluded.

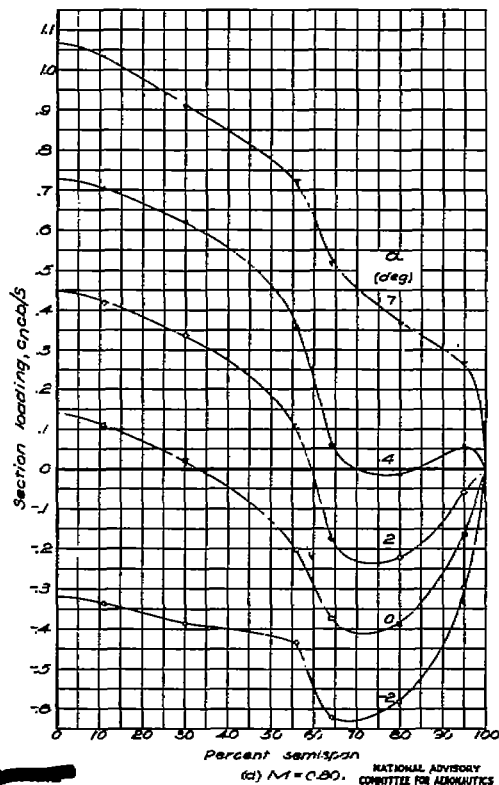
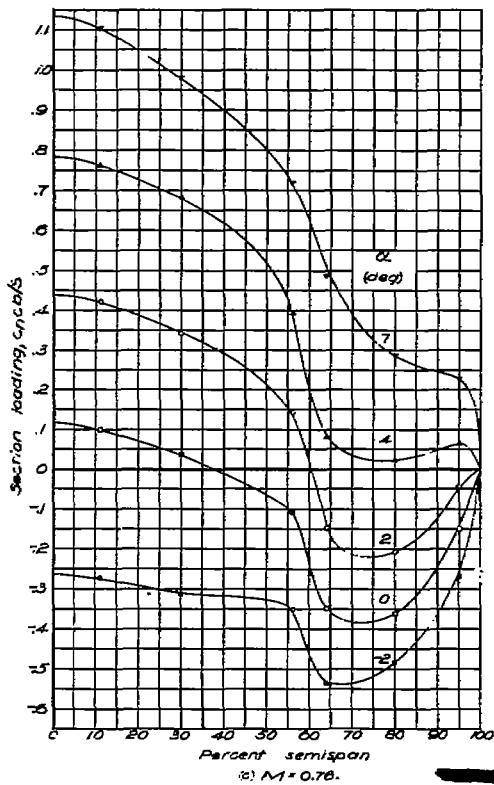
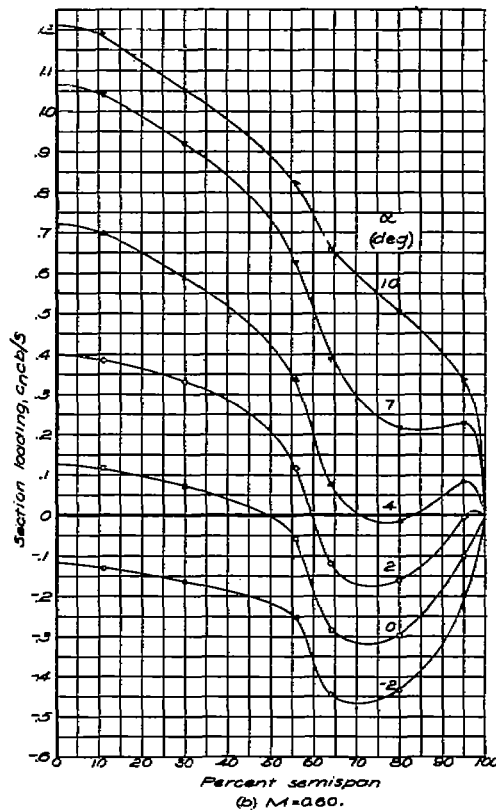
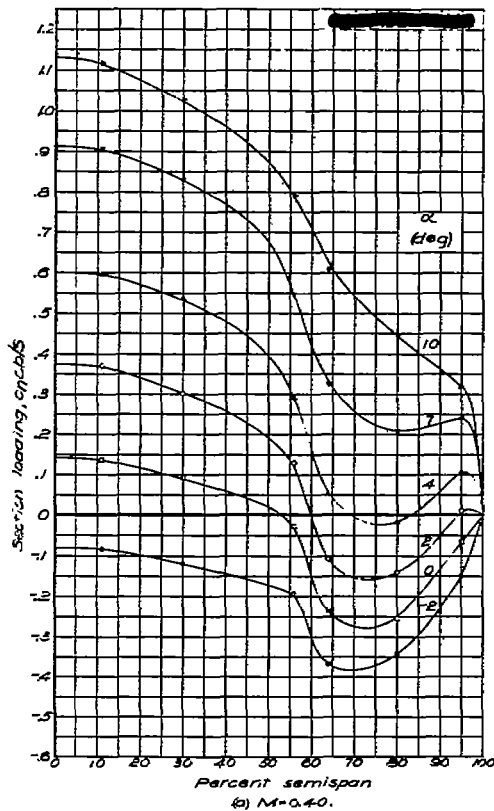


Figure 22. — Spanwise variation in section loading. $\delta_a = 0.0^\circ$ for $M \leq 0.76$, $\delta_a = -0.3^\circ$ for $M \geq 0.80$; $\frac{t}{c} = 0.06$, $\frac{x}{c} = 0.60$.

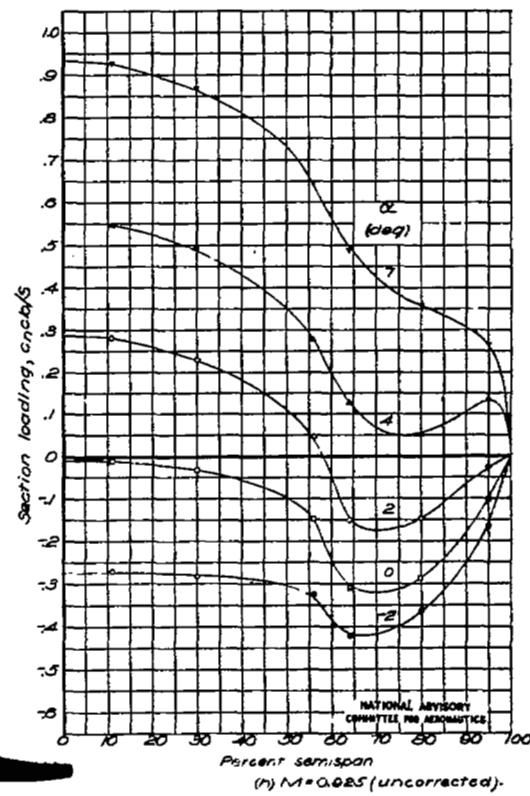
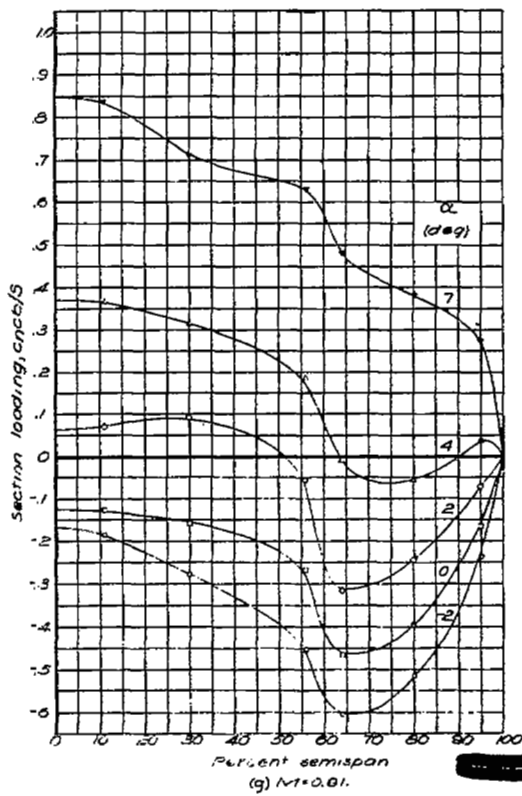
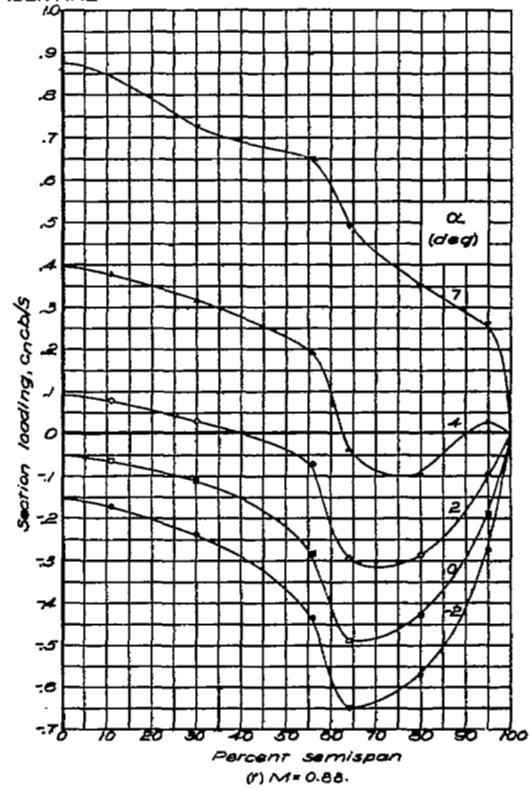
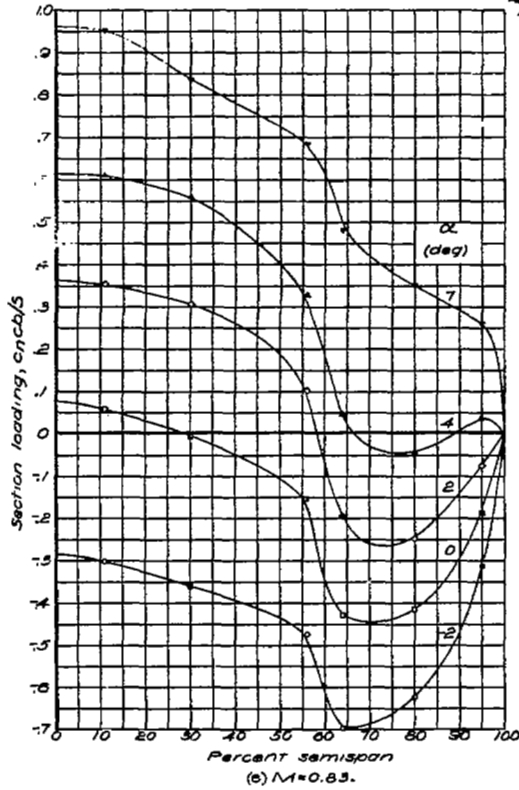


Figure 22. — Concluded.

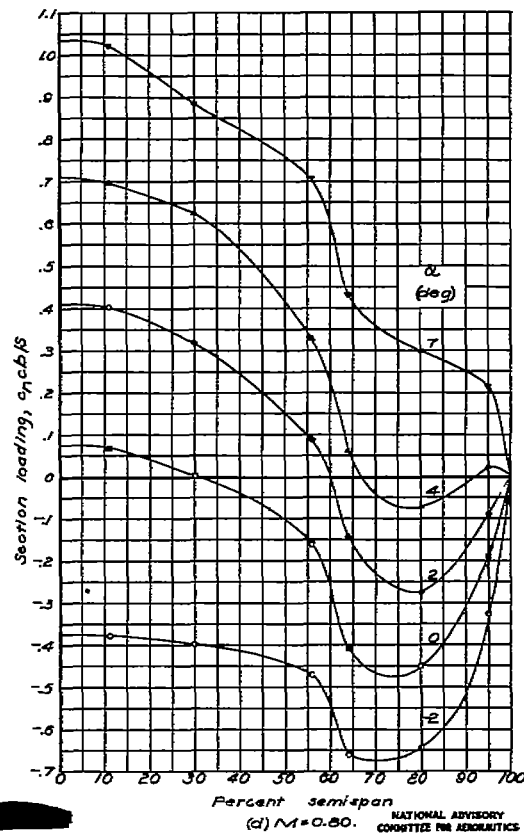
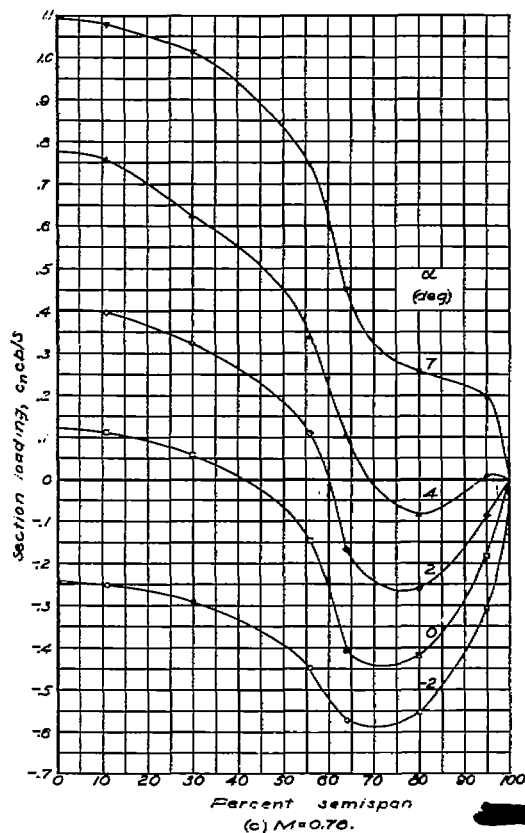
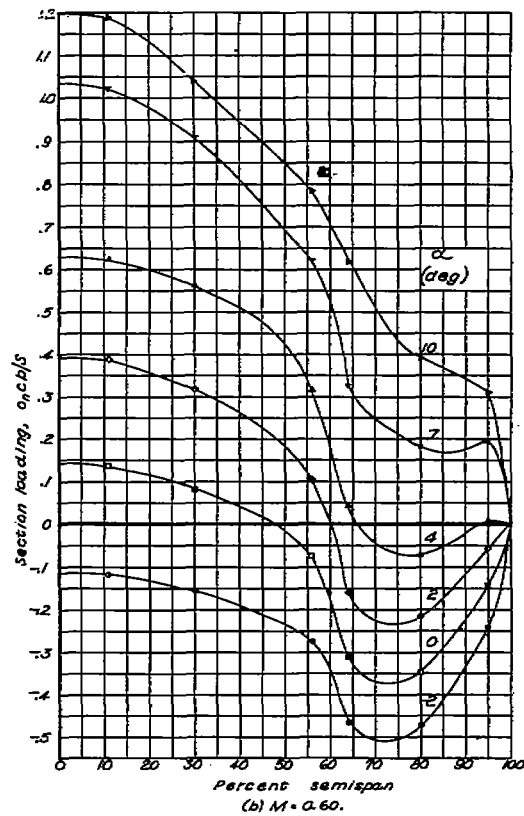
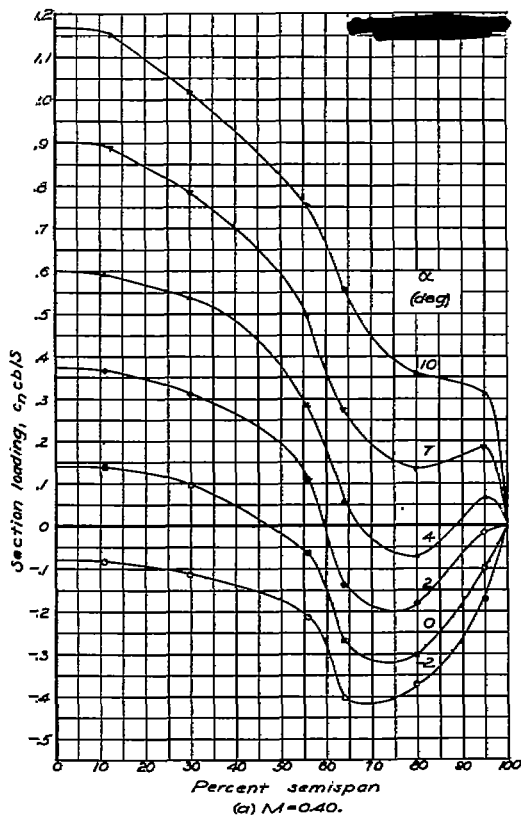


Figure 23 .— Spanwise variation in section loading. $\delta_a = -3.3^\circ$; $h/c = 0.06$; $x/c = 0.60$.

NATIONAL ADVISORY
COMMITTEE FOR AERONAUTICS

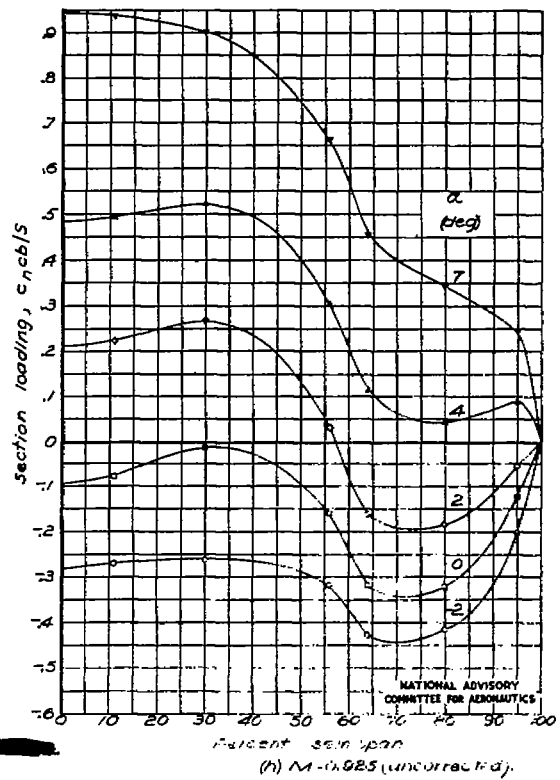
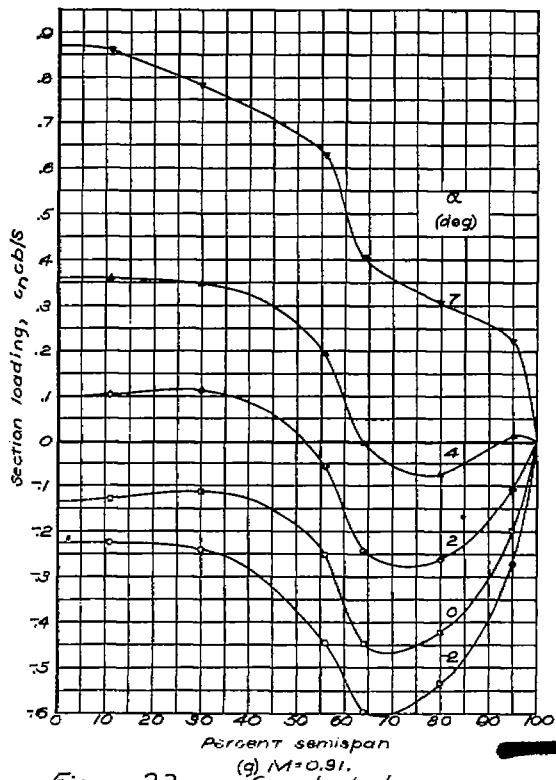
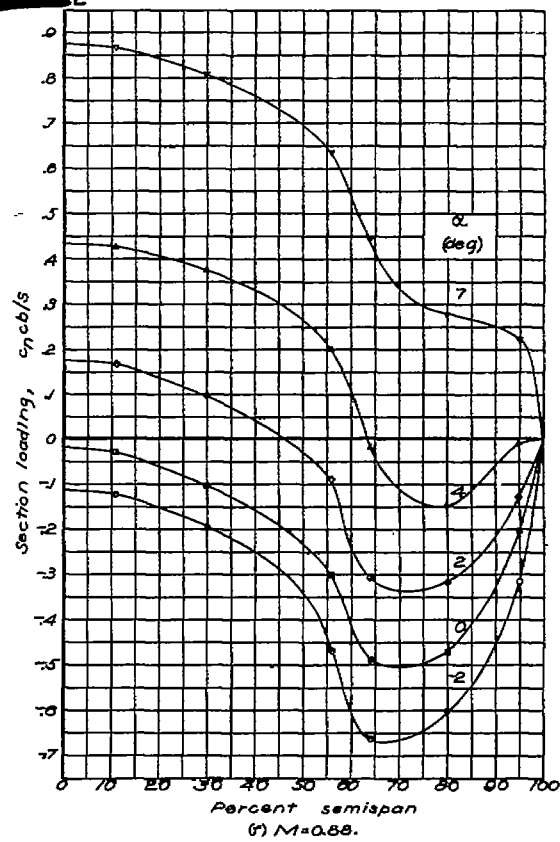
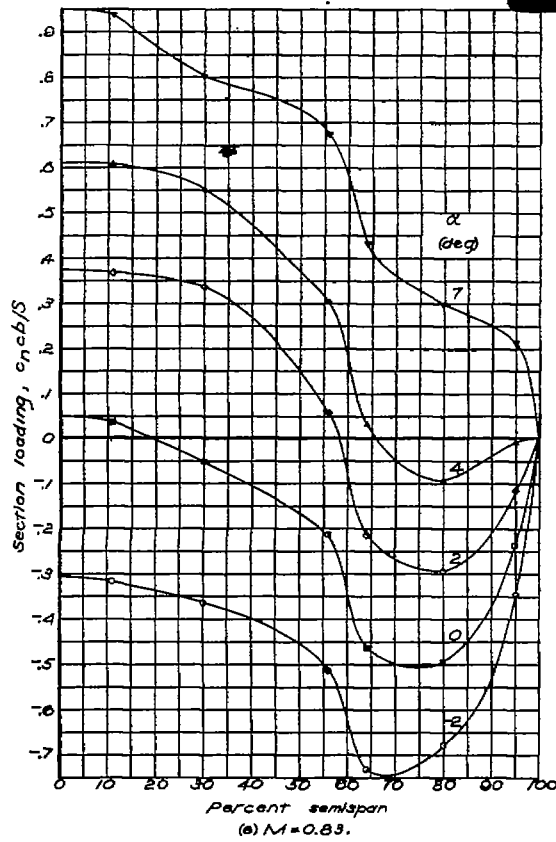


Figure 23. — Concluded.

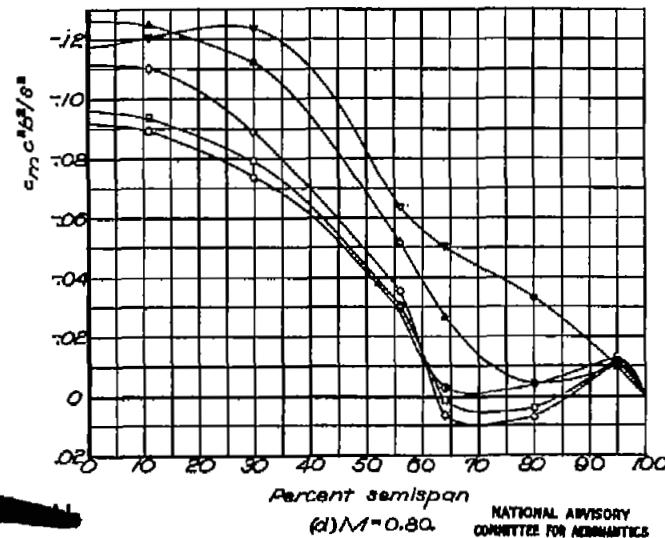
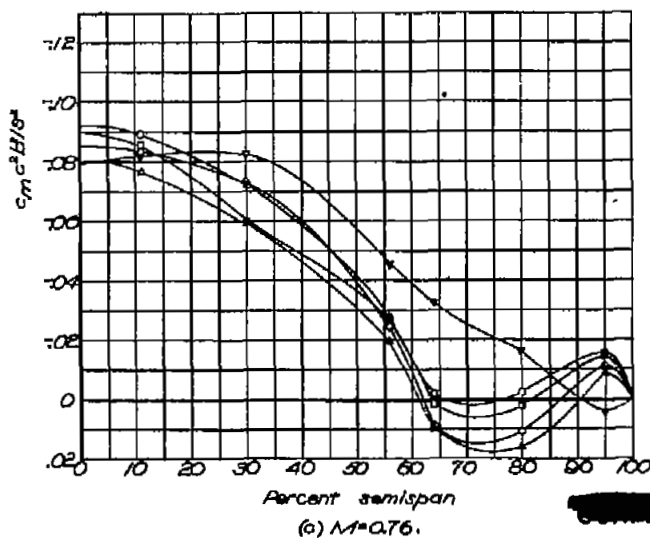
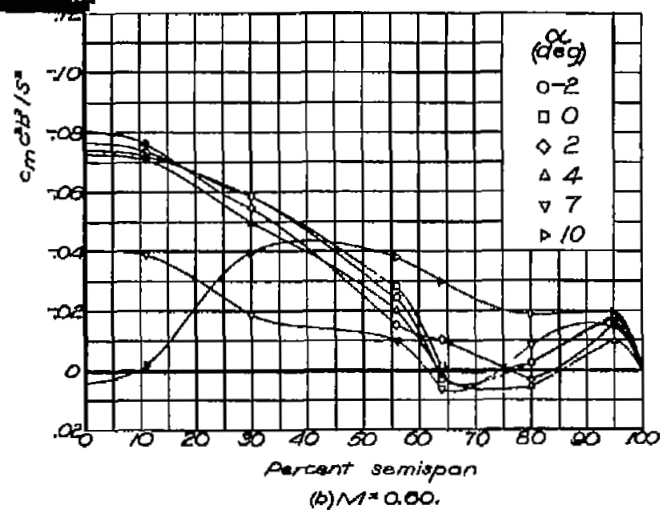
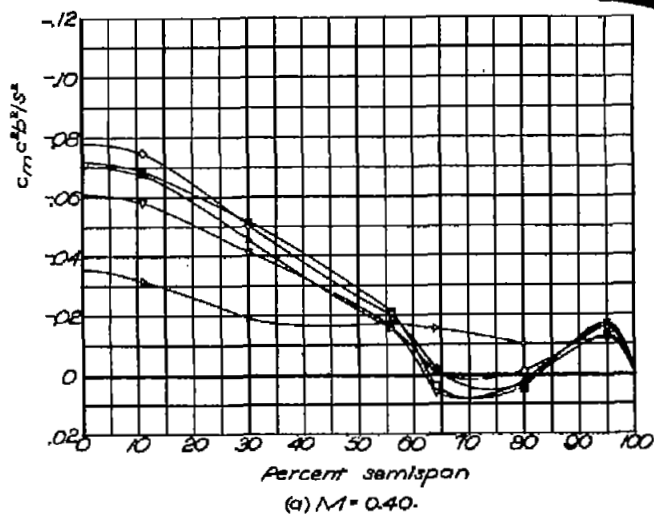


Figure 24.—Spanwise variation in section moment factor. $\delta\alpha=0.5^\circ$;
 $\frac{h_s}{c}=0.03$, $\frac{x_s}{c}=0.70$.

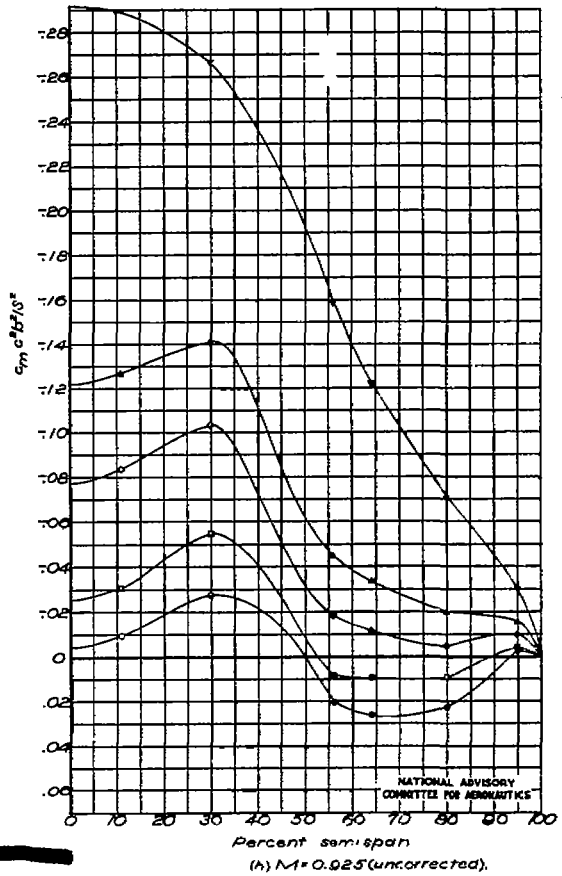
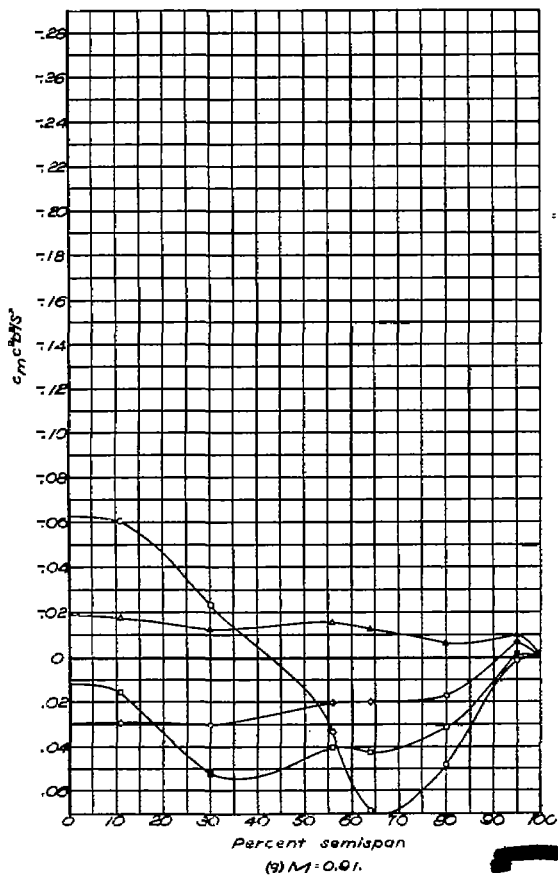
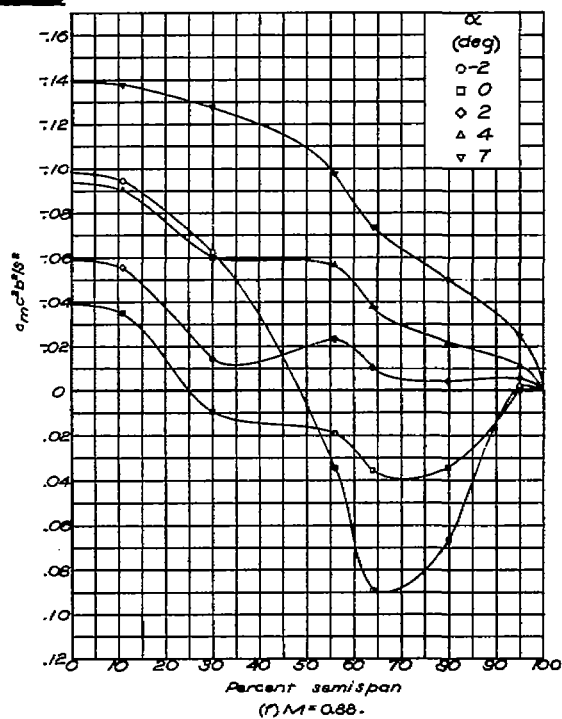
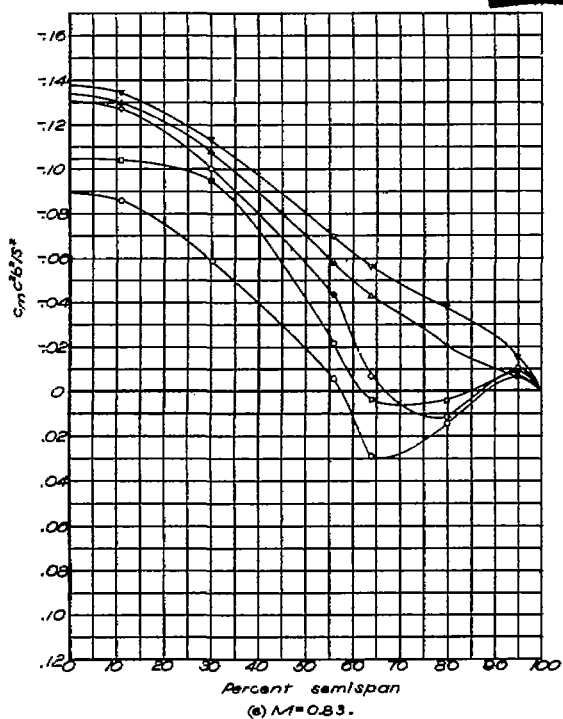


Figure 24 .— Concluded.

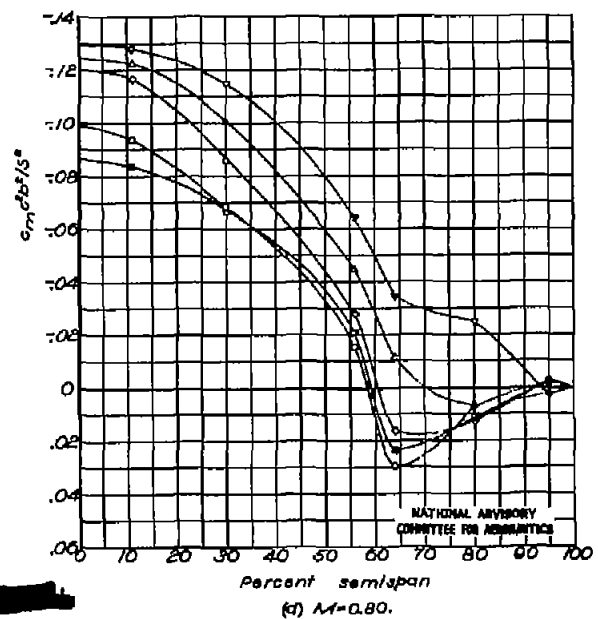
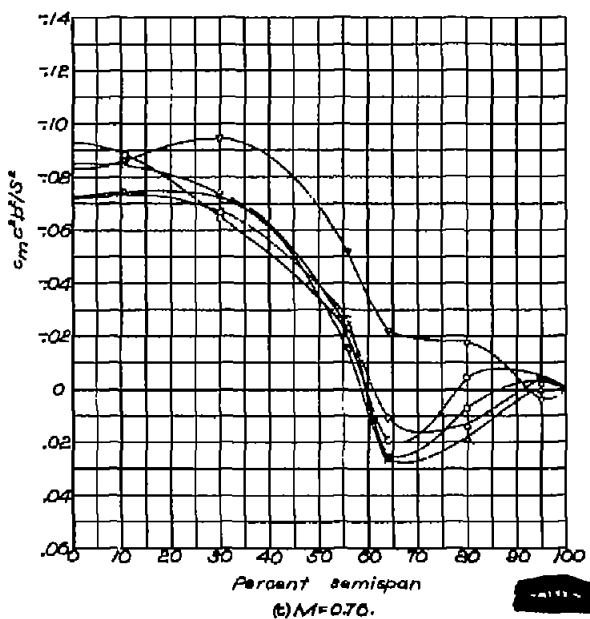
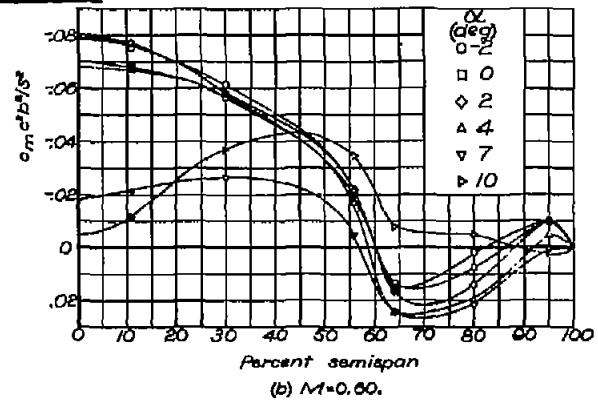
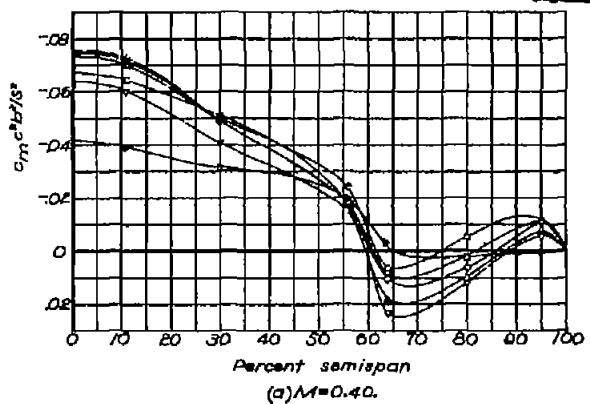


Figure 25. — Spanwise variation in section moment factor. $\delta_a = -3.3^\circ$;
 $\frac{X_2}{c} = 0.03$, $\frac{X_2}{c} = 0.70$.

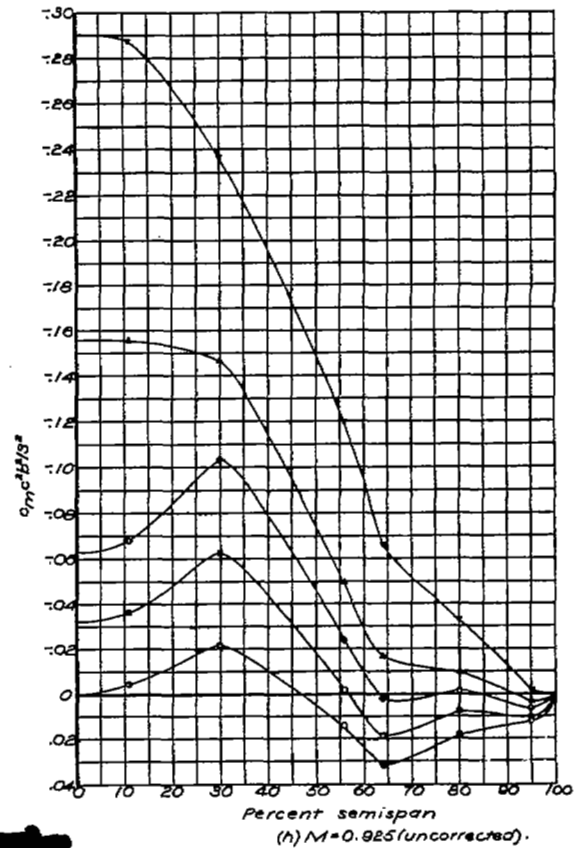
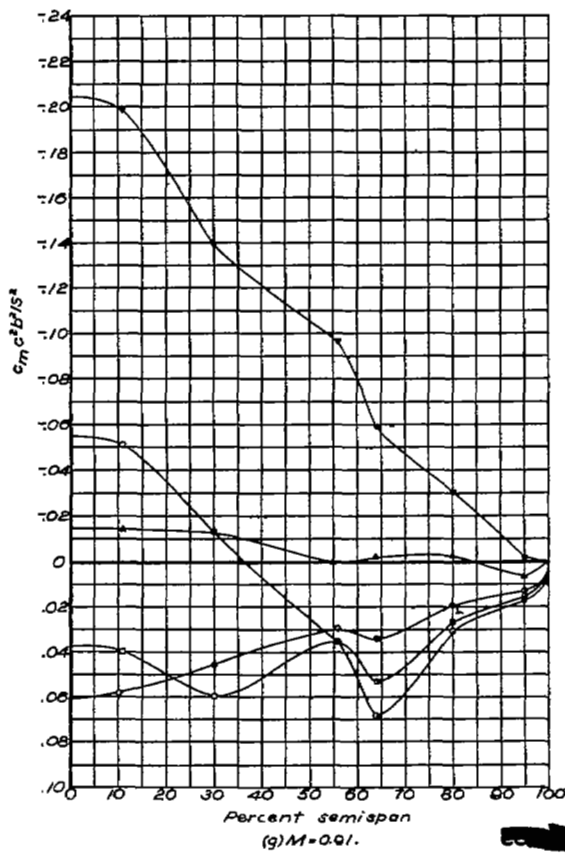
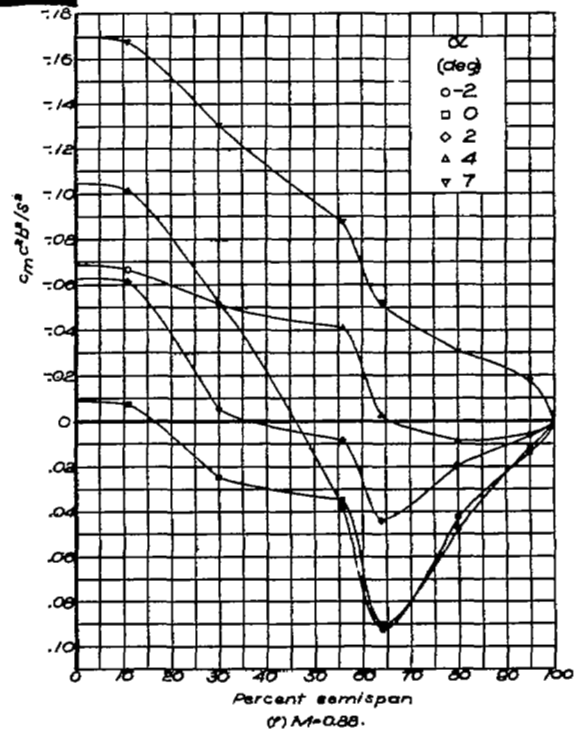
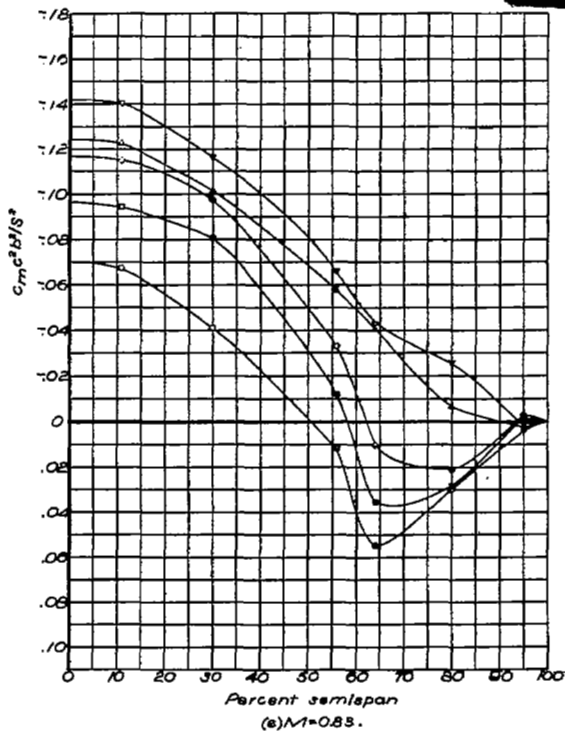


Figure 25.— Concluded.

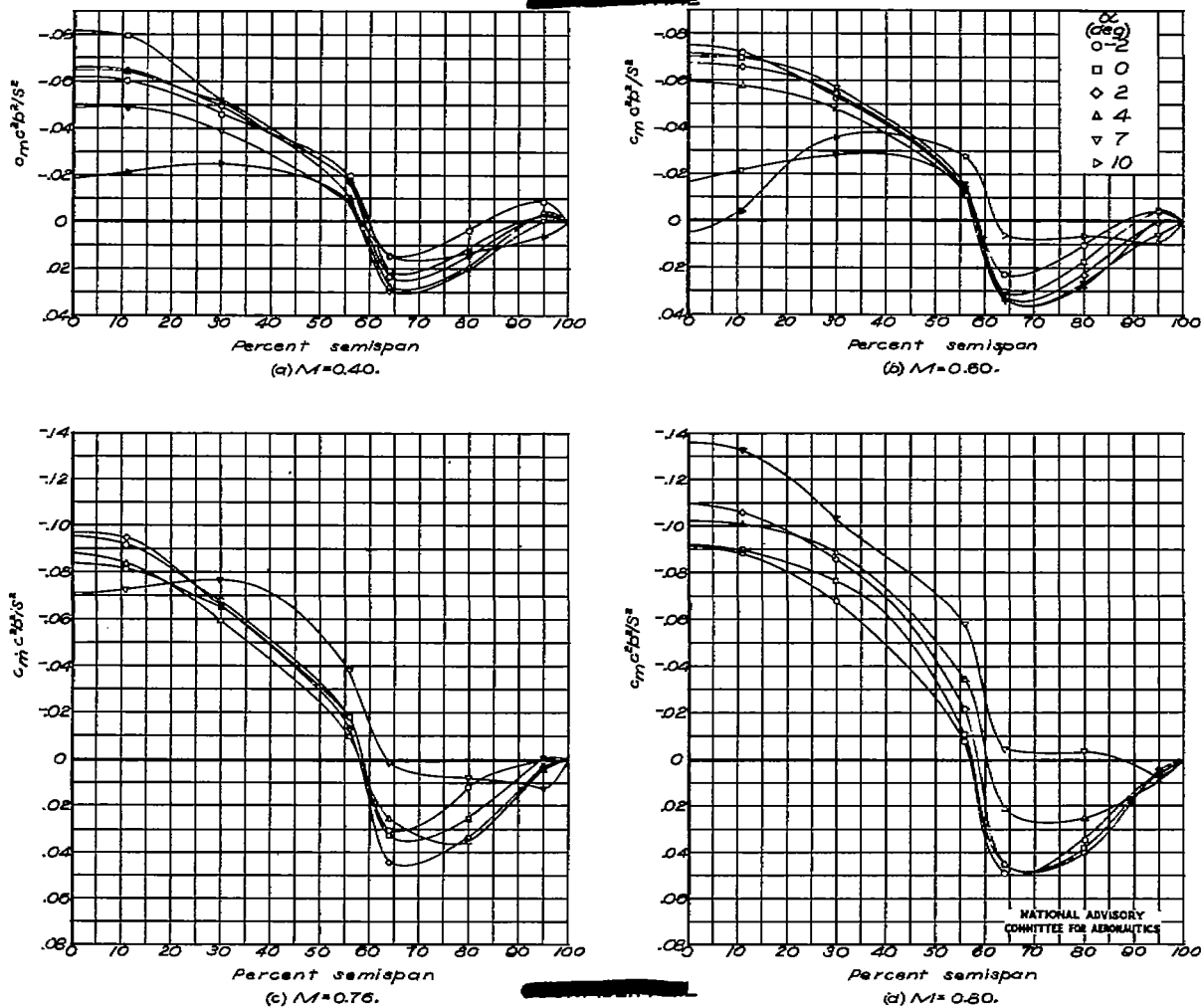


Figure 26.— Spanwise variation in section moment factor. $\delta_a = -5.6^\circ$;
 $\frac{r_s}{c} = 0.03$, $\frac{x_s}{c} = 0.70$.

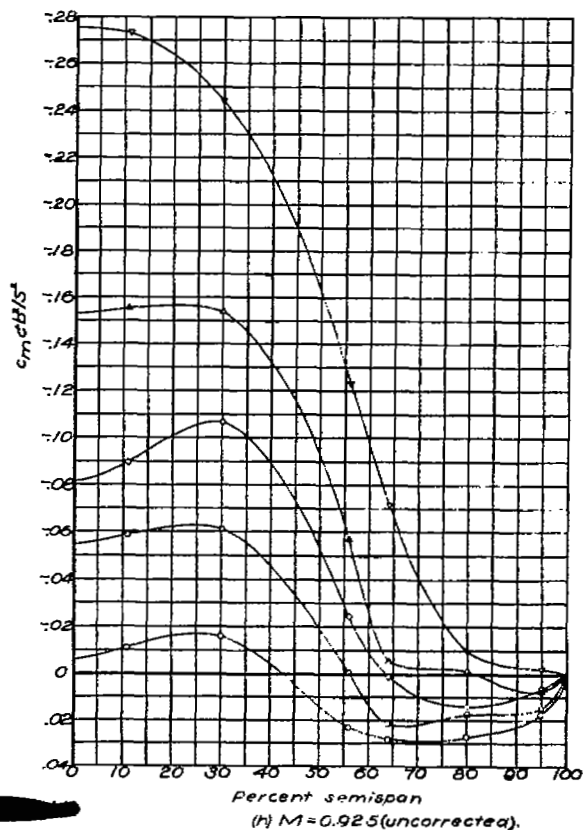
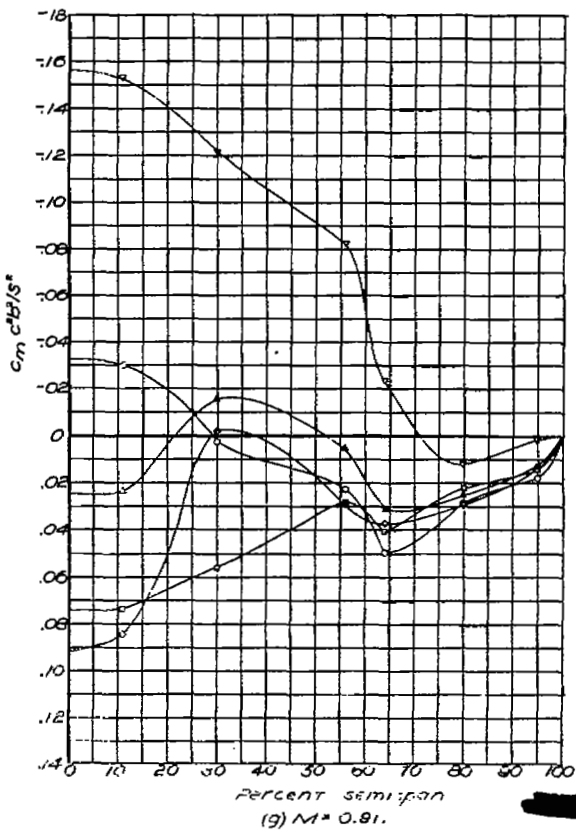
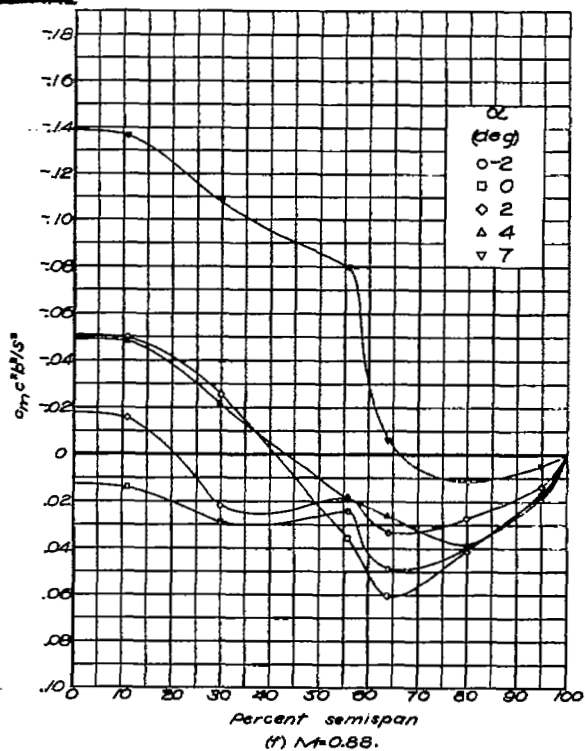
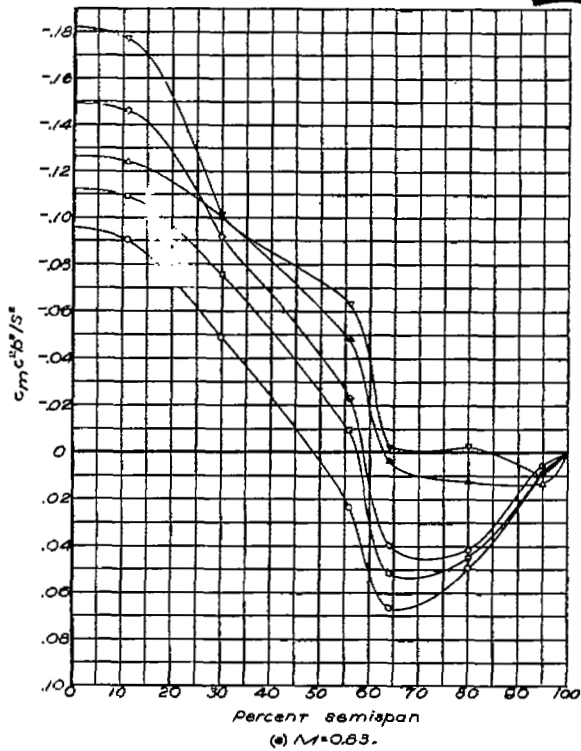


Figure 26. — Concluded.

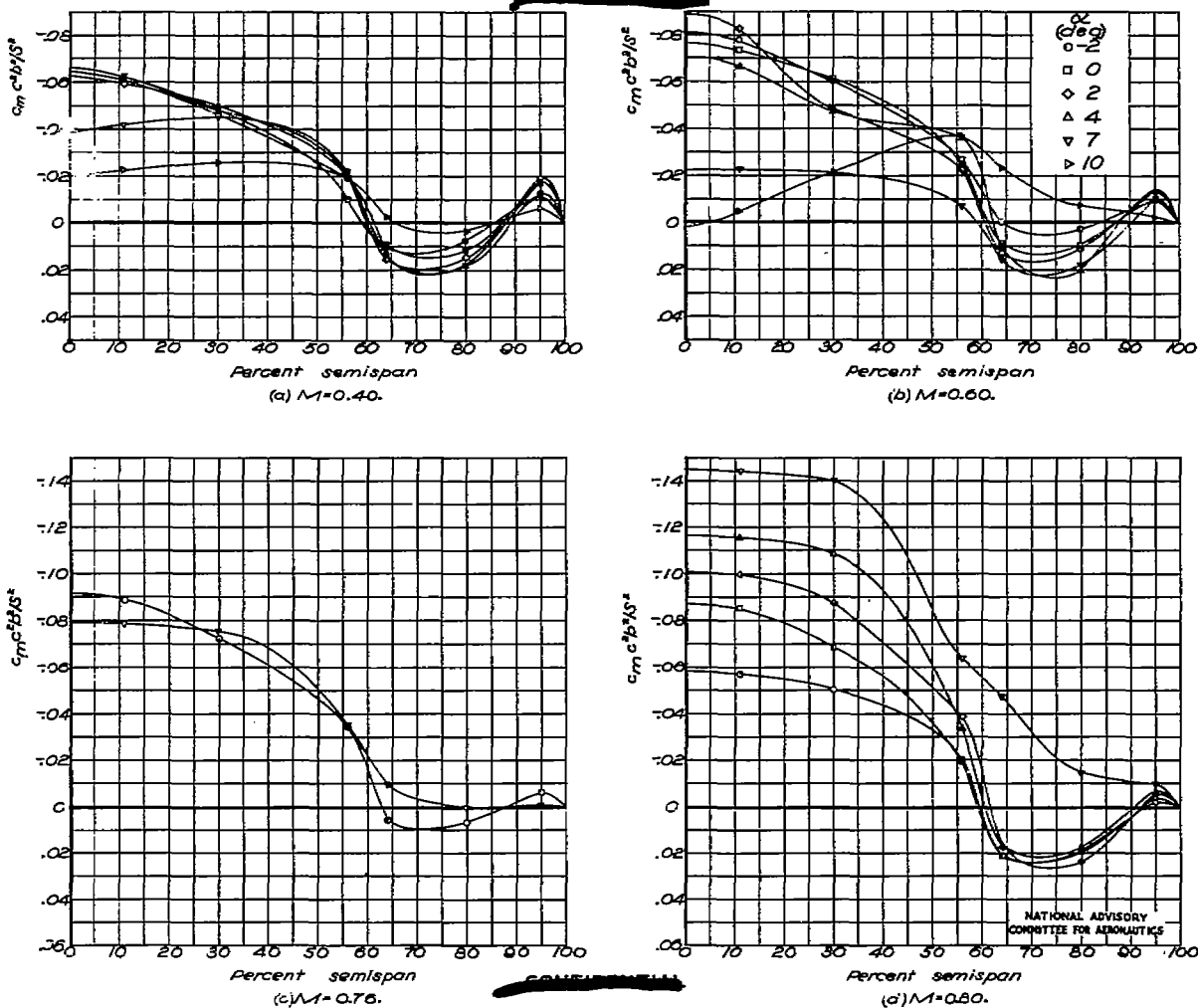


Figure 27.— Spanwise variation in section moment factor. $\delta\alpha=0.0^\circ$;
 $\frac{h_s}{c}=0.06$, $\frac{x_s}{c}=0.70$.

~~CONFIDENTIAL~~

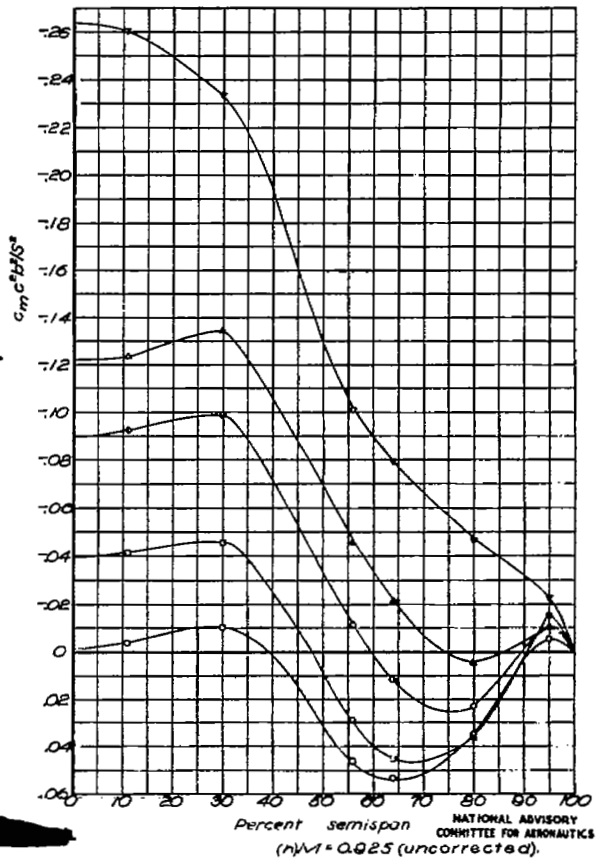
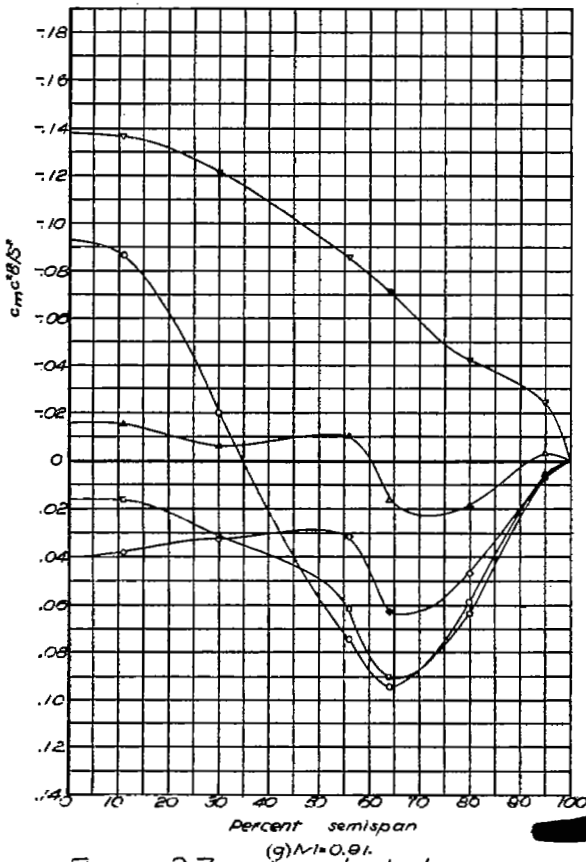
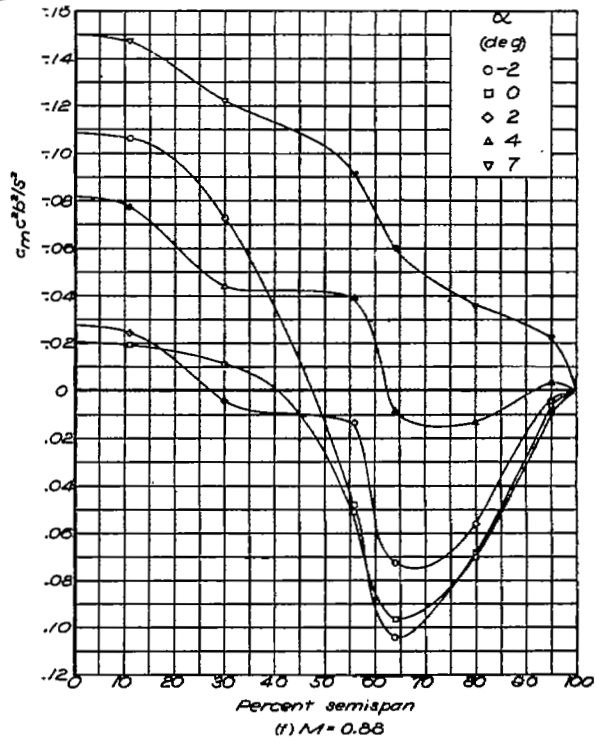
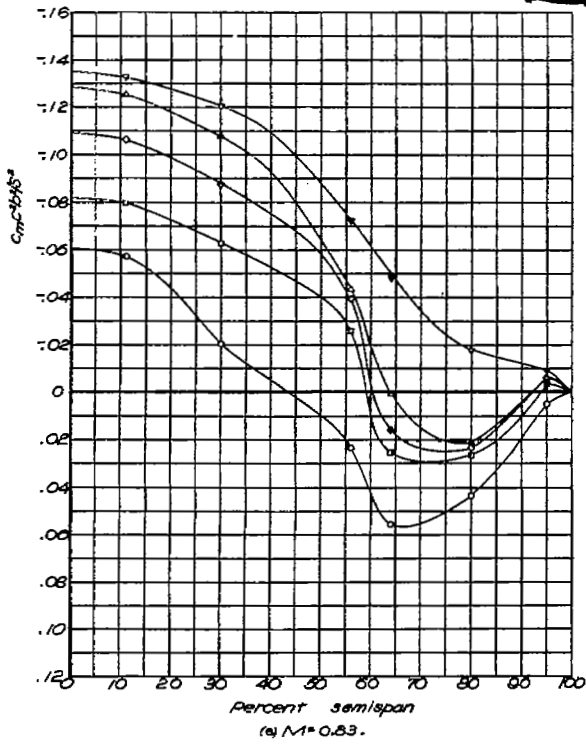


Figure 27. — Concluded.

NATIONAL ADVISORY
COMMITTEE FOR AERONAUTICS

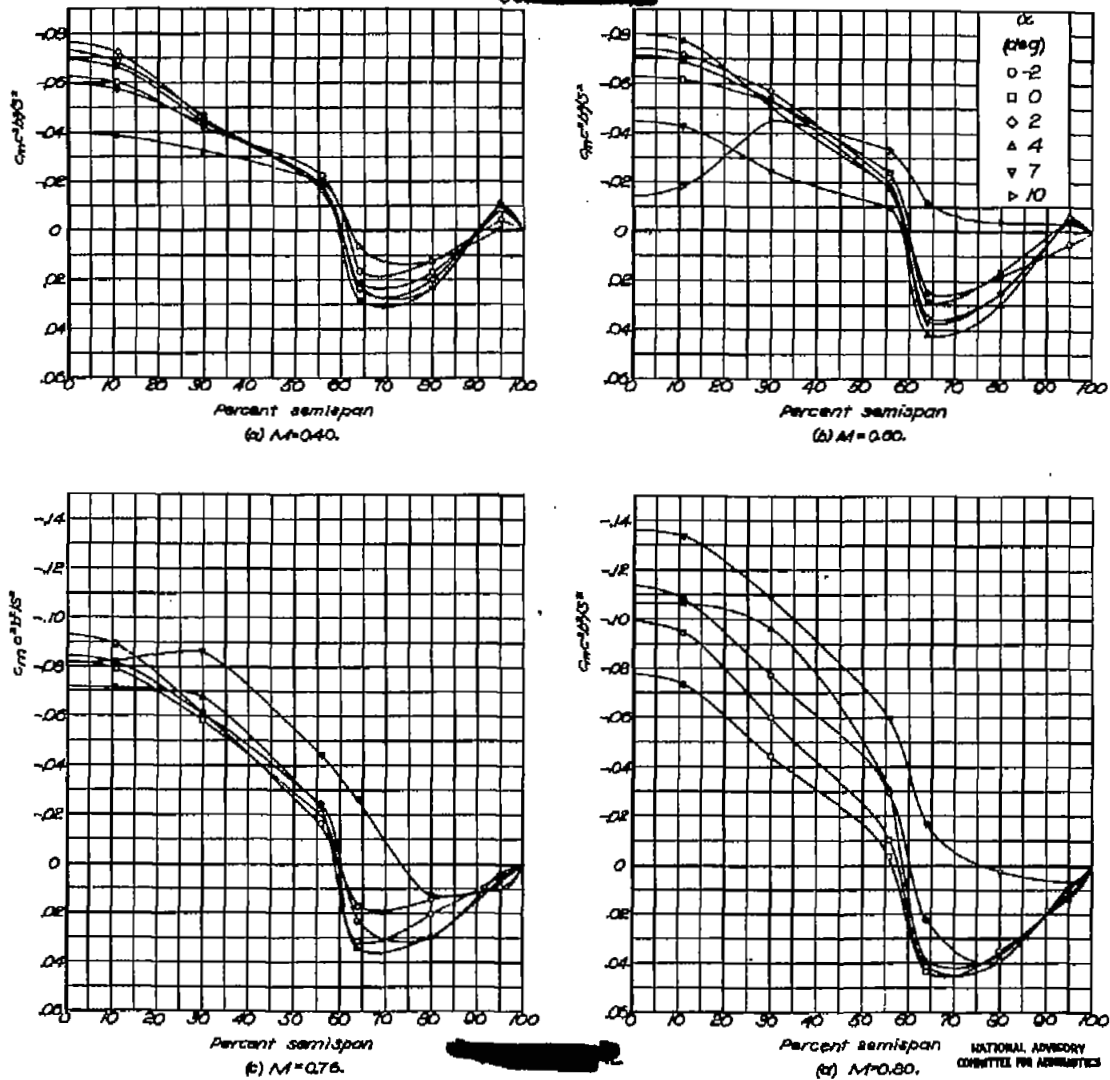


Figure 2B. — Spanwise variation in section moment factor. $\delta_0 = -3.3^\circ$
 $\frac{h_s}{c} = 0.06$, $\frac{x_s}{c} = 0.70$.

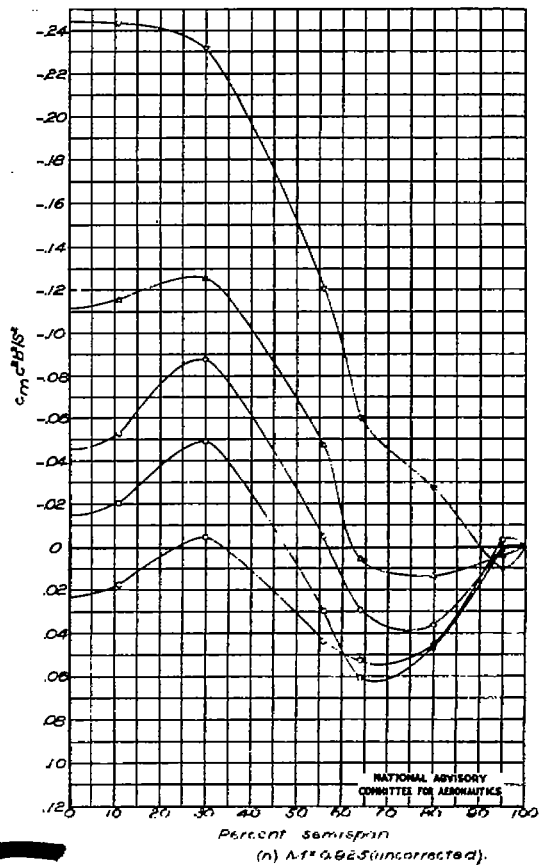
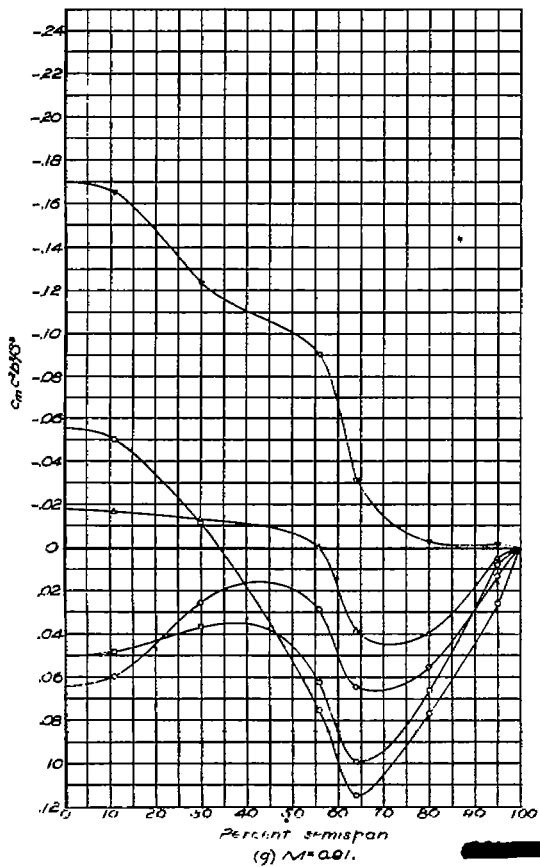
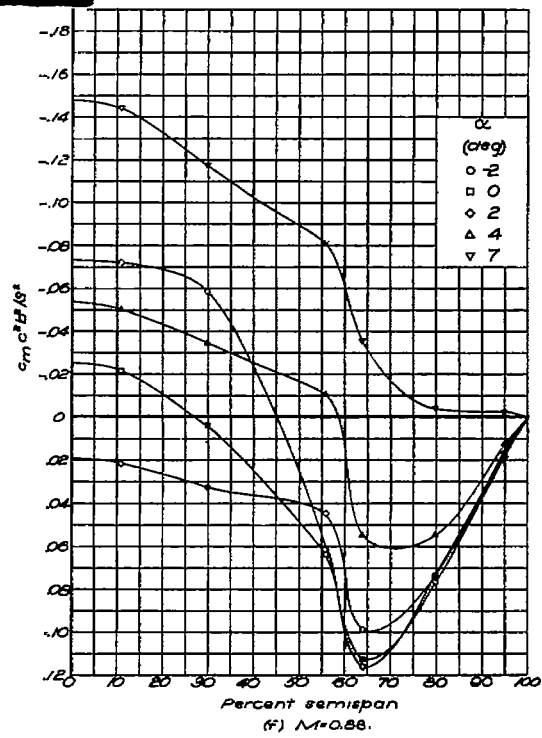
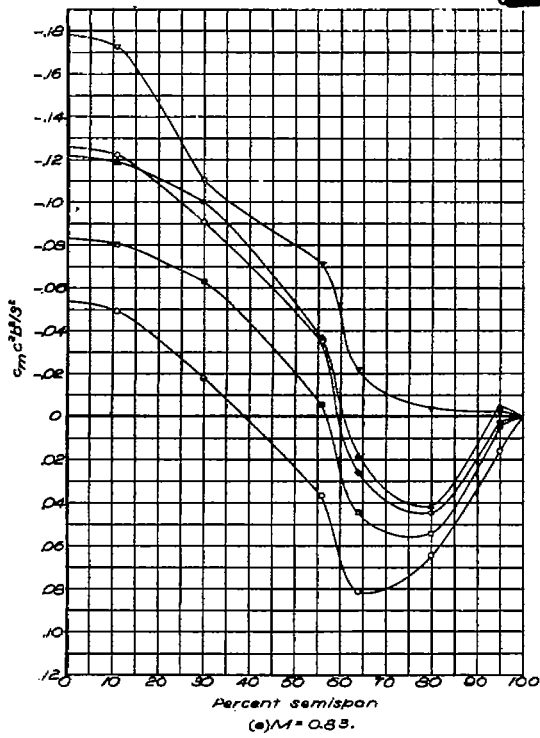
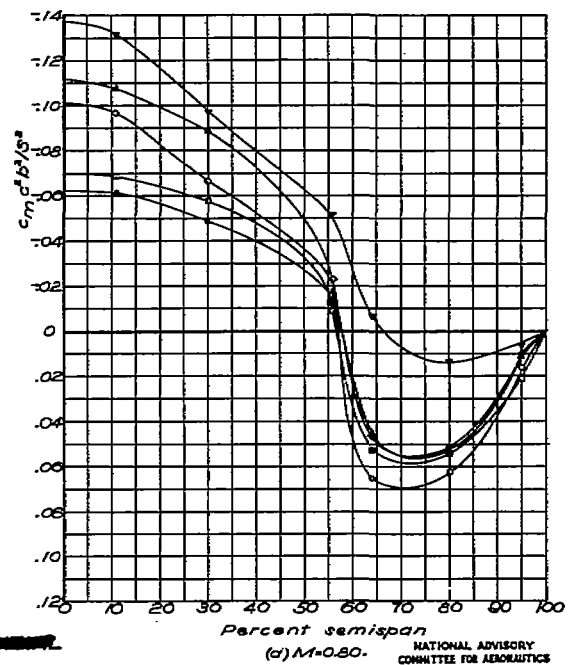
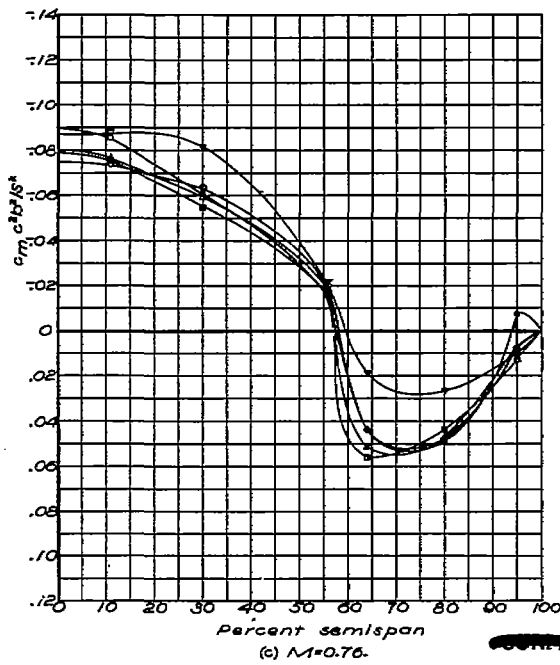
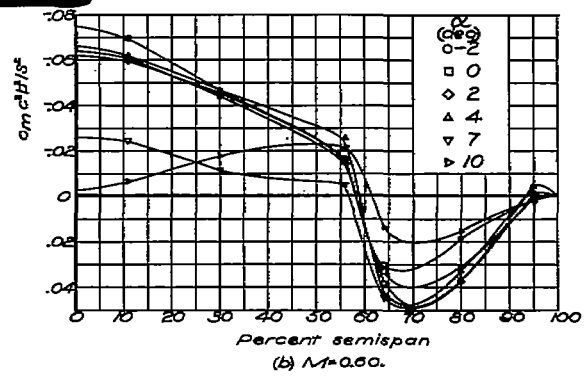
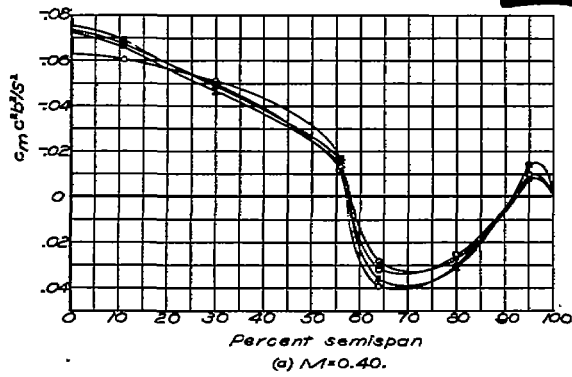


Figure 28. — Concluded.

~~CONFIDENTIAL~~



~~CONFIDENTIAL~~

NATIONAL ADVISORY
COMMITTEE FOR AERONAUTICS

Figure 29.—Spanwise variation in section moment factor. $\delta_a = -5.5^\circ$;
 $\frac{h_s}{c} = 0.06$, $\frac{x_s}{c} = 0.70$.

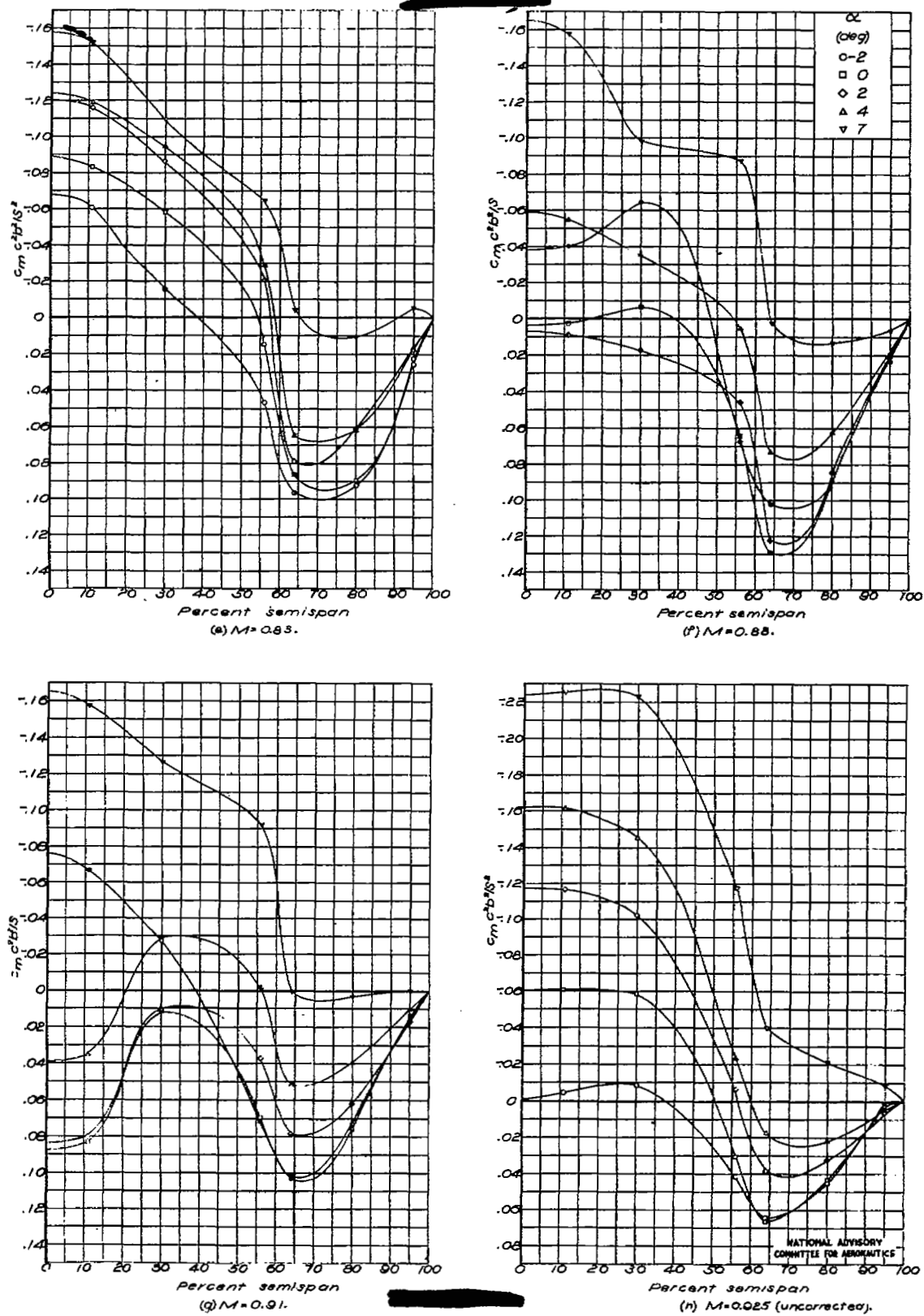


Figure 29.—Concluded.

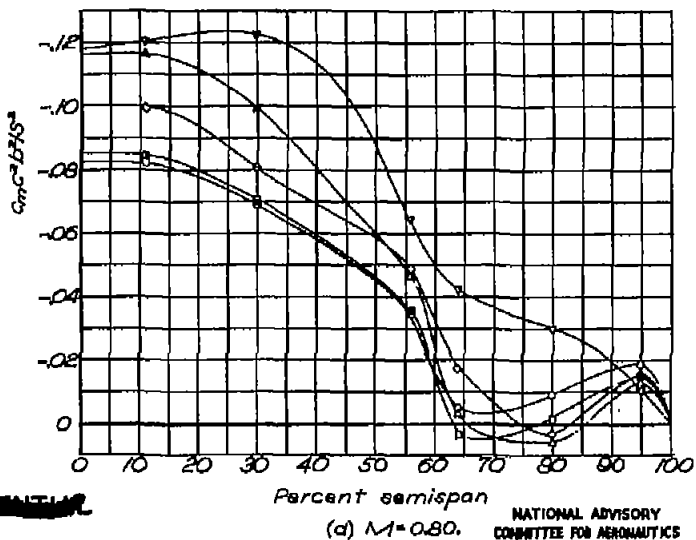
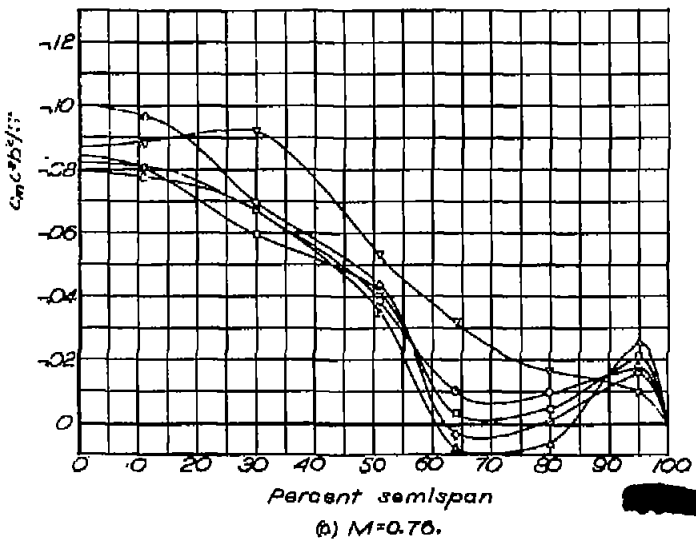
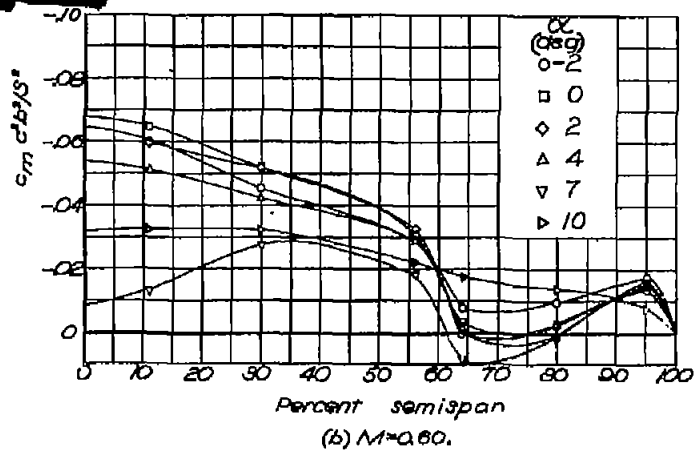
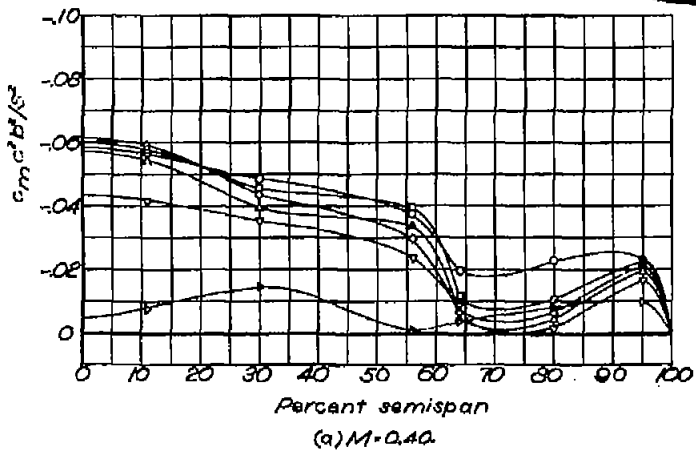


Figure 30.—Spanwise variation in section moment factor. $\delta\alpha=0.0^\circ$;
 $\frac{h_s}{c}=0.03$, $\frac{x_s}{c}=0.60$.

NATIONAL ADVISORY
 COMMITTEE FOR AERONAUTICS

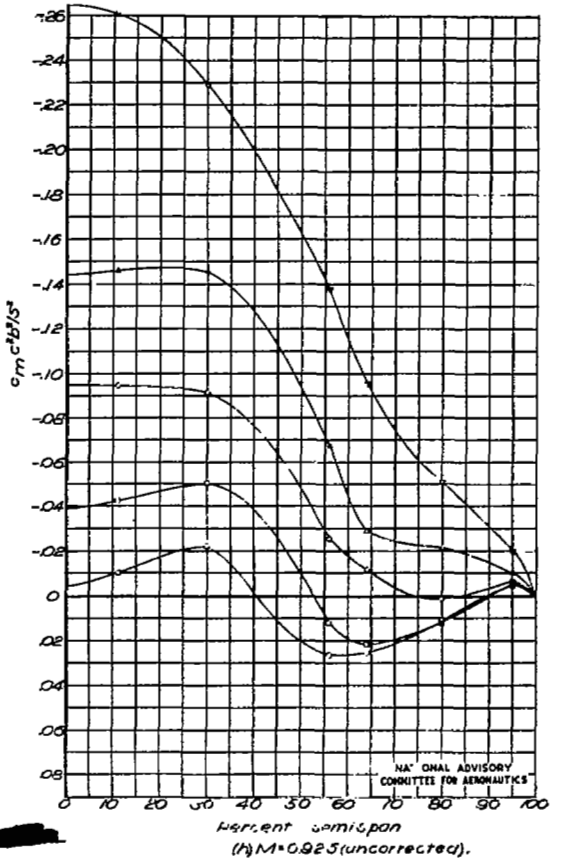
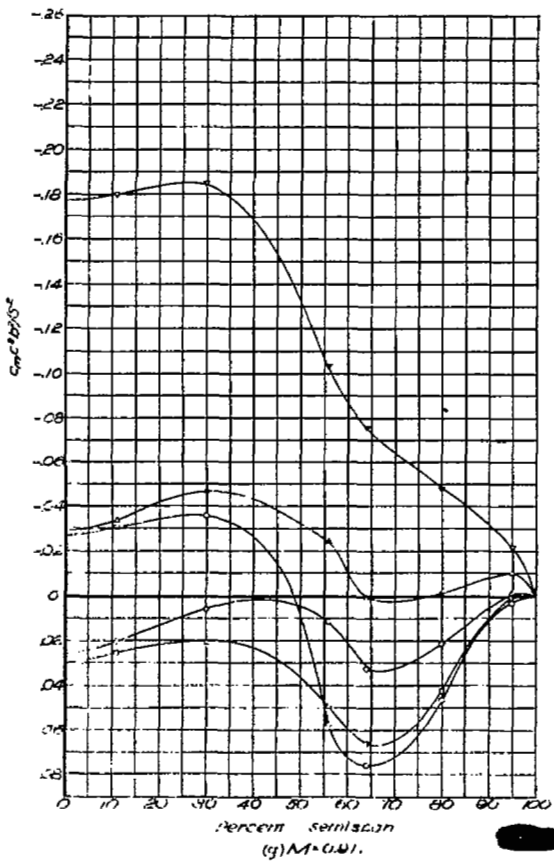
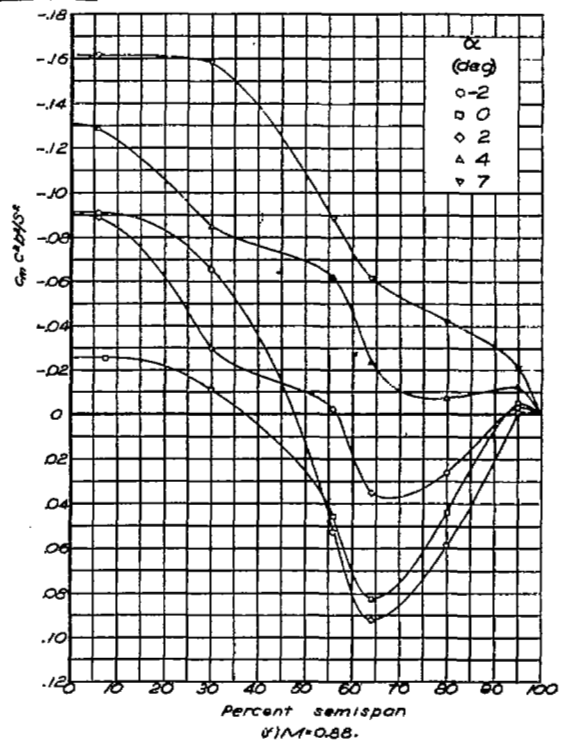
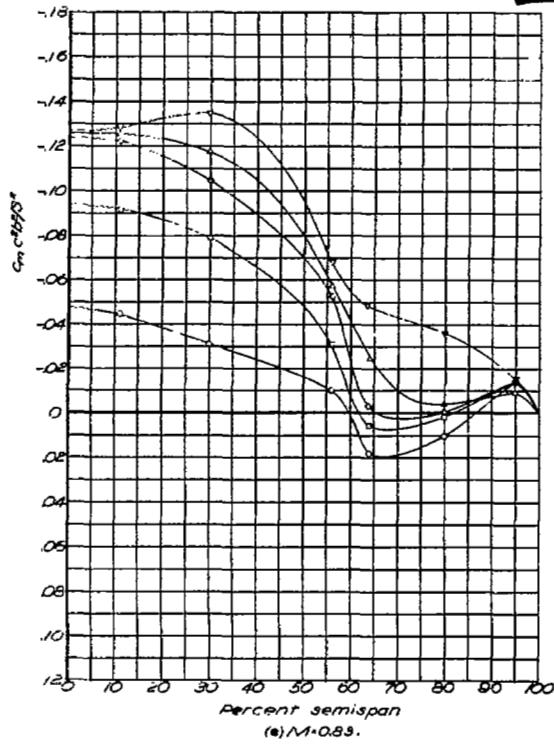


Figure 30. — Continued.

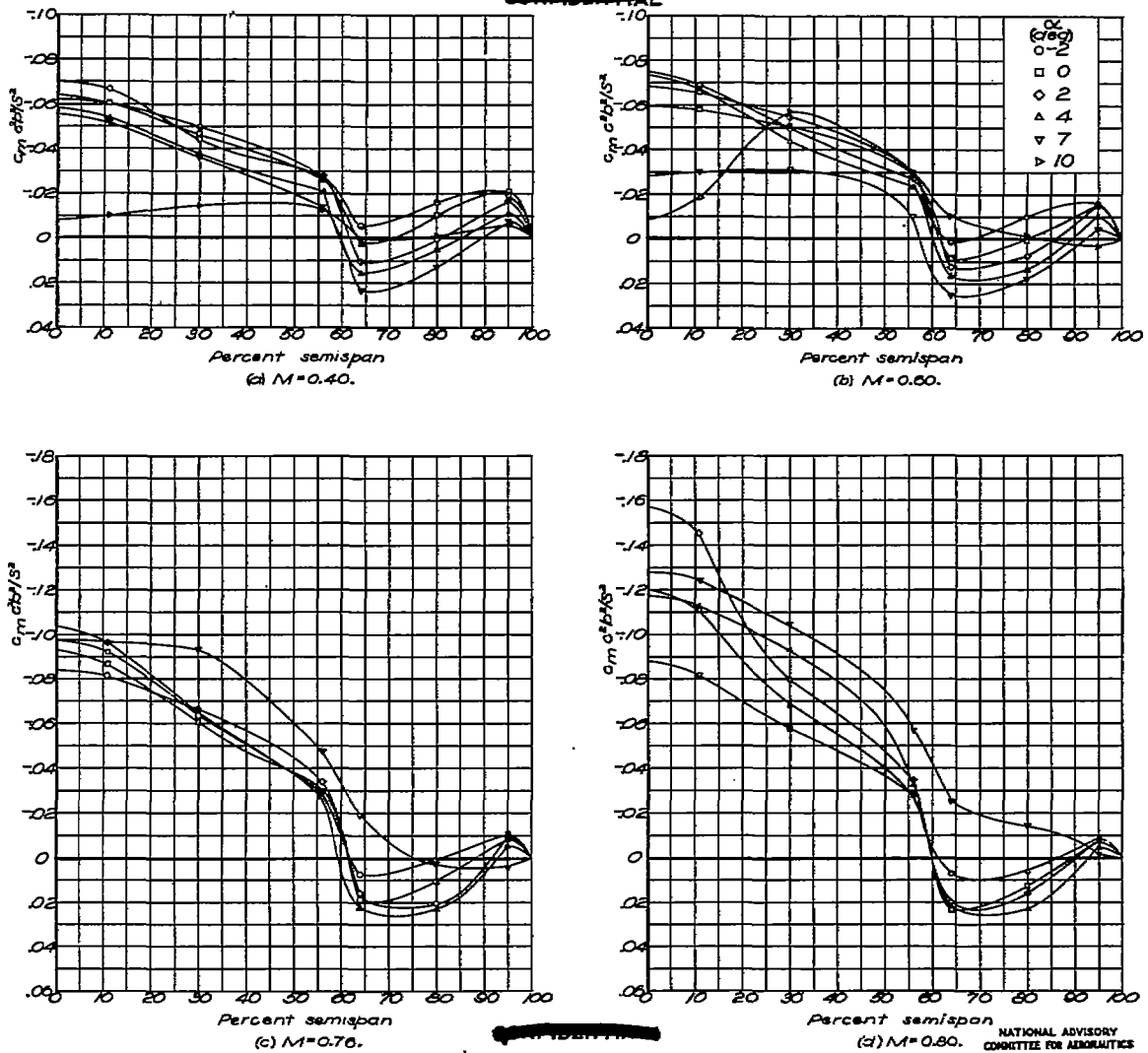


Figure 31.— Spanwise variation in section moment factor. $\delta_q = -3.3$;
 $\frac{h_s}{c} = 0.03$; $\frac{x_s}{c} = 0.60$.

NATIONAL ADVISORY
 COMMITTEE FOR AERONAUTICS

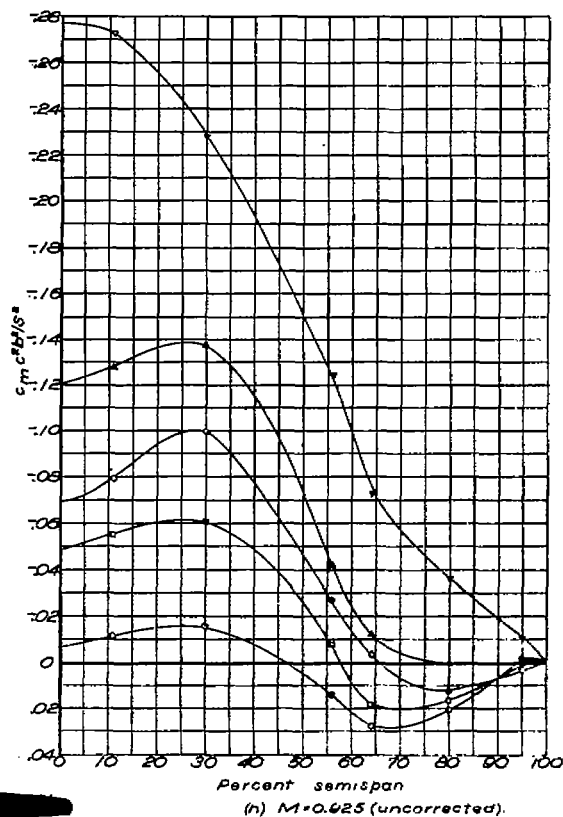
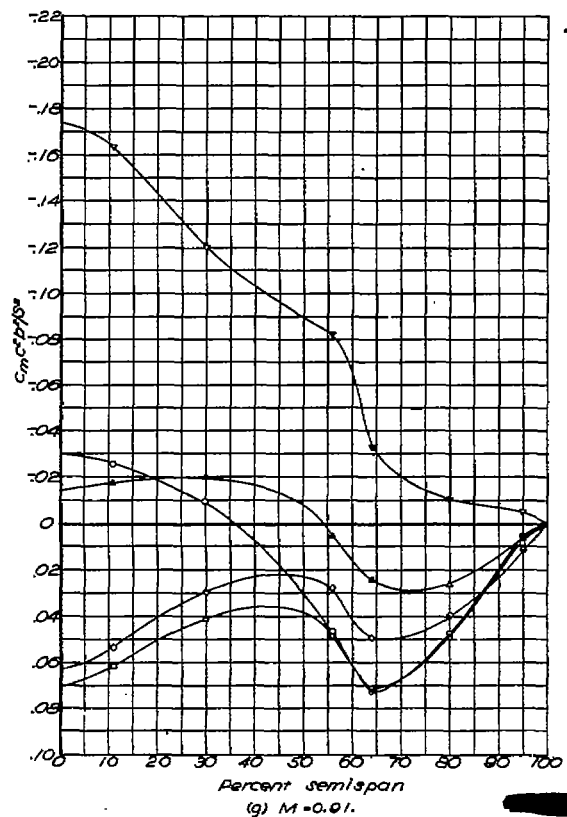
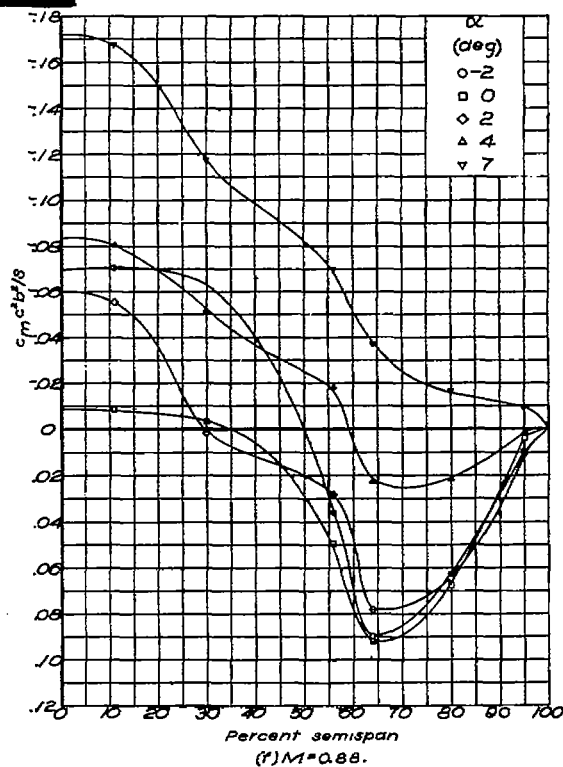
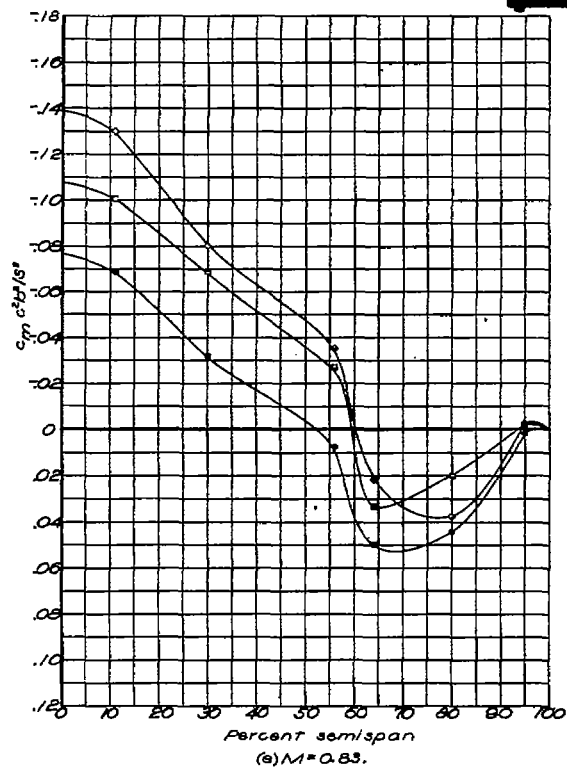


Figure 31 .— Concluded.

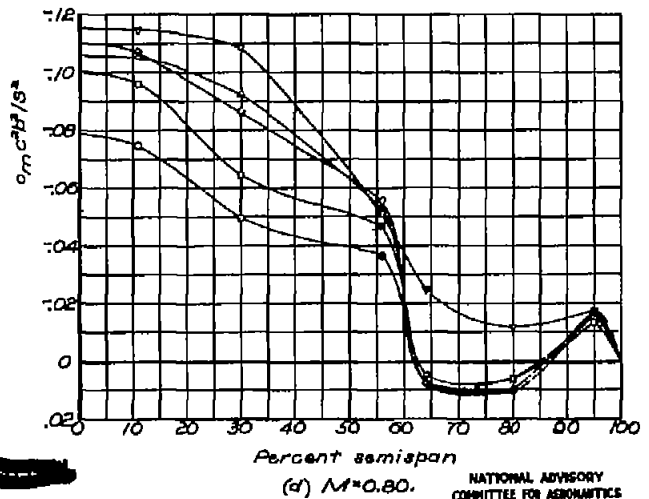
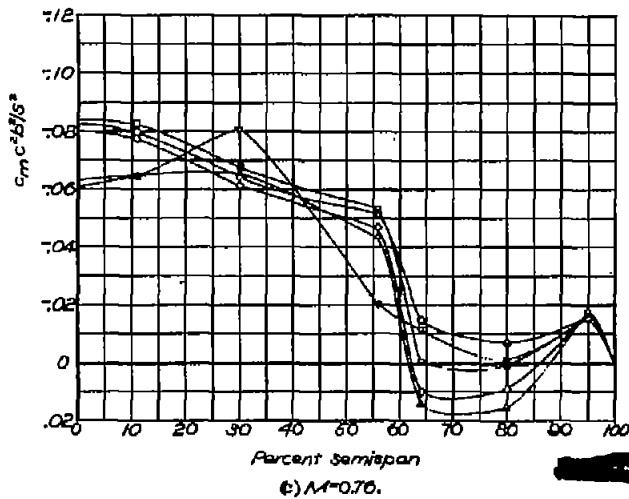
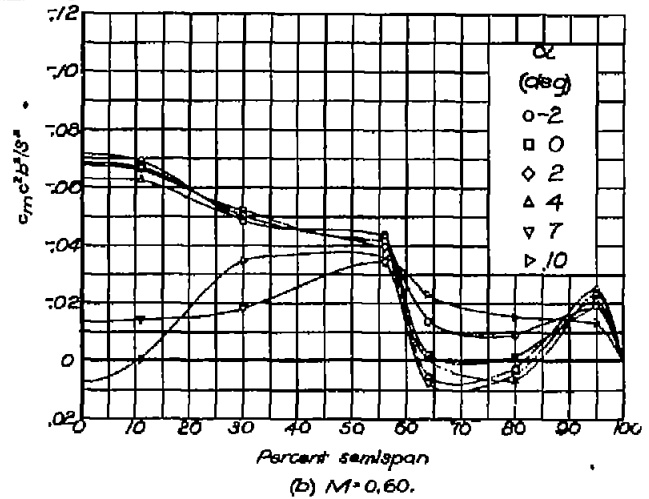
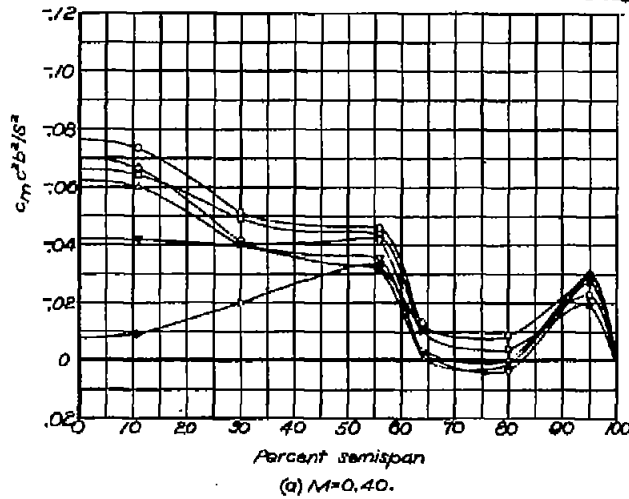


Figure 32. — Spanwise variation in section moment factor. $\delta_a=0.0^\circ$ for $M \leq 0.76$, $\delta_a=-0.3^\circ$ for $M \geq 0.80$; $\frac{h_s}{c}=0.06$, $\frac{x_s}{c}=0.60$.

NATIONAL ADVISORY COMMITTEE FOR AERONAUTICS

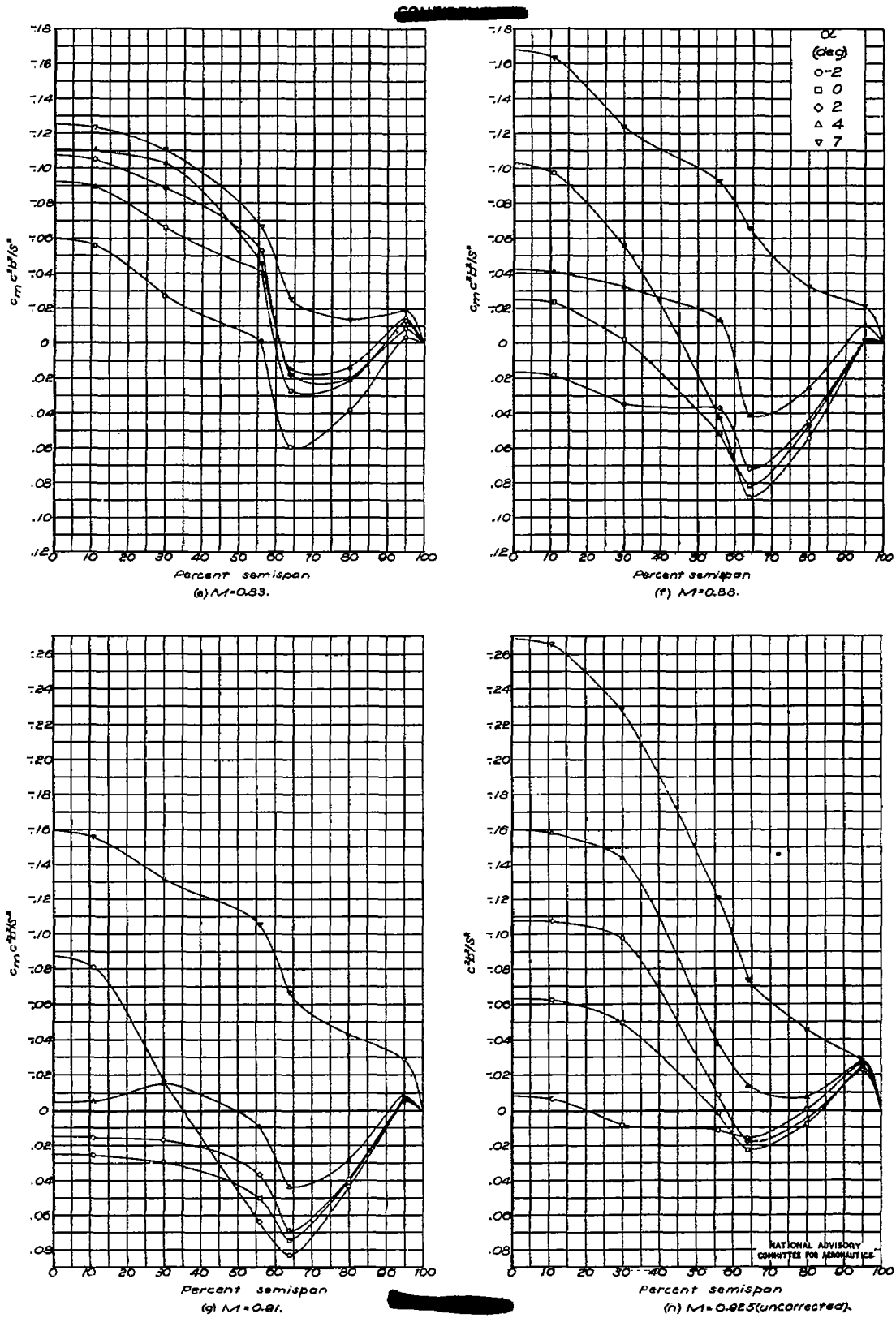


Figure 32.— Concluded.

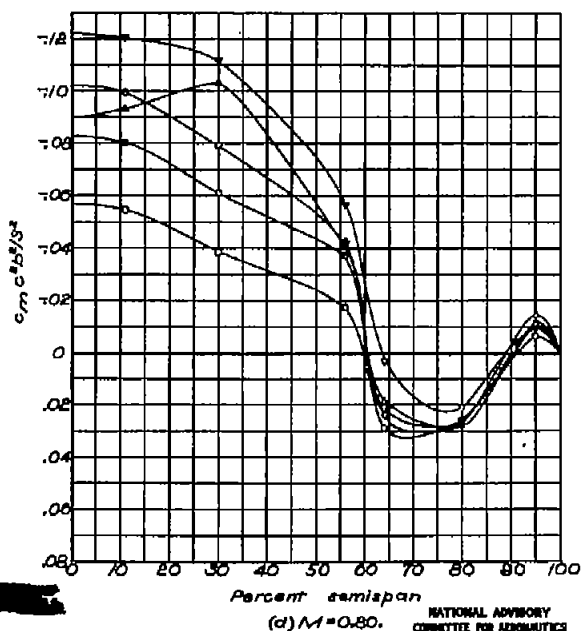
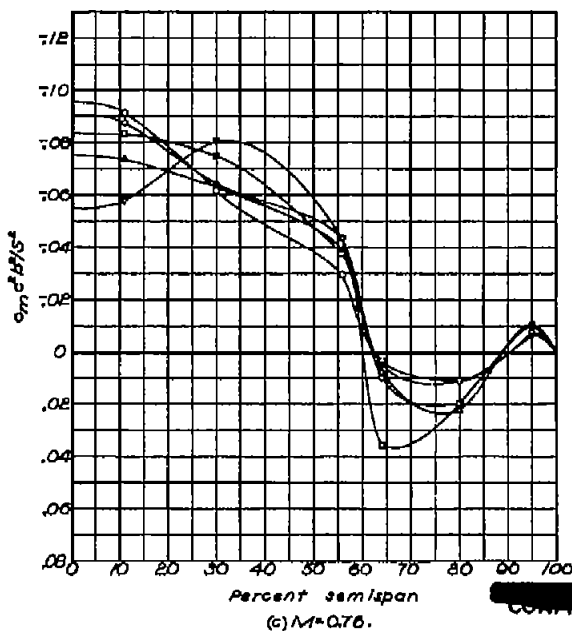
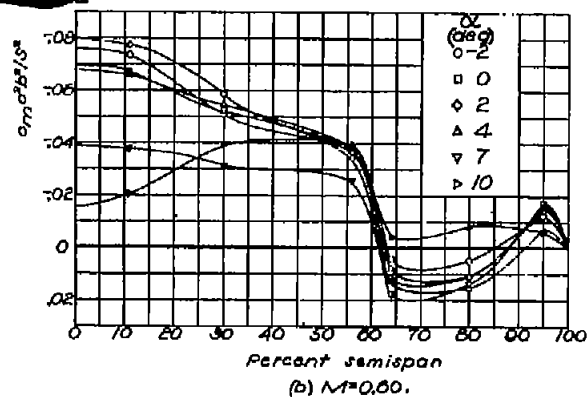
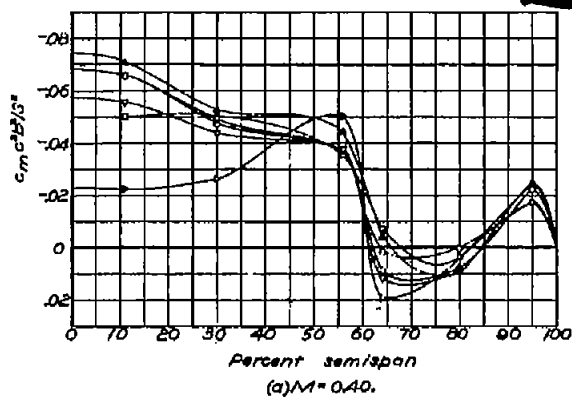


Figure 33.—Spanwise variation in section moment factor. $\delta\alpha = -3.3^\circ$; $\frac{h_s}{c} = 0.06$, $\frac{x_s}{c} = 0.60$.

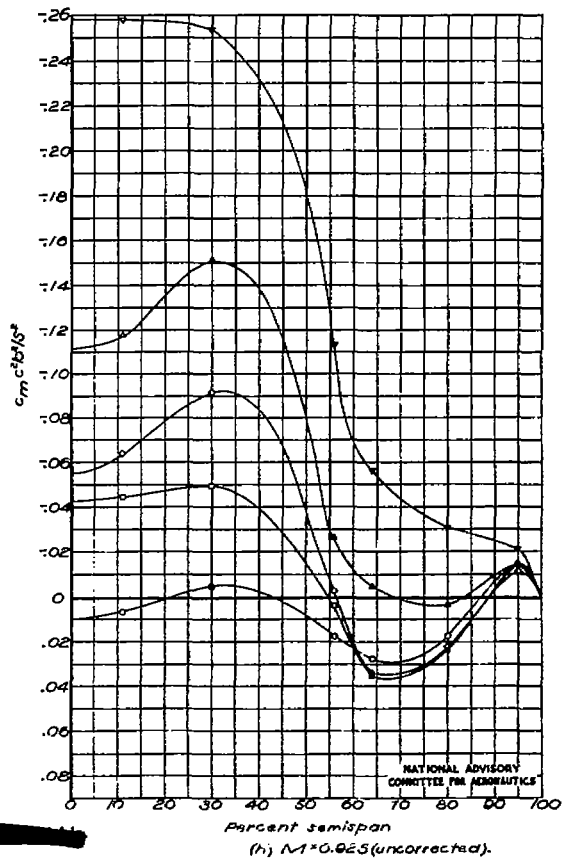
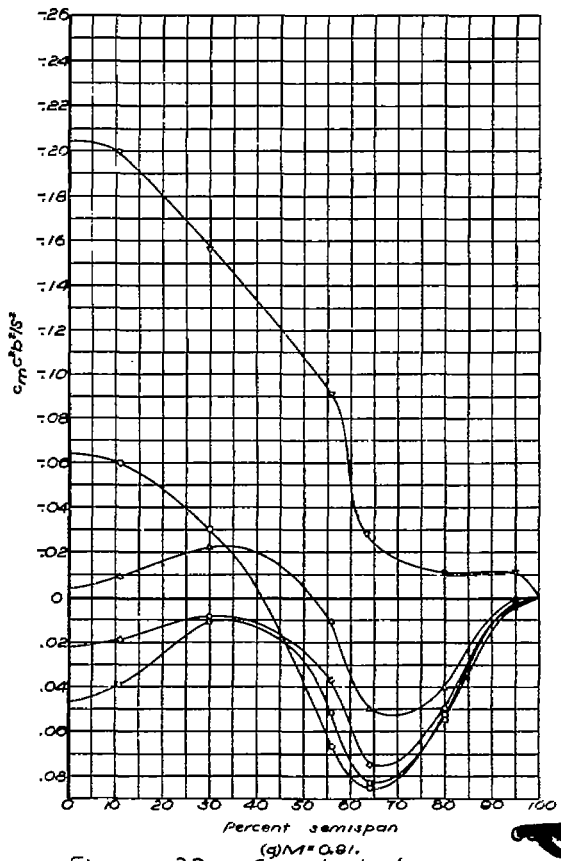
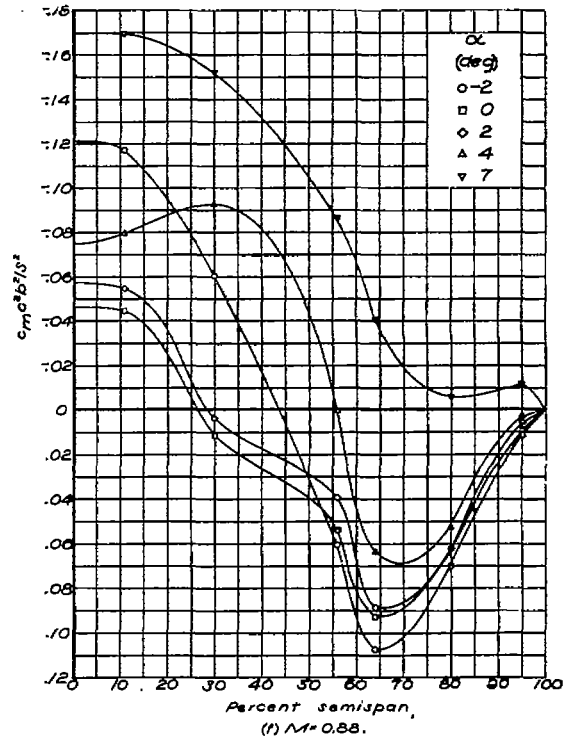
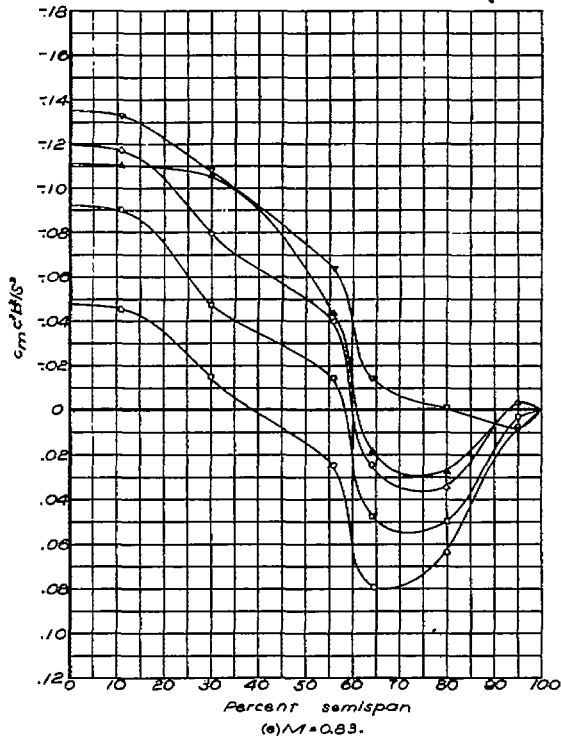
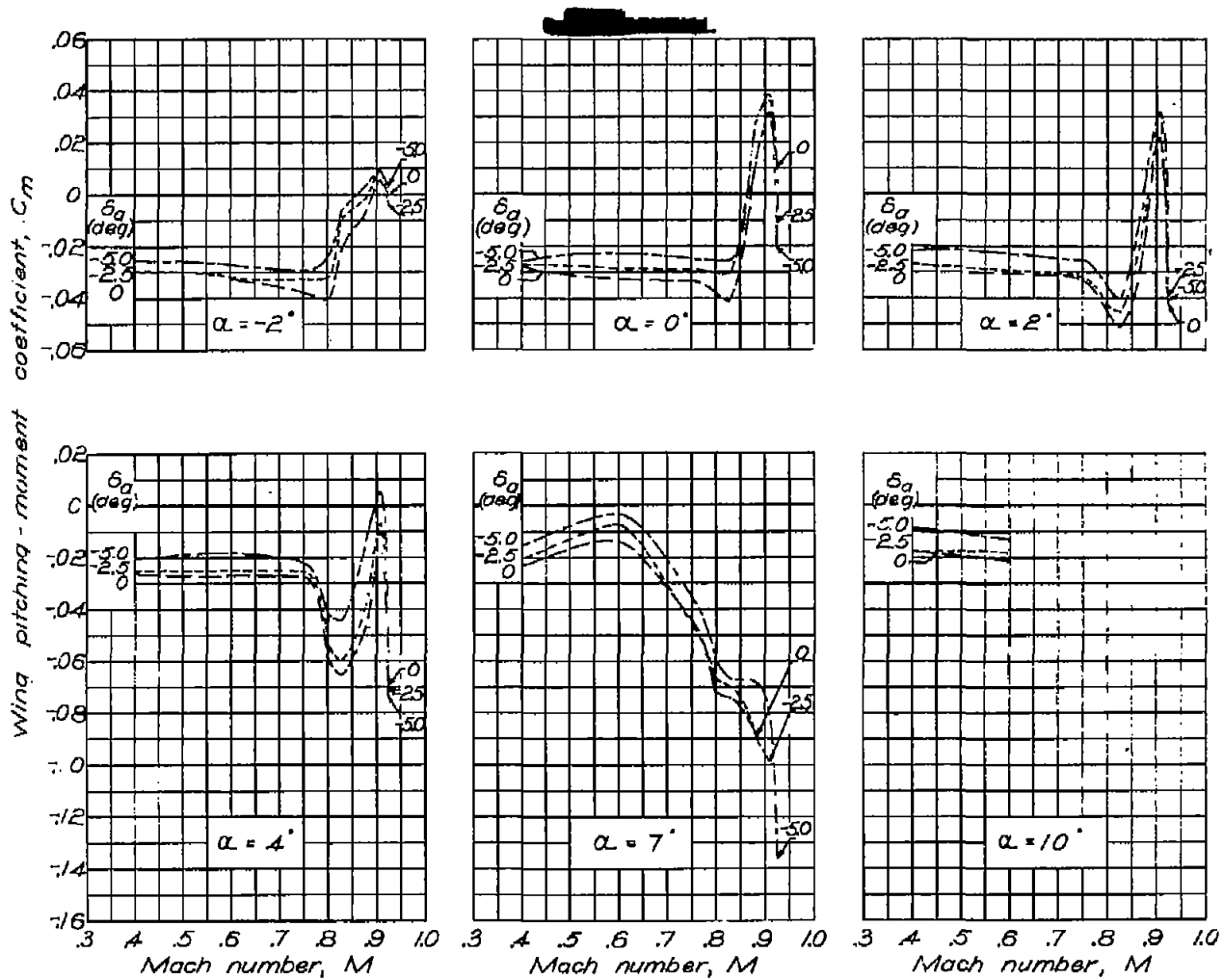


Figure 33.—Concluded.

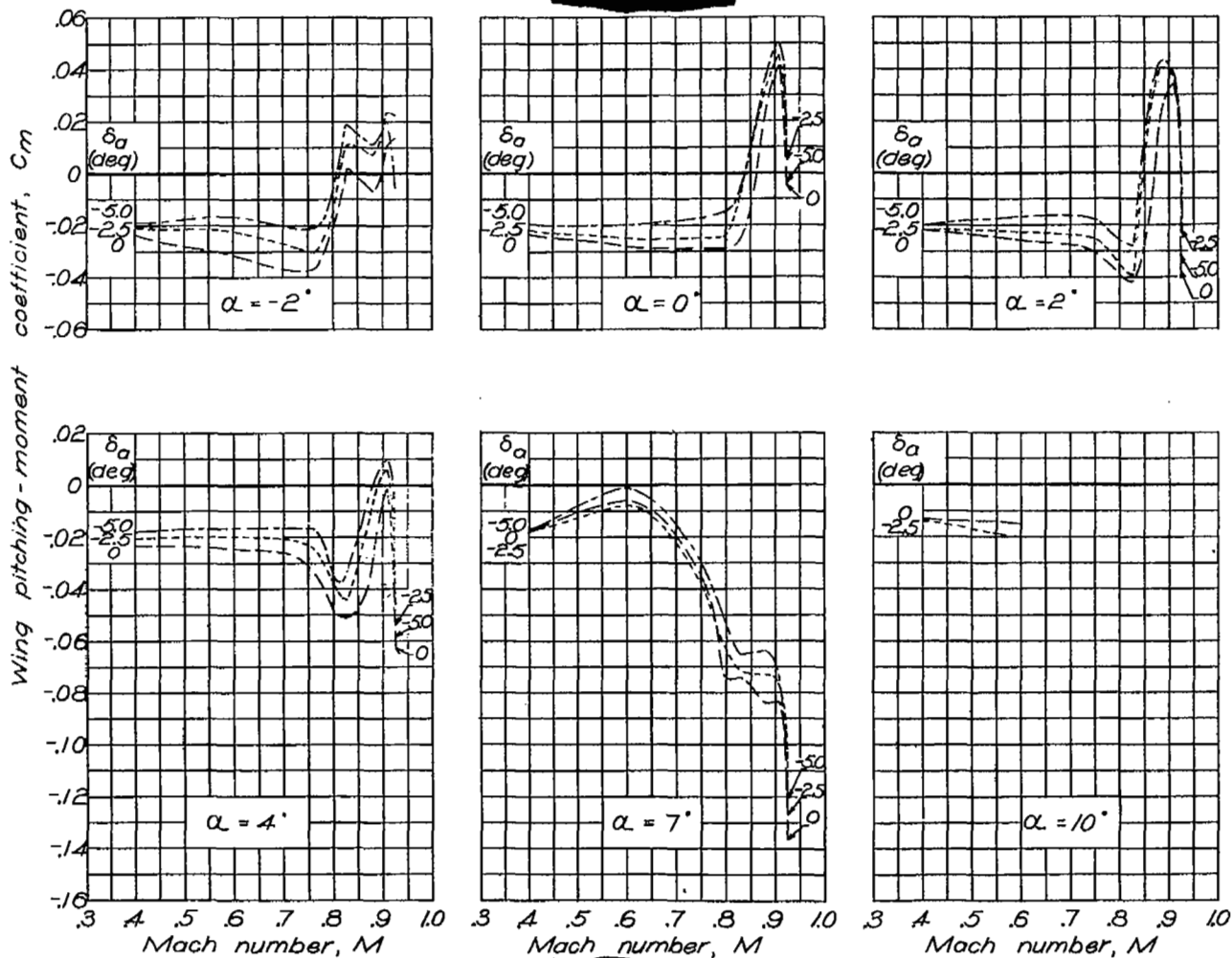
NATIONAL ADVISORY
COMMITTEE FOR AERONAUTICS



(a) $\frac{h_s}{c} = 0.03$; $\frac{x_s}{c} = 0.70$.

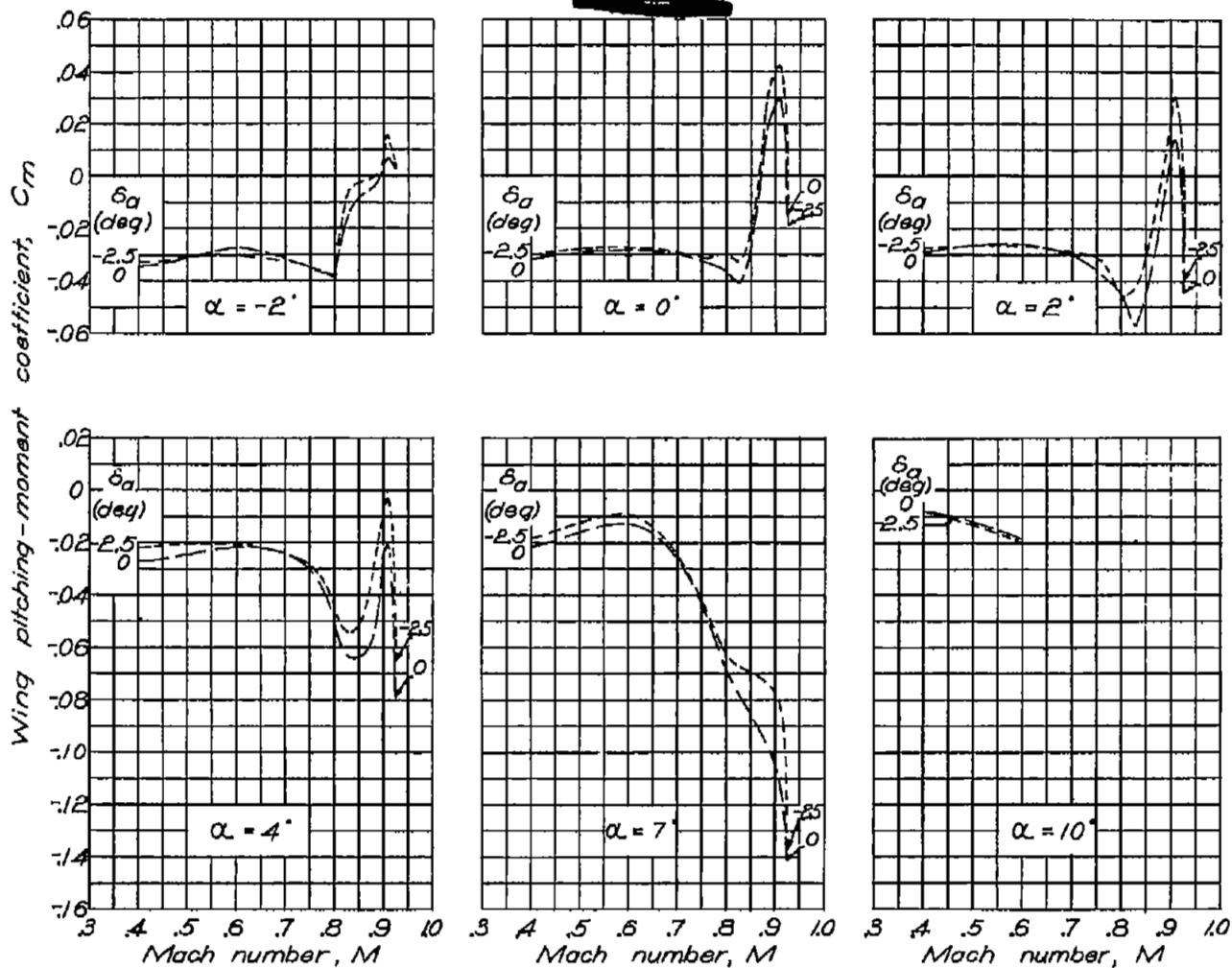
NATIONAL ADVISORY
COMMITTEE FOR AERONAUTICS

Figure 34.—Variation of wing pitching-moment coefficient with Mach number.



(b) $\frac{h_s}{c} = 0.06$; $\frac{x_s}{c} = 0.70$.

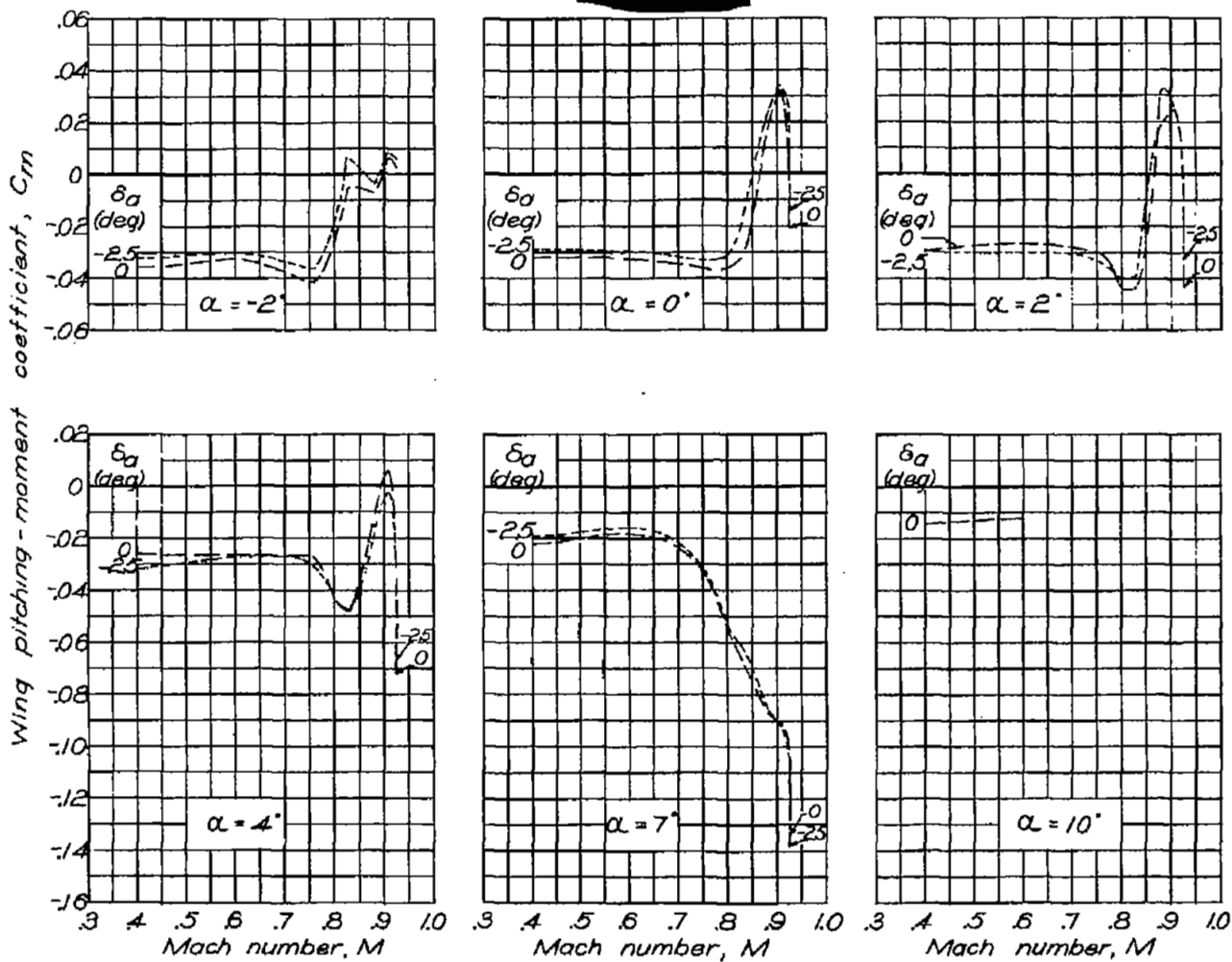
Figure 34. — Continued.



(c) $\frac{h_s}{c} = 0.03$; $\frac{x_s}{c} = 0.60$.

NATIONAL ADVISORY
COMMITTEE FOR AERONAUTICS

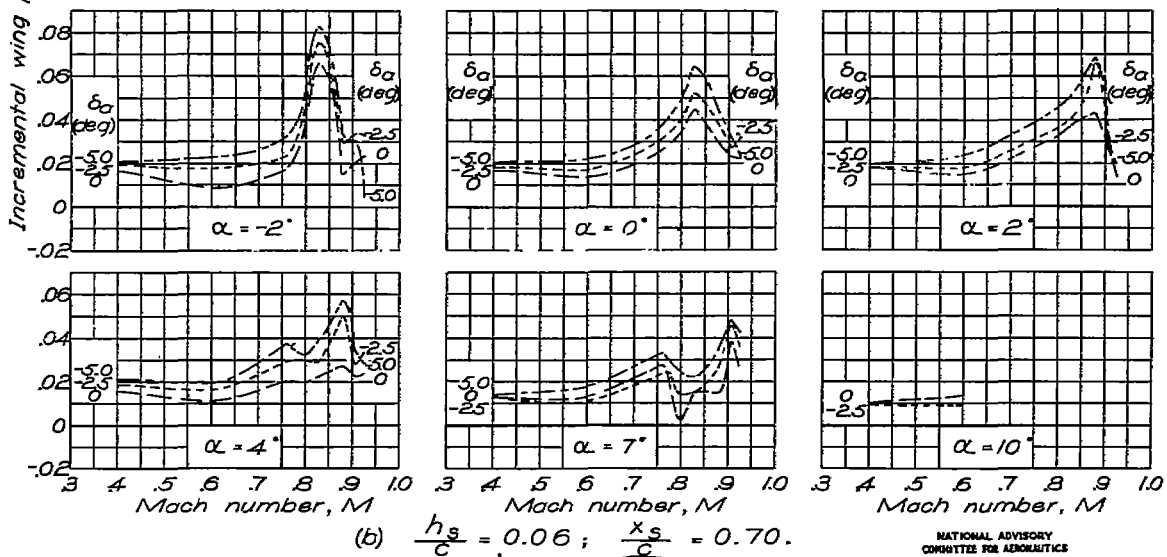
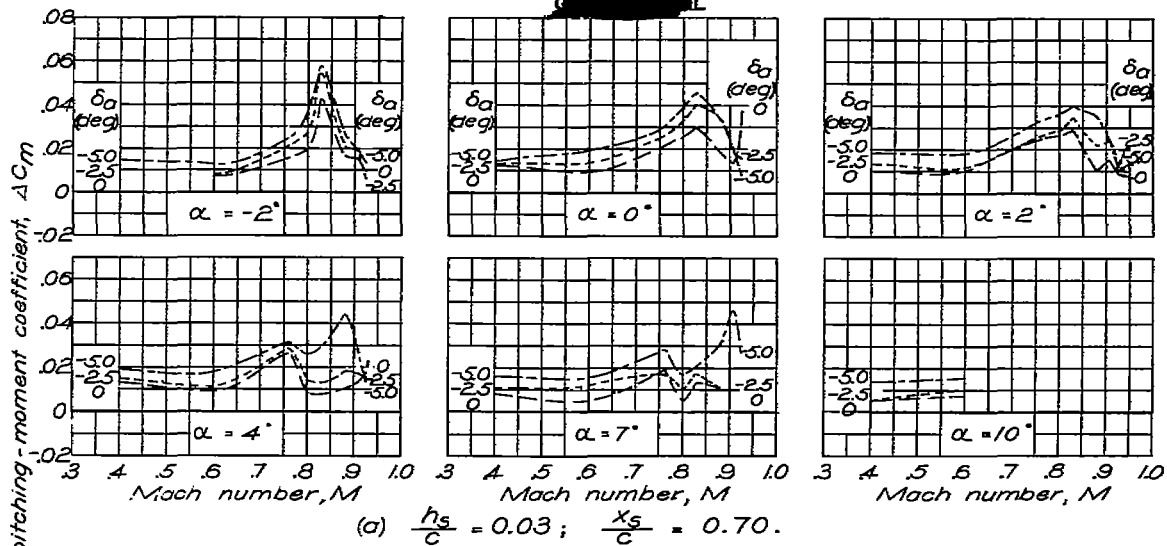
Figure 34.— Continued.



NATIONAL ADVISORY
COMMITTEE FOR AERONAUTICS

(d) $\frac{h_s}{c} = 0.06$; $\frac{x_s}{c} = 0.60$.

Figure 34. — Concluded.



NATIONAL ADVISORY
COMMITTEE FOR AERONAUTICS

Figure 35.- Incremental wing pitching-moment coefficient due to spoiler projection and aileron deflection. Unsealed aileron.

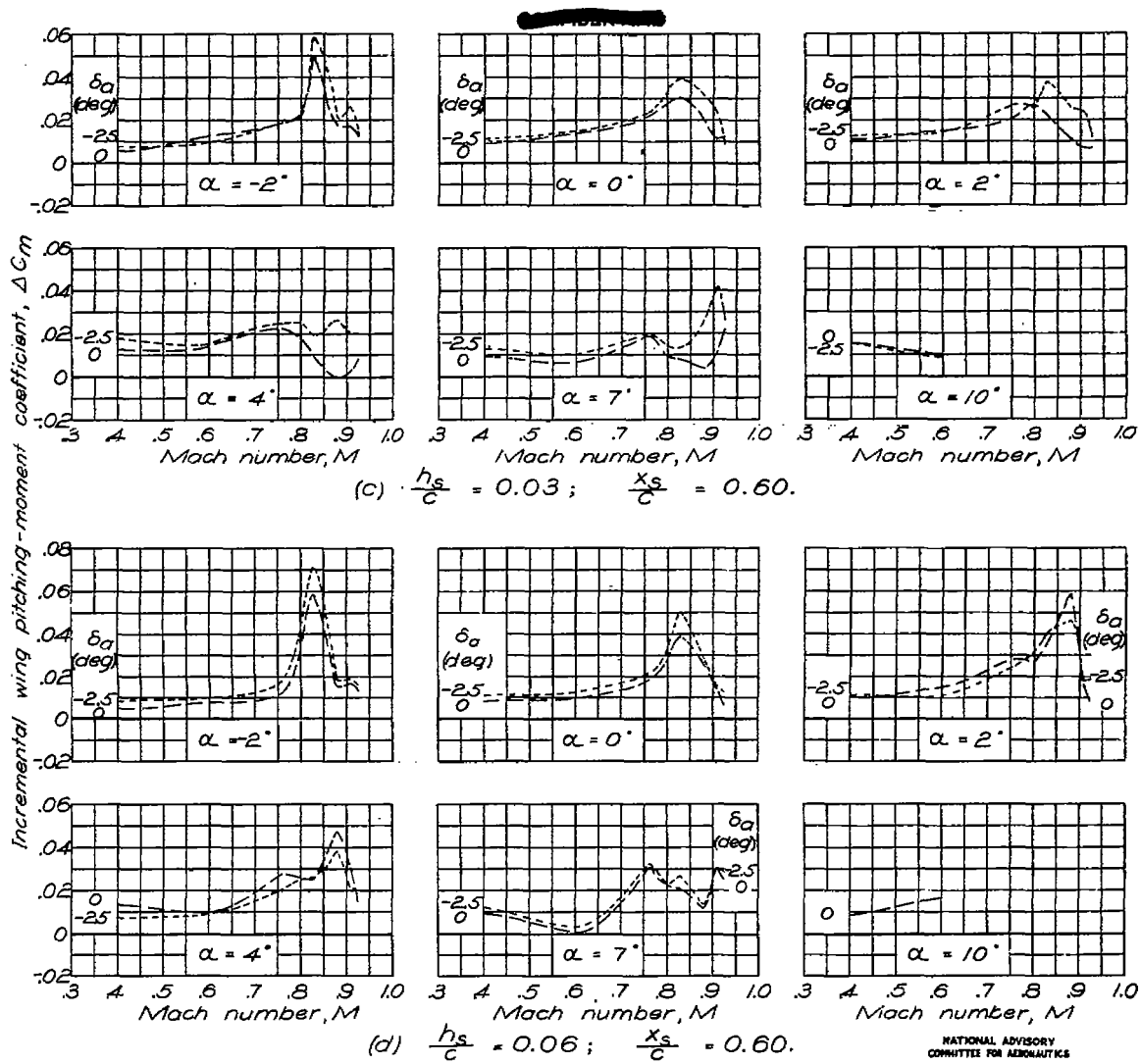
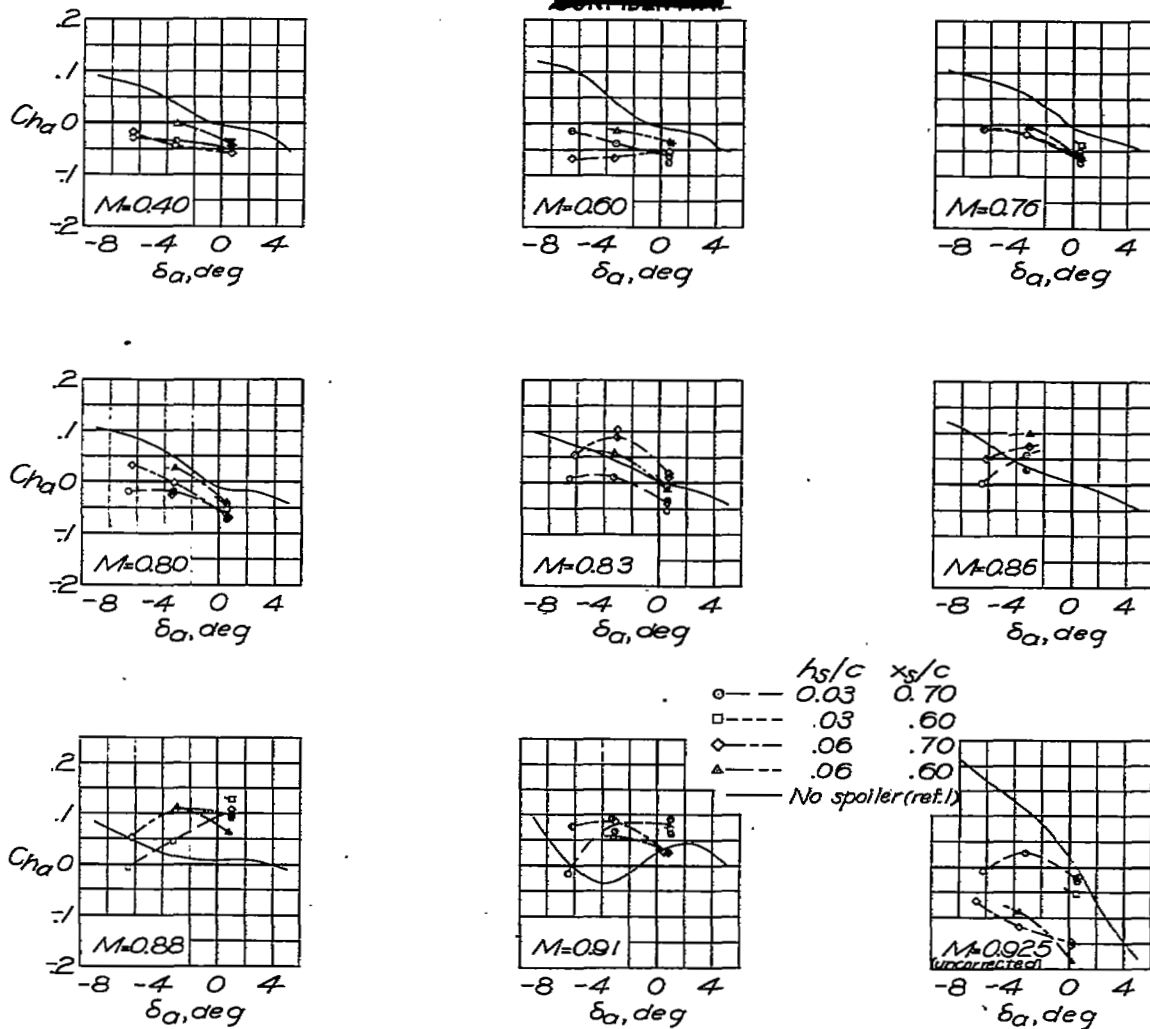


Figure 35. - Concluded.



NATIONAL ADVISORY
COMMITTEE FOR AERONAUTICS

Figure 36. — Variation of aileron hinge-moment coefficient with aileron deflection. Unsealed aileron.

~~CONFIDENTIAL~~

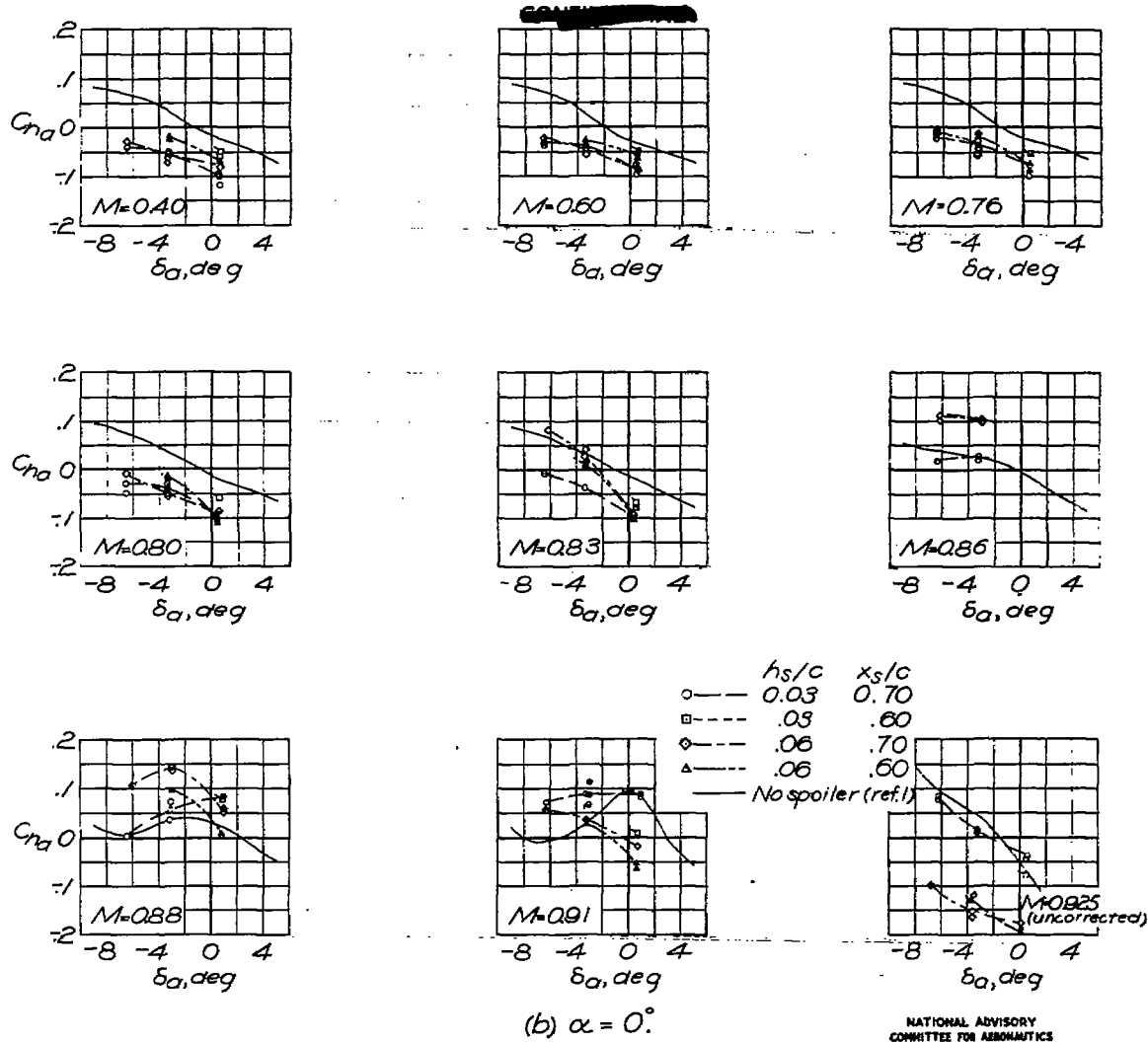
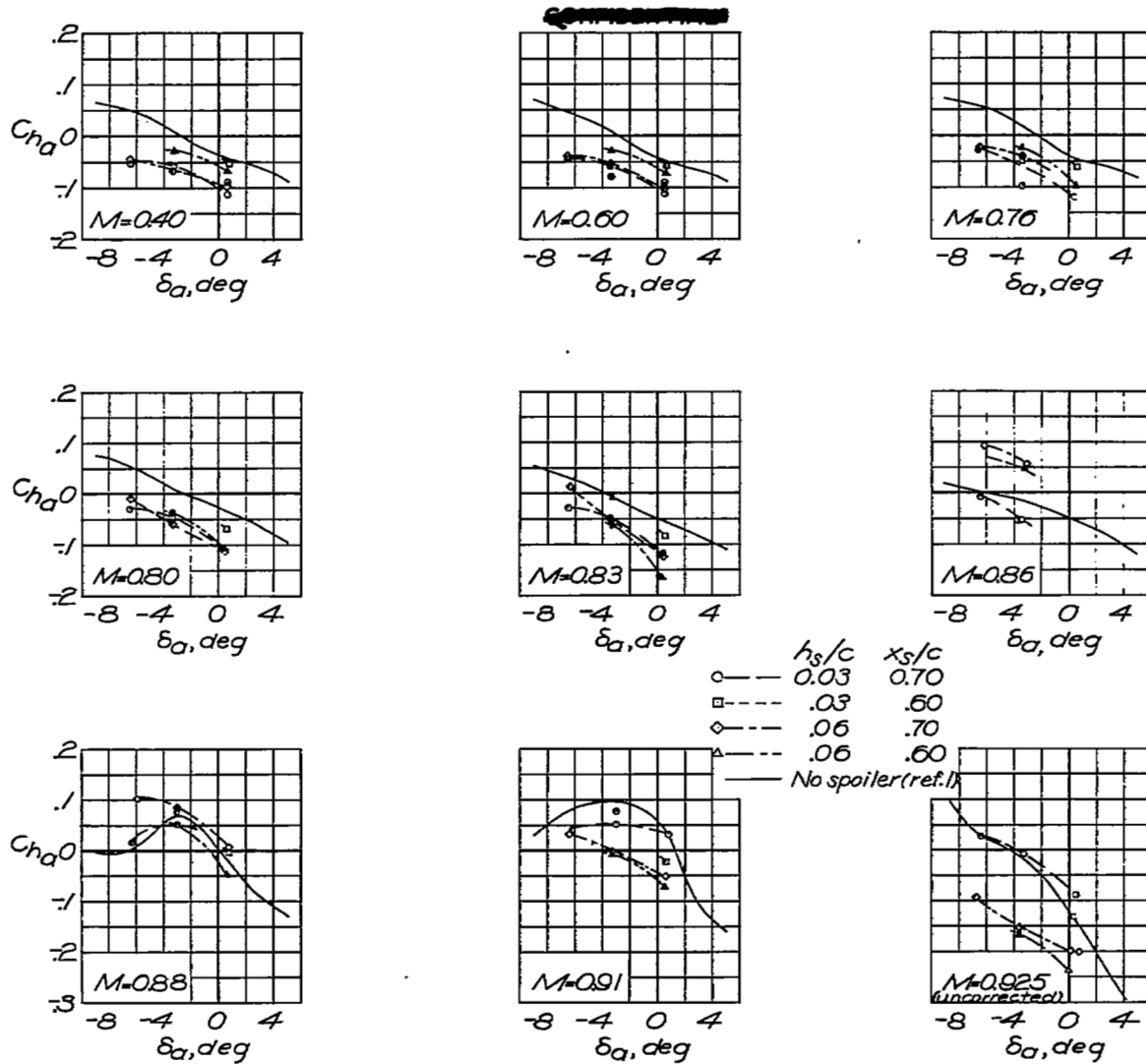
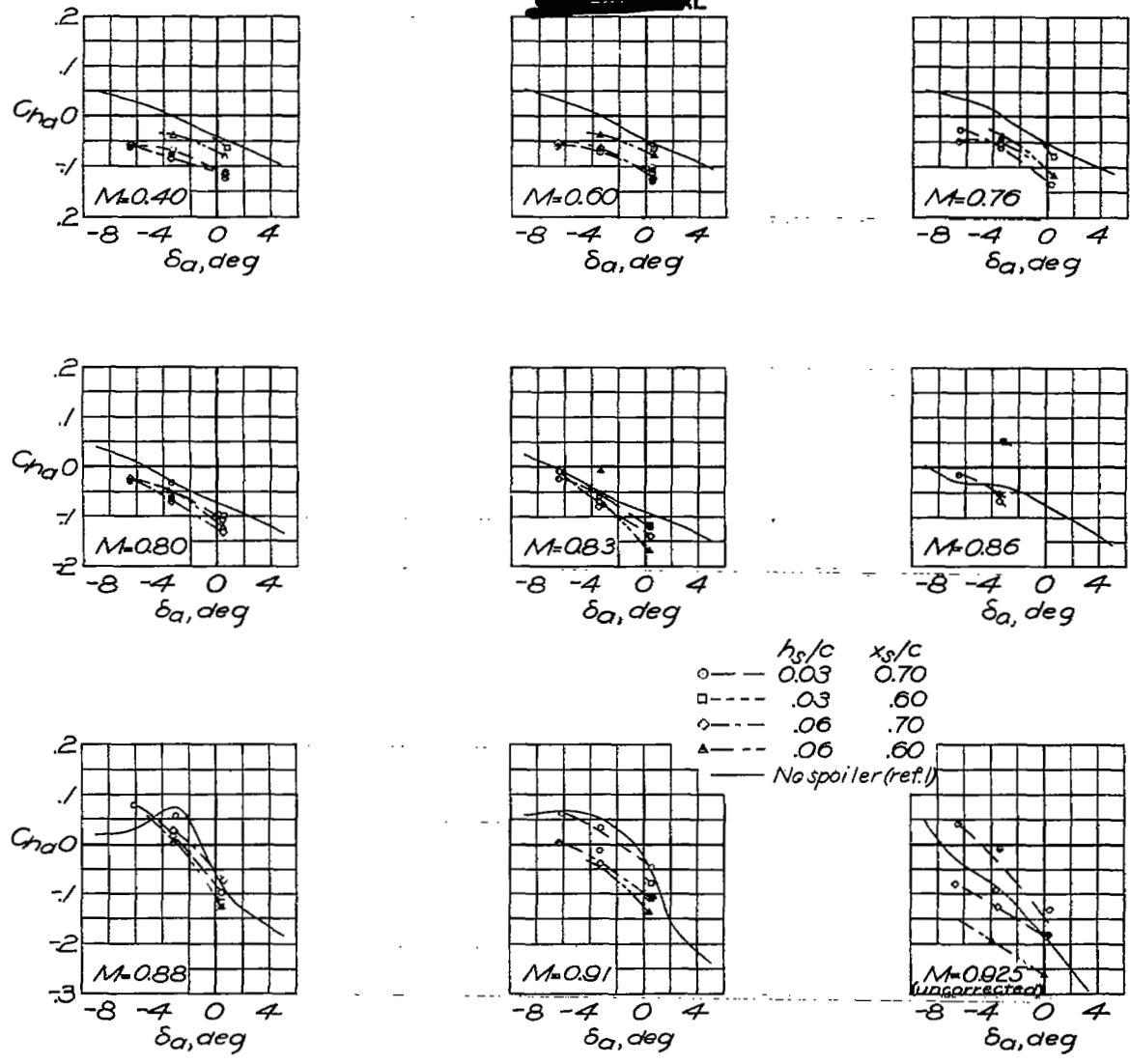


Figure 36.—Continued.



(c) $\alpha = 2^\circ$

Figure 36.—Continued.



(d) $\alpha = 4^\circ$.

Figure 36.-Continued.

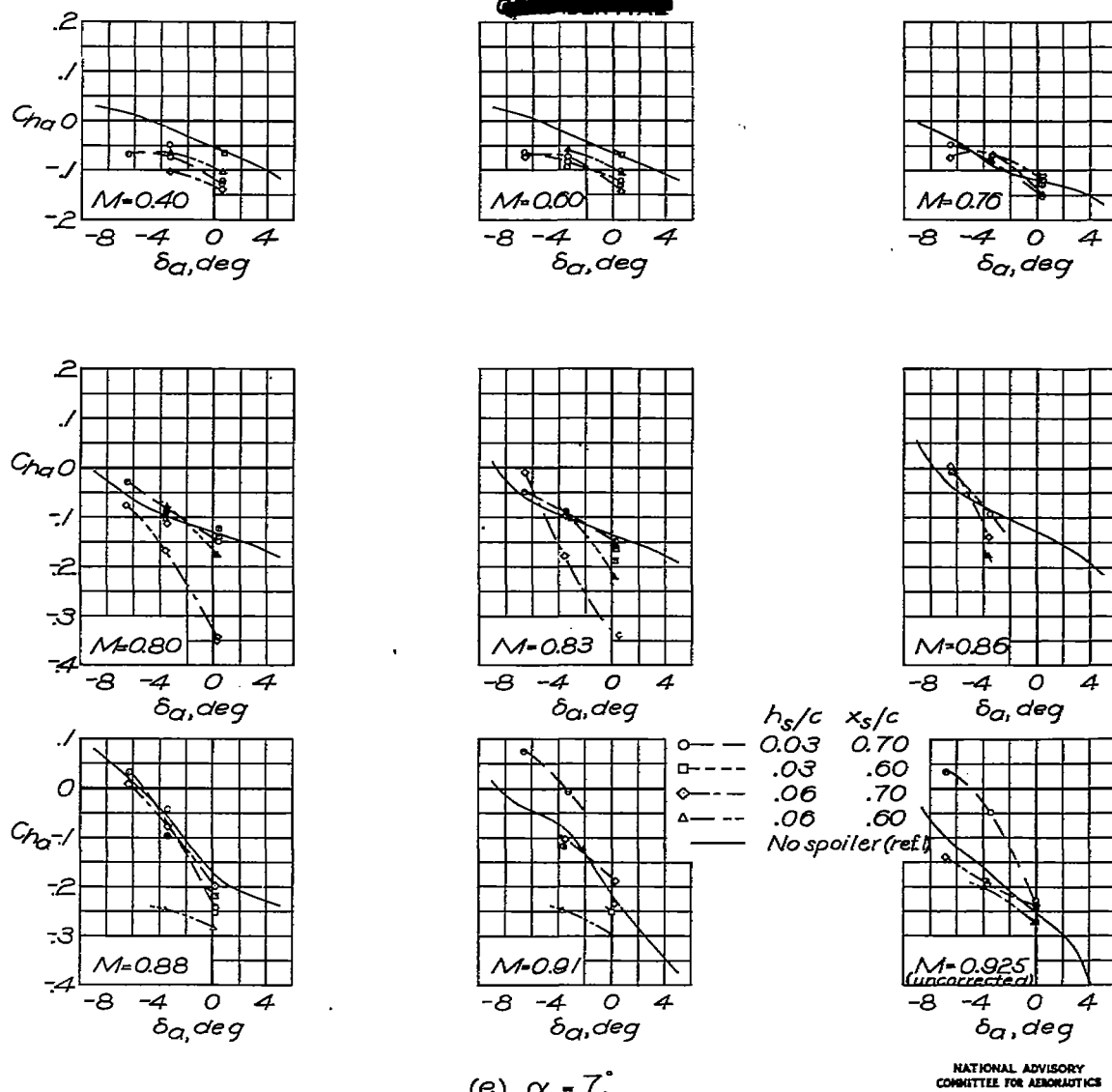
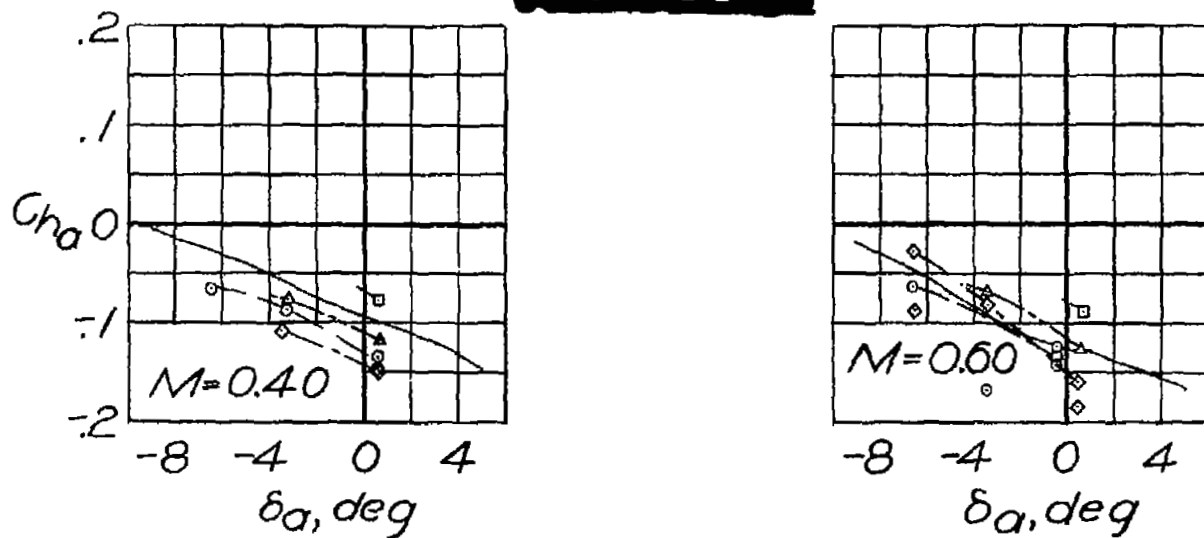


Figure 36 .- Continued.

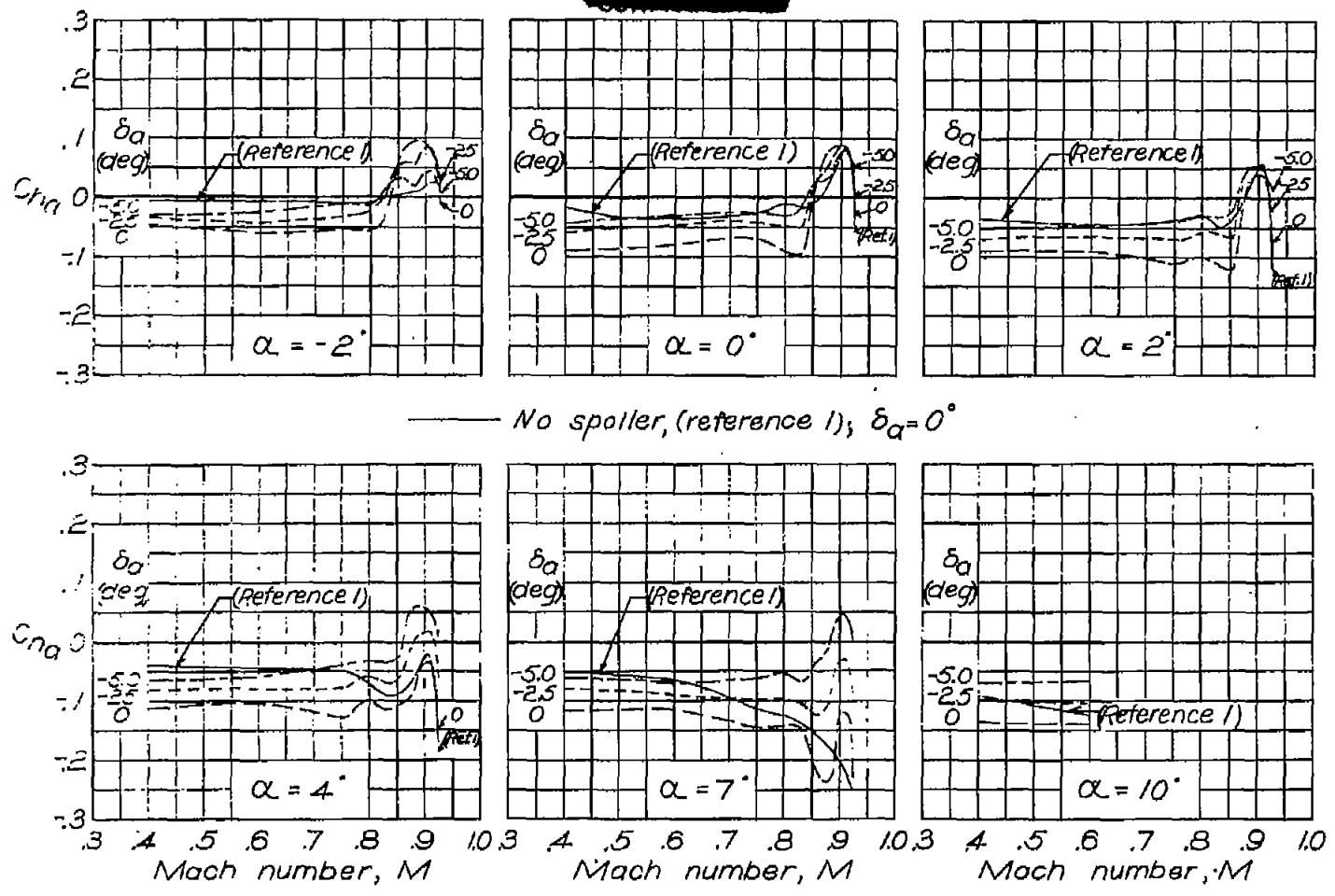


	h_s/c	x_s/c
○ —	0.03	0.70
□ - - -	.03	.60
◇ - - -	.06	.70
△ - - -	.06	.60
—	No spoiler (ref. 1)	

NATIONAL ADVISORY
COMMITTEE FOR AERONAUTICS

(f) $\alpha = 10^\circ$

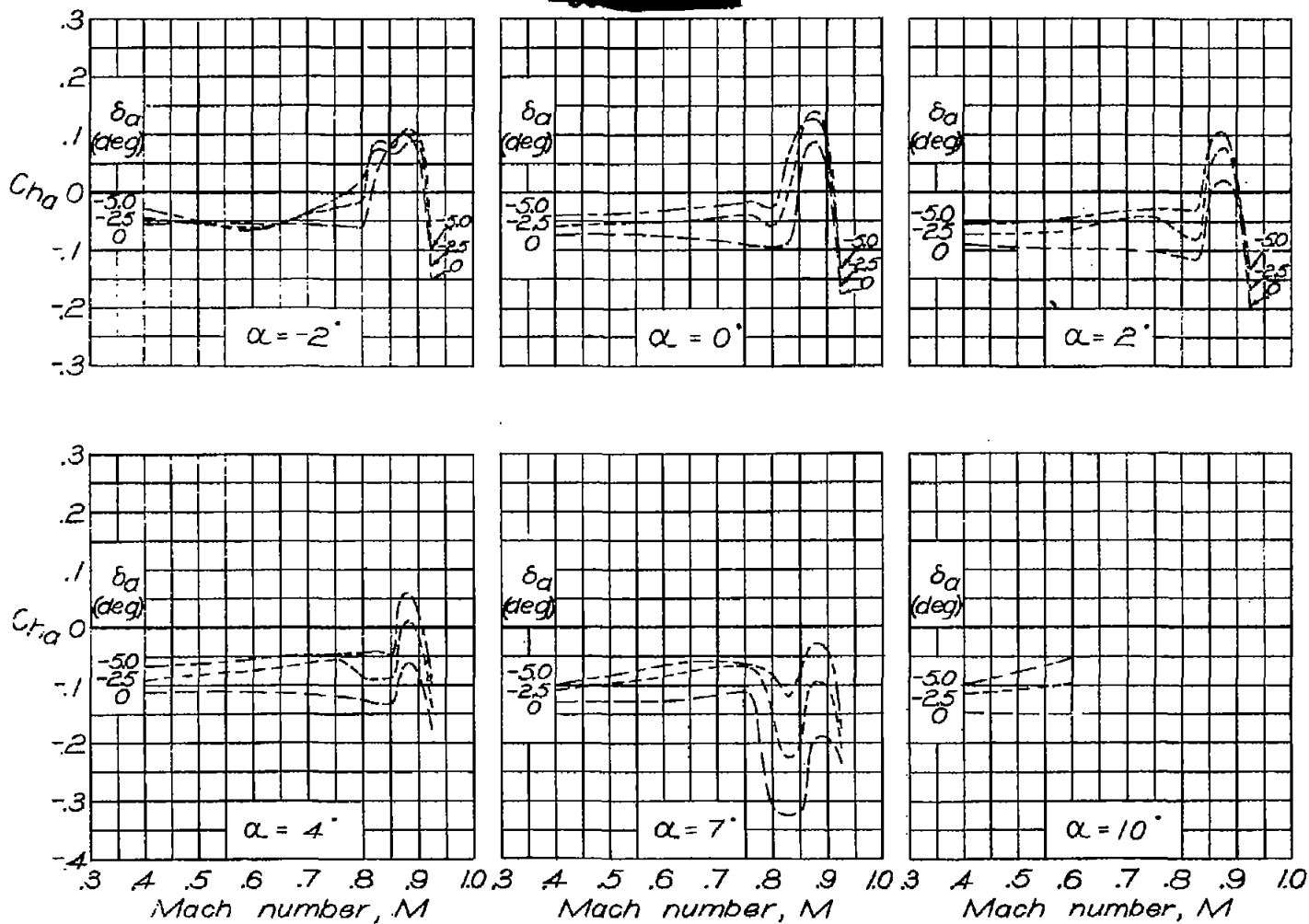
Figure 36.—Concluded.



(a) $\frac{h_s}{c} = 0.03$; $\frac{x_s}{c} = 0.70$.

NATIONAL ADVISORY
COMMITTEE FOR AERONAUTICS

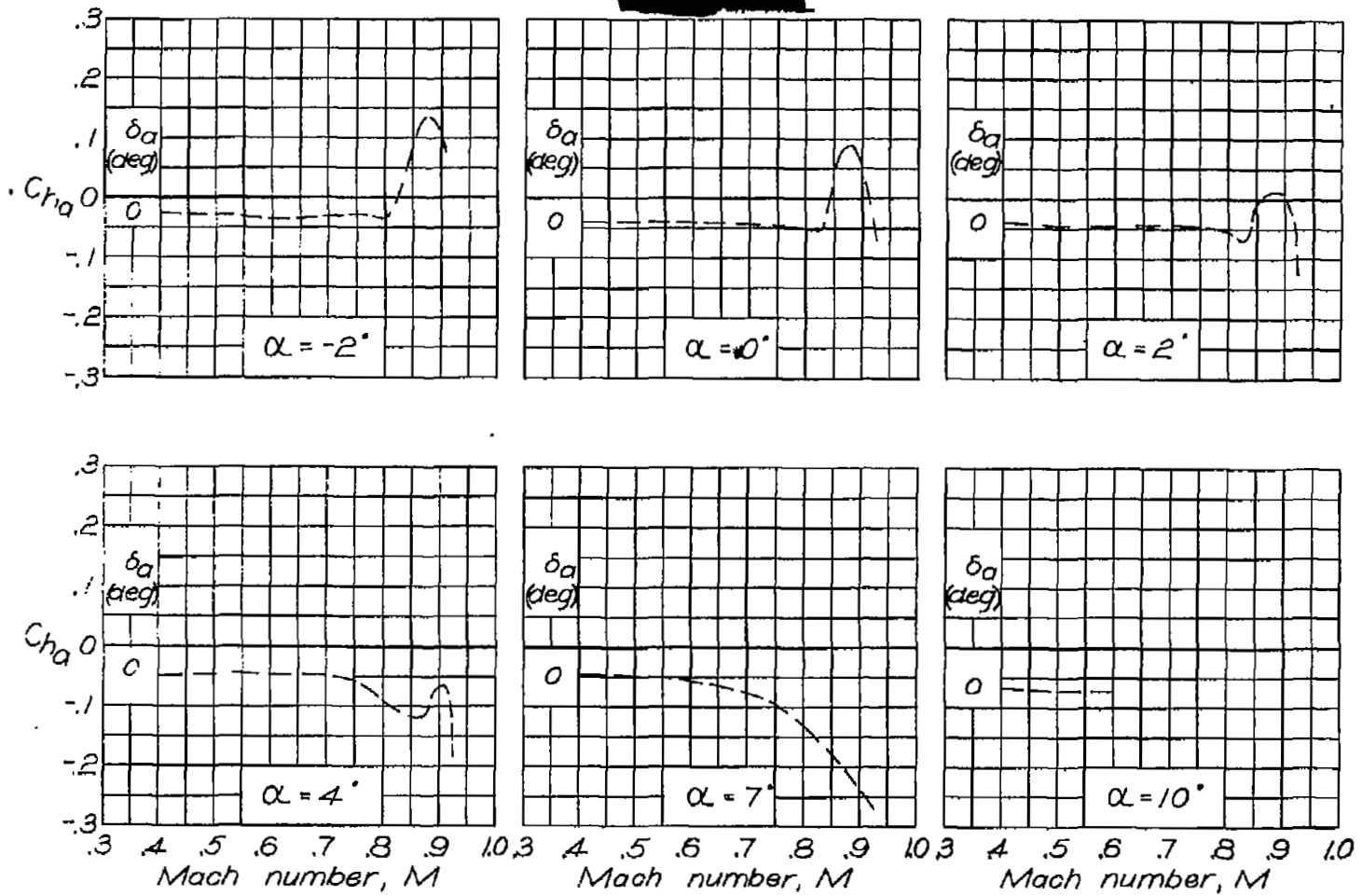
Figure 37.—Variation of hinge-moment coefficient with Mach number. Unsealed aileron.



(b) $\frac{h_s}{c} = 0.06$; $\frac{x_s}{c} = 0.70$.

NATIONAL ADVISORY
COMMITTEE FOR AERONAUTICS

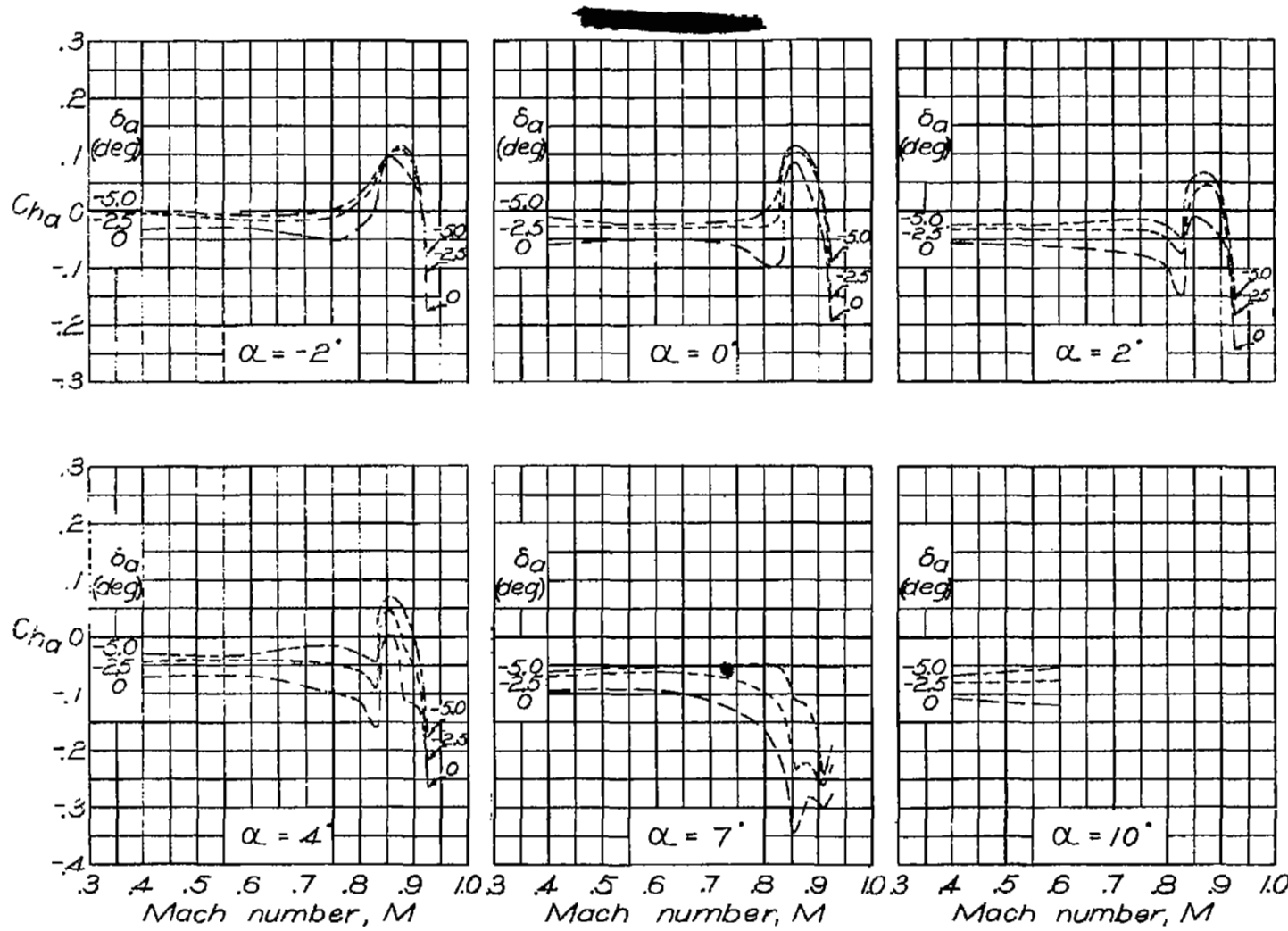
Figure 37.—Continued.



(c) $\frac{h_s}{c} = 0.03$; $\frac{x_s}{c} = 0.60$.

NATIONAL ADVISORY
COMMITTEE FOR AERONAUTICS

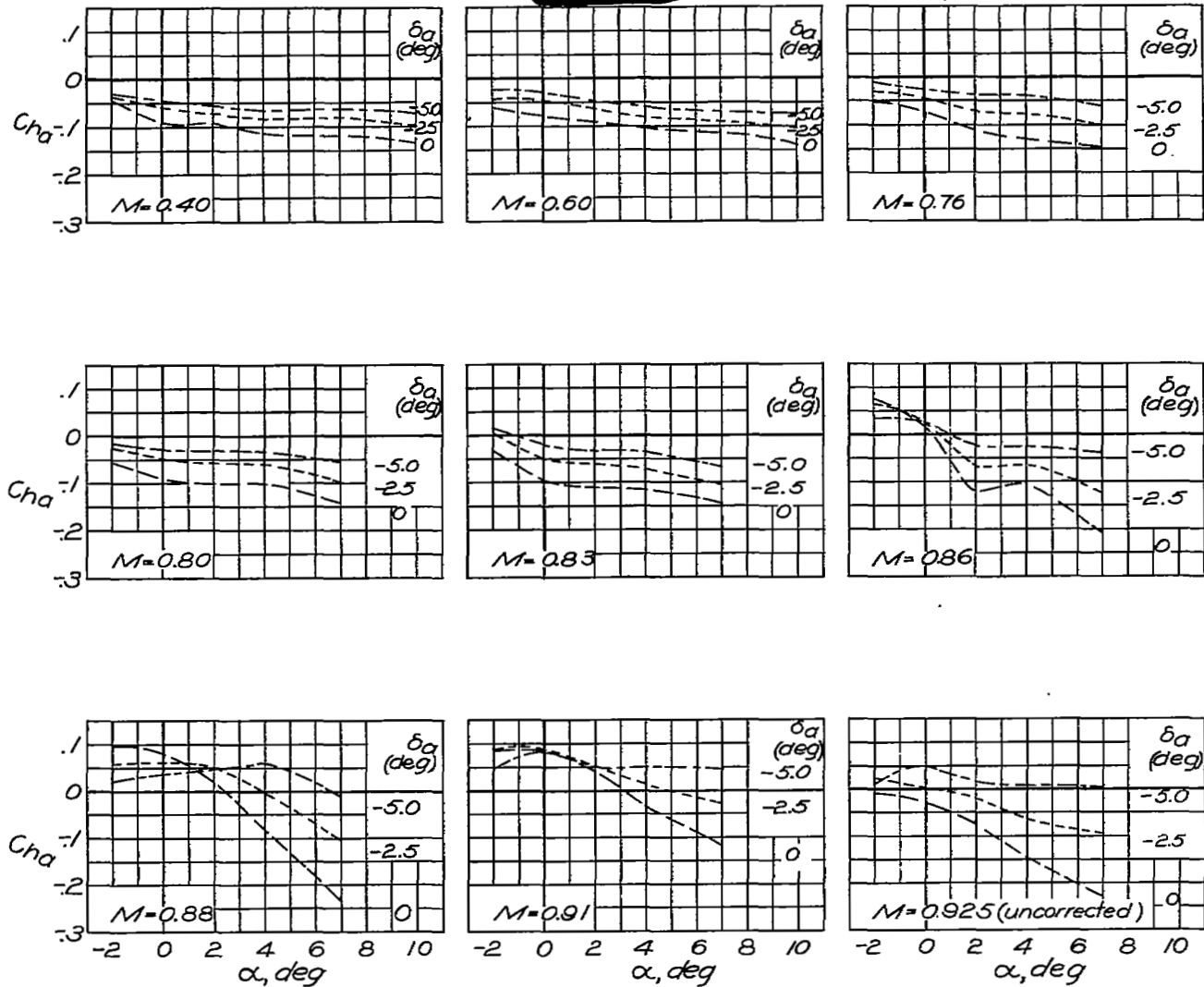
Figure 37. — Continued.



(d) $\frac{h_s}{c} = 0.06$; $\frac{x_s}{c} = 0.60$.

Figure 37. — Concluded.

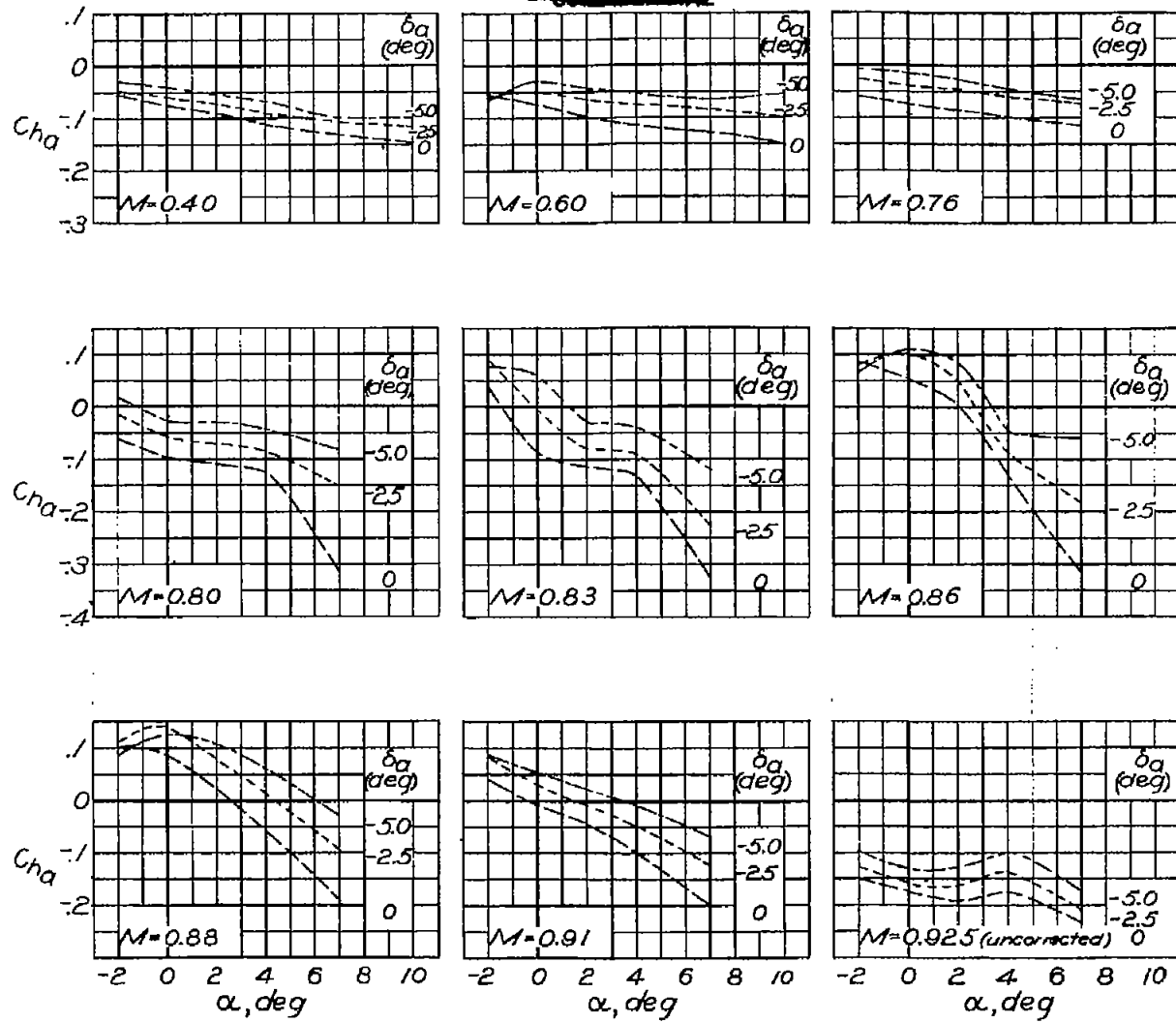
NATIONAL ADVISORY
COMMITTEE FOR AERONAUTICS



(a) $\frac{h_s}{c} = 0.03$; $\frac{x_s}{c} = 0.70$.

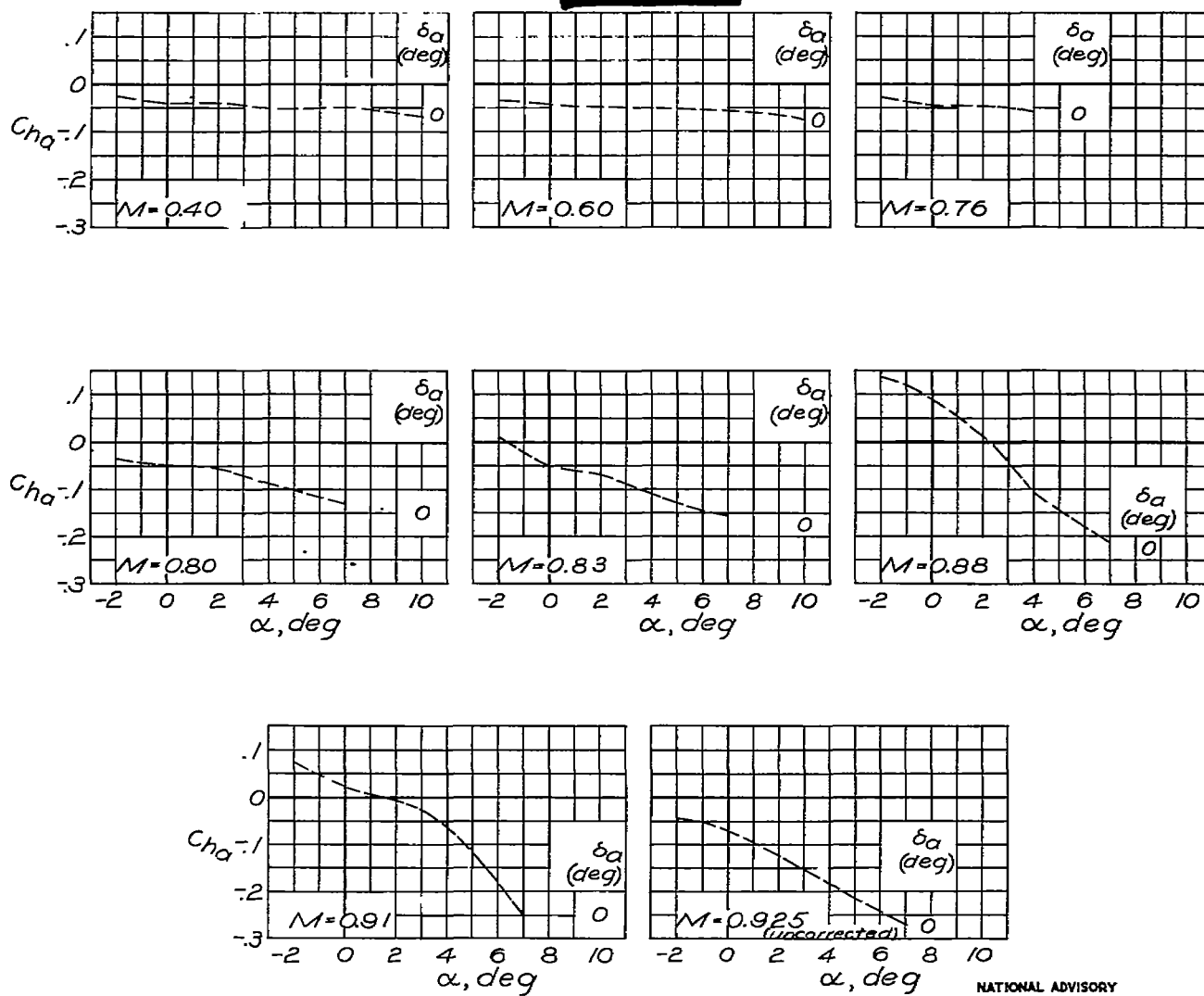
NATIONAL ADVISORY
COMMITTEE FOR AERONAUTICS

Figure 38 .— Variation of aileron hinge-moment coefficient with angle of attack .Unsealed aileron.



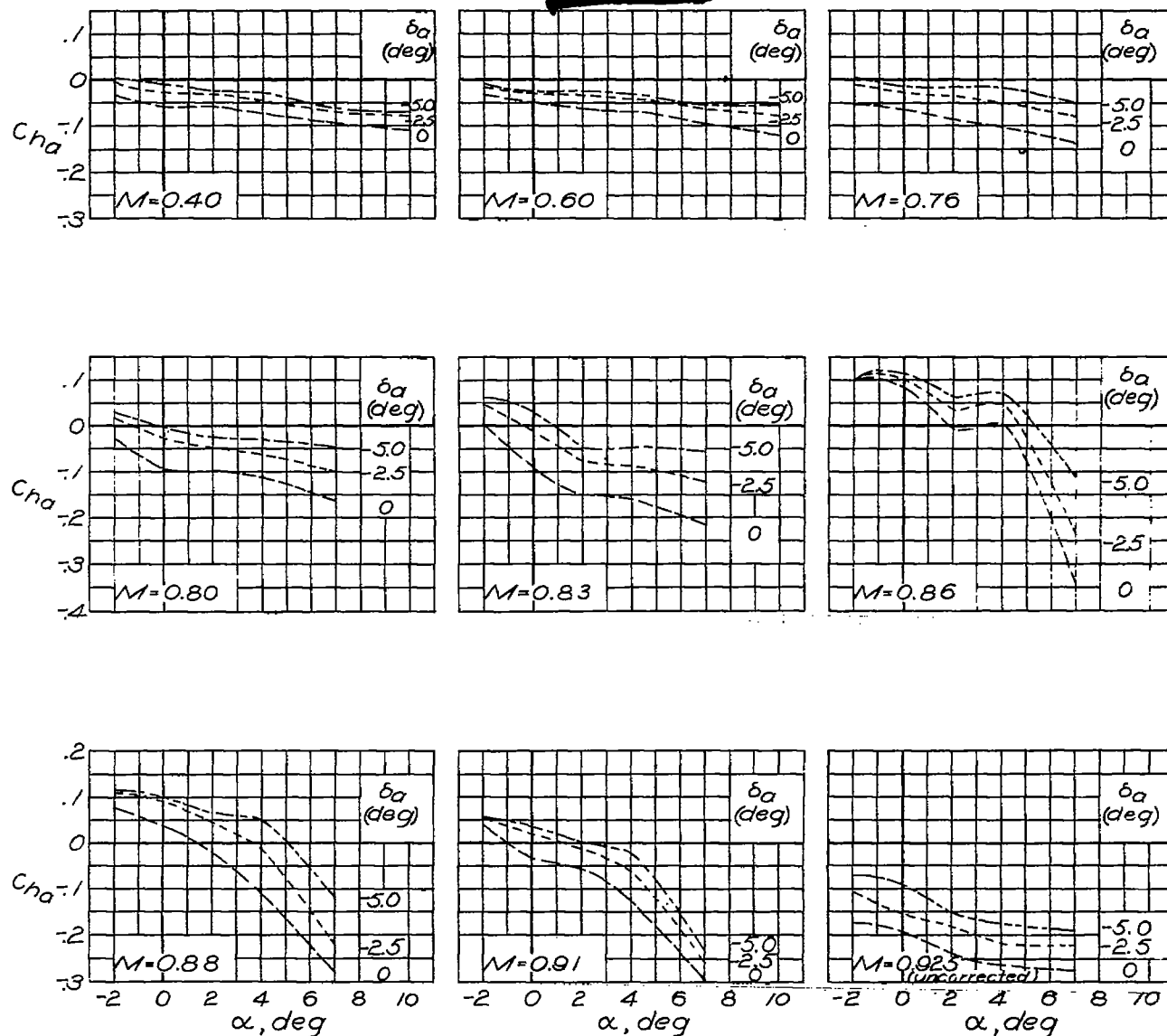
(b) $\frac{h_s}{c} = 0.06$; $\frac{x_s}{c} = 0.70$.

Figure 38 — Continued.



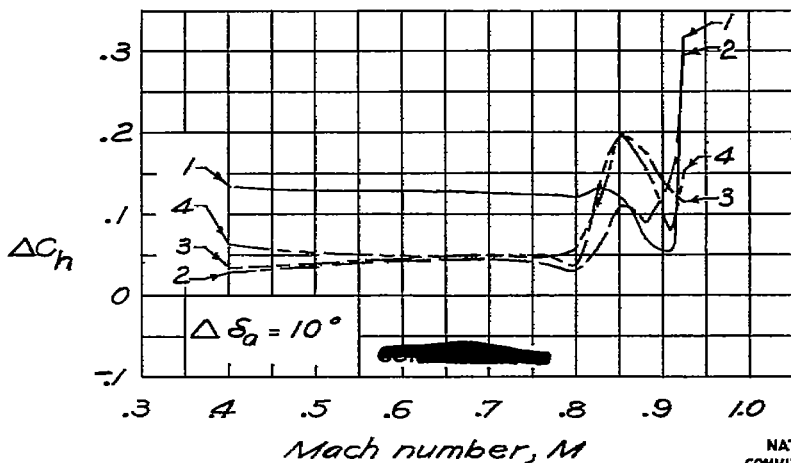
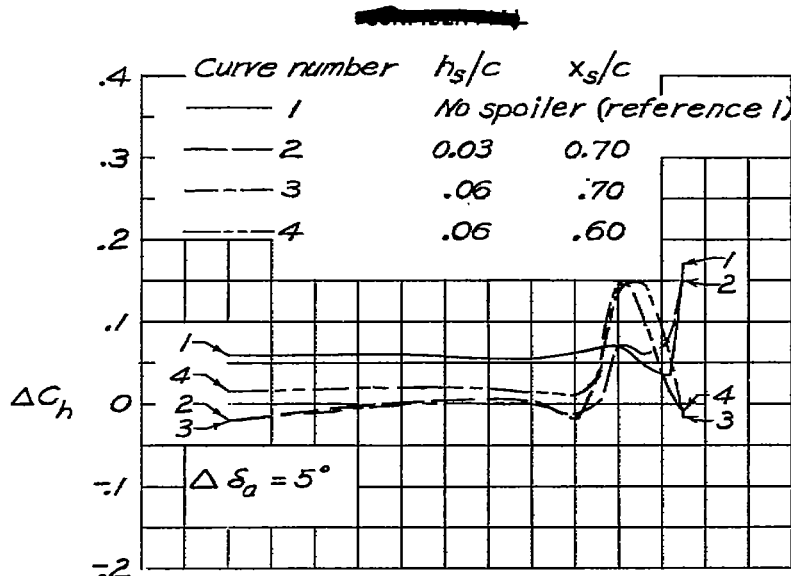
(c) $\frac{h_s}{c} = 0.03$; $\frac{x_s}{c} = 0.60$.

Figure 38. — Continued.



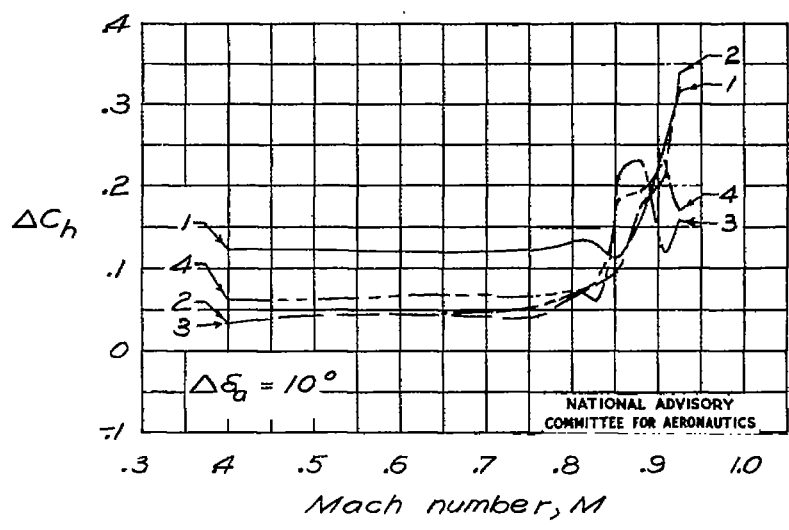
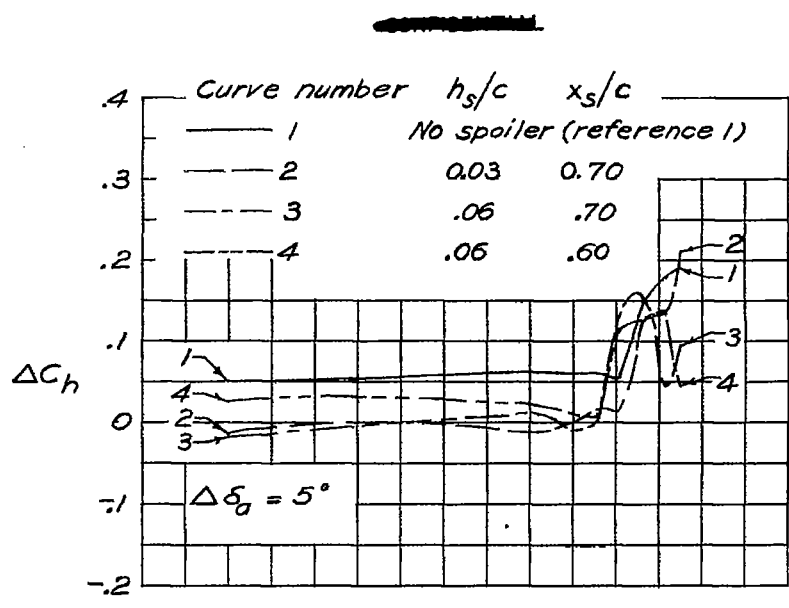
(d) $\frac{h_s}{c} = 0.06$; $\frac{x_s}{c} = 0.60$.

Figure 38 .— Concluded .



NATIONAL ADVISORY
COMMITTEE FOR AERONAUTICS

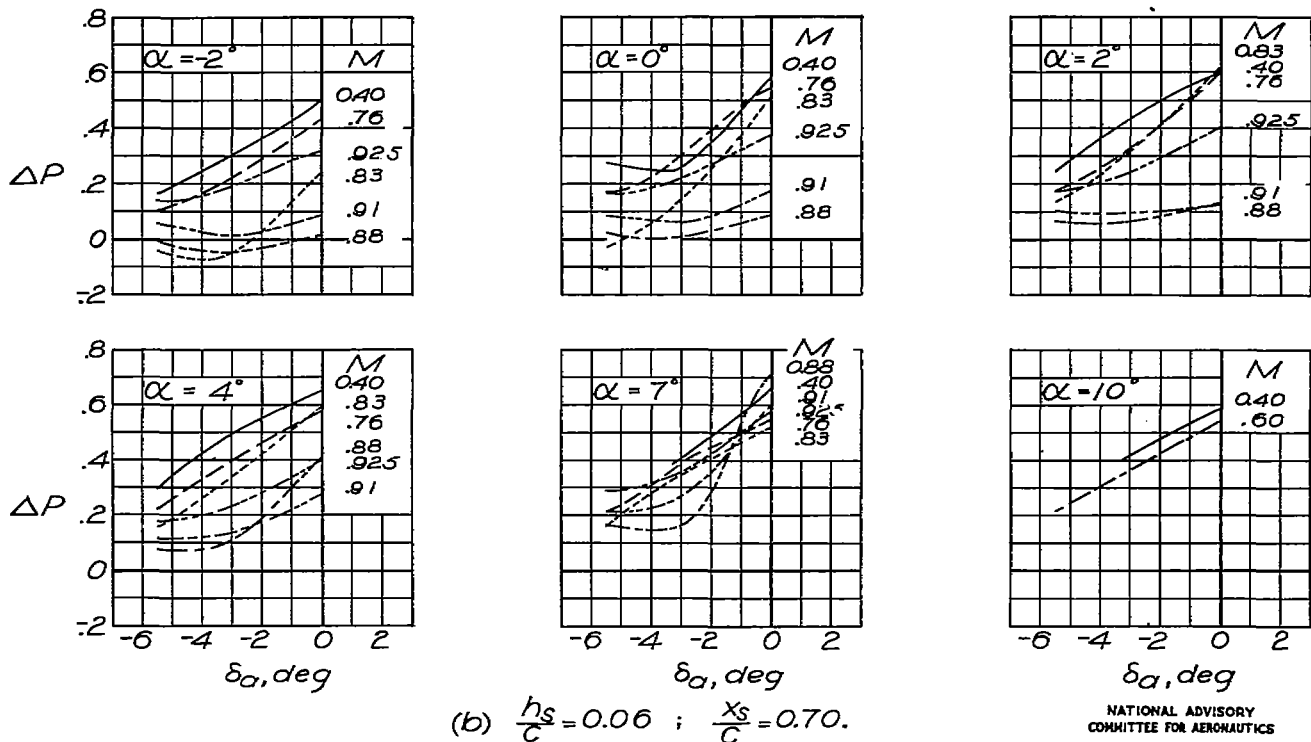
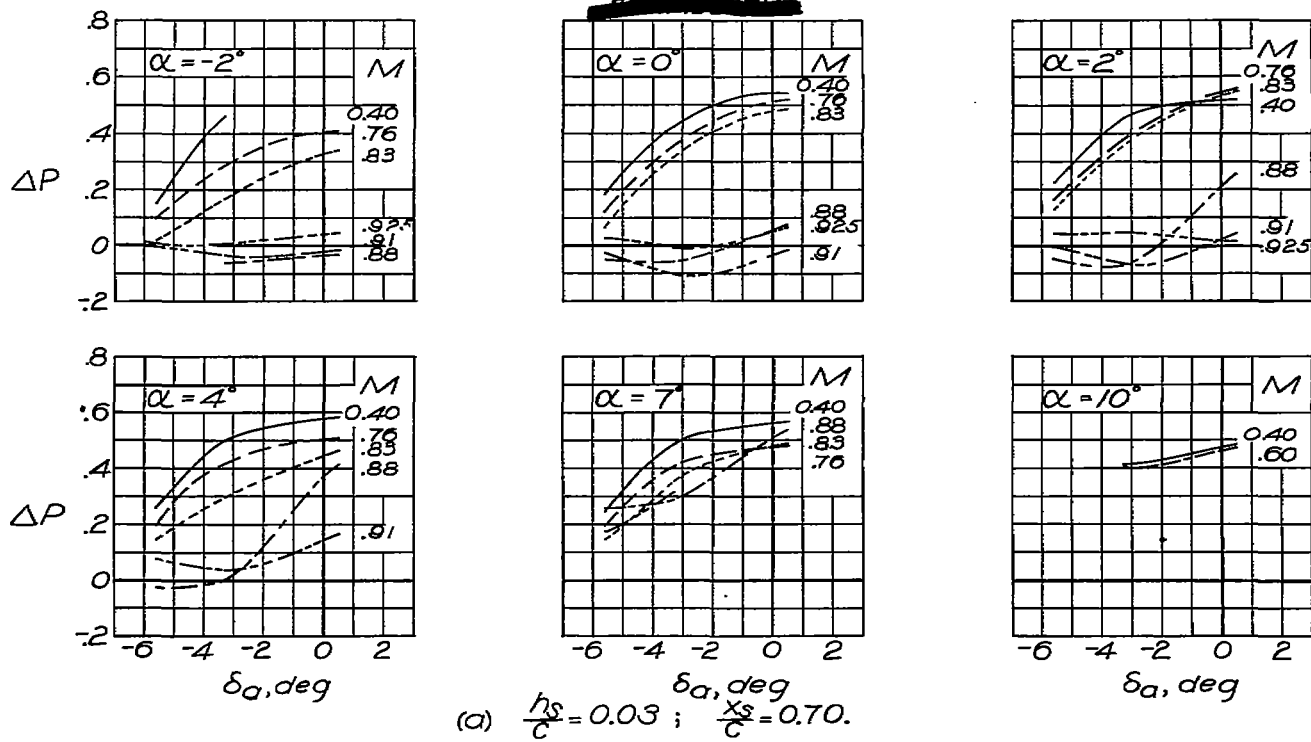
Figure 39.—Comparison of effect of compressibility on hinge-moment coefficient of ailerons at non-differential deflections with and without spoiler ahead of up-going aileron.



(b) $\alpha = 2^\circ$.

Figure 39.- Concluded.

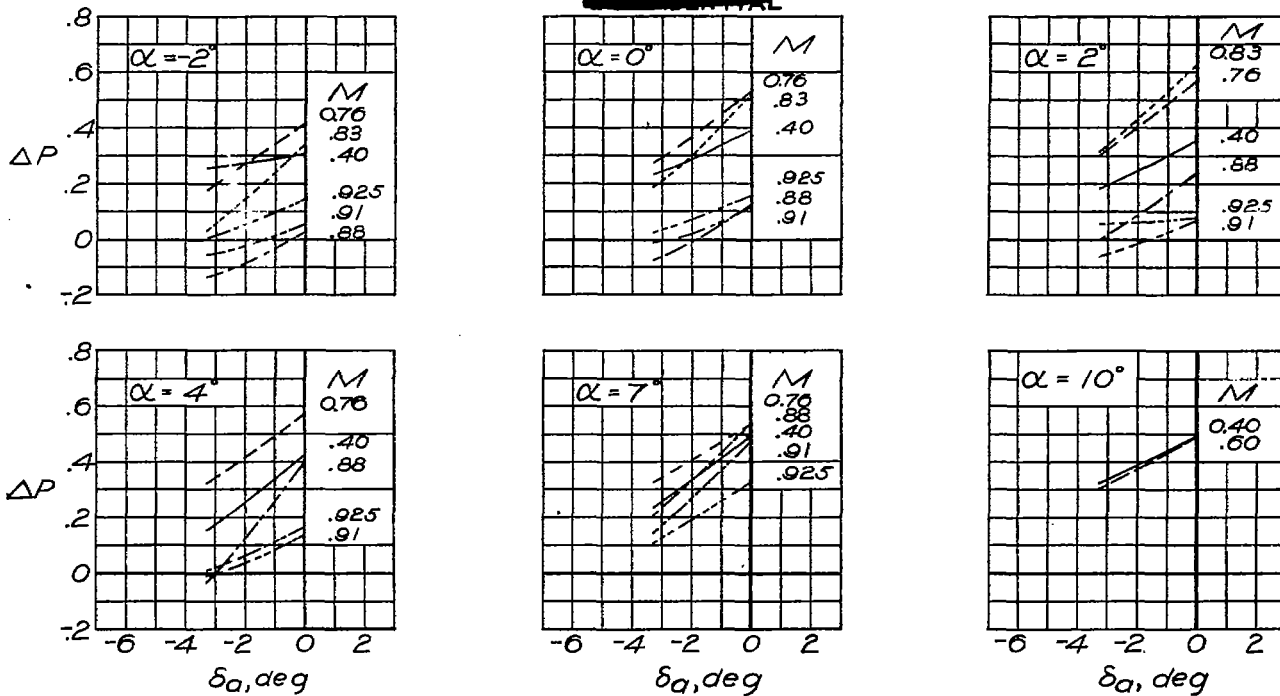
~~CONFIDENTIAL~~



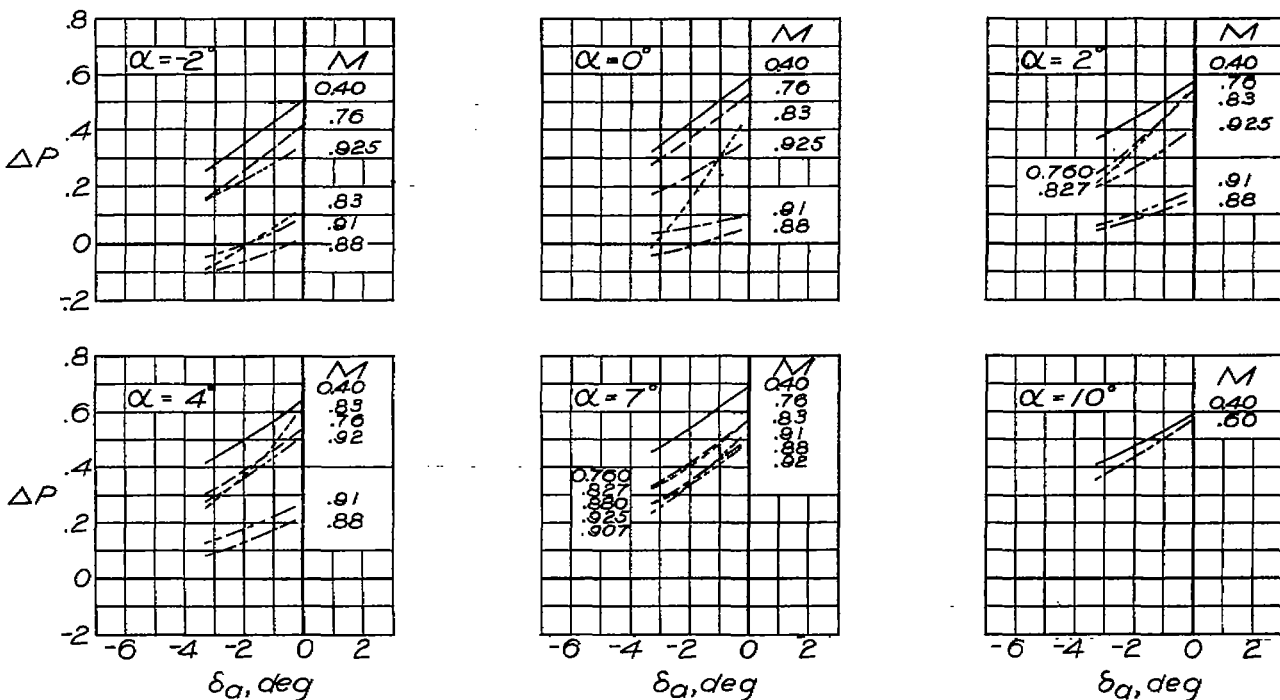
NATIONAL ADVISORY
COMMITTEE FOR AERONAUTICS

Figure 40.—Variation of resultant pressure coefficient across aileron seal.

Fig. 40c,d



(c) $\frac{h_s}{c} = 0.03$; $\frac{x_s}{c} = 0.60$.



(d) $\frac{h_s}{c} = 0.06$; $\frac{x_s}{c} = 0.60$.

NATIONAL ADVISORY
COMMITTEE FOR AERONAUTICS

Figure 40. — Concluded.

014363635

NASA Technical Library



3 1176 01436 3635